Combining microstructural analysis with EPMA monazite geochronology to constrain progressive stages of orogenesis in the Appalachians

Volume I: Text.

Thesis submitted by

Nicholas John Lisowiec BSc(Hons) *Adelaide*

in December 2005

for the degree of Doctor of Philosophy

in the School of Earth Sciences

James Cook University

STATEMENT OF ACCESS

I, the undersigned, author of this work, understand the James Cook University will make this thesis available for use within the University Library and, via the Australian Digital Thesis network, for use elsewhere.

I understand that, as an unpublished work, a thesis has significant protection under the Copyright Act and I do not wish to place further restriction on access to this work.

_____________________ _____________

Nicholas Lisowiec Date

STATEMENT OF SOURCES

DECLARATION

I declare that this thesis is my own work and has not been submitted in any other form for another degree or diploma at any university of other institution of tertiary education. Information derived from published or unpublished work of others has been acknowledged in the text and a list of references is given.

Nicholas Lisowiec Date

STATEMENT ON THE CONTRIBUTION OF OTHERS

T.H. Bell provided supervision, guidance and editorial assistance for this body of work. Funding for fieldwork and analyses was provided from an ARC Large grant to T.H. Bell, and a JCU Doctoral Merit Research Scheme grant to myself. Stipend support was received from a JCU School of Earth Sciences and an Australian Postgraduate Award (APA) Scholarship.

Kevin Blake provided invaluable assistance in setting up and running the EPMA and contributed significant amounts to the techniques used here. Paul Evins provided technical and data handling advice and reviewed earlier versions of this thesis, which lead to significant improvements. Discussions with Cameron Huddlestone-Holmes, David Donald and Joe Pyle, helped improve the statistical sections of the thesis. Cameron also helped with obtaining some of the data. Joe contributed advice on technical issues, and reviewed an earlier version of the first chapter, which resulted in substantial changes and improvements.

ACKNOWLEDGEMENTS

I would like to thank Tim Bell for giving me the opportunity to firstly do a PhD and then encourage me to complete it (pretty much) within the planned timeframe, especially after the first 12 months were a failure. Andrew Ham and Cameron Huddlestone-Holmes are particularly thanked for helping me initially refocus my project, during Tim's absence.

Kevin Blake is thanked for his invaluable assistance and his continuing efforts to setup and refine the techniques used in this study. Without Kevin, this project would not have happened. Paul Evins is also thanked for his efforts in helping develop the techniques of monazite analysis and chemical dating at all levels. Discussions with Paul have helped me define many of the concepts and strategies used during the project.

I would like to thank past and present members of SAMRI and other individuals within the department. The people around me during my time at JCU have made the experience enjoyable, and helped me learn a lot.

My family down in Adelaide are thanked for encouraging me to initially make the trek to North Queensland and being wiling to help me whenever I needed it ever since.

Finally, I would like to save my biggest thank you to (and), whose love and support has always been appreciated. The final year of PhD has been interesting and eventful and we have only become closer because of it.

TABLE OF CONTENTS: VOLUME I

TABLE OF CONTENTS: VOLUME II

THESIS INTRODUCTION AND OUTLINE

Introduction

Microstructural relationships between porphyroblasts and the matrix have been frequently used to infer the relative timing of porphyroblast growth in deformed and metamorphosed terrains (Bell and Rubenach, 1983; Bell et al., 1986; Schulz, 1990; Barker, 1994; Williams, 1994). Although the interpretation of inclusion trail geometries is still controversial (Bell et al., 1992; Passchier et al., 1992; Williams and Jiang, 1999; Ikeda et al., 2002), quantification, by way of foliation intersection/inflection axes preserved in porphyroblasts (FIAs), has shown that long histories and multiple periods of growth can be preserved (Bell and Hayward, 1991; Bell et al., 1995; Bell et al., 1998). As such, inclusion trails have been used to locally track the deformation and metamorphic history that predates the development of the matrix foliations that are finally preserved in rocks (Bell and Hickey, 1999; Stallard and Hickey, 2001; Stallard et al., 2003; Bell et al., 2004; Cihan and Parsons, 2005).

Whilst relative timing constraints on numerous sample suites have been obtained using the FIA method, chemical and absolute time data for these interpretations is required. Microstructurally, successive portions of garnet porphyroblasts generally do not correlate with the chemical zoning patterns of major cations, despite these porphyroblasts preserving a multi-stage growth history (e.g. Bell and Kim, 2004). One explanation for this has been based around the effects of deformation partitioning and reactivation of pre-existing foliations controlling the location and timing of porphyroblast growth (Bell et al., 2004). In these models, differentiated crenulation cleavage development stops porphyroblast growth because the resultant strain softening prevents microfracture, which is essential for the rapid access of components to and from the growth site. When later deformation resumes, porphyroblast growth resumes provided the deformation partitions through that location, until differentiated cleavage again begins to develop, and growth again ceases. If no significant changes have occurred in temperature (T), pressure (P) or composition (X), then on resumption of growth there should be no (or little) effect on compositional zoning. The ability to constrain absolute time and test whether this is the case is, therefore, very important. Fine-scale isotopic dating of garnet is difficult and expensive, particularly when inclusion-rich porphyroblasts are the subject of study (e.g. DeWolf et al., 1996; Vance et al., 1998; Prince et al., 2000). The dating of accessory minerals such as monazite provides a viable alternative for constraining different generations of porphyroblast growth and/or foliation development.

Monazite [(LREE)PO_4] incorporates appreciable amounts of Th and U and is highly resistant to Pb-loss through either volume diffusion (Seydoux-Guillaume et al., 2002; Cherniak et al., 2004), or metamictisation (Ewing and Haaker, 1980; Meldrum et al., 1997). Consequently, it is widely used to date metamorphic, igneous and hydrothermal events. Monazite contains little or no common Pb (Parrish, 1990). Therefore, it can be chemically dated in-situ on the electron probe microanalyser (e.g. Suzuki and Adachi, 1991; Montel et al., 1996; Rhede et al., 1996; Cocherie et al., 1998; Crowley and Ghent, 1999; Williams et al., 1999; Jercinovic and Williams, 2005; Pyle et al., 2005). Advantages of the electron probe microanalyser (EPMA) include the small spatial resolution (down to 1 μm), minimal sample damage and the ability to get compositional data for each spot analysed. High detection limits (which generally preclude dating monazites younger than approximately 50 Ma), large errors in precision, and the inability to assess potential discordancy between ^{238}U-^{206}Pb and ^{235}U-^{207}Pb ages, are some potential problems (Montel et al., 1996; Cocherie and Albarede, 2001). However, used within its limits, monazite dating on the EPMA has the potential to provide crucial absolute time constraints on both porphyroblast growth and foliation development (Bell and Welch, 2002; Williams and Jercinovic, 2002).

Whilst monazite is an ideal accessory mineral to date garnet growth events, it is not necessarily present around the garnet isograd. The monazite stability field in metapelites commonly appears to be at a higher grade than that of garnet. Consequently, it is mostly present as inclusions in garnet porphyroblast rims and/or higher grade phases. This restricted one of the aims in this study, the dating of FIA events, which, at present, has only been attempted by Bell and Welch (2002). Nevertheless, both detailed microstructural and monazite analyses have been combined to solve particular metamorphic and deformation timing problems within the Appalachians of eastern North America. Three different areas are examined, two in the southern Appalachians and the third in the New England. Between these regions, over 150 million years of orogenesis, within three major events are recorded. The protocol for analysing monazite was (and still is) a continual process of refinement and learning. As such, the data presented here reflects this natural progression, and some of the methods used during the early parts of this project were improved on in the later parts. The data presented here has been obtained as accurately as possible and where any doubts existed regarding the results they were either re-checked using the current EPMA setup or addressed within the thesis.

Thesis Outline

The thesis consists of four sections, each written as independent bodies of work with the intention that they will be submitted as papers for publication in international journals. The chapters follow a progression from early work involving data handling and determining the precision of EPMA monazite ages, to combining monazite and garnet chemistry, microstructural classification and chemical ages to interpret the metamorphic and deformational history of the study areas. The main text of the thesis is in Volume I and figures and tables are presented in Volume II. References are given at the end of each section in Volume I and appendices are included at the end of Volume II.

The first chapter addresses how different studies have quoted precision errors in EPMA monazite ages, particularly with the “single-spot” method (where an “age” is calculated from the Pb, Th, U concentration for each data point). Two different techniques have been used, one utilising counting statistics and the other the variation within a group of individual ages/dates. By comparing the methods with a dataset from a homogeneous monazite grain, the potential underestimation of precision from counting statistics is highlighted. This chapter is a major revision of a manuscript submitted to Chemical Geology in late 2004.

The second chapter follows on from above by evaluating a non parametric (bootstrap) method for calculating precision errors in heterogeneous monazite grains/domains. Methods to chemically and microstructurally interpret individual grains in metamorphic rocks are also presented. These techniques are applied to data from the Murphy Syncline, North Carolina with the results addressing previous uncertainties as to whether regional metamorphism was Taconic (Ordovician), Acadian (Silurian-Devonian), or a combination of both events.

A narrow, fault-bounded belt of meta-sediments and meta-volcanics that extends across northern Georgia is the subject of Chapter 3. These rocks have an uncertain metamorphic age, although they contain excellent microstructures, both within garnet porphyroblasts and the matrix that potentially record a prolonged metamorphic history. Whilst the rare monazite inclusions prevented a detailed study of the porphyroblast history, the data that was obtained provides interesting insights into the metamorphic and structural development of the region.

The final chapter presents the results of an extensive study to determine the earliest stages of porphyroblast growth within meta-pelites from north-central Massachusetts. The rocks here contain multiple FIA sets within the porphyroblasts, despite the matrix having been heavily sheared late in the metamorphic history. Qualitative analysis of garnet-monazite equilibrium was undertaken in some samples to correlate monazite ages to periods of garnet porphyroblast growth. The results are interpreted with respect to the possible pattern of early metamorphism and the also the tectonic setting of metamorphism prior to shearing.

References

Barker, A.J., 1994. Interpretation of porphyroblast inclusion trails: limitations imposed by growth kinetics and strain rates. Journal of Metamorphic Geology, 12, 681-694.

Bell, T.H., Forde, A. and Wang, J., 1995. A new indicator of movement direction during orogenesis: measurement technique and application to the Alps. Terra Nova, V. 7, 500-508.

Bell, T.H., Ham, A.P. and Kim, H.S., 2004. Partitioning of deformation along an orogen and its effects on porphyroblast growth during orogenesis. Journal of Structural Geology, 26, 825-845.

Bell, T.H. and Hayward, N., 1991. Episodic metamorphic reactions during orogenesis; the control of deformation partitioning on reaction sites and reaction duration. Journal of Metamorphic Geology, 9, 619-640.

Bell, T.H. and Hickey, K.A., 1999. Complex microstructures preserved in rocks with a simple matrix; significance for deformation and metamorphic processes. Journal of Metamorphic Geology, 17, 521-535.
Bell, T.H., Hickey, K.A. and Upton, G.J.G., 1998. Distinguishing and correlating multiple phases of metamorphism across a multiply deformed region using the axes of spiral, staircase and sigmoidal inclusion trails in garnet. Journal of Metamorphic Geology, 16, 767-794.
Bell, T.H., Johnson, S.E., Davis, B., Forde, A., Hayward, N. and Witkins, C., 1992. Porphyroblast inclusion-trail orientation data; eppure non son girate! Journal of Metamorphic Geology, 10, 295-307.
Bell, T.H. and Kim, H.S., 2004. Preservation of Acadian deformation and metamorphism through intense Alleghanian shearing. Journal of Structural Geology, 26, 1591-1613.
Bell, T.H. and Rubenach, M.J., 1983. Sequential porphyroblast growth and crenulation cleavage development during progressive deformation. Tectonophysics, 92, 171-194.
Bell, T.H., Rubenach, M.J. and Fleming, P.D., 1986. Porphyroblast nucleation, growth and dissolution in regional metamorphic rocks as a function of deformation partitioning during foliation development. Journal of Metamorphic Geology, 4, 37-67.
Bell, T.H. and Welch, P.W., 2002. Prolonged Acadian orogenesis: revelations from foliation intersection axis (FIA) controlled monazite dating of foliations in porphyroblasts and matrix. American Journal of Science, 302, 549-581.
Cherniak, D.J., Watson, E.B., Grove, M. and Harrision, T.M., 2004. Pb diffusion in monazite: A combined RBS/SIMS study. Geochimica et Cosmochimica Acta, 68 (4), 829-840.
Cihan, M. and Parsons, A., 2005. The use of porphyroblasts to resolve the history of macro-scale structures: an example from the Robertson River Metamorphics, North-Eastern Australia. Journal of Structural Geology, 27, 1027-1045.
Cocherie, A. and Albarede, F., 2001. An improved U-Th-Pb age calculation for electron microprobe dating of monazite. Geochimica et Cosmochimica Acta, 65 (24), 4509-4522.
Cocherie, A., Legendre, O., Peucat, J.J. and Kouamelan, A.N., 1998. Geochronology of polygenetic monazites constrained by in situ electron microprobe Th-U-total lead determination: Implications for lead behaviour in monazite. Geochimica et Cosmochimica Acta, 62 (14), 2475-2497.
Crowley, J.L. and Ghent, E.D., 1999. An electron microprobe study of the U-Th-Pb systematics of metamorphosed monazite: the role of Pb diffusion versus overgrowth and recrystallization. Chemical Geology, 157, 285-302.
DeWolf, C.P., Ziessler, C.J., Halliday, A.N., Mezger, K. and Essene, E.J., 1996. The role of inclusions in U-Pb and Sm-Nd garnet geochronology: Stepwise dissolution experiments and trace uranium mapping by fission track analysis. Geochimica et Cosmochimica Acta, 60, 121-134.
Ewing, R.C. and Haaker, R.F., 1980. The metamict state: Implications for radiation damage in crystalline waste forms. Nuclear and Chemical Waste Management, 1, 51-57.
Ikeda, T., Shimobayashi, N., Wallis, S.R. and Tsuchiyama, A., 2002. Crystallographic orientation, chemical composition and three dimensional geometry pf sigmoidal garnet: evidence for rotation. Journal of Structural Geology, 24, 1633-1646.

Jercinovic, M.J. and Williams, M.L., 2005. Analytical perils (and progress) in electron microprobe trace element analysis applied to geochronology: Background acquisition, interferences, and beam irradiation effects. American Mineralogist, 990, 526-546.

Meldrum, A., Boatner, L.A. and Ewing, R.C., 1997. Displacive radiation effects in the monazite- and zircon-structure orthophosphates. Physical Review B, 56, 13805-13814.

Montel, J.-M., Foret, S., Veschambre, M., C, N. and Provost, A., 1996. Electron microprobe dating of monazite. Chemical Geology, 131, 37-53.

Parrish, R.R., 1990. U-Pb dating of monazite and its application to geological problems. Canadian Journal of Earth Science, 27, 1431-1450.

Passchier, C.W., Trouw, R.A.J., Zwart, H.J. and Vissers, R.L.M., 1992. Porphyroblast rotation: eppur si muove? Journal of Metamorphic Geology, 10, 283-294.

Prince, C.I., Kosler, J., Vance, D. and Gunther, D., 2000. Comparison of laser ablation ICP-MS and isotope dilution REE analyses - implications for Sm–Nd garnet geochronology. Chemical Geology, 168, 255-274.

Pyle, J.M., Spear, F.S., Wark, D.A., Daniel, C.G. and Storm, L.C., 2005. Contributions to the precision and accuracy of chemical ages of monazite. American Mineralogist, 90, 547-577.

Rhede, D., Wendt, I. and Förster.H.-J., 1996. A three-dimensional method for calculating independent chemical U/Pb- and Th/Pb-ages of accessory minerals. Chemical Geology, 130, 247-253.

Schulz, B., 1990. Prograde-retrograde P-T-t-deformation path of Austroalpine micaschists during Variscan continental collision (Eastern Alps). Journal of Metamorphic Geology, 8, 629-643.

Seydoux-Guillaume, A.-M., Paquette, J.-L., Wiedenbeck, M., Montel, J.-M. and Heinrich, W., 2002. Experimental resetting of the U-Th-Pb systems in monazite. Chemical Geology, 191, 165-181.

Stallard, A.R. and Hickey, K.A., 2001. Shear zone vs folding origin for spiral inclusion trails in the Canton Schist. Journal of Structural Geology, 23 (12), 1845-1864.

Stallard, A.R., Hickey, K.A. and Upton, G.J., 2003. Measurement and correlation of microstructures: the case of foliation intersection axes. Journal of Metamorphic Geology, 21 (3), 241-252.

Suzuki, K. and Adachi, M., 1991. Precambrian provenance and Silurian metamorphism of the Tsubonosawa paragneiss in the South Kitakami terrane, Northeast Japan, revealed by the chemical Th-U-total Pb isochron ages of monazite, zircon and xenotime. Geochemical Journal, 25, 357-376.

Vance, D., Meier, M. and Oberli, F., 1998. The influence of high U-Th inclusions on the U-Th-Pb systematics of almandine-pyrope garnet: results of a combined bulk dissolution, stepwise-leaching, and SEM study. Geochimica et Cosmochimica Acta, 62, 3527-3540.

Williams, M.L., 1994. Sigmoidal inclusion trails, punctuated fabric development and interactions between metamorphism and deformation. Journal of Metamorphic Geology, 12, 1-21.

Williams, M.L. and Jercinovic, M.J., 2002. Microprobe monazite geochronology: putting absolute time into microstructural analysis. Journal of Structural Geology, 24, 1013-1028.

Williams, M.L., Jercinovic, M.J. and Terry, M.P., 1999. Age mapping and dating of monazite on the electron microprobe: Deconvoluting multistage tectonic histories. Geology, 27 (11), 1023-1026.
Williams, P.F. and Jiang, D., 1999. Rotating garnets. Journal of Metamorphic Geology, 17, 367-378.

CHAPTER 1

PRECISION ESTIMATION IN ELECTRON MICROPROBE MONAZITE DATING: REPEATED MEASUREMENTS VERSUS STATISTICAL (POISSON) BASED CALCULATIONS

Abstract

Quoted errors on electron microprobe monazite ages may not reflect true errors arising from natural variation in the data, and potentially lead to incorrect or misleading geological interpretations. The precision of single-spot analyses, where ages are calculated from the Pb, U and Th concentrations from a single analysis and then combined with others to generate an average age, are most significant in this regard. A comparison between the classical method based on a description of the variability of multiple measurements and a more electron microprobe specific method using Poisson (counting) statistics shows that the results from each will generally be different. Sixty analyses from a compositionally homogenous monazite grain were used as a data set to enable the two methods to be compared, and the results show that Poisson statistics underestimates the real precision of electron microprobe analyses. More accurate estimates of the true precision are achievable using confidence intervals derived from standard errors of the mean, as long as homogenous grains and/or domains are analysed.

1. Introduction

With many different laboratories around the world attempting to analyse monazite for geochronological purposes on the electron microprobe (EMP), many different approaches have appeared (e.g., Suzuki and Adachi, 1991; 1994; Montel et al., 1996; Rhede et al., 1996; Cocherie et al., 1998; Crowley and Ghent, 1999; Williams et al., 1999; Scherrer et al., 2000). Two different ways to calculate an age have been developed; an isochron-type method (Suzuki and Adachi, 1991; 1994; Rhede et al., 1996; Cocherie et al., 1998; Cocherie and Albarede, 2001; Crowley and Ghent, 1999) and a single-point/average method (Montel et al., 1996). Unlike the isochron methods, the single-point technique does not require variations between the U/Pb and Th/Pb ratios within the monazite, and therefore a unique age (τ) can be calculated from the concentrations of Pb, U, and Th by iteratively solving the equation:

$$\begin{aligned} Pb = & \frac{Th}{232}\left[\exp\left(\lambda^{232}\tau\right)-1\right]208+\frac{U}{238.04}0.9928\times\left[\exp\left(\lambda^{238}\tau\right)-1\right]206 \\ & +\frac{U}{238.04}0.0072\times\left[\exp\left(\lambda^{235}\tau\right)-1\right]207 \end{aligned} \qquad (1)$$

where Pb, U, Th are concentrations in ppm, and λ^{232}, λ^{235}, λ^{238} are the radioactive decay constants of ^{232}Th, ^{235}U and ^{238}U respectively. Multiple age analyses are then averaged within a distinct compositional (or age) domain.

Regardless of the method used to date monazite, there will be both quantifiable and non-quantifiable sources that will contribute to an error on the age (e.g., Pyle et al., 2005). Identifying these sources is the first step to reducing error, and this is the only course of action where the contribution of an uncertainty is unknown. Since the accuracy of EMP monazite ages can only be estimated (usually by comparing to previously dated material), the precision or repeatability of the measurements is the only uncertainty that can be placed on an age. In previous studies, single-point/domain age (precision) errors have been calculated in two different ways. The first method (e.g., Williams and Jercinovic, 2002) uses multiple measurements from a "compositional domain" (that is assumed to be homogenous), and the error is representative of the variability of the accumulated measurements. The other (more complicated) technique uses statistical equations, calculated based on the theory of EMP analysis to describe the precision (e.g., Montel et al., 1996). Both of these methods have flaws which will be examined, and both methods have been incorrectly used. Thorough evaluations and guidelines of how to use the techniques are given below.

The technical aspect of obtaining ages from monazite will not be assessed, nor will the methods for increasing precision or accuracy be discussed. However, the variability that exists within the data and the way in which uncertainties can be calculated that reflect the true nature of EMP dating will be considered in detail. The data used in this study was obtained from EMP analysis of a portion of the well-characterised Manangotry monazite from SE Madagascar (Foster et al., 2002; Oelkers and Poitrasson, 2002; Horstwood et al., 2003).

2. Precision in monazite dating

2.1. Repeated measurements on a "compositional domain"

In most cases the precision of any experiment can be determined by taking repeated measurements (RM); however EMP analysis of monazite has some inherent complications. Long count times (several minutes) are required for monazite analysis (e.g., Montel et al., 1996; Cocherie et al., 1998; Williams and Jercinovic, 2002), and repeated/extended measurements on a spot can lead to damage to both the conductive coating (Jercinovic and Williams, 2005) and the surface of the monazite (Pyle et al., 2005), effectively invalidating subsequent analyses. As a consequence, homogeneous (compositional) domains have to be identified by single element mapping (Williams et al., 1999) and/or backscattered electron (BSE) imaging (Scherrer et al., 2000). By taking multiple analyses from within a single domain, the resultant ages can be combined and the average considered as being representative of the true age of that domain. The precision of the age will be related to the variability in individual age measurements.

Previous studies (Bell and Welch, 2002; Williams and Jercinovic, 2002) have used the standard error of the mean (the standard deviation of the mean age divided by the square root of the number of measurements) to describe the precision of the age. This however makes the assumption that the age is completely independent from the Pb, U and Th concentrations (and their associated uncertainties), which is not actually the case (see below). In essence, the authors in these studies are assuming that the errors in reproducibility are random and as long as the EMP is "sampling" from a homogenous, normally distributed (Gaussian) age domain, the variability of multiple measurements of the mean is an estimate of the precision of the age. This assumption will be tested below.

Although this method has merit, it can easily be unintentionally misused, particularly where the degree of homogeneity is uncertain. It is also important to note that the precisions calculated this way should be quoted as confidence intervals for the mean (C.I.) rather than just standard errors (S.E.) of the mean, in order for the reliability of quoted ages to be more explicitly conveyed. When the sample size is small (generally n<30), the use of the Student's t distribution is required to compute the confidence interval (Snedecor and Cochran, 1989). Therefore, to obtain a confidence interval for the population mean (in this case the true chemical age), a value of t should be multiplied by the standard error. For a 95% confidence interval, with infinite degrees of freedom the t-value is 1.96 (equivalent to the normal (Z) score for this C.I.), but becomes progressively larger as the degrees of freedom (sample size) are reduced. For larger sample sets, the Z-score should be used. Therefore, the age errors in both Bell and Welch (2002) and Williams and Jercinovic (2002), could be at least double those published, which would have significant implications for the geological interpretations presented in those studies.

2.2. Poisson statistics in electron microprobe analysis

An alternate method for determining the precision of a monazite age is to consider what controls the scatter of results that is inherent in the x-ray measurement process. The number of x-rays that are produced (from a given sample) and which interact with the EMP detectors are random in time, but have a fixed mean value (Goldstein et al., 1992). Ancey et al. (1977) showed that Poisson (counting) statistics (PS) can be used to describe the precision of an analysis, assuming that systematic errors are negligible. A thorough discussion on EMP precision in monazite analysis is given in Pyle et al. (2005). Only an overview of the relevant statistics is given here.

According to Poisson statistics, if N is the number of pulses counted by the detector, the variance (σ^2) is N and the standard deviation (σ) is given by $N^{1/2}$ (Scott et al., 1995). By combining count rates on both the peak (P) and background (B), the standard deviation of the net peak count rate ($\sigma_{P\text{-}B}$) becomes:

$$\sigma_{P\text{-}B} = \sqrt{\frac{N_P}{t_P^2} + \frac{N_B}{t_B^2}} \tag{2}$$

where t is time in seconds. The relative standard deviation ($\varepsilon_{P\text{-}B}$) is therefore calculated as:

$$\varepsilon_{P\text{-}B} = \sqrt{\frac{N_P}{t_P^2} + \frac{N_B}{t_B^2}} \Bigg/ \left(\frac{N_P}{t_P} - \frac{N_B}{t_B} \right) \tag{3}$$

The standard deviation of the k-ratio[1] can then be calculated by combining the relative standard deviation for both the standard and the unknown (Pyle et al., 2005) using basic error propagation techniques (assuming all covariance terms equal zero), such that:

$$\varepsilon_{P-B,\,k-ratio} = \sqrt{\varepsilon^2_{P-B,\,std} + \varepsilon^2_{P-B,\,unk}} \tag{4}$$

Assuming that no other factors affect the precision throughout the analysis (see Other Considerations below), this statistic can be used as an estimate of the error of the concentration for the unknown being measured.

When using this approach, the uncertainties on Pb, U and Th need to be propagated through Eq. (1). However, the general formula for propagation of error (e.g., Bevington, 1969) cannot be directly applied as it is a transcendental equation that cannot be solved with respect to age (τ). Previous studies that appear to use the Poisson statistics approach (Montel et al., 1996; Crowley and Ghent, 1999; Goncalves et al., 2004) are not clear as to exactly how an age error is generated. In this study a Monte

[1] The k-ratio of an element is the measured intensity on the unknown (I_{unk}), divided by the measured intensity of the standard (I_{std}). This value is proportional to the concentration (C) of the element being measured i.e. k-ratio = I_{unk}/Istd α C.

Carlo approach is used to propagate concentration errors through equation (1) and is explained in detail below.

2.3. Other considerations

In both techniques, two potential sources of uncertainty are commonly overlooked. The first relates to the errors associated with interfering x-ray peaks, a technical difficulty inherent to monazite analysis (Scherrer et al., 2000; Pyle et al., 2002). Recently however, the actual contribution of these has been quantified and shown to be negligible in most cases (Pyle et al., 2005). Therefore the (relative) k-ratio error above can generally be assumed to be representative of the concentration error (in the PS approach) and the error correction will be ignored for now in both approaches.

The second source of uncertainty that is commonly neglected is that associated with the matrix composition and ZAF/PAP/phi-rho-Z corrections. Variations in the matrix composition will influence the matrix-corrected Pb, U and Th concentration values and thus the precision of the matrix element measurements should be accounted for. An example of a method for quantifying the contribution of the matrix correction error with respect to an age is briefly outlined in Montel et al. (1996), with another in (Pyle et al., 2005). In the latter study, calculated ages varied by only ± 1 Ma when individual elements were increased by approximately two standard deviations relative to an average pelitic monazite composition (for a 2000 ppm Pb monazite). Similar results have been found using analyses of the monazite below. For simplicity, no attempt has been made to include this in the error calculations presented below.

2.4. Comparing the different methods

Although the two methods of estimating the precision of EMP ages are fundamentally different, and cannot (directly) be statistically compared to each other, it is still an important exercise to use a large, internally consistent data set to illustrate the difference in the final result. It is arguable that the error calculated by taking multiple analyses on a truly age-homogenous sample/domain will (essentially) always be larger than that calculated via the PS approach, as the RM method will absorb additional systematic errors (e.g. spectrometer drift, uncertainty in standard composition, sample damage, pulse shift etc) that cannot be accounted or corrected for (at this stage) when using counting statistics (e.g., Goldstein et al., 1992). Note that these systematic errors should (and usually are) minimised in any EMP dating protocol, but can still be statistically significant, particularly for large data sets. In very rare circumstances, the cancelling effect of multiple compensatory systematic errors may result in the error generated by repeated measurements being smaller than that from Poisson statistics. The possibility of this phenomenon is expected to become rarer with increasing sample size, as the effect of systematic errors will tend to become more pronounced. As a general rule, samples with errors that fall into this category should be re-analysed, if possible to prevent misleading results. Some idea of the effect of systematic errors in the experimental data can be gained by repeating the exercise with a theoretical data set and comparing the results. Details of the methods are presented below.

3. Methods

3.1. Analytical conditions for monazite data

A single, homogenous fragment of a 1 cm Manangotry monazite crystal was analysed 60 times using the JEOL JXA-8200 electron probe microanalyser at the Advanced Analytical Centre (AAC) at James Cook University. The assumption of compositional (thus age) homogeneity was based on BSE images of the fragment and numerous (>50) previous analyses over a 12 month period. A beam diameter of 5 μm was used with a 15 kV accelerating voltage and 200 nA sample current. A "full composition" analysis was used, in which all elements thought to be present in monazite were analysed during the routine. The standards were analysed five times prior to the measurement of the monazite at 15kV, 20nA, 5 μm beam diameter, and the average value was used for each element. Interference corrections of Th and Y on Pb Mα and Th on U Mβ were applied as in Scherrer et al. (2000) and Pyle et al. (2002). Both the YPO_4 and ThO_2 standards were analysed three times at monazite analytical conditions and correction factors were calculated from the averages. The X-ray lines for the REEs were chosen to avoid and/or minimise any interfering peaks (e.g., Pyle et al., 2002). Automated peak searches were conducted every six analyses for the majority of elements (excluding Pb and U), in an attempt to correct for any spectrometer drift/peak shift. The Armstrong-CITZAF (phi-rho-Z) matrix correction program (Armstrong, 1988; Armstrong, 1991) was used. Since both the sample and standards were carbon coated, the absorbed current was recorded over time (for several analyses) to determine whether coat damage/beam effects could be identified (e.g., Jercinovic and Williams, 2005). Full analytical details can be found in Table 1.

3.2. Monte Carlo simulation

Monte Carlo (MC) simulation is a method that can be used to propagate uncertainties through complex functions such as equation (1). In essence, the method is based on repeated calculation of a result, using randomly generated data as inputs (e.g., Anderson, 1976). If the random input data is constrained by uncertainties, the accumulated results will produce an uncertainty distribution for the function being investigated. In this example, normally distributed (pseudo) random concentration values, constrained by their calculated errors/uncertainties (1σ), were generated. The "Mersenne Twister", mt19937 (Matsumoto and Nishimura, 1998) pseudo-random number generator (implemented in the NtRand add-in for Microsoft Excel) was used to produce the numbers. All analytical errors were calculated based on the statistical equations outlined above. 10000 sets of Pb, U and Th pseudo-random concentration values were used for each analysis, and an age was calculated from equation (1) for each set. The accumulated results were assumed to represent the result of 10000 repeated measurements of Pb, U and Th concentrations, at the same location on the monazite. Since the results are normally distributed, the 95% confidence interval for the mean (i.e. the individual age) is calculated by multiplying the standard deviation by 1.96. Further details of the procedure can be found in Appendix A.

4. Results and Discussion

4.1. Measured concentrations, ages and errors

The results of the 60 analyses, with (interference-corrected) Pb, U and Th concentrations, ages, progressive standard errors (of the mean) and progressive 95% confidence intervals calculated for each point are given in Table 2. Using the RM method, the average age for the total is 545.7 Ma, with a standard error of 1.48 m.y., and a 95% confidence interval on the age of ± 2.97 m.y[2]. This is ca. 10 million years below the isotopic age of 555 ± 1 Ma determined for this monazite (Horstwood et al., 2003). Under normal circumstances, the Student's-t value might not be considered neccesary to calculate confidence intervals when n > 30, but for continuity across all the analyses, it is used in this exercise. The same analyses, with concentration errors calculated as above, and the results of the MC error propagation technique are shown in Table 3. Combining the independently calculated errors for the MC technique by a weighted average procedure (e.g., Bevington, 1969), gave a final error for the 60 analyses of 1.74 m.y. (95% C.I.). A MSWD for this age of 2.8 was calculated using Isoplot v3.1 (Ludwig, 2003). Full analytical results can be found in Appendix B.

Insights into the additional error from the matrix correction were obtained by calculating the ages based upon the maximum and minimum cumulative 2σ counting statistical variation in matrix elements for the first analysis presented herein (Table 4). The 2σ precision errors of these elements were obtained using the counting statistics

[2] It is common practise to quote ages and errors in EMP chemical ages rounded up to the nearest whole number, but due to the magnitude of the error values being compared, decimal places have been used here.

equations above. The 2σ maximum and minimum concentrations were then input into the matrix correction, corresponding Pb + U + Th concentrations were obtained and these were input into the age equation. From these values it was ascertained that the maximum, additional 2σ precision error related to the matrix correction be around 1-2 million years for each analysis on the Manangotry grain. For accumulated results, such as those presented in this study, this value should become negligible.

Systematic increases or decreases in the data were investigated by linear regressions to the concentration data. For the purpose of this study, differences were considered significant if they were greater than the average 2σ k-ratio (concentration) error for each element. Based upon these guidelines, no significant spectrometer drift was identified on Pb or U (Fig. 1a, b), but an increase in count-rate (and hence concentration) was noticed on Th (Fig. 1c). As a result, the linear trend of calculated age decreases by about 2.4% over the duration of the exercise (Fig. 1d), probably accounting for a significant portion of the underestimation of the "true" age. The reason for the increase in Th concentration with increasing analytical number is uncertain, particularly since the spectrometer recording Th counts automatically conducted a peak search every 6 analyses (hence any spectrometer drift should have been corrected for). A possible compositional change in the monazite itself cannot be ruled out as the grid pattern of the analyses potentially supports an increase in Th concentration across the grain, where a combination of REEs could be substituting for Th (Spear and Pyle, 2002). The only REE that significantly decreased over time was Gd (nearly 25% or 0.1 wt % of total), so this could be one of the substituting cations. However, if the changes in measured Th, Gd and also Nd (~ 6%) are monazite composition related, they do not correspond with any known exchange vectors. Numerous previous analyses have given no insight into this phenomenon, thus the causes for the systematic increases/decreases remain uncertain, but are most likely related to technical issues such as spectrometer drift, sample damage etc. This may also have become more significant as a result of the large number of analyses performed on the same grain during this experiment. The results of fitting linear trends to the elemental concentration data over the 60 analyses is shown in Table 5.

Recordings of the absorbed current over time were taken for several analyses to determine whether the carbon coat was damaged by continuous electron beam exposure during the (approximately) 6 minute analytical period (thus creating additional error). Fig. 2 shows a representative plot of absorbed current over time for one of the analyses, as the results of all recordings showed similar trends. The plot shows that the absorbed current varied by less than 0.5 nA over the course of the analysis, indicating that the carbon coat was sufficient for the analytical conditions used and was not being significantly damaged. This appears to be similar to the findings in Jercinovic and Williams (2005), where different beam conditions and durations were tested, although according to those results, a decrease in absorbed current may have been encountered if longer count times were used (see Jercinovic and Williams (2005) for more details).

Before the error values were compared, the assumption that the analyses were taken from a normally distributed age domain (required for the RM method to be statistically valid) was tested. A quantile-quantile (q-q) plot of the age data (Fig. 3) indicates the calculated ages have an approximately normal distribution. Additionally, using a Shapiro-Wilk Test for normality ($p = 0.52$), the hypothesis ($p > 0.05$) that the data comes from a normally distributed age population was upheld.

4.2. Comparing the error values

.

The weighted average error using the Poisson/Monte Carlo technique (1.74 m.y.) is approximately 40% less than the error calculated from the standard error of the means (2.97 m.y.). The progressive error values (for increasing numbers of analyses) is summarised in Fig. 4, which shows that the RM technique produces error values that are consistently greater than that of the PS/MC approach, after approximately 10 analyses. Although the Th concentration systematically increases during the exercise, most of the difference identified in Fig. 4 is evident before the Th increases noticeably (Fig. 1c), and thus is not the major factor in the difference between the two methods. Evidence that the PS/MC approach underestimates the precision of multiple EMP analyses can be seen in Fig. 5; which shows the distribution of the individual age measurements (with 95% C.I. error bars) around the (sample) mean. Assuming that the sample mean approximates the population mean, then if the age measurements are obtained by taking 60 random samples from a normal distribution, then all but 2 to 3 of the intervals should include the population mean (Siegel, 1988). This is clearly not the case. The calculated MSWD of 2.8 also indicates that the analytical errors are underestimated in this method (Ludwig, 2003). This illustrates that there is either substantial systematic error (a portion of which has already be identified above) that cannot be accounted for using PS, and/or there is a problem with the way in which the concentration errors are propagated through equation (1).

4.3. Assessment of the Monte Carlo technique

The use of normally distributed (pseudo) random concentration values in the Monte Carlo approach is rooted in the implicit assumption that generation of X-rays during EMP analysis occurs with a normal distribution. This was based on the fact the distribution of a large number of counts recorded by the detectors in an EMP analysis will be approximately normal (Goldstein et al., 1992). Although this need not necessarily be the case for accumulated concentration values, it has already been shown that the age distribution is approximately normal and thus one would expect the concentration values to be approximately normal as well. Quantile-quantile plots for the Pb and U concentrations (Fig. 6) support this (Th was excluded due to the systematic increase in the data outlined above), and thus this assumption is considered reasonable.

The MC technique was tested by generating simulated concentration data (again using normally distributed random numbers) and running the data though both methods to compare the results. The mean of the 60 experimental values for both the concentration and standard deviation (counting error) was used as the mean and standard deviation of the simulated data (Table 6). 400 concentration values were generated for Pb, U and Th, all with identical errors (for simplicity). The results (Fig. 7) show that the output of the MC technique should approximate that of the RM method, if the concentration errors reflect true analytical precision. It is therefore implied that the large difference in errors calculated by the two methods, using the experimental data above, is purely related to the fact that Poisson statistics is inadequate to calculate the true precision in measured concentration values.

Since the controlling factor in the MC output is the nature of the random numbers used, two other pseudo-random number generators (PRNG) besides the Mersenne Twister (mt19937) were tested with this data, namely "ran2" (Press et al., 1992) and the default PRNG in Excel 2002. Interestingly, the differences in age error output between mt19937 and ran2 algorithms was only around 1% (for 10000 iterations), but the difference between mt19937 and the default Excel PRNG was approximately 40%. Incidentally, this is similar to the difference noted between the PS/MC and RM methods above, but this is purely coincidental. The merits (and analyses of randomness) of the former PRNGs are discussed in their respective publications, but there is evidence that the Excel PNRG is inadequate for this exercise as it has failed several standard tests of randomness (Microsoft Knowledge Base, 2004). A new version was included in Excel 2003, but was not tested in this study. For the purpose of this exercise, the choice of the mt19937 algorithm over ran2 was probably trivial, particularly as they are both included in the NtRand add-in (and therefore easily implemented). However, since ran2 has a shorter period length than mt19937 (2×10^{18} vs 2^{19937}-1) and shows a correlation bias, based on a one-dimension random walk test (Proykova, 2000), the mt19937 algorithm was preferred.

4.4. Potential uses of Poisson statistics

Poisson statistics is still useful in the chemical dating of monazite. As it is the largest controlling factor in the precision of EMP analyses, it can be used as a benchmark to estimate the magnitude of additional non-quantifiable sources of error. Comparisons between concentration errors calculated via both PS and RM can help identify which elements in the protocol have large additional errors, such that they may be reduced (e.g., Jercinovic and Williams, 2005; Pyle et al., 2005). The most important element to consider in this case is Pb, since its concentration is highly correlated to calculated age. Consequently, reducing Pb error is critical in reducing age error (e.g. Fig. 8).

Both concentration and age errors derived via PS can also be useful for identifying compositional/age domains at a far greater resolution than either BSE images and/or chemical (or age) maps. Although images provide the framework for deciding where quantitative analyses are performed, the (estimated) errors can be used to cluster points into more accurately constrained domains. Owing to the results above, a guideline for differentiating domains could be based on the 3σ level of significance, where a domain would be considered significantly different if the 3σ concentration errors of either the calculated ages or individual element concentrations do not overlap those from previous analyses. However, this would need to be assessed on a case-by-case basis and individuals would need to make decisions based on their own results. In certain cases, this procedure may potentially save the need to run time consuming elemental maps prior to EMP dating.

5. Conclusions

Since the precision of EMP monazite ages cannot be adequately estimated using a combined Poisson statistics and Monte Carlo simulation approach, there is no other option at this stage than to calculate an error from repeated measurements on a homogenous domain. Therefore, some doubt exists on the validity of interpretations in previous studies that have used this procedure (e.g., Montel et al., 1996; 2000; Crowley and Ghent, 1999; Goncalves et al., 2004) and also studies that estimate and/or calculate Poisson-derived concentration uncertainties for isochron methods (e.g., Cocherie et al., 1998; Cocherie and Albarede, 2001). The use of Poisson statistics may aid in identifying systematic error that, by its nature cannot be accounted for, and if additional errors are found to be small or negligible in a particular EMP dating protocol, the use of the Monte Carlo propagation technique presented here may give insights into expected age deviations and/or domains. Future work in attempting to quantify and/or reduce these additional errors will advance the field greatly.

6. References

Ancey, M., Bastenaire, F. and Tixier, R., 1977. The statistical control and optimization of x-ray intensity measurements. Journal of Physics D: Applied Physics, 10, 817-830.

Anderson, G.M., 1976. Error propagation by the Monte Carlo method in geochemical calculations. Geochimica et Cosmochimica Acta, 40, 1533-1538.

Armstrong, J.T., 1988. Quantitative analysis of silicate and oxide materials: Comparison of Monte Carlo, ZAF and Φ (ρz) procedures. In: D.E. Newbury (Editor), Microbeam Analysis. San Francisco Press.

Armstrong, J.T., 1991. Quantitative elemental analysis of individual microparticles with electron beam instruments. In: K.F.J. Heinrich and D.E. Newbury (Editors), Electron Probe Quantitation. Plenum Press.

Bell, T.H. and Welch, P.W., 2002. Prolonged Acadian orogenesis: revelations from foliation intersection axis (FIA) controlled monazite dating of foliations in porphyroblasts and matrix. American Journal of Science, 302, 549-581.

Bevington, P.R., 1969. Data Reduction and Error Analysis for the Physical Sciences. McGraw-Hill, New York.

Cocherie, A. and Albarede, F., 2001. An improved U-Th-Pb age calculation for electron microprobe dating of monazite. Geochimica et Cosmochimica Acta, 65 (24), 4509-4522.

Cocherie, A., Legendre, O., Peucat, J.J. and Kouamelan, A.N., 1998. Geochronology of polygenetic monazites constrained by in situ electron microprobe Th-U-total lead determination: Implications for lead behaviour in monazite. Geochimica et Cosmochimica Acta, 62 (14), 2475-2497.

Crowley, J.L. and Ghent, E.D., 1999. An electron microprobe study of the U-Th-Pb systematics of metamorphosed monazite: the role of Pb diffusion versus overgrowth and recrystallization. Chemical Geology, 157, 285-302.

Foster, G., Gibson, H.D., Parrish, R.R., Horstwood, M., Fraser, J. and Tindle, A., 2002. Textural, chemical and isotopic insights into the nature and behaviour of metamorphic monazite. Chemical Geology, 191, 183-207.

Goldstein, J.I., Newbury, D.E., Echlin, P., Joy, D.C., Romig, A.D., Lyman, C.E., Fiori, C. and Lifshin, E., 1992. Scanning Electron Microscopy and X-ray Microanalysis 2nd Ed. Plenum Press, New York.

Goncalves, P., Nicollet, C. and Montel, J.-M., 2004. Petrology and in situ U-Th-Pb monazite geochronology of ultrahigh-temperature metamorphism from the Andriamena mafic unit, north-central Madagascar. Significance of a petrographical P-T path in a polymetamorphic context. Journal of Petrology, 45 (10), 1923-1957.

Horstwood, M.S.A., Foster, G.L., Parrish, R.R., Noble, S.R. and Nowell, G.M., 2003. Common-Pb corrected in situ U-Pb accessory mineral geochronology by LA-MC-ICP-MS. Journal of Atomic Spectrometry, 18, 837-846.

Jercinovic, M.J. and Williams, M.L., 2005. Analytical perils (and progress) in electron microprobe trace element analysis applied to geochronology: Background acquisition, interferences, and beam irradiation effects. American Mineralogist, 990, 526-546.

Ludwig, K.R., 2003. User's manual for Isoplot 3.0; a geochronological toolkit for Microsoft Excel, Berkeley Geochronology Centre, Special Publication No. 4.

Matsumoto, M. and Nishimura, T., 1998. Mersenne Twister: A 623-dimensionally equidistributed uniform pseudorandom number generator. ACM Transactions on Modelling and Computer Simulations: Special Issue on Uniform Random Number Generation, 8, 3-30.

Montel, J.-M., Foret, S., Veschambre, M., C, N. and Provost, A., 1996. Electron microprobe dating of monazite. Chemical Geology, 131, 37-53.

Montel, J.-M., Kornprobst, J. and Vielzeuf, D., 2000. Preservation of old U-Th-Pb ages in shielded monazite: example from the Beni Bousera Hercynian kinzigites (Morocco). Journal of Metamorphic Geology, 18, 335-342.

Oelkers, E.H. and Poitrasson, F., 2002. An experimental study of the dissolution stoichiometry and rates of a natural monazite as a function of temperature from 50 to 230 °C and pH from1.5 to 10. Chemical Geology, 191, 73-87.

Press, W.H., Teukolsky, S.A., Vetterling, W.T. and Flannery, B.P., 1992. Numerical Recipes in C: The Art of Scientific Computing, Second Edition. Cambridge University Press.

Proykova, A., 2000. How to improve a random number generator. Computer Physics Communications, 124, 125-131.

Pyle, J.M., Spear, F.S. and Wark, D.A., 2002. Electron Microprobe Analysis of REE in Apatite, Monazite and Xenotime: Protocols and Pitfalls. Reviews in Mineralogy and Geochemistry, 48, 337-362.

Pyle, J.M., Spear, F.S., Wark, D.A., Daniel, C.G. and Storm, L.C., 2005. Contributions to the precision and accuracy of chemical ages of monazite. American Mineralogist, 90, 547-577.
Rhede, D., Wendt, I. and Förster.H.-J., 1996. A three-dimensional method for calculating independent chemical U/Pb- and Th/Pb-ages of accessory minerals. Chemical Geology, 130, 247-253.
Scherrer, N.C., Engi, M., Gnos, E., Jakob, V. and Liechti, A., 2000. Monazite analysis; from sample preparation to microprobe age dating and REE quantification. Schweizerische Mineralogische und Petrographische Mitteilungen, 80 (1), 93-105.
Scott, V.D., Love, G. and Reed, S.J.B., 1995. Quantitative Electron-Probe Microanalysis (2nd edition). Ellis Horwood Ltd, Chichester.
Siegel, A.F., 1988. Statistics and Data Analysis. John Wiley & Sons, New York.
Snedecor, G.W. and Cochran, W.G., 1989. Statistical Methods, Eighth Edition. Iowa State University Press.
Spear, F.S. and Pyle, J.M., 2002. Apatite, Monazite, and Xenotime in Metamorphic Rocks. Reviews in Mineralogy and Geochemistry, 48, 293-335.
Suzuki, K. and Adachi, M., 1991. Precambrian provenance and Silurian metamorphism of the Tsubonosawa paragneiss in the South Kitakami terrane, Northeast Japan, revealed by the chemical Th-U-total Pb isochron ages of monazite, zircon and xenotime. Geochemical Journal, 25, 357-376.
Suzuki, K. and Adachi, M., 1994. Middle Precambrian detrital monazite and zircon from the Hida gneiss on Oki-Dogo Island, Japan: their origin and implications for the correlation of basement gneiss of Southwest Japan and Korea. Tectonophysics, 235, 277-292.
Williams, M.L. and Jercinovic, M.J., 2002. Microprobe monazite geochronology: putting absolute time into microstructural analysis. Journal of Structural Geology, 24, 1013-1028.
Williams, M.L., Jercinovic, M.J. and Terry, M.P., 1999. Age mapping and dating of monazite on the electron microprobe: Deconvoluting multistage tectonic histories. Geology, 27 (11), 1023-1026.

CHAPTER 2

OVERPRINTING ACADIAN AMPHIBOLITE-GRADE OROGENESIS IN THE TACONIC APPALACHIAN BLUE RIDGE: NEW AGES AND APPROACHES USING MONAZITE

Abstract

No adequate guidelines exist for handling compositionally heterogeneous EPMA monazite data. Fine-scale compositional domains within metamorphic monazite grains may be representative of different growth events, but can also reflect subtle changes associated with cation availability during continuous growth. The precision of EPMA monazite ages is mostly a function of composition and can be approximated by a normal (Gaussian) distribution. Combining data from different chemical zones within a single grain generally contravenes assumptions of normality, but comparisons with a non-parametric (bootstrap) method, show that this is not significant enough to affect results. This is illustrated using data from the Murphy Syncline in the North Carolina Appalachians. Microstructurally controlled dating of monazite grains in these samples indicates an initial staurolite-kyanite-grade (Taconian) event (ca. 450 Ma), was locally overprinted by staurolite-grade metamorphism, some 50 million years later during the Acadian. However, the latter event is not preserved throughout the region. The actual distribution of metamorphism appears to be controlled by Acadian deformation being preferentially partitioned through either one or both limb(s) of the syncline, leaving the hinge zone preserving exclusively Taconic textures.

1. Introduction

Monazite is widely used to date igneous, metamorphic and hydrothermal events. Dating techniques that constrain the ages of metamorphism and/or deformation with in-situ grains are advantageous because direct chronological links can be made with specific reactions, textures, or microstructures. Since its introduction (Suzuki et al., 1991), numerous studies (e.g., Montel et al., 1996; Rhede et al., 1996; Cocherie et al., 1998; Crowley and Ghent, 1999; Williams et al., 1999; Pyle et al., 2005 and other references herein), involving the chemical dating of monazite on the electron probe microanalyser (EPMA) has established the method as a viable technique. The advantages of using the EPMA include the small spatial resolution (down to 1 μm), minimal sample damage and associated compositional data for each spot analysed. Some disadvantages include high detection limits (which generally preclude dating monazites younger than approximately 50 Ma), large errors in precision, and the inability to assess potential discordancy between ^{238}U-^{206}Pb and ^{235}U-^{207}Pb ages (although statistical methods can be used to detect discordancy between U-age and Th-age, if it exists (e.g., Suzuki and Adachi, 1991; Rhede et al., 1996; Cocherie et al., 1998; Cocherie and Albarede, 2001)). Used within its limits, monazite dating on the EPMA can play an important role in reconstructing the timing of events in complex petrogenetic sequences.

With any in-situ method, it is important to understand the reactions and/or processes that lead to the formation of the mineral being dated (Foster et al., 2000; Foster et al., 2002; Catlos et al., 2002; Pyle et al., 2001; Pyle and Spear, 2003). Monazite is known to be involved in reactions with other REE-accessory phases such as allanite, apatite, epidote, and titanite (e.g., Catlos et al., 2002), but also major phases such as garnet (Pyle et al., 2001). Linking monazite to such reactions increases the power of the chronometer immensely as ages can then be put into a pressure-temperature (P-T) context. The behaviour of monazite during foliation development and/or shearing is also important as monazite can recrystallise during deformation, resetting its Th-U-Pb systematics (Ayers et al., 1999) and allowing periods of active deformation to be dated (Shaw et al., 2001; Bell and Welch, 2002; Williams and Jercinovic, 2002). Regardless of the in-situ dating method used, a combined chemical analysis microstructural/textural analysis is essential in fully interpreting metamorphic monazite ages.

This paper will focus on compositional and microstructural classification and EPMA ages of monazite from staurolite and kyanite grade metapelites from the Murphy Syncline in the southern Appalachians, USA. Particular attention will be given to the statistical treatment of the age data, including the assessment of a bootstrap method (Efron and Tibshirani, 1993) for dealing with non-parametric (e.g., mixed composition) age data. By carefully comparing both the chemistry and ages of monazites firstly within a single grain and then between grains in different textural/microstructural settings it is shown that, important insights into the P-T-D-t history of the southern Appalachians can be established.

2. Data handling/reduction background

The approach for EPMA data treatment/reduction used here is similar to that proposed in Williams et al. (2006). In essence, individual Th, U and Pb dates from distinct compositional domains are grouped together based on the assumption that they represent random samples from a distinct age population (in the case of EPMA data, a normal (Gaussian) population). With this method, each domain can be placed into its own unique context, unlike isochron techniques that require a fundamental (and significant) variation in Th-U-Pb in order for an age to be calculated (e.g., Suzuki and Adachi, 1991; Suzuki and Adachi, 1994; Rhede et al., 1996; Cocherie et al., 1998; Cocherie and Albarede, 2001). The other benefit of this technique is that analytical error can be assessed in a way that relies purely on the statistical variation between measurements rather than counting statistics alone (potentially accounting for uncertainties such as spectrometer drift, sample damage, pulse shift etc). This is critical considering the amount counting statistics can underestimate the real analytical precision during extended EPMA sessions (Chapter 1).

Domains may be representative of different reactions that produce or consume monazite, or hydrothermal or deformation events that result in the dissolution and precipitation of monazite (Williams et al., 2006). Two major types of compositional domain exist in monazite, the first associated with the incorporation of Th (and/or U), through either the brabantite (Th or U + Ca = 2REE) or huttonite (Th or U + Si = REE + P) exchanges, and the second related to Y substituting for REEs (Spear and Pyle, 2002). Due to counting statistics, compositional zones related to the concentrations of Th, U (and thus radiogenic Pb) define the overall precision of calculated ages (Pyle et al., 2005; Williams et al., 2006). Thus, if EPMA analyses are obtained from more than one of these domains, the resultant dataset will essentially be a mixture of samples from different populations. This can commonly occur, particularly when fine scale heterogeneities within monazite grains (e.g., igneous oscillatory zoning, exsolution lamellae, compositional variation associated with fractures, inclusions, partitioning of cations etc), combined with technical limitations (e.g., beam diameter) are taken into account.

The processes associated with compositional variation can occur over a short time period and/or over an interval that is unresolvable using the EPMA. If this is the case, multiple compositional domains may have equivalent mean ages. A combination of these is referred to as a "date domain" herein, and the mean date of these domains is more representative of the average age of monazite growth rather than the age of a distinct monazite growth event. Assuming data obtained from date domains is neither extremely non-normal or has very large outliers, parametric (classical) statistics are generally robust enough (e.g., Siegel, 1988) to estimate empirical distribution parameters for these "mixed" datasets. Therefore, as long as the timing of monazite growth within a date domain is insignificant (checked via plots or statistical tests), precision errors can be essentially calculated using the same approach as with compositional domains. This can be expanded further to datasets from heterogeneous monazite grains, where no compositional domains can be analysed. However, these scenarios may be more problematical as assessing the distribution of small, compositionally complex datasets is not feasible. The use of non parametric statistics avoids assumptions regarding the underlying distribution of the data and thus the application of these techniques is tested below.

3. Regional geology

The Murphy Syncline extends from south-west North Carolina into northern Georgia and nearby Tennessee (Fig. 1) and forms part of the western Blue Ridge of the Appalachian Orogeny (Hatcher, 1987b). The western Blue Ridge is separated from the Valley and Ridge to the northwest by the Great Smoky and Greenbrier Faults, and from the eastern Blue Ridge by the Hayesville Fault. The rocks in the study area (Fig. 2) are meta-sediments from the late PreCambrian to early Cambrian Murphy Belt and Great Smoky Groups (Mohr, 1973; Hatcher, 1987b; Wiener and Merschat, 1992). The Murphy Syncline is isoclinal, with a moderately south-east dipping axial plane, and has been interpreted to be a D_1 structure that formed either prior to or during regional metamorphism (Mohr, 1973). Metamorphic grade ranges from greenschist to amphibolite facies, with the lowest grades in the core of the syncline. Traditionally, the metamorphic peak in the western Blue Ridge was thought to have been reached during the Taconic Orogeny (ca. 450 Ma), with little, if any effect from the latter Acadian or Alleghanian events (e.g., Glover et al., 1983; Hatcher, 1987b; Rodgers, 1987). Evidence for Acadian metamorphism however is numerous and includes stratigraphic interpretations based on fossil assemblages (Unrug and Unrug, 1990; Unrug et al., 2000), a 412 ± 6 Ma U-Pb staurolite age (Brosky and Odom, 2002), and recent (ca. 400 Ma) EPMA/Ion microprobe monazite ages (Kohn and Malloy, 2004). Based on $^{40}Ar/^{39}Ar$ whole-rock/phyllite and U-Pb zircon techniques respectively, Connelly and Dallmeyer (1993) and Miller et al. (2000) have argued for a polymetamorphic history with both Taconic and Acadian (up to amphibolite grade) events recorded within the western Blue Ridge.

4. Sample selection and analytical procedures

4.1. Microstructural/textural classification

Four samples containing garnet and staurolite porphyroblasts from around the Murphy Syncline were used in this study. All were taken from formations within the Great Smoky Group, in particular the Grassy Branch (CH22), Copper Hill (CH27) and Ammons Formations (CH35, CH62). Garnet porphyroblasts generally contain sigmoidal inclusion trails that were either truncated by an inclusion-free rim or the matrix, whereas staurolite (and kyanite where present) frequently preserve crenulations, millipede structures or generally straight inclusion trails that are continuous with, but curved into the matrix foliation. Garnet porphyroblasts are commonly enclosed by larger staurolite and/or kyanite porphyroblasts. Several generations of overprinting crenulations were identified within the matrix.

Monazite is less prevalent or non existent as inclusions in garnet, compared to the other porphyroblastic phases, but is common throughout the matrix. Once monazite was located, the setting of each grain relative to preserved textures and microstructures (Table 1) was interpreted. Individual monazites were selected for analysis based on the following: (1) size and quality of polish of the grain, (2), representation of unique of microstructural/textural settings, and (3) confidence of monazite correlation to microstructural/textural setting. Overall, 18 monazite grains were analysed, 8 of which occur as inclusions in porphyroblasts.

4.2. EPMA analysis

Thin sections were polished with 1 micron diamond paste and carbon-coated to approx 250 Å. BSE images were obtained for all monazite grains prior to quantitative analysis to identify compositional domains and/or assess zoning profiles Analyses were conducted on the JEOL JXA-8200 Superprobe at James Cook University using a 3 μm beam diameter (unless otherwise specified), accelerating voltage of 15 kV and Faraday cup current of 200 nA.. The elements Si, P, Ca, Y, La, Ce, Pr, Nd, Sm, Gd, Dy, Pb, Th and U were measured in a single analysis, with extended count times on Pb, U and Th to optimise statistical precision for chemical age dating. Calibrations were performed on the standards at 15kV and 20nA. The interferences of ThMζ and YLγ on PbMα, and ThMγ on UMβ were corrected post-analysis, using correction factors obtained from analysing the Th and Y standards (e.g., Scherrer et al., 2000; Pyle et al., 2002). All other background positions avoid interfering peaks and were selected based on wavelength scans of 8 well-characterised monazite grains with Th concentrations ranging from 2 to 11 wt %. Two-point linear backgrounds were used as no curvature or abnormality above baseline was detected in the area between chosen background points. Collimators were opened to maximum (3 mm), PHA settings were optimized and the Armstrong-CITZAF (phi-rho-z) matrix correction program (Armstrong, 1988; Armstrong, 1991) was used. Full details of the setup are given in Table 2.

The precision of each element in each individual analysis was calculated based on counting statistics using the equations in Scott et al. (1995) and Pyle et al. (2005). In addition to the elemental standards, a fragment of 555 ± 1 Ma Manangotry monazite (Horstwood et al., 2003) was used as a "consistency age standard" and was routinely analysed prior to and after the unknown monazites. Results of these analyses are included with the results of the unknowns.

4.3. Age calculation and error propagation

BSE images, combined with quantitative elemental data were used to identify compositional domains in individual grains rather than elemental maps. In most cases BSE variation can be correlated with Th and/or Y zoning (e.g., Spear and Pyle, 2002). Multiple analyses were taken from within recognisable BSE domains, and once the quantitative data was available, individual points were re-allocated into different zones/domains if required. Within each domain, individual dates[3] were calculated by inserting the Th, U, Pb concentrations into the age equation of Montel et al. (1996). A mean date was calculated for each domain and 95% confidence intervals (CI) were generated by multiplying the standard error of the mean (SE) with the Student's-t value for (n-1) degrees of freedom (Siegel, 1988).

Where compositional domains could not be adequately separated, and/or individual data points sampled more than one domain, the Y, Th and U composition of all affected points were plotted with respect to their calculated dates (with associated 95% CI counting statistical errors obtained via Monte Carlo simulation (Chapter 1)) to assess the level of date-variation. If the individual dates correlated with a compositional change and/or the data looked bimodal or mixed, attempts were made to separate it into date-domains. This was only practical for larger datasets where trends could be reliably identified. For the purpose of this study, CIs for all data in this category were calculated using both parametric and nonparametric (bootstrap) methods. Datasets with less than 5 analyses were not used for age calculation.

[3] Based on the recommendation in Williams et al. (2006), the terminology "date" is used to describe individual numbers calculated via the age equation. This value may or may not have geological significance. "Age" is used when the result (date or combination of dates) is interpreted to have geological significance.

Once the mean and confidence intervals were calculated for all domains, data from different monazite grains and/or domains were grouped together (where possible) based on additional information such as chemical signature and/or textural setting. Where domains could be interpreted to be representative of a geologically significant event, the datasets were then combined via the weighted average procedure in Isoplot v3.10 (Ludwig, 2003).

4.4. Analytical concerns

A 3 µm beam diameter is considered to be the best compromise between spatial resolution and sample/C-coat damage with this setup. Numerous recordings during this study of absorbed current (nA) as a function of time (Fig. 3a), indicate that for a 3 µm beam diameter the absorbed current generally decreased only a minimal amount (between 0-5 nA), and the severity of bright spots (in BSE) was significantly less than with a 1 or 2 µm electron beam. Changes in absorbed current are thought to indicate a disequilibrium build-up of charge and/or changing electron emission characteristics, whereas the "bright spots" could be related to a compositional change (i.e. elemental loss) during analysis (see Jercinovic and Williams (2005) for more details). Although not yet fully quantified, the use of a focussed beam appears to affect the measurement of P and the LREEs (e.g., La, Ce, Pr, Nd), resulting in an increase in counts on those elements over extended periods (Kevin Blake, pers. comm.). The elemental measurement order in the protocol used here was devised to minimise this phenomena, such that only minor matrix elements were measured towards the end of the analysis (Fig. 3b). The effects of a focussed (1 µm) beam on the measurement of Th, U and Pb do not appear significant at this stage but are still being investigated.

4.5. Bootstrap method

In essence, bootstrap methods allow us to assess the variability of our data (i.e. calculate a CI for the mean) where the sampling distribution is not known (Fisher, 1993). This is common for small datasets (typical of EPMA monazite analyses), and where the precisions of individual analyses (counting statistics) are variable (see above). The fundamental idea involved in bootstrapping is that a resample with replacement of a random sample from a certain population is again a random sample of that population (Efron and Tibshirani, 1993). Thus the collected data can be re-sampled multiple times and empirical distributions of population parameters (such as the mean and confidence intervals) can be derived. In this study, we used the classical non-parametric bootstrap (e.g., Efron and Tibshirani, 1993; Fisher, 1993), where our original dataset was re-sampled, with replacement such that the bootstrapped sample was the same size as our original dataset. The mean of this sample became our first bootstrap estimate and the procedure was repeated 10,000 times, such that 10,000 bootstrap estimates were generated. This part of the procedure was executed using the Microsoft Excel® "bootstrap add-in" from Barreto and Howland (2005), which utilises the fast multiple recursive random number generator (FMRG) of Deng and Lin (2000) to randomly resample the data. The output was checked for skewness/acceleration from normality (via a histogram), and also the degree of bias (comparison of the mean of the bootstrap distribution to the mean of the original data). Because these statistics for the data presented herein were (and should be) negligible, bootstrap CIs were estimated by multiplying the standard deviation of the bootstrap distribution, by the corresponding t-value, for n-1 degrees of freedom (Efron and Tibshirani, 1993). Extensions to the technique used here are given in Hall (1992) and Efron and Tibshirani (1993).

5. Monazite chemistry and Th-U-Pb dates

Mean “dates” (including errors) and the description of each monazite domain in which a mean date was calculated are shown in Table 3. The full dataset, including monazite compositions and counting errors are presented in Appendix C.

5.1. Sample CH22

Monazite was analysed in two different textural settings, as inclusions in staurolite and as elongate grains lying parallel to the matrix foliation (Table 3). The dominant inclusion trails in staurolite porphyroblasts appear continuous and curve into the matrix foliation, which was crenulated synchronous with the growth of this porphyroblastic phase. The two monazite grains within staurolite are interpreted to pre-date those in the matrix, although their relative timing is uncertain. Of the monazite grains analysed, zoning patterns (mostly dominated by Th) vary considerably but chemically all were similar, with the exception of one grain enclosed by staurolite (140-mnz1) that was characterised by a distinctly lower Y content (Fig. 4a). The monazites with distinct cores and rims (e.g., 30-mnz1) appear to have a trend from high Th/U, low Ce/Y in the core to lower Th/U, higher Ce/Y in the rims (Fig. 4b, c). In all cases the intra-granular variation in Y was minimal, indicating that Ce variation is related to the Th concentration. Based on generally unresolvable Th-compositional complexity and minimal Y variability, most of the ages and errors for these monazites were calculated based on date domains rather than compositional domains (with the exception of the relatively homogeneous 30-mnz2). The mean dates of all the monazites are in the range 434-457 Ma and all lie within calculated error, including (the low Y) monazite 140-

mnz1. As the data cannot be statistically separated in this sample, a weighted mean of 443 ± 8 Ma (MSWD = 1.07) was calculated and is considered to represent the average age of monazite growth in this rock (Fig. 4d).

Although not distinctly different in age, three possible explanations for the distinctly low Y monazite are proposed: (1) both staurolite-enclosed monazite grains crystallised at (unresolvable) different times, the first in a lower Y environment and the latter in a higher Y matrix composition, similar to that recorded in monazite grains preserved in the matrix, (2) both monazite grains crystallised at essentially the same time, but the low Y-monazite crystallised in proximity to a synchronous Y-sequestering phase, locally limiting Y availability, or (3) the cracks that indirectly link both inclusions to the matrix (Fig. 5a, b), may have acted as a fluid pathway in the case of monazite 0-mnz4, with related compositional effects. Of these mechanisms (1) is possible, but cannot be confirmed microstructurally due to uncertainties in the relative timing relationships between these inclusions. Mechanism (2) is unlikely as the most obvious Y-sequestering phase is garnet and this clearly pre-dates staurolite (there is no evidence for any other Y bearing mineral in the vicinity). The third mechanism is difficult to asses, due to uncertainties as to how monazite behaves when exposed to fluid, although apparent resetting of monazite inclusions within porphyroblasts, that are connected to the matrix by cracks have been reported (DeWolf et al., 1993; Montel et al., 2000; Carson et al., 2004). Based on available data, the most likely explanation is that the low Y grain (0-mnz4) grew either synchronous with garnet or preceding Y-enrichment of the matrix as garnet resorbed during staurolite growth. This would explain the higher Y contents of all other monazite grains, and implies that they must be younger than the low-Y grain.

5.2. Sample CH27

All analysed monazite grains in this sample lie within the matrix (Table 3). Grains 20-mnz1 and 20-mnz2 show little compositional variation, and are interpreted to lie within the same dominant (although weakly crenulated) matrix foliation (Fig. 6a, b). However, a third grain (50-mnz2), with a distinct homogenous core, and complexly zoned rim lies within an earlier foliation that was subsequently crenulated by both foliations described above (Fig. 6c, d). The zoning in this grain is dominated by both U + Th variation, which is higher in the core than in the rim. Patches of similar BSE brightness and contrast elsewhere in the grain possibly indicate that the high U + Th zone is not necessarily confined just to the core. The correlation between Th/U and Ce/Y in this grain is also reverse to that observed in CH22 (Fig. 6e). Monazite grains 20-mnz1 and 20-mnz2 were considered compositional domains, but mean dates for the core and rim of (grain) 50-mnz2 were calculated separately. Since both these values were near identical, and the high U zone may not be confined to the core, all data was combined into a single date domain (Fig. 6f). The mean dates for all three grains are in the range 442-451 Ma and the weighted mean of 443 ± 5 Ma (MSWD = 0.50) is considered to represent the age of foliation development (pre-S_C) during the later stages of ductile deformation in this sample (Fig. 6f).

5.3. Sample CH35

Monazite in a variety of textural and microstructural settings was analysed in this sample, including inclusions in garnet, kyanite and grains in the matrix (Table 3). Garnet porphyroblasts clearly predate staurolite and kyanite, with staurolite appearing to predate kyanite, although both phases have inclusion trails that curve into the matrix.

Foliations within the graphite-rich matrix are difficult to correlate across the thin section due to multiple overprinting crenulation events and reactivation of older foliations, particularly around porphyroblasts. The compositional zoning in the monazite grains examined varied in complexity, but two grains were distinctly different from the others (Fig. 7a). The first is an inclusion in a garnet rim (mnz3), which is associated with xenotime (Fig. 7b). Its chemical zoning is dominated by Y + Dy variation, with both of these elements generally increasing towards the rim in contact with xenotime and/or garnet (Fig. 7c), possibly indicating that one or both of these phases is controlling the distribution of these elements. The most chemically distinct monazite is a relatively homogeneous grain (mnz6) situated within a large crack (with associated bt-ms-qtz-pl infill) in a staurolite porphyroblast (Fig. 7d). This grain has a different chemical signature (depleted in Y + HREE), relative to the other monazites in the sample (Fig. 6e), and appears to have precipitated in the crack sometime after staurolite growth.

As most of the monazite grains in this sample were chemically heterogeneous, very few chemical domains were adequately analysed. Mean dates for each grain (regardless of core/rim separations) were calculated based on a lack of clear evidence for more than one stage of growth (a possible exception being mnz4). The mean dates for mz1-mnz5 are all within error of each other (range: 424-464 Ma), however mnz6 is clearly different with a mean date of 310 ± 25 Ma. A weighted mean of 455 ± 19 Ma (MSWD = 3.1) was calculated for all monazite grains, excluding mnz6 (Fig. 7f), the large error and MSWD possibly indicating multiple stages of growth that were not resolvable with the data collected.

The origin of the ca. 310 Ma age for grain mnz6 (in staurolite) is uncertain. Like the monazite CH22-140-mnz1 discussed above, this grain could be interpreted as being the result of infiltrating fluids that fully or partially reset the chemical composition, including the U-Th-Pb systematics, in a previously crystallised monazite grain (e.g., DeWolf et al., 1993; Montel et al., 2000; Carson et al., 2004). However, uncertainties surrounding monazite behaviour in the presence of fluids makes this only a tentative possibility. No other monazite grains with similar chemistry or age were found in this sample (approximately 10 monazites in the vicinity of this grain were analysed once in an effort to locate a similar monazite grain), which hampers interpretation. Based on both chemical and textural observations, it is mostly likely that this grain crystallised from (post-peak) metamorphic fluids, after the staurolite porphyroblast was cracked during brittle deformation.

5.4. Sample CH62

In this sample monazite grains were analysed as inclusions in staurolite porphyroblasts and grains aligned parallel/sub-parallel to the matrix foliation. The inclusion trails in staurolite are continuous with and curve into the weakly crenulated matrix foliation. The staurolite clearly post-dates the cores of the garnet porphyroblasts, which have inclusion trails truncated by an inclusion free-rim, but the relationship between the garnet porphyroblast rims and the staurolite is uncertain. Three out of the four monazite grains analysed (one in staurolite and two in the matrix) were found to have three very distinct domains (inner core-A, outer core-B and rim), with Th varying from around 8 wt % in core-A, down to 1 wt % in the rims (Fig. 8a, b, c). The chemical variation between core-A and core-B appears entirely related to incorporation of Th into the monazite structure (i.e. related to brabantite and huttonite exchanges). However, the rim is also characterised by much lower Y and HREE concentrations, indicating that additional exchanges occurred during latter growth (Fig. 8 d,e). The remaining monazite grain (mnz3) in the sample has a complex chemistry (patchy zoning in BSE), and the analysed portion of this grain is interpreted to be either an intermediate zone between core-B and the rim (as identified above), or the result mixed analyses between of these zones.

Although three distinct zones were identified chemically, analyses from core-A and core-B were combined due to similar Y (+ HREE) contents and calculated dates. Two distinct mean dates can be separated in grains mnz1, mnz2 and mnz4. The weighted mean of the core zones of these grains is 451 ± 7 Ma (MSWD = 0.03), whereas that of the rim zones is 398 ± 20 Ma (MSWD = 0.49). This provides a clear indication of multiple stages of monazite growth in this sample (Fig. 7f). The poorly defined mean date for mnz3 of 440 ± 47 Ma supports the interpretation of mixed analyses suggested above. The irregular shape of the core zones in grains mnz1, 2, and 4 (defined from BSE images) could indicate partial dissolution and precipitation around ca. 400 Ma, leaving behind only a portion of a relict core. An alternative interpretation is that the core may be poorly defined in this thin section orientation (e.g., elongate normal to strike) and the rim may be an overgrowth, leaving the relict core essentially intact (this was not investigated). This uncertainty makes interpretation of the older phase of growth difficult. Staurolite must almost certainly postdate 400 Ma monazite growth, and most likely occurred within the same time frame. Based on the unlikely scenario that the monazite isograd in this sample is below that of garnet (and no monazite inclusions in garnet were located), it seems reasonable to assume that the garnet porphyroblast cores grew around 450 Ma, along with the first generation of monazite. This implies that some 50 million years later, a second period of metamorphism resulted in the garnet porphyroblast rims, additional monazite and also the growth of staurolite porphyroblasts.

6. Discussion

6.1. Evaluation of technique

In all cases the bootstrap CI is between 5-10 % smaller than that calculated using parametric techniques, even when applied to significantly Th-zoned samples. As the bootstrap is a consequence of the central limit theorem, the distribution of the bootstrap estimates will tend to become normal as n increases. Therefore, bootstrap CIs correspond well to classical methods for approximately normally distributed data (i.e. compositional domains). However, since the differences between the two methods are also minimal for mixed composition data, it would appear that this data can also be adequately represented by a normal distribution. It seems that representative confidence intervals are achievable by calculating a confidence interval from the SE for Th-U-Pb zoned monazites, as long as compositional variation is independent of age. The bootstrap approach can still be worthwhile as the output distribution can be used as an approximation of the sampling distribution to asses how skewness, for example, will affect the calculated CI. Significant skewness should also raise immediate suspicion that data sampling was inadequate (mixed) and/or instrument error occurred. This may not be obvious with limited data (Fig. 9). Although corrections for bias and acceleration (BC_a) are possible for bootstrap distributions (Efron and Tibshirani, 1993; Hall, 1992), this should not be required for EPMA data for the above reasons. In summary, the bootstrap can be used as a guide in interpreting EPMA dates from both relatively homogeneous and mixed composition monazites, but generally is not required to calculate CIs because classical (parametric) methods appear adequate. Importantly, the use of the bootstrap cannot make up for a poor sampling strategy, or a small number of samples.

The ultimate goal in EPMA monazite dating is to maximise the number of data points in a compositional domain, such that precise ages can be obtained for each stage of growth. Nevertheless, the data presented above highlights the usefulness of this protocol, which due to current technical limitations compromises both spatial resolution and precision to reduce accuracy errors (e.g., increasing beam diameter and reducing total analytical time to minimise sample damage). As a result, interpreting individual domains is more complex. The results both here and elsewhere (Zhu and O'Nions, 1999a; Pyle et al., 2001; Spear and Pyle, 2002) would suggest that Y (+ HREE) variation can be used as an indicator of distinct monazite growth events. This correlation can be easily checked in zoned monazite grains and assumptions regarding growth events can be made without compositional domains being accurately identified or sampled. Continued efforts will attempt to improve the resolution, precision and accuracy of the protocol presented here, with the goal of potentially being able to date multiple stages of monazite growth within a single orogenic event.

6.2. Interpretation of ages

The majority of the monazite ages can be correlated to the Taconic Orogeny, with the rims of the monazites in sample CH62 linked to the Acadian. Within this sample, there is clear evidence for two distinct periods of monazite growth, with staurolite growth also interpreted to accompany the second stage. The data presented here corresponds with numerous Taconic isotopic ages for the region (e.g., Glover et al., 1983) and also post-Taconic (ca. 400 Ma) ages for monazite (Kohn and Malloy, 2004), staurolite (Brosky and Odom, 2002), and zircon (Miller et al., 2000). These results also support the interpretation of two distinct metamorphic periods as alluded to by Connelly and Dallmeyer (1993) and Miller et al. (2000), with further evidence that the Acadian event (although not preserved everywhere), must have been of a similar grade to that reached in the Taconic. The overall range of ages is reflective of the low precision technique used here, but the interpretation that monazite grew at different stages between samples is also quite likely.

These ages provide solid evidence that the sediments of the Great Smoky Group were deposited prior to the Ordovician and/or cannot be conformable with the Walden Creek Group in this region (if the paleontological data of Unrug et al. (2000) is correct). All samples studied tend to contain well preserved Taconic matrix monazites. If these grains are detrital, it would require that all these sediments originated from rocks metamorphosed in the Taconic. Whilst this cannot be ruled out, it does not explain the apparent lack of younger grains that should have grown in response to st-ky grade metamorphism. It is far more likely that these Taconic monazite grains grew during the metamorphism of the current host rocks, particularly as these samples have experienced several generations of foliation development, which should have deformed and recrystallised most relict grains (Bell and Welch, 2002).

The ca. 310 Ma age of the crack-infill monazite (CH35-mz6) corresponds to the Alleghanian Orogeny. This event is largely interpreted to be associated with the westward transport of thrust sheets as a result of the collision of Laurentia with Africa (e.g., Hatcher, 1987b; Hatcher and Goldberg, 1991). Rb-Sr isotopic resetting in intensely deformed Blue Ridge and Piedmont mylonites at 302 ± 5 Ma (Van Camp and Fullagar, 1982) and 307 ± 5 Ma (Su and Fullagar, 1995), correspond to the age presented here, but the extent of these ages are not known and no regional scale Alleghanian metamorphism has been found in this portion of the southern Appalachians. Nevertheless, this grain is tentatively interpreted be the result of Alleghanian brittle deformation opening cracks within the porphyroblasts, allowing infiltrating fluids to precipitate monazite and other metamorphic minerals, without noticeably affecting the Taconic metamorphic assemblage in this sample.

6.3. Tectonic framework

Whilst no attempts will be made to define the duration or continuity of the Taconic or Acadian orogenies in the western Blue Ridge based on the data presented here, there is convincing evidence in sample CH62 that metamorphism and deformation accompanied both events and there was a significant hiatus (around 50 m.y.) in between. Evidence for either or both these events are increasing (see references above), which suggests that they both affected the region and the peak metamorphic conditions may have been similar. Clearly, evidence for both the Taconic and Acadian events is not present throughout the western Blue Ridge and Taconic isotope data plus Taconic chemical ages from this study dominate. As both events affected the western Blue Ridge, the distribution of metamorphism may be explained in the context of deformation partitioning (Moecher and Wintsch, 1994; Bell et al., 1998; Bell et al., 2004). Moecher and Wintsch (1994) have shown how metamorphic textures can remain unaffected when the deformation partitions into surrounding zones during later metamorphic events, and similar interpretations have been used to explain multiple generations of garnet growth across an outcrop (Bell et al., 1998) and regionally (Bell et al., 2004).

More data would be required to make a proper interpretation, although it seems that the location of the only sample examined here preserving Acadian metamorphism relative to the Murphy Syncline may be important. This sample (CH62) is the only one clearly from the limb of the fold, as the other three, which all contain Taconic metamorphic textures exclusively, are closer to the hinge. Therefore during Acadian tectonism, deformation may have preferentially partitioned along this limb, locally developing crenulations and driving porphyroblast growth prior to the development of a new crenulation cleavage (Bell et al., 2005). This may or may not have also occurred on the opposite limb (samples from this limb would be required to check this). The lack of any apparent deformation and/or metamorphism of this age in the other samples indicates that the deformation at this time partitioned on this side of the hinge, as well as into rocks further north, accounting other Acadian metamorphic ages within the western Blue Ridge (e.g., Kohn and Malloy, 2004).

7. Conclusions

1. Despite technical limitations, the EPMA is a useful tool for dating monazite, and is more than adequate for distinguishing distinct Palaeozoic (and older) metamorphic events with intervals of approximately 50 million years.

2. As previously recognised (e.g., Zhu and O'Nions, 1999a; Spear and Pyle, 2002), Y and HREE intra-grain variation can be a useful indicator of distinct monazite growth events.

3. Defining chemical domains on the basis of Th and/or U variation is not critical, but is preferred if domains are large enough as statistical error and correlations to monazite forming reactions will improve.

4. The bootstrap and/or other nonparametric techniques are generally not required for EPMA monazite data as parametric methods are robust enough and serious deviations from normality are probably related to mixed ages and/or instrumental error.

5. The western Blue Ridge experienced an initial Taconic (ca. 450 Ma) metamorphic episode, which was locally overprinted by an amphibolite facies event during the Acadian (ca. 400 Ma).

6. Based on the dominance of Taconic monazite grains within these samples, it is unlikely that the Great Smoky Group sediments are correlative with the Walden Creek Group.

8. References

Armstrong, J.T., 1988. Quantitative analysis of silicate and oxide materials: Comparison of Monte Carlo, ZAF and Φ (ρz) procedures. In: D.E. Newbury (Editor), Microbeam Analysis. San Francisco Press.

Armstrong, J.T., 1991. Quantitative elemental analysis of individual microparticles with electron beam instruments. In: K.F.J. Heinrich and D.E. Newbury (Editors), Electron Probe Quantitation. Plenum Press.

Ayers, J.C., Miller, C., Gorisch, B. and Milleman, J., 1999. Textural development of monazite during high-grade metamorphism: Hydrothermal growth kinetics, with implications for U,Th-Pb geochronology. American Mineralogist, 84, 1766-1780.

Barreto, H. and Howland, F.M., 2005. Introductory Econometrics: Using Monte Carlo Simulation with Microsoft Excel. Cambridge University Press, 800 pp.

Bell, T.H., Ham, A.P., Hayward, N. and Hickey, K.A., 2005. On the development of gneiss domes. Australian Journal of Earth Sciences, 52, 183-204.

Bell, T.H., Ham, A.P. and Kim, H.S., 2004. Partitioning of deformation along an orogen and its effects on porphyroblast growth during orogenesis. Journal of Structural Geology, 26, 825-845.

Bell, T.H., Hickey, K.A. and Upton, G.J.G., 1998. Distinguishing and correlating multiple phases of metamorphism across a multiply deformed region using the axes of spiral, staircase and sigmoidal inclusion trails in garnet. Journal of Metamorphic Geology, 16, 767-794.

Bell, T.H. and Welch, P.W., 2002. Prolonged Acadian orogenesis: revelations from foliation intersection axis (FIA) controlled monazite dating of foliations in porphyroblasts and matrix. American Journal of Science, 302, 549-581.

Brosky, R. and Odom, L., 2002. U-Pb staurolite age of metamorphism in the western Blue Ridge, Southern Appalachians. Geological Society of America, Abstracts with Programs, 34, 342.

Carson, C.J., Berman, R.G., R.A., S., Sanborn-Barrie, M., Skulski, T. and Sandeman, H.A.I., 2004. Age constraints on the Paleoproterozoic tectonometamorphic history of the Committee Bay region, western Churchill Province, Canada; evidence from zircon and in situ monazite SHRIMP geochronology. Canadian Journal of Earth Sciences, 41, 1049-1076.

Catlos, E.J., Gilley, L.D. and Harrison, T.M., 2002. Interpretation of monazite ages obtained via in situ analysis. Chemical Geology, 188, 193-215.

Cocherie, A. and Albarede, F., 2001. An improved U-Th-Pb age calculation for electron microprobe dating of monazite. Geochimica et Cosmochimica Acta, 65 (24), 4509-4522.

Cocherie, A., Legendre, O., Peucat, J.J. and Kouamelan, A.N., 1998. Geochronology of polygenetic monazites constrained by in situ electron microprobe Th-U-total lead determination: Implications for lead behaviour in monazite. Geochimica et Cosmochimica Acta, 62 (14), 2475-2497.

Connelly, J.B. and Dallmeyer, R.D., 1993. Polymetamorphic evolution of the western Blue Ridge: Evidence from $^{40}Ar/^{39}Ar$ whole-rock slate/phyllite and muscovite ages. American Journal of Science, 293 (4), 322-359.

Crowley, J.L. and Ghent, E.D., 1999. An electron microprobe study of the U-Th-Pb systematics of metamorphosed monazite: the role of Pb diffusion versus overgrowth and recrystallization. Chemical Geology, 157, 285-302.

Deng, L.-Y. and Lin, D.K.J., 2000. Random Number Generation for the New Century. The American Statistician, 54, 145-150.

DeWolf, C.P., Belshaw, N. and O'Nions, R.K., 1993. A metamorphic history from micron-scale $^{207}Pb/^{206}Pb$ chronometry of Archean monazite. Earth and Planetary Science Letters, 120, 207-220.

Efron, B. and Tibshirani, R., 1993. An Introduction to the Bootstrap. Chapman & Hall, New York.
Fisher, N.I., 1993. Statistical Analysis of Circular Data. Cambridge University Press, 277 pp.
Foster, G., Gibson, H.D., Parrish, R.R., Horstwood, M., Fraser, J. and Tindle, A., 2002. Textural, chemical and isotopic insights into the nature and behaviour of metamorphic monazite. Chemical Geology, 191, 183-207.
Foster, G., Kinny, P., Vance, D., Prince, C. and Harris, N., 2000. The significance of monazite U-Th-Pb age data in metamorphic assemblages; a combined study of monazite and garnet chronometry. Earth and Planetary Science Letters, 181, 327-340.
Glover, L., Speer, J.A., Russell, G.S. and Farrar, S.S., 1983. Ages of Regional Metamorphism and Ductile Deformation in the Central and Southern Appalachians. Lithos, 16 (3), 223-245.
Hall, P., 1992. The Bootstrap and Edgeworth Expansion. Springer Series in Statistics. Springer-Verlag, New York.
Hatcher, R.D., Jr, 1987. Tectonics of the Southern and Central Appalachian Internides. Annual Review of Earth and Planetary Sciences, 15, 337-362.
Hatcher, R.D., Jr. and Goldberg, S.A., 1991. The Blue Ridge geologic province. In: J.W. Horton, Jr. and V.A. Zullo (Editors), The Geology of the Carolinas (Carolina Geological Society Fiftieth Anniversary Volume). Univ. Tenn. Press, Knoxville, TN, pp. 11-35.
Horstwood, M.S.A., Foster, G.L., Parrish, R.R., Noble, S.R. and Nowell, G.M., 2003. Common-Pb corrected in situ U-Pb accessory mineral geochronology by LA-MC-ICP-MS. Journal of Atomic Spectrometry, 18, 837-846.
Jercinovic, M.J. and Williams, M.L., 2005. Analytical perils (and progress) in electron microprobe trace element analysis applied to geochronology: Background acquisition, interferences, and beam irradiation effects. American Mineralogist, 990, 526-546.
Kohn, M.J. and Malloy, M.A., 2004. Formation of monazite via prograde metamorphic reactions among common silicates: Implications for age determinations. Geochimica et Cosmochimica Acta, 68, 101-113.
Ludwig, K.R., 2003. User's manual for Isoplot 3.0; a geochronological toolkit for Microsoft Excel, Berkeley Geochronology Centre, Special Publication No. 4.
Miller, B.V., Stewart, K., G., Miller, C.F. and Thomas, C.W., 2000. U-Pb ages from the Bakersville, North Carolina eclogite; Taconian eclogite metamorphism followed by Acadian and Alleghanian cooling. Geological Society of America, Abstracts with Programs, 32, 62.
Moecher, D.P. and Wintsch, R.P., 1994. Deformation induced reconstitution and local resetting of mineral equilibria in polymetamorphic gneisses: tectonic and metamorphic implications. Journal of Metamorphic Geology, 12, 523-538.
Mohr, D.W., 1973. Stratigraphy and structure of part of the Great Smoky and Murphy belt groups, western North Carolina. American Journal of Science, 273-A, 41-71.
Montel, J.-M., Foret, S., Veschambre, M., C, N. and Provost, A., 1996. Electron microprobe dating of monazite. Chemical Geology, 131, 37-53.
Montel, J.-M., Kornprobst, J. and Vielzeuf, D., 2000. Preservation of old U-Th-Pb ages in shielded monazite: example from the Beni Bousera Hercynian kinzigites (Morocco). Journal of Metamorphic Geology, 18, 335-342.

Pyle, J.M. and Spear, F.S., 2003. Four generations of accessory-phase growth in low-pressure migmatites from SW New Hampshire. American Mineralogist, 88, 338-351.

Pyle, J.M., Spear, F.S., Rudnick, R.L. and McDonough, W.F., 2001. Monazite-xenotime-garnet equilibrium in metapelites and a new monazite-garnet thermometer. Journal of Petrology, 42, 2083-2107.

Pyle, J.M., Spear, F.S. and Wark, D.A., 2002. Electron Microprobe Analysis of REE in Apatite, Monazite and Xenotime: Protocols and Pitfalls. Reviews in Mineralogy and Geochemistry, 48, 337-362.

Pyle, J.M., Spear, F.S., Wark, D.A., Daniel, C.G. and Storm, L.C., 2005. Contributions to the precision and accuracy of chemical ages of monazite. American Mineralogist, 90, 547-577.

Rhede, D., Wendt, I. and Förster.H.-J., 1996. A three-dimensional method for calculating independent chemical U/Pb- and Th/Pb-ages of accessory minerals. Chemical Geology, 130, 247-253.

Rodgers, J., 1987. The Appalachian-Ouachita Orogenic Belt. Episodes, 10, 259-266.

Scherrer, N.C., Engi, M., Gnos, E., Jakob, V. and Liechti, A., 2000. Monazite analysis; from sample preparation to microprobe age dating and REE quantification. Schweizerische Mineralogische und Petrographische Mitteilungen, 80 (1), 93-105.

Scott, V.D., Love, G. and Reed, S.J.B., 1995. Quantitative Electron-Probe Microanalysis (2nd edition). Ellis Horwood Ltd, Chichester.

Shaw, C.A., Karlstrom, K.E., Williams, M.L., Jercinovic, M.J. and McCoy, A.M., 2001. Electron-microprobe monazite dating of ca. 1.71-1.63 Ga and ca. 1.45-1.38 Ga deformation in the Homestake shear zone, Colorado: Origin and early evolution of a persistent intracontinental tectonic zone. Geology, 29, 739-742.

Siegel, A.F., 1988. Statistics and Data Analysis. John Wiley & Sons, New York.

Spear, F.S. and Pyle, J.M., 2002. Apatite, Monazite, and Xenotime in Metamorphic Rocks. Reviews in Mineralogy and Geochemistry, 48, 293-335.

Su, Q. and Fullagar, P.D., 1995. Rb-Sr and Sm-Nd Isotopic Systematics During Greenschist Facies Metamorphism and Deformation: Examples from the Southern Appalachian Blue-Ridge. Journal of Geology, 103 (4), 423-436.

Suzuki, K. and Adachi, M., 1991. Precambrian provenance and Silurian metamorphism of the Tsubonosawa paragneiss in the South Kitakami terrane, Northeast Japan, revealed by the chemical Th-U-total Pb isochron ages of monazite, zircon and xenotime. Geochemical Journal, 25, 357-376.

Suzuki, K. and Adachi, M., 1994. Middle Precambrian detrital monazite and zircon from the Hida gneiss on Oki-Dogo Island, Japan: their origin and implications for the correlation of basement gneiss of Southwest Japan and Korea. Tectonophysics, 235, 277-292.

Suzuki, K., Adachi, M. and Tanaka, T., 1991. Middle Precambrian provenance of Jurassic sandstone in the Mino Terrane, central Japan: Th-U-total Pb evidence from an electron microprobe monazite study. Sedimentary Geology, 75, 141-147.

Unrug, R., Ausich, W.I., Bednarczyk, J., Cuffy, R.J., Mamet, B.L., Palmes, S.L. and Unrug, S., 2000. Paleozoic age of the Walden Creek Group, Ocoee Supergroup, in the western Blue Ridge, southern Appalachians: Implications for evolution of the Appalachian margin of Laurentia. Geological Society of America Bulletin, 112, 982-996.

Unrug, R. and Unrug, S., 1990. Paleontological evidence of Paleozoic age for the Walden Creek Group, Ocoee Supergroup, Tennessee. Geology, 18, 1041-1045.

Van Camp, S.G. and Fullagar, P.D., 1982. Rb-Sr whole-rock ages of mylonites from the Blue Ridge and Brevard Zone of North Carolina. Northeastern and Southeastern combined section meetings Abstracts with Programs - Geological Society of America, 14, 92-93.

Wiener, L.S. and Merschat, C.E., 1992. Geological map of south-western North Carolina including adjoining south-eastern Tennessee and northern Georgia. Division of Land Resources, North Carolina Department of Environment, Health and Natural Resources.

Williams, M.L. and Jercinovic, M.J., 2002. Microprobe monazite geochronology: putting absolute time into microstructural analysis. Journal of Structural Geology, 24, 1013-1028.

Williams, M.L., Jercinovic, M.J., Goncalves, P. and Mahan, K., 2006. Format and philosophy for collecting, compiling, and reporting microprobe monazite ages. Chemical Geology, 225, 1-15.

Williams, M.L., Jercinovic, M.J. and Terry, M.P., 1999. Age mapping and dating of monazite on the electron microprobe: Deconvoluting multistage tectonic histories. Geology, 27 (11), 1023-1026.

Zhu, X.K. and O'Nions, R.K., 1999. Monazite chemical composition: some inplications for monazite geochronology. Contributions to Mineralogy and Petrology, 137, 351-363.

CHAPTER 3

ALLEGHANIAN AMPHIBOLITE FACIES TECTONISM WITHIN THE SOUTHERN BLUE RIDGE APPALACHIANS

Abstract

Small (< 30 μm) monazite inclusions within garnet porphyroblasts and the matrix from the Dahlonega Gold Belt, northern Georgia Appalachians have been chemically dated using the EPMA. Each garnet porphyroblast preserves up to three generations of inclusion trails and monazite inclusions were correlated to periods of foliation development and/or porphyroblast growth, using a combination of microstructural and chemical techniques. Monazite grains within the matrix and garnet porphyroblast rims mostly correlate with the development of the dominant pervasive schistosity, preserved across the belt. The age of the inclusions within the cores of porphyroblasts cannot be separated from those in the rims and the matrix. The weighted mean of all grains analysed is 322 ± 4 Ma (MSWD = 1.4), which is interpreted to represented the average age of metamorphism above the monazite isograd. This indicates that these rocks underwent metamorphism during the early Alleghanian, rather than during the Late Acadian (ca 365 Ma) as was previously assumed. Preservation of the earlier event cannot be ruled out, as monazite inclusions can only be correlated to the early stages of garnet porphyroblast growth in one sample. These ages fit within a narrow window for Alleghanian metamorphism, prior to thrust sheet movement within the Piedmont and Blue Ridge of the southern Appalachians, as a result of continental collision with Africa. The lack of Alleghanian metamorphism in surrounding belts is possibly related to deformation preferentially partitioning through this narrow, fault bounded belt, with little effect on adjacent rocks.

1. Introduction

The Palaeozoic tectonic history within the southern Appalachians has been interpreted to be the result of a series of compressional events, culminating with the collision of the North American continent with Africa in the Alleghanian Orogeny (e.g., Hatcher, 1972; 1987b; Butler, 1973). The Blue Ridge Province (Fig. 1) contains most of this orogenic history, and is separated from the weakly-metamorphosed Valley and Ridge to the northwest by the Blue Ridge fault system, and from the Inner Piedmont province to the southeast by the Brevard Fault Zone (King, 1955; Hatcher, 1972). The Gossan-Lead, Holland Mountain, Hayesville and Allatoona Faults divide the province into two contrasting terranes referred to as the eastern and western Blue Ridge (Hatcher, 1978). The majority of the metamorphism in the Blue Ridge has been correlated to the earlier Taconic and/or Acadian events (Butler, 1973; Glover et al., 1983; Connelly and Dallmeyer, 1993; Goldberg and Dallmeyer, 1997; Miller et al., 2000) with the Alleghanian interpreted to be mostly a deformational event, responsible for the transport of thrust sheets towards the continental interior (Hatcher, 1987b; Hatcher and Goldberg, 1991). The realisation that the Blue Ridge consists of a series of thrust sheets, each with a different tectonic history (e.g., Hatcher, 1978; Hatcher and Odom, 1980) has complicated regional interpretations but gives important insights into prolonged orogeneses that are only recorded locally.

This study examines a small portion of the multiply deformed Dahlonega Gold Belt of the eastern Blue Ridge, in northern Georgia, using a combination of detailed microstructural analysis and electron probe microanalyser (EPMA) monazite dates. Attempts will be made to directly link monazite growth events to particular microstructures preserved in both porphyroblasts and within the matrix, to put absolute time constraints on deformation (e.g., Bell and Welch, 2002; Williams and Jercinovic, 2002). The small spatial resolution of EPMA (down to 1 μm) makes this the preferred geochronological technique for small inclusions in porphyroblasts, although it is limited by the relatively large errors in precision (e.g., Montel et al., 1996; Cocherie and Albarede, 2001). Other assumptions and background information pertinent to EPMA monazite dating are covered in Chapter 2.

2. Regional geology

The Dahlonega Gold Belt traditionally refers to a NE-trending belt of gold occurrences across northern Georgia, generally confined to the New Georgia Group (Abrams and McConnell, 1984; German, 1989). Extensions of this unit into North Carolina (Otto Formation of Hatcher (1987a)), and subsequent studies have led to the term now referring to a belt of metasediments and metavolcanics defined by the Allatoona-Soque River and Chattahoochee faults (Settles et al., 2001b; Bream et al., 2004). Sedimentation is thought to be related to a Late Cambrian/Early Ordovician Laurentian arc system, based on interpreted evidence for syndeposition with emplacement of the Sally Free mafic complex (Settles et al., 2001a).

At least four fold events have been identified in the Dahlonega Gold Belt. The first generated recumbent isoclinal folds with NE-trending axes (Abrams and McConnell, 1984), that were later refolded by upright northeast trending F_2 structures, responsible for the majority of present day outcrop patterns (German, 1989).

Subsequent fold events (F_3) were less intense, essentially refolding $F_{1/2}$ structures, with later warping during F_4 (Abrams and McConnell, 1984). Metamorphism ranged from biotite to kyanite grade and has been interpreted to have occurred around 365 Ma, based on the extrapolation of ^{40}Ar-^{39}Ar hornblende and biotite cooling ages from the Inner Piedmont to the southeast (Dallmeyer, 1978; German, 1989). The Allatoona Fault, which marks the northern boundary of the Dahlonega Gold Belt, truncates metamorphic isograds across to the Ocoee Supergroup (German, 1989; Holm and Farmer, 2002), and has been interpreted to indicate post-metamorphic movement.

3. Sample selection and methods

3.1. Description of samples

Twenty one samples, containing garnet porphyroblasts (up to 8 mm), with the mineral assemblage grt + ms + bt + qtz + ilm ± st ± ky ± pl ± rt ± chl ± gr ± tur (abbreviations from Kretz (1983)), taken between the localities of Canton and Dawsonville were checked for monazite in this study (Fig. 2). Garnet cores typically preserve sigmoidal inclusion trails (defined by quartz), and are generally truncated by relatively inclusion-poor rims, creating a clear core-rim textural boundary (Fig. 3). Crenulations were also frequently preserved (Fig. 3, 4). Inclusion trails in the rims are characterised by ilmenite and graphite and mostly appear continuous with the matrix. (Fig. 3b, d). Stallard et al. (2003) conducted extensive microstructural work on these rocks and identified at least 4 stages of garnet growth by measuring foliation intersection/inflection axes preserved in the porphyroblasts.

Where present, staurolite was generally associated with garnet rims, and has inclusions trails (defined by graphite), that are continuous with, but weakly deflected into the dominant matrix foliation (Fig. 3). In one example (CA17a), where staurolite is more abundant, both staurolite and garnet rims preserve the same structures in non-adjacent portions of the rock, indicating relatively synchronous growth (Fig. 4). Minor kyanite, preserving inclusion trails similar to staurolite was found in three graphite-rich samples (CA19, 20, 23), all from essentially the same locality. Evidence for retrogression is limited, but local replacement of garnet and/or biotite by chlorite was noted in several samples. The dominant matrix foliation defines a penetrative north-east striking schistosity (with approximate 50° dip in samples examined herein). This foliation is sub-parallel to the axial planes of micro- and meso-scale isoclinal folds (Stallard and Hickey, 2001) and is locally crenulated, defining a weak axial plane foliation

3.2. Sample selection and monazite locating procedure

All the samples were checked for monazite using the secondary electron (SEM) mode combined with qualitative energy-dispersive spectrometry (EDS) spot analyses on the JEOL JXA-8200 Superprobe at James Cook University. Monazite grains larger than 5 μm were easily located using this technique, but smaller grains probably went unnoticed. Because inclusions in and around porphyroblasts were targeted first, this procedure took less than 30 minutes per thin section, although this time was reduced if no monazite grains were located. Where monazite was found as inclusions in porphyroblasts, additional sections were examined. Monazite was also found to be present in the matrix of most samples (Table 1). Notable exceptions include the three kyanite-bearing samples listed above. A few samples contained monazite as inclusions in garnet and/or staurolite and four of these samples were selected for analysis. A summary of the microstructural/textural setting of monazites analysed is given in Table 2.

3.3. EPMA analysis

Thin sections were polished with 1 micron diamond paste and carbon-coated to approx 250 Å. BSE images were obtained for all monazite grains prior to quantitative analysis to identify compositional domains and/or assess zoning profiles Analyses were conducted on the JEOL JXA-8200 Superprobe at James Cook University using a 3 μm beam diameter (unless otherwise specified), accelerating voltage of 15 kV and Faraday cup current of 200 nA.. The elements Si, P, Ca, Y, La, Ce, Pr, Nd, Sm, Gd, Dy, Pb, Th and U were measured in a single analysis, with extended count times on Pb, U and Th to optimise statistical precision for chemical age dating. Calibrations were performed on the standards at 15kV and 20nA. The interferences of ThMζ and YLγ on PbMα, and ThMγ on UMβ were corrected post-analysis, using correction factors obtained from analysing the Th and Y standards (e.g., Scherrer et al., 2000; Pyle et al., 2002). All other background positions avoid interfering peaks and were selected based on wavelength scans of 8 well-characterised monazite grains with Th concentrations ranging from 2 to 11 wt %. Two-point linear backgrounds were used as no curvature or abnormality above baseline was detected in the area between chosen background points. Collimators were opened to maximum (3 mm), PHA settings were optimized and the Armstrong-CITZAF (phi-rho-z) matrix correction program (Armstrong, 1988; Armstrong, 1991) was used. Full details of the setup are given in Table 3.

The precision of each element in each individual analysis was calculated based on counting statistics using the equations in Scott et al. (1995) and Pyle et al. (2005). In addition to the elemental standards, a fragment of 555 ± 1 Ma Manangotry monazite (Horstwood et al., 2003) was used as a "consistency age standard" and was routinely analysed prior to and after the unknown monazites. Results of these analyses are included with the results of the unknowns.

In addition to the above, a single Y-elemental map was obtained for a garnet in sample CA17a. Operating conditions included an accelerating voltage of 15 kV, Faraday cup current of 1.10 μA, beam diameter/step size of 10 μm and dwell time of 120 milliseconds/pixel. The map was processed using the program ImageJ v. 1.34s (Rasband, 1997-2005).

3.4. Analytical concerns

Due to the size of many of the monazite grains analysed in this study (< 10 μm), a 1 μm beam diameter was regularly used to increase spatial resolution. This resulted in high totals for each analysis (101-103 wt %), compared to when a 3 or 5 μm beam was used (99-100 wt %). Recordings of absorbed current (nA) as a function of time (Fig. 5a) indicate that the absorbed current generally decreased when a 1 μm beam was used, but the total amount was variable (possibly a function of composition and quality of C-coat). In addition, the post-analysis bright spots (in BSE) on the surface of the monazites were more significant than when a defocused beam was used. Changes in absorbed current are thought to indicate a disequilibrium build-up of charge and/or changing electron emission characteristics, whereas the "bright spots" could be related to a compositional change (i.e. elemental loss) during analysis (see Jercinovic and

Williams (2005) for more details). Neither of these processes appear to have a significant effect on the measurement of Th, U or Pb (Fig. 5b) and hence no effect on the calculated ages. However, P and the LREE (e.g., La, Ce, Pr, Nd) concentrations appear to increase with a focussed beam, when measured late in the analysis and explain the (2-3 wt %) increase in totals (Kevin Blake pers. comm.). The protocol used here was later modified to minimise this, and the measurement order of elements was changed such that only backgrounds and minor matrix elements were being measured towards the end of the analysis (Fig. 5c). However, the majority of the analyses presented here were conducted using the earlier protocol. For referencing purposes, this will be designated "protocol A", while the modified version will be "protocol B". Whilst the concentrations of the LREEs, in protocol B are overestimated, this only had a minor effect on the matrix correction and is discussed below.

3.5. Monazite age and error calculation

BSE images, combined with quantitative elemental data were used to identify compositional domains in individual grains rather than elemental maps. In most cases BSE variation can be correlated with Th and/or Y zoning (e.g., Spear and Pyle, 2002). Where possible, multiple analyses were taken from within recognisable BSE domains, and once the quantitative data was available, individual points were re-allocated into different zones/domains if required. Individual dates were calculated for each point by inserting the Th, U, Pb concentrations into the age equation of Montel et al. (1996). Where compositional domains in a particular grain were either too small to adequately analyse, or the result of continuous compositional variation, the Y, Th and U composition of all analysed points were plotted with respect to their calculated dates (with associated 95% CI counting statistical errors obtained via Monte Carlo simulation (see Chapter 1)). If no significant correlation existed between these components and the calculated date, then these points were allocated into a date-domain. A mean date was calculated for each domain and 95% confidence intervals (CI) were generated by multiplying the standard error of the mean (SE) with the Student's-t value for (n-1) degrees of freedom (Siegel, 1988; Snedecor and Cochran, 1989).

Once the mean and confidence intervals were calculated for all domains, data from different monazite grains and/or domains were grouped together (if possible) based on additional information, such as chemical signature and/or textural setting. Where domains could be interpreted to be representative of a geologically significant event, the datasets were then combined via the weighted average procedure in Isoplot v3.10 (Ludwig, 2003).

4. Results

A total of fifteen monazite grains, in several different microstructural/textural settings were analysed and chemically dated. Mean "dates" (including errors) and summaries of the chemistry of each grain are shown in Table 4. The full dataset, including monazite compositions and counting errors are presented in Appendix D.

4.1. CA5

One small monazite grain (170E-mnz1), lying in the rim of a garnet porphyroblast (Fig. 6a) was analysed in sample CA5. The inclusion trails in this portion of the porphyroblast are continuous with the dominant matrix foliation, indicating that the growth of the porphyroblast rim probably occurred during the final (weak) stage of (sub-horizontal) crenulation development in this sample. The grain analysed is elongate and lies sub-parallel to the curved-portion of the inclusion trails (Fig. 6a). Only four analyses of this grain were possible, which resulted in a mean date of 327 ± 42 Ma. Excess Si, from the surrounding garnet was identified in the data (Fig. 6b), based on the expected concentration from the huttonite exchange in monazite (see Spear and Pyle, 2002, for more details). The contribution of this to the error is addressed below.

Three monazite grains were analysed in the matrix (Fig. 6 c, d, e), one is elongate, parallel to S_m (170E-mnz2), another is partially elongate relative to S_m (0E-mnz1), and the third grain has a blocky shape, but also lies within S_m (0E-mnz2). Grains 170E-mnz2 and 0E-mnz2 have relatively similar Y concentration values of approx 1.65 wt % (although 0E-mnz2 has a larger range in values), but 0E-mnz2 has two distinct Y zones of ca. 0.9 wt % and 1.6 wt % (Fig. 6f). This variation is correlative to Th, and is thought to indicate multiple stages of growth, with the second (higher Y) stage possibly corresponding with the growth of the other two monazites. If this is the case, it is not resolvable with the mean dates of the grains, as they all lie within error of each other (Table 4). Not enough data exists to calculate separate mean dates for the two zones in 0E-mnz1 either, as only four spots were analysed in the low-Y zone and three in the other (two are thought to be mixed or possibly be part of an intermediate zone).

4.2. CA14

Two small monazite grains, both lying elongate and sub-parallel/parallel to S_m, were analysed in sample CA14 (Fig. 7). Some Y and Th variation exists within these grains, although no chemical domains can be identified due to the lack of obtainable analyses. Both grains have near identical mean dates of 311 ± 31 Ma (mnz2) and 312 ± 40 Ma (mnz3).

4.3. CA17a

All monazite grains analysed in this sample are elongate and parallel to the preserved inclusion trails in garnet porphyroblasts (Fig. 8). Two grains lie within the core and two within the rim. The cores of garnet porphyroblasts are interpreted to have grown during the early stages of sub-horizontal differentiated crenulation cleavage, now preserved as inclusion trails within the rim and also the dominant matrix foliation. The rim is interpreted to have grown during sub-vertical crenulation development, responsible for the weak crenulation cleavage within the matrix. The intra-grain chemical trend (Th, U and Y decreasing and Ce increasing) is similar from core outwards for all grains, (Fig. 9a), but the two that lie within the cores of the porphyroblasts (mnz1, mnz4) have a slightly higher Th content than those in the rims. In addition there is a trend towards a higher Y content from monazite inclusions in the core relative to those in the rim, most evident in mnz4 (closest to grt core) and mnz2 (closest to grt rim). This however, does not correlate to the Y zoning of the garnet porphyroblast containing grains mnz1 and mnz2 (Fig. 9b, c), which shows a continuous depletion towards the rim. These trends reflect differences in Th and Y availability and possibly different ages of the monazite grains in the cores of the garnet porphyroblasts relative to those in the rims (see below). However, the mean dates of all four grains are within error (Table 4), indicating that any age difference between successive stages of monazite growth within this sample is unresolvable.

4.4. CA30

A total of five monazite grains were analysed in CA30, three as inclusions within garnet porphyroblasts and two within the matrix. Within the porphyroblasts, one (0B-mnz2) lay on the edge of a core zone and two (0E-mnz1, 0G-mnz1) lay in the inclusion trail free rim (Fig. 10). The lack of inclusions in the garnet rims makes the relative timing relationship with the matrix foliation uncertain, and also inhibits adequate correlation of these monazite grains relative to garnet. However, the grain interpreted to be within the outer edge of the garnet porphyroblast core, appears aligned with the core inclusion trails. This grain also has a distinctive high U, low Y chemistry relative to the others (Fig. 11), indicating increased U and decreased Y availability at the time of crystallisation, and potentially signifying that this grain is a different age to those in the garnet rim. Like sample CA17a above, the mean dates of all monazite inclusions within garnet are within error (Table 4), again highlighting an unresolvable age difference between potentially two stages of monazite growth.

The monazite grains analysed within the matrix (0E-mnz2, 0G-mnz2) were found to have a relatively similar composition, although the latter has slightly more intra-grain Th variation. This grain is also more elongate, parallel to S_m (Fig. 12). The calculated mean dates of both grains are similar (326 ± 27 Ma and 335 ± 23 Ma respectively) and within error of the matrix grains from other samples.

4.5. Additional errors from excess LREE or Si

An attempt to semi-quantify the effect on the resultant dates due to excess LREE concentrations in "protocol A" (see above) was made by comparing the concentrations of La, Ce, Pr and Nd to monazite grains with similar Th, U and Y contents analysed with "protocol B". As such, additional LREE concentrations were roughly estimated to be around 5% (each), which easily accounts for the additional 2-3 wt % in measured concentration totals inherent in this protocol. Reducing the concentrations of La, Ce, Pr, Nd in the matrix correction by this amount has only a minimal effect on the Pb, U and Th concentrations and the calculated date decreases by less than 0.1 Ma.

Several of the analyses of monazite inclusions in garnet (CA5-170E-mnz1, in particular), contain excess Si that appears to be due to the electron beam partially sampling a portion of the surrounding porphyroblast (Table 4). Unintentional sampling of surrounding/adjacent minerals in EPMA analyses generally can be attributed to operator/instrumental error, and such analyses are usually discarded. In the examples here, the size of the monazite grains relative to the electron beam meant that even slight inaccuracies in beam alignment resulted in minor co-sampling of garnet. Whilst the analytical error associated with grain edges is not certain (possible scattering of X-rays), it appears not to significantly effect the relative measurements of Pb, U and Th (although the intensities may be reduced). In addition, any potential interference relating to Y in garnet (expected to be minimal) will be corrected for as the YLγ on PbMα overlap is already addressed in the monazite analytical protocol. Due to the minimal number of monazite inclusions in garnet suitable for dating and their small size, these analyses were retained here and an assessment made based on the potential effect the matrix correction. In the case of CA5-170E-mnz1, an additional 1 wt % SiO_2

was thought to be derived from garnet. This value was estimated by comparing measured SiO_2 to the expected amount that should be incorporated in the monazite structure due to the huttonite exchange (Fig. 6b). Excess CaO is considered negligible based on an assumption of SiO_2 being roughly an order of magnitude greater than CaO in a typical pelitic garnet. Removing the excess Si (in the matrix correction) increases the calculated dates by less than 1 Ma. As a result, all monazite grains with excess Si in one or more analyses have an additional ± 1 Ma included in the CI displayed in Table 4. The additional errors associated with excess LREE concentrations in protocol A (± 0.1 Ma) are ignored.

5. Discussion

5.1. Monazite behaviour during foliation development

During the latter stages of differentiated crenulation cleavage development, the matrix reconstitutes as deformation and metamorphism take place (Bell, 1986). This involves the deformation, recrystallisation, dissolution and solution transfer and removal of non-platy minerals (such as quartz), from the zones of progressive shearing, and the recrystallisation of the phyllosilicates left behind in the cleavage seams (Bell and Cuff, 1989). Monazite grains in this environment should plastically deform and recrystallise or be plastically deformed along their margins, dissolved, undergo solution transfer and nucleate as new grains in zones of progressive shortening (Bell and Welch, 2002). Both these processes would also be expected to reset the Th-U-Pb isotope systematics of the grains (Bell and Welch, 2002). Many of the monazite grains analysed in this study are elongate, lie sub-parallel to parallel with the trend of the matrix foliation and (some) show chemical zoning from the core towards the tips (e.g., Fig. 6, 8). Thus they are interpreted to have nucleated and grown, or recrystallised during the final stages of differentiated crenulation cleavage development, with the zoning representing changing cation availability during continuous growth or new growth over recrystallised grains. If this is the case, the age of monazite grains in this microstructural setting should be the same as the foliation in which they lie. The rotation and/or elongation of previous grains without isotopic resetting, is only likely to occur during the early stages (1 and 2) of crenulation development, prior to the reconstitution of the matrix. In this case, the ages of the grains should represent the age of the foliation being crenulated.

Factors such as grain size (both matrix and monazite), shape, direction of compression relative to pre-existing grains, and the stage of differentiated crenulation cleavage development may result in only partial progression of these processes. As such portions of grains may survive deformation. For example, a grain within sample CA5 (0E-mnz1) preserves evidence of an earlier foliation event, with subsequent (over) growth related to the development of a later foliation (Fig. 13). The growth history is supported by distinct Y-domains, and in this case, the "tails" on the grain indicate the shear sense (Fig. 13) during the development of the differentiated crenulation cleavage (S_m). Similar overgrowths on relic grains in other studies have been used to date distinct deformational events (e.g., Shaw et al., 2001; Williams and Jercinovic, 2002). Clearly, the behaviour of monazite during foliation development is highly variable and each grain needs to be interpreted individually.

5.2. Correlation of monazite grains to periods of foliation development and/or porphyroblast growth

The elongate monazite inclusions, lying parallel to the inclusion trails in the garnet porphyroblasts in sample CA17a, are most important in testing the assumption that grains in successive fabrics should be younger. The two monazite inclusions within the core are interpreted to have grown during the development of the sub-vertical foliation, which was later overgrown by garnet during the early stages of sub-horizontal differentiated crenulation cleavage development. The monazite grains in the rims of these garnets are also interpreted to have grown during this latter event. Therefore, the timing of garnet porphyroblast core growth should be able to be constrained to the interval between the ages of these two groups of monazite grains. However, this interval is too close to resolve with the data obtained in this study (see above). Nevertheless, the Y content of the grains may be a more useful indicator of differences in timing. As outlined above, the trend of increasing Y content within monazite grains towards the porphyroblast rims is opposite to the Y zoning of the garnet porphyroblast(s), which shows a continuous depletion towards the rim (Fig. 9b, c).

When xenotime and monazite coexist, xenotime is thought to buffer the activity of YPO_4 in monazite, partitioning Y more strongly at lower grades, with the value of this coefficient decreasing with increasing temperature (Pyle et al., 2001). In essence the activity of the YPO_4 component in monazite will increase with increasing T. When xenotime reacts out, Y is then partitioned between garnet and monazite, thus the YPO_4 content of monazite becomes a function of metamorphic grade, the monazite/garnet ratio and the effective bulk composition of Y (which is probably enriched due to xenotime breakdown). Whilst the modal (volumetric) uptake of Y by garnet is 2-3 orders of magnitude greater than monazite (Pyle et al., 2001), the decreased ability of garnet to partition Y as T increases (Pyle and Spear, 2000) may result in more Y being incorporated into growing monazite. In the case of sample CA17a, the earliest monazite grain analysed (Mnz1) is interpreted to have co-existed with xenotime and is situated within the garnet porphyroblast core (Fig. 8d). The actual core of this (monazite) grain has a lower Y content relative to the cores of the other analysed grains (Fig. 9a). Based on the argument above, subsequent monazite grains in equilibrium with xenotime should incorporate more Y as the temperature increases, but the demise of xenotime from the system after the growth of the garnet core removed the mass-balance constraint for Y partitioning. Nevertheless, the combination of xenotime breakdown within the matrix and the decreased ability of garnet to partition Y as T increases, still explains the presence of monazite grains with higher Y contents preserved within the garnet porphyroblast rims, and thus a subsequent foliation. This would strongly suggest that the monazite grains in the garnet porphyroblast rims postdate the grains within the cores (and also xenotime), supporting the assumption that the age of elongate monazite grains, within and parallel to a foliation generally represent when that foliation formed. The actual monazite intra-grain Y decrease (related to an increase in Ce and decrease Th, U) can be possibly caused by local constraints associated with nearby garnet porphyroblast growth removing and sequestering some of the available Y that would otherwise have been incorporated into monazite.

Within sample CA30, a similar pattern of a lower Y monazite grain (0B-mnz2), lying sub-parallel to inclusion trails within the (edge of the) core of a garnet porphyroblast, compared to higher Y grains (0E-mnz1, 0G-mnz1) within the rims is also observed. Although no Y or xenotime location maps were obtained for this sample, this might still suggest that the ages of these monazite grains should be different. The mean date of the monazite inclusion within the core (309 ± 22 Ma) probably represents the age of the foliation that is now preserved as inclusion trails within that portion of the garnet. The lack of inclusion trails within the porphyroblast rims implies that grains 0E-mnz1 and 0G-mnz1 can only be used to constrain the maximum timing of the surrounding garnet growth.

The monazite inclusion (170E-mnz1) within the rim of the garnet porphyroblast in sample CA5 is interpreted to be a grain that was rotated during the development of the weak crenulation, synchronous with the growth of the porphyroblast rim. Assuming that no recrystallisation or internal deformation of this grain occurred, the mean date (327 ± 42 Ma) represents the maximum age for growth of the porphyroblast rim. Based on microstructural relationships, this grain should be equivalent in age to 170E-mnz2, which lies elongate and parallel to the sub-vertical S_m and possibly grain 0E-mnz2, although this correlation is less certain. As discussed above, these grains must postdate the earliest stage of grain 0E-mnz1, although the tails on this grain are most likely the same age. Unfortunately, no adequate mean date could be calculated for this initial stage of monazite growth, thus no tighter constraints can be placed on the timing of garnet porphyroblasts in this sample.

The three monazite grains in sample CA5, interpreted to have formed/recrystallised during the development of S_m can be correlated to microstructurally equivalent grains in samples CA14 (grains within S_m), CA17a (grains within garnet porphyroblast rims), and CA30 (grains within S_m). The weighted mean of these nine monazite grains is 324 ± 9 Ma (MSWD = 1.7), which represents the best estimate of the age of the development of S_m and the maximum age of the garnet porphyroblast rims within these samples (Fig. 14a). The weighted mean of all grains dated in this study (Fig. 14b) is 322 ± 4 Ma (MSWD = 1.4), which signifies the average

age of peak metamorphism (more specifically, metamorphism above the monazite isograd) in these samples.

5.3. Interpretation of ages

Although monazite was analysed in several different microstructural and textural settings, the mean dates of all the grains are inseparable (range: 304-335 Ma, without errors), with a weighted mean of 322 ± 4 Ma (MSWD = 1.4). Therefore, these monazite grains record ages that correlate to the Alleghanian Orogeny, which is very significant given this event previously was not known to cause regional metamorphism this far inland. Whilst only limited time constraints can be placed on the timing of garnet growth, it would appear that all porphyroblast growth occurred during the Alleghanian in sample CA17a. Many of the porphyroblasts in other samples preserve additional sets and/or different orientations of inclusion trails (Stallard and Hickey, 2001; Stallard et al., 2003), possibly indicating different ages of porphyroblast growth. Despite this, it would appear that all garnet grade (and above) metamorphism in this portion of the Dahlonega Gold Belt occurred during the Alleghanian. Further work would be required to confirm this assumption. The inseparable mean dates of monazite grains in two distinct foliations (e.g., sample CA17a) also possibly indicates that deformation was relatively continuous throughout this period.

Analyses on the Manangotry standard (Table 4), would suggest (at 95 % confidence) that the maximum error in accuracy for the data presented here be around ± 18 m.y. (based on the largest error interval on Manangotry relative to the assumed age of 555 ± 1 Ma). Most of the analyses on this standard resulted in mean dates below, but within error of this age, implying that these results presented herein are more likely to be younger than their true ages, rather than older. Nevertheless, it would be highly unlikely that the interpretation that these monazite grains preserve Alleghanian ages would change with more accurate analyses.

5.4. Tectonic implications of ages

Alleghanian metamorphism and ductile deformation in this portion of the Appalachians does not fit into any previously published tectonic synthesis. Regional metamorphism and deformation related to this event has been recognised in the Kiokee (Snoke et al., 1980; Secor et al., 1986), Raleigh (Russell et al., 1985) and Kings Mountain belts (Horton et al., 1987), and corresponding terrains further north into Virginia and Maryland. In the vicinity of the Dahlonega Gold Belt, only evidence of Taconic and/or Acadian metamorphism has been reported (Dallmeyer, 1978; Dallmeyer, 1988; Kish, 1990; Connelly and Dallmeyer, 1993; Goldberg and Dallmeyer, 1997; Miller et al., 2000). Assuming that the movement of the Blue Ridge Thrust Complex was ca. 310-300 Ma (based on Rb-Sr resetting in mylonites (Su and Fullagar, 1995)), the ages presented here can be placed in a suitable timeframe for metamorphism prior to or synchronous with the commencement of thrusting. More work to constrain the extent of these ages is required, but it is proposed that after Early Ordovician deposition of the rocks examined in this study, initial burial was driven by the collision of Avalon during the Acadian Orogeny. Some metamorphism and deformation around this time may have occurred, and cannot be ruled out with the available data. Assuming that these rocks remained relatively deep in the crust, deformation and/or further burial associated with the earliest stages of the collision with Africa, during the Alleghanian may have either preferentially partitioned into these rocks, or affected a wider area than currently exposed. Continued compression resulted in the development of numerous thrusts, culminating in the detachment along which the Piedmont and Blue Ridge provinces were thrust towards the continental interior as part of a massive thrust sheet (Hatcher, 1987b; Hatcher and Goldberg, 1991). Movement associated with early thrusting during the waning stages of ductile deformation, may have contributed to the present day orientation of the matrix foliation(s).

Whilst the setting of Alleghanian metamorphism within this portion of the Appalachians presented above is preliminary and explains the results obtained here, the lack of Alleghanian metamorphism in adjacent terrains still needs to be addressed; particularly east of the Chattahoochee Fault. In the vicinity of this study, the Chattahoochee Fault separates Dahlonega Belt rocks from higher grade migmatitic rocks (eastern Sandy Springs Group), essentially defining a distinct tectonic and lithologic boundary between the gold belt and the rest of the eastern Blue Ridge (German, 1989). Muscovite and biotite $^{40}Ar/^{39}Ar$ ages, from within the eastern Blue Ridge (Dallmeyer, 1988), record similar ages to this study (ca. 325 – 305 Ma), although these have been interpreted to date postmetamorphic (Acadian) cooling through the closure temperature of these minerals. One tentative theory would be that these ages record resetting of isotopic systematics in response to Alleghanian thermal effects, with no discernable impact on higher-grade metamorphic textures. This would also imply that the metamorphism in this terrain occurred earlier in the Acadian than previously thought. Therefore, if Alleghanian amphibolite facies metamorphism did not affect these rocks, then it seems that either deformation partitioned exclusively through the Dahlonega Gold Belt, leaving adjacent rocks unaffected, or these effects are not preserved at present surface levels.

6. References

Abrams, C.E. and McConnell, K.I., 1984. Geologic Setting of Volcanogenic Base and Precious Metal Deposits of the West Georgia Piedmont: A Multiply Deformed Metavolcanic Terrain. Economic Geology, 79, 1521-1539.

Armstrong, J.T., 1988. Quantitative analysis of silicate and oxide materials: Comparison of Monte Carlo, ZAF and Φ (ρz) procedures. In: D.E. Newbury (Editor), Microbeam Analysis. San Francisco Press.

Armstrong, J.T., 1991. Quantitative elemental analysis of individual microparticles with electron beam instruments. In: K.F.J. Heinrich and D.E. Newbury (Editors), Electron Probe Quantitation. Plenum Press.

Bell, T.H., 1986. Foliation development and reactivation in metamorphic rocks: the reactivation of earlier foliations and decrenulation due to shifting patterns of deformation partitioning. Journal of Metamorphic Geology, 4, 421-444.

Bell, T.H. and Cuff, C., 1989. Dissolution solution transfer diffusion versus fluid flow and volume loss during deformation/metamorphism. Journal of Metamorphic Geology, 7, 425-447.

Bell, T.H. and Welch, P.W., 2002. Prolonged Acadian orogenesis: revelations from foliation intersection axis (FIA) controlled monazite dating of foliations in porphyroblasts and matrix. American Journal of Science, 302, 549-581.

Bream, B.R., Hatcher, R.D., Jr., Miller, C.F. and Fullagar, P.D., 2004. Detrital zircon ages and Nd isotopic data from the Southern Appalachian crystalline core, Georgia, South Carolina, North Carolina, and Tennessee: New provenance constraints for part of the Laurentian margin. In: R.P. Tollo, L. Corriveau, J. McLelland and M.J. Bartholomew (Editors), Proterozoic tectonic evolution of the Grenville Orogen in North America. Geological Society of America Memoir, Boulder, Colorado, pp. 459-475.

Butler, J.R., 1973. Paleozoic deformation and metamorphism in part of the Blue Ridge thrust sheet, North Carolina. American Journal of Science, 273-A, 72-88.

Cocherie, A. and Albarede, F., 2001. An improved U-Th-Pb age calculation for electron microprobe dating of monazite. Geochimica et Cosmochimica Acta, 65 (24), 4509-4522.

Connelly, J.B. and Dallmeyer, R.D., 1993. Polymetamorphic evolution of the western Blue Ridge: Evidence from ^{40}Ar/^{39}Ar whole-rock slate/phyllite and muscovite ages. American Journal of Science, 293 (4), 322-359.

Dallmeyer, R.D., 1978. (super 40) Ar/ (super 39) Ar incremental-release ages of hornblende and biotite across the Georgia Inner Piedmont; their bearing on late Paleozoic-early Mesozoic tectonothermal history. American Journal of Science, 278 (2), 124-149.

Dallmeyer, R.D., 1988. Late Paleozoic tectonothermal evolution of the western Piedmont and eastern Blue Ridge, Georgia: Controls on the chronology of terrane accretion and transport in the southern Appalachian orogen. Geological Society of America Bulletin, 100 (5), 702-713.

German, J.M., 1989. Geologic Setting and Genesis of Gold Deposits of the Dahlonega and Carroll County Gold Belts, Georgia. Economic Geology, 84 (4), 903-923.

Glover, L., Speer, J.A., Russell, G.S. and Farrar, S.S., 1983. Ages of Regional Metamorphism and Ductile Deformation in the Central and Southern Appalachians. Lithos, 16 (3), 223-245.
Goldberg, S.A. and Dallmeyer, R.D., 1997. Chronology of Paleozoic metamorphism and deformation in the Blue Ridge thrust complex, North Carolina and Tennessee. American Journal of Science, 297, 488-526.
Hatcher, R.D., Jr., 1972. Developmental Model for the Southern Appalachians. Geological Society of America Bulletin, 83 (9), 2735-2760.
Hatcher, R.D., Jr., 1978. Tectonics of the western Piedmont and Blue Ridge, Southern Appalachians: Review and speculation. American Journal of Science, 278 (3), 276-304.
Hatcher, R.D., Jr., 1987a. Bedrock geology and regional geologic setting of Coweeta Hydrologic Laboratory in the eastern Blue Ridge. In: W.T. Swank and D.A. Crossley, Jr. (Editors), Forest hydrology and ecology at Coweeta, Ecological Studies 66. Springer-Verlag, Berlin, pp. 81-92.
Hatcher, R.D., Jr., 1987b. Tectonics of the Southern and Central Appalachian Internides. Annual Review of Earth and Planetary Sciences, 15, 337-362.
Hatcher, R.D., Jr. and Goldberg, S.A., 1991. The Blue Ridge geologic province. In: J.W. Horton, Jr. and V.A. Zullo (Editors), The Geology of the Carolinas (Carolina Geological Society Fiftieth Anniversary Volume). Univ. Tenn. Press, Knoxville, TN, pp. 11-35.
Hatcher, R.D. and Odom, A.L., 1980. Timing of thrusting in the southern Appalachians, USA: model for orogeny? Journal of the Geological Society, 137, 321-327.
Holm, C.S. and Farmer, M.R., 2002. Detailed geologic mapping of the eastern/western Blue Ridge terrane bounding Allatoona Fault of northwestern Georgia. Geological Society of America, Abstracts with Programs, 34 (2), 11.
Horstwood, M.S.A., Foster, G.L., Parrish, R.R., Noble, S.R. and Nowell, G.M., 2003. Common-Pb corrected in situ U-Pb accessory mineral geochronology by LA-MC-ICP-MS. Journal of Atomic Spectrometry, 18, 837-846.
Horton, J.W., Jr., Sutter, J.F., Stern, T.W. and Milton, D.J., 1987. Alleghanian Deformation, Metamorphism, and Granite Emplacement in the Central Piedmont of the Southern Appalachians. American Journal of Science, 287, 635-660.
Jercinovic, M.J. and Williams, M.L., 2005. Analytical perils (and progress) in electron microprobe trace element analysis applied to geochronology: Background acquisition, interferences, and beam irradiation effects. American Mineralogist, 990, 526-546.
King, P.B., 1955. A geologic section across the southern Appalachians. An outline of the geology in the segment in Tennessee, North Carolina, and South Carolina. In: R.J. Russell (Editor), Guides to southeastern geology. Geological Society of America, New York, pp. 332-373.
Kish, S.A., 1990. Timing of Middle Paleozoic (Acadian) Metamorphism in the Southern Appalachians - K-Ar Studies in the Talladega Belt, Alabama. Geology, 18, 650-653.
Kretz, R., 1983. Symbols for rock-forming minerals. American Mineralogist, 68, 277-279.
Ludwig, K.R., 2003. User's manual for Isoplot 3.0; a geochronological toolkit for Microsoft Excel, Berkeley Geochronology Centre, Special Publication No. 4.

Miller, B.V., Stewart, K., G., Miller, C.F. and Thomas, C.W., 2000. U-Pb ages from the Bakersville, North Carolina eclogite; Taconian eclogite metamorphism followed by Acadian and Alleghanian cooling. Geological Society of America, Abstracts with Programs, 32, 62.

Montel, J.-M., Foret, S., Veschambre, M., C, N. and Provost, A., 1996. Electron microprobe dating of monazite. Chemical Geology, 131, 37-53.

Pyle, J.M. and Spear, F.S., 2000. An empirical garnet (YAG) - xenotime thermometer. Contributions to Mineralogy and Petrology, 138, 51-58.

Pyle, J.M., Spear, F.S., Rudnick, R.L. and McDonough, W.F., 2001. Monazite-xenotime-garnet equilibrium in metapelites and a new monazite-garnet thermometer. Journal of Petrology, 42, 2083-2107.

Pyle, J.M., Spear, F.S. and Wark, D.A., 2002. Electron Microprobe Analysis of REE in Apatite, Monazite and Xenotime: Protocols and Pitfalls. Reviews in Mineralogy and Geochemistry, 48, 337-362.

Pyle, J.M., Spear, F.S., Wark, D.A., Daniel, C.G. and Storm, L.C., 2005. Contributions to the precision and accuracy of chemical ages of monazite. American Mineralogist, 90, 547-577.

Rasband, W.S., 1997-2005. ImageJ. U. S. National Institutes of Health, Bethesda, Maryland, USA, http://rsb.info.nih.gov/ij/.

Russell, G.S., Russell, C.W. and Farrar, S.S., 1985. Alleghanian deformation and metamorphism in the eastern North Carolina Piedmont. Geological Society of America Bulletin, 96, 381-387.

Scherrer, N.C., Engi, M., Gnos, E., Jakob, V. and Liechti, A., 2000. Monazite analysis; from sample preparation to microprobe age dating and REE quantification. Schweizerische Mineralogische und Petrographische Mitteilungen, 80 (1), 93-105.

Scott, V.D., Love, G. and Reed, S.J.B., 1995. Quantitative Electron-Probe Microanalysis (2nd edition). Ellis Horwood Ltd, Chichester.

Secor, D.T., Snoke, A.W., Bramlett, K.W., Costello, O.P. and Kimbrell, O.P., 1986. Character of the Alleghanian orogeny in the southern Appalachians: Part I. Alleghanian deformation in the eastern Piedmont of South Carolina. Geological Society of America Bulletin, 97, 1319-1328.

Settles, D.J., Bream, B.R. and Hatcher, R.D., 2001a. The Sally Free mafic complex and associated mafic rocks of the Dahlonega gold belt; evidence of Ordovician arc volcanism and intrusion northwest of Dahlonega, Georgia. Geological Society of America, Abstracts with Programs, 33 (6), 262.

Settles, D.J., Hatcher, R.D. and Bream, B.R., 2001b. Tectonostratigraphic relationships that define a fundamental Appalachian Terrane boundary within the central Blue Ridge of North Georgia. Geological Society of America, Abstracts with Programs, 33 (2), 66.

Shaw, C.A., Karlstrom, K.E., Williams, M.L., Jercinovic, M.J. and McCoy, A.M., 2001. Electron-microprobe monazite dating of ca. 1.71-1.63 Ga and ca. 1.45-1.38 Ga deformation in the Homestake shear zone, Colorado: Origin and early evolution of a persistent intracontinental tectonic zone. Geology, 29, 739-742.

Siegel, A.F., 1988. Statistics and Data Analysis. John Wiley & Sons, New York.

Snedecor, G.W. and Cochran, W.G., 1989. Statistical Methods, Eighth Edition. Iowa State University Press.

Snoke, A.W., Kish, S.A. and Secor, D.T., Jr., 1980. Deformed Hercynian granitic rocks from the Piedmont of South Carolina. American Journal of Science, 280, 1018-1034.
Spear, F.S. and Pyle, J.M., 2002. Apatite, Monazite, and Xenotime in Metamorphic Rocks. Reviews in Mineralogy and Geochemistry, 48, 293-335.
Stallard, A.R. and Hickey, K.A., 2001. Shear zone vs folding origin for spiral inclusion trails in the Canton Schist. Journal of Structural Geology, 23 (12), 1845-1864.
Stallard, A.R., Hickey, K.A. and Upton, G.J., 2003. Measurement and correlation of microstructures: the case of foliation intersection axes. Journal of Metamorphic Geology, 21 (3), 241-252.
Su, Q. and Fullagar, P.D., 1995. Rb-Sr and Sm-Nd Isotopic Systematics During Greenschist Facies Metamorphism and Deformation: Examples from the Southern Appalachian Blue-Ridge. Journal of Geology, 103 (4), 423-436.
Williams, M.L. and Jercinovic, M.J., 2002. Microprobe monazite geochronology: putting absolute time into microstructural analysis. Journal of Structural Geology, 24, 1013-1028.

CHAPTER 4

PRESERVATION OF MULTIPLE STAGES OF PORPHYROBLAST AND MONAZITE GROWTH THROUGH INTENSE ALLEGHANIAN DEFORMATION AND METAMORPHISM

Abstract

Quantitative compositional analyses and chemical dates of 37 monazite grains in 9 different samples from the north eastern flank of the Pelham Dome, north central Massachusetts, show that the majority of preserved metamorphic textures are Late Pennsylvanian (Alleghanian) in age. However, some garnet porphyroblasts which preserve an extended microstructural history contain monazite inclusions that are up to 60 million years older than those dated within the bulk of the metamorphic mineral assemblage. Where possible, these monazite grains are correlated to periods of garnet porphyroblast growth using qualitative indicators such as yttrium maps, to infer equilibrium between the phases. The ages show that garnet-grade, Late Acadian metamorphism is preserved within these samples, despite subsequent garnet, staurolite and kyanite garnet occurring in the later event. Late Pennsylvanian deformation and metamorphism culminated in intense shearing, which truncated all foliations defined by inclusion trails in porphyroblasts as a result of the rocks of the Northfield Syncline being thrust a large distance south-ward over the gneisses in the Pelham Dome.

1. Introduction

Three Palaeozoic orogenic events dominate in the New England Appalachians; the Taconian (Middle to Late Ordovician), the Acadian (Latest Silurian to Middle Devonian), and the Alleghanian (Permian). These events are interpreted to be a result of the collision of the southern margin of Laurentia with an island arc, collision between Laurentia with the Avalon micro-continent, and collision between Laurentia (and accreted terrains) with Africa (Robinson et al., 1998). Although the effects of these events generally trend progressively to the east (Armstrong et al., 1992), significant overprinting plus local variations in intensity and timing complicate correlation of metamorphism with particular events (e.g., Tucker and Robinson, 1990; Moecher and Wintsch, 1994; Moecher, 1999). An increasing number of isotopic ages (both igneous and metamorphic) do not fit into the regionally defined episodes mentioned above (Robinson et al., 1992; Thomson et al., 1992), indicating that Appalachian orogenesis was more complex than originally realised.

Garnet porphyroblasts have been used extensively in orogenic belts such as the Appalachians to gain insights into the pressure-temperature path (e.g., Tracy et al., 1976; Spear and Selverstone, 1983) and the foliation development history (Bell and Hayward, 1991; Williams, 1994; Stallard and Hickey, 2001; Bell et al., 2003). Inclusion trails commonly record extended histories of foliation development, because porphyroblasts grow episodically (assuming thermodynamic equilibrium criteria are met) as a consequence of deformation partitioning through different portions of the crust at different times (Bell et al., 1998; Bell et al., 2004). This allows determination of the deformation and metamorphic history that predates the development of matrix foliations that are finally preserved in a rock (Bell and Hickey, 1999; Bell and Kim, 2004). Whilst garnet porphyroblasts may record growth zoning profiles for a particular sample, several of the possible pulses of growth may not be chemically detectable, due to variation in the distribution of deformation partitioning (Bell et al., 2004). Therefore, in multiply tectonised terrains, characterisation of the earlier stages of metamorphism and deformation requires the correlation of inclusion trails across a region. One such method is the measurement of foliation intersection/inflection axes preserved in porphyroblasts (FIAs), to determine the relative timing of porphyroblast growth region (Bell et al., 1998; Stallard et al., 2003; Bell et al., 2004; Cihan and Parsons, 2005).

Radiogenic minerals such as monazite are commonly included in garnet and can be dated to provide a maximum timing constraint on the enveloping phase. If interpreted to have grown during the development of the foliation responsible for preserved inclusion trails, the age of these monazite grains represents the age of the foliation that immediately pre-dates porphyroblast growth (e.g., Bell et al., 1986). Where monazite grains can be dated in multiple generations of inclusion trials (e.g., different FIAs), constraints on porphyroblast growth can become more clearly defined, and used to demonstrate episodic porphyroblast growth across a region (e.g., Bell and Welch, 2002). Demonstrating equilibrium between monazite and garnet (Pyle et al., 2001), can lead to absolute ages being translated to surrounding sections of porphyroblasts, further constraining the age of a point along a P-T path. Since metamorphic monazite inclusions are commonly small and compositionally complex, chemical dating using the fine spatial resolution of the electron probe microanalyser (EPMA) is the preferred approach for this work. This technique is proving to be increasingly popular (e.g., Suzuki and Adachi, 1991; Montel et al., 1996; Cocherie et al., 1998; Williams et al., 1999; Bell and Welch, 2002; Goncalves et al., 2004), and compares well with ages obtained via isotopic methods (Montel et al., 1996; Kohn and Malloy, 2004; Dahl et al., 2005; Pyle et al., 2005).

This study will present the results of chemical dating of monazite in schists that overly the north eastern margin of the Pelham Dome, Massachusetts. The samples contain monazite inclusions in garnet (and staurolite) porphyroblasts that span the range of FIA sets determined for the region as well as the matrix and record an extended metamorphic history. All monazite grains are correlated (where possible) to the microstructures in which they lie and for selected samples, yttrium elemental maps of garnet porphyroblasts were used to qualitatively assess the equilibrium between phases. This provided some insight into the earliest recorded metamorphism in this portion of New England.

2. Geological background

The Pelham Dome, a series of Late Ordovician gneisses, and a cover sequence of Ordovician, Silurian and Devonian meta-sedimentary and meta-volcanic rocks (Fig. 1) are the main constituents of this portion of the Bronson Hill anticlinorium (Tucker and Robinson, 1990; Robinson et al., 1992; Robinson et al., 1998). The Late Proterozoic gneisses within the Pelham Dome represent the only known exposure of this age in the region and have been interpreted to be a fragment of the Avalon micro-continent, thrust beneath surrounding rocks during the late Palaeozoic (Getty and Gromet, 1992). Late Acadian (ca. 360 Ma) metamorphism, as evident in the granulite facies central Massachusetts metamorphic high was thought to be widespread, but was overprinted around the vicinity of the Pelham Dome in the Late Pennsylvanian (Robinson et al., 1998). As a consequence, U-Pb dating of monazite, zircon and titanite grains, plus ^{40}Ar-^{39}Ar ages from hornblende in the dome gneisses and the cover sequences has resulted in ages around 300-290 Ma (Spear and Harrison, 1989; Harrison et al., 1989; Tucker and Robinson, 1990; Robinson et al., 1992). On the eastern flank of the Pelham Dome (Fig. 2), relict Late Acadian Kfs-Sil-Grt assemblages have been documented within the Ordovician (?) Mount Mineral Formation (Moecher, 1999), overprinted by Ky-St grade metamorphism in the Late Pennsylvanian. The contact between the cover sequences and the Pelham Dome is characterised by pervasively sheared rocks (locally mylonitic), with a strong, top-to-the-south N-S mineral elongation lineation (Peterson and Robinson, 1993), that is also present in and around the dome.

3. Description of samples and previous work

Eight Grt + St ± Ky (mineral abbreviations from Kretz (1983)) grade samples of Devonian Littleton Formation and a sample from the Mount Mineral Formation were used in this study (Fig. 2). Seven of the Littleton samples were taken from within the Northfield Syncline, on the northern flank of the Pelham Dome with the other from the Wendell Syncline (Table 1). All samples contain garnet porphyroblasts with inclusion trails (truncated by the matrix foliation) enabling a correlation between deformation and relative timing of mineral growth. As such a complex deformation history has been recognised using the FIA method, on an extended sample set, which includes the samples described herein (Bell et al., 2004; Bell and Kim, 2004). This work showed that growth of multiple generations of garnet porphyroblasts has preserved FIAs trending successively SE-NW, SW-NE, W-E, NNW-SSE and SSW-NNE. The samples for monazite dating were chosen as they cover the range of FIAs identified above, and thus the largest possible period of deformational and metamorphic history. A subsequent study (Kim and Bell, 2005), provided P-T estimates for the early stages of garnet porphyroblast growth in five samples, two of which (K53, M54) are included here. The location of monazite inclusions with respect to preserved microstructures in garnet porphyroblasts prevented an attempt to date FIAs as in Bell and Welch (2002). The microstructural/textural location of each monazite dated is outlined in Table 2.

4. Analytical procedures

4.1. EPMA analysis

Thin sections were polished with 1 micron diamond paste and carbon-coated to approx 250 Å. BSE images were obtained for all monazite grains prior to quantitative analysis to identify compositional domains and/or assess zoning profiles Analyses were conducted on the JEOL JXA-8200 Superprobe at James Cook University using a 3 μm beam diameter (unless otherwise specified), accelerating voltage of 15 kV and Faraday cup current of 200 nA. The elements Si, P, Ca, Y, La, Ce, Pr, Nd, Sm, Gd, Dy, Pb, Th and U were measured in a single analysis, with extended count times on Pb, U and Th to optimise statistical precision for chemical age dating. Calibrations were performed on the standards at 15kV and 20nA. The interferences of ThMζ and YLγ on PbMα, and ThMγ on UMβ were corrected post-analysis, using correction factors obtained from analysing the Th and Y standards (e.g., Scherrer et al., 2000; Pyle et al., 2002). All other background positions avoid interfering peaks and were selected based on wavelength scans of 8 well-characterised monazite grains with Th concentrations ranging from 2 to 11 wt %. Two-point linear backgrounds were used as no curvature or abnormality above baseline was detected in the area between chosen background points. Collimators were opened to maximum (3 mm), PHA settings were optimized and the Armstrong-CITZAF (phi-rho-z) matrix correction program (Armstrong, 1988; Armstrong, 1991) was used. Full details of the setup are given in Table 3.

The precision of each element in each individual analysis was calculated based on counting statistics, using the equations in Scott et al. (1995) and Pyle et al. (2005). A fragment of 555 ± 1 Ma Manangotry monazite (Horstwood et al., 2003) was used as a "consistency age standard", and was regularly analysed over the period that the data was obtained (Fig. 3).

Yttrium elemental maps of garnet were obtained using the following operating conditions; an accelerating voltage of 15 kV, Faraday cup current of 1.10 μA, beam diameter/step size of 10 μm and dwell time of 120 milliseconds/pixel. Maps were processed using the program ImageJ v. 1.34s (Rasband, 1997-2005).

4.2. Analytical concerns

Most of the of analytical concerns relating to protocols "B" and "C" are addressed in Chapters 2 and 3, and the majority of that discussion is applicable here. A particular concern with regard to protocol "A" are the uncertainties related to using "fixed" elemental concentrations for the matrix correction. This is difficult to assess as most "compositional domains" are not large enough to obtain sufficient Y, Pb, Th and U analyses and an additional analysis for the matrix elements. Furthermore, domains are generally not truly homogeneous and some variation usually exists between the spot locations. The affect on calculated dates with respect to varying the concentration of fixed elements in the matrix correction was discussed in Pyle et al. (2005). In that study, the calculated dates varied by only ± 1 Ma when individual elements were increased by approximately two standard deviations relative to an average pelitic monazite composition. A similar value was obtained in Chapter 1 by calculating dates for the maximum and minimum cumulative 2σ counting statistical variation in elements, based on measurements on the Manangotry standard. Note that this value is the maximum estimate of an additional precision error intrinsic to all analyses presented here. Although the fixed elemental data in protocol “A” were obtained from the sample being analysed, and input into the matrix correction (using Th as the compositional indicator of each point), the accuracy of these values relative to the real composition is not known. However, based on the data above it is anticipated that on the effect on the error will be in the order of ± 1 Ma and probably no more than ± 5 Ma relative to the analyses in protocols “B” and “C”. Several single spot analyses using “C” were obtained to verify some of the ages presented where “A” was used and were found to be comparable.

4.3. Monazite age and error calculation

BSE images, combined with quantitative elemental data were used to identify compositional domains in individual grains rather than elemental maps. In most cases BSE variation can be correlated with Th and/or Y zoning (e.g., Spear and Pyle, 2002). Where possible, multiple analyses were taken from within recognisable BSE domains, and once the quantitative data was available, individual points were re-allocated into different zones/domains if required. Individual dates were calculated for each point by inserting the Th, U, Pb concentrations into the age equation of Montel et al. (1996). Where compositional domains in a particular grain were either too small to adequately analyse, or the result of continuous compositional variation, the Y, Th and U composition of all analysed points were plotted with respect to their calculated dates (with associated 95% CI counting statistical errors obtained via Monte Carlo simulation (see Chapter 1)). If no significant correlation existed between these components and the calculated date, then these points were allocated into a date-domain. A mean date was calculated for each domain and 95% confidence intervals (CI) were generated by multiplying the standard error of the mean (SE) with the Student's-t value for (n-1) degrees of freedom (Siegel, 1988; Snedecor and Cochran, 1989).

Once the mean and confidence intervals were calculated for all domains, data from different monazite grains and/or domains were grouped together (if possible) based on additional information, such as chemical signature and/or textural setting. Where domains could be interpreted to be representative of a geologically significant event, the datasets were then combined via the weighted average procedure in Isoplot v3.10 (Ludwig, 2003).

5. Results and interpretation

A total of 37 monazite grains were analysed, 21 of which are inclusions in garnet porphyroblasts, 5 in staurolite porphyroblasts and 11 in the matrix. The results of mean dates calculated for each domain and/or grain can be viewed in Table 4. Two major groupings of the mean dates were identified; one above 330 Ma and the other below 320 Ma. Samples preserving older ages and/or those with Y-maps are examined in detail first, whereas the other samples are more briefly summarised. The full dataset, including the composition measured at each point and associated counting errors can be seen in Appendix E. Summaries of the results for each sample are given below.

5.1. K38

Sample K38 contains a monazite inclusion associated with a smaller xenotime grain lying just inside the truncated relic porphyroblast core (Fig. 4a). This association is most evident in the Y-map (Fig. 4b, c), where the core, characterised by a smooth, minor decrease in Y is truncated by a ring of quartz inclusions and an abrupt, irregular change in Y content. This monazite grain (Mnz6) has a relatively consistent Y concentration, but the analyses on the edge, adjacent to the quartz inclusion appear to be characterised by a Y and/or U decrease (Fig. 4d). These domains are visible in the BSE image (Fig. 4e), and appear similar to intergrowth zones (e.g., Zhu and O'Nions, 1999b). The mean date of this combined domain appears different to the bulk of the grain: 350 ± 8 Ma (bulk of grain) and 305 ± 38 Ma (intergrowth zone), although, the lack of analyses on the latter zone resulted in a large CI. A comparison of the relatively homogeneous Y-content of both the garnet and monazite (on the scale of the monazite grain) would suggest that both phases were potentially in equilibrium when they grew (Table 8: Pyle et al., 2001). If this is the case, the core of the garnet porphyroblast should also be approximately this age. Therefore, after a hiatus in garnet growth (of uncertain duration), shearing against the relict porphyroblast rim and/or resorption, must have affected the monazite grain along the non-enclosed boundary. As a result, a small portion of the grain possibly recrystallised with a slightly different chemistry, or some components (such as Pb) leached out into the matrix, either partially or fully resetting the isotope systematics. Resumption of porphyroblast growth must have commenced post-monazite alteration. A mean date of a different monazite grain in the rim of another porphyroblast (Mnz2: Fig. 4f), was calculated at 300 ± 12 Ma, which supports at least two distinct stages of garnet growth in this sample. Other monazite grains, one in a staurolite porphyroblast and two in the matrix have slightly younger mean dates (Table 4), probably indicating that these postdate garnet rim growth.

5.2. K53

Two monazite grains in this sample are interpreted to lie within the core of garnet porphyroblasts. One (Mnz1) lies sub-parallel to the curved portion of the inclusion trails in the core (Fig. 5a), and is characterised by two high Th core zones (> 9 wt %), decreasing towards the rim (2.5-3 wt %), corresponding with a much less intense decrease in Y content (Fig. 5b). The Y map of this garnet porphyroblast (Fig. 5c, d), shows an original, euhedral inner-core (also defined by a truncation of inclusion trails), a subsequent, semi-euhedral, oscillatory-zoned outer core (median) followed by a relatively Y-depleted rim. This monazite grain appears to pre-date or be synchronous with the first appearance of xenotime (Fig. 5c). Therefore the Y available for growing monazite must have been mostly controlled by the amount that was/had been fractionated into the garnet porphyroblast. The monazite grain here appears to have crystallised concentrically from possibly two original cores, with no obvious signs of resorption. Assessment of potential equilibrium between the phases depends on whether this monazite grain grew synchronously with the foliation that defines the inclusion trails in the porphyroblast core. Based on its microstructural position, it is considered that the bulk of the grain grew prior to garnet, during the development of a sub-vertical foliation. The inner core of the garnet porphyroblast grew during the development of a subsequent sub-horizontal differentiated crenulation cleavage, possibly rotating the monazite grain slightly into its present microstructural position. Some additional growth may have occurred during this event, but this is not obvious. Therefore, most, if not all of this grain probably predates garnet growth. The mean date of this grain is 365 ± 14 Ma, which also corresponds to the mean date (356 ± 24 Ma) of another inclusion (Mnz2) within a different porphyroblast (Fig. 6a). Due to the angle of the thin section cut, the microstructural setting of the second monazite grain relative the surrounding porphyroblast is less clear. However, both predate the same period of garnet growth as both grains lie within the ring defined by xenotime inclusions (Fig. 5c, 6a). Significantly, two inclusions (Fig 6a, b, c) in the rim of this second porphyroblast have mean dates of 295 ± 8 Ma and 287 ± 20 Ma respectively, indicating a later stage of monazite growth over 50 millions years after the inclusions preserved in the core.

Two grains (Mnz6, Mnz7) were analysed in staurolite porphyroblasts in this sample. The grains have mean dates of 288 ± 9 Ma and 300 ± 15 Ma respectively, which is similar to those in the garnet porphyroblast rims. A grain (Mnz8) within the strain shadow of a garnet porphyroblast in this sample (Fig. 6d) has a mean date of 343 ± 24 Ma, suggesting that it essentially survived the effects of matrix deformation that partitioned around the porphyroblast. The poorly defined mean (due to a large range of individual dates), may be the result of some localised modification, although overall this grain has retained the age of the monazite inclusions in the porphyroblast cores. This would also imply that an earlier stage of garnet porphyroblast growth must have occurred to preserve the older monazite grains and also protect grains, such as this from the effects of subsequent deformation.

5.3. K63

Two inclusions (Mnz2, Mnz3) within sample K63 appear to lie within the core of a garnet porphyroblast, although there were no microstructural relationships such as inclusion trails that could be used to confirm this (Fig. 7a). Both grains are small (one is fractured or a combination of two adjacent grains), and have similar compositions characterised by a very high Th content (between 10-14 wt %), and a Y content above 1 wt %. This is in contrast to grain Mnz1, which is, interpreted to lie in the rim of another porphyroblast (Fig. 7b), with a much lower Th (< 2 wt %) and Y (< 0.2 wt %) content (Fig. 7c). The mean dates of the “core” grains are 334 ± 11 and 337 ± 10 Ma respectively, whereas the “rim” inclusion has a distinctively lower mean of 271 ± 24 Ma. This latter mean date is similar to those obtained from a grain in a staurolite porphyroblast (278 ± 23 Ma) and a grain, lying partially elongate and parallel to the matrix foliation (281 ± 19 Ma) within this sample. Although the correlation between monazite and garnet growth is not clear in this sample, at least two stages of garnet porphyroblast growth seem reasonable (like the samples above).

5.4. K45

In sample K45 a monazite grain located in the core/median portion of a garnet porphyroblast was analysed (Fig. 8a, b). The grain lies sub-parallel to the inclusion trails and shows only minor chemical variation, with Y (+ Dy) and Th decreasing slightly towards the porphyroblast rim (Fig. 8b). The Y map of the garnet porphyroblast displays a concentric zoning pattern, also with a decrease in Y towards the rim (Fig. 8c). In addition, xenotime appears to have been absent during the growth of this monazite grain (Fig. 8c). As such, any monazite grain that grew in equilibrium with the porphyroblast core should have a higher Y content to that of a grain that grew in equilibrium with the rim. The observation that the monazite grain analysed here displays this trend, indicates that the higher Y-domain (relict core?) crystallised first, with the lower domain forming after the (growing) garnet porphyroblast had fractionated additional Y from the matrix. The mean date of this monazite grain is 310 ± 9 Ma, and is interpreted to represent the average age of the core/median section of garnet. The age of the rim (defined by low Y) is unknown, although, it must predate the matrix foliation which truncates the inclusions trails in the rim. An elongate monazite grain (Mnz2), lying parallel to the matrix foliation in this sample (Fig. 8d) has a mean date of 289 ± 6 Ma, providing a lower limit for the growth of the garnet porphyroblast rim.

5.5. Other Samples

A grain (Mnz1) in sample K52 that appears to lie within the core of a garnet porphyroblast (Fig. 9a) has a mean date of 287 ± 34 Ma. However, another grain (Mnz2: Fig. 9b), within the median zone of the same porphyroblast (between core and rim), with a similar, but slightly lower Th and Y content has a seemingly young mean of 254 ± 31 Ma. Both these grains are in contrast with an inclusion (Mnz3) in the very rim of the porphyroblast (Fig. 9c), with a very high Th (> 12 wt %) and low Y (< 0.4 wt %) content, which has a mean date of 300 ± 4 Ma. In the same sample, a grain within the core of a staurolite porphyroblast (297 ± 12 Ma) and two within the matrix (296 ± 11 and 282 ± 11 Ma) were analysed. The matrix grains should post-date garnet porphyroblast growth, thus the accuracy of the younger mean date above is questionable. As a result, the correlations between the monazite inclusions and the surrounding porphyroblast are uncertain in this sample.

A small monazite inclusion lying at a high angle to the inclusion trails in a porphyroblast was analysed in sample K103. The mean date of this poorly constrained grain was 307 ± 22 Ma, which is indistinguishable from another grain, clearly within a porphyroblast rim with a mean of 304 ± 19 Ma. Two elongate grains, lying parallel to the matrix foliation, have slightly younger (but within error) mean dates of 299 ± 9 and 294 ± 16 Ma respectively.

A monazite grain within a garnet porphyroblast rim and another lying elongate and parallel to the matrix foliation in sample K31, have indistinguishable mean dates of 295 ± 9 and 289 ± 10 Ma respectively. In addition, two grains within the garnet porphyroblast rims of sample K59 have similar mean dates of 294 ± 23 and 273 ± 10 Ma respectively.

Three monazite inclusions within the garnet porphyroblast rims and one within the matrix in sample M54 (Mount Mineral Formation), appear to preserve two different ages, one around 310 Ma and the other around 290 Ma (Table 4). The actual mean dates are poorly constrained due to a lack of analyses, but the younger date corresponds with a chemically distinct rim on the grains (Fig. 10). Clearly, the age of the garnet porphyroblast rims in this sample must be no older than the youngest age preserved in these monazite grains. If this age is in fact around 290 Ma, similar constraints exist on late garnet porphyroblast growth, compared to the other samples from the Northfield and Wendell synclines.

5.6. Accuracy of results

The accuracy of the data here can only be semi quantified by comparing analyses on the Manangotry age standard to isotopic data, during the period of this study. In this time frame, five representative datasets (n = 10) on this standard were obtained (Fig. 3), with a weighted mean of 549 ± 3 Ma. Since the best estimate of the age of this standard is 555 ± 1 Ma (Horstwood et al., 2003), the results presented above may be slightly younger than they actually are. This apparent discrepancy is unlikely to affect any of the interpretations presented here, as most of the mean dates and weighted means already include relatively large errors.

5.7. Summary of Northfield and Wendell syncline samples

Several different stages of garnet porphyroblast growth are evident from the results presented here (Fig. 11a), which supports both the microstructural interpretations and (where applicable) Y-zoning profiles. The earliest stages of growth are most likely related to deformation and metamorphism during the Late (Neo)-Acadian event that also affected rocks further east, in the central Massachusetts metamorphic high (Thomson et al., 1992; Robinson et al., 1998). The duration of this event has been constrained by Robinson et al. (1998) as being within 366-350 Ma, and four monazite grains (three as inclusions in garnet porphyroblasts) from this study, lie within this window. These grains probably approximate the earliest phase of garnet porphyroblast growth in these samples. The two monazite grains from within sample K63 with mean dates of 334 ± 11 and 337 ± 10 Ma respectively, lie just below this time period (Fig. 11a, b). These dates could represent either a later phase of deformation and metamorphism or extended duration of this Late Acadian event. There is also the possibility that they resulted from analytical error (see above).

The majority of the monazite inclusions in the garnet porphyroblast rims, and two from within the cores lie within or close to (Fig. 11b) the relatively narrow time interval previously recorded for the Late Pennsylvanian event of 300-290 Ma (Spear and Harrison, 1989; Harrison et al., 1989; Tucker and Robinson, 1990; Robinson et al., 1992). Only two grains lie below the lower boundary and may be explained as the result of the same analytical error discussed above. The weighted mean for all monazite inclusions in the rims of garnet porphyroblasts (Fig. 11b) is 295 ± 6 Ma (MSWD = 3.9). The large MSWD probably indicates that not all these grains are actually the same age. However, there is most certainly at least one distinct period of garnet porphyroblast growth (possibly all growth in some samples) that can be attributed to metamorphism and deformation during the Late Pennsylvanian.

Garnet growth during the Late Pennsylvanian probably ceased when staurolite production started, as the growth of the latter phase probably involved the breakdown of garnet. The monazite inclusions in staurolite porphyroblasts certainly appear to correlate with this event (Fig. 11c). The weighted mean for these five grains is 292 ± 6 Ma (MSWD = 1.04), which is essentially indistinguishable from that of the inclusions in the garnet rims. Some evidence that garnet porphyroblast growth resumed after staurolite production stopped is evident in Fig. 5c. This Y map shows a high-Y annulus near the rim of the porphyroblast, similar to those described in (Pyle and Spear, 1999). These features were interpreted to be the result of garnet resorption during production of staurolite, releasing Y into matrix, followed by the cessation of staurolite growth and resumption of garnet production in a Y- enriched environment. If this annulus is the result of this process, it may have also occurred in other samples (in which Y-maps were not obtained), and thus (portions of) garnet porphyroblast rims may actually have different ages between samples. This may be a partial reason for the large MSWD calculated for the garnet porphyroblast rim inclusions above.

In the majority of samples, monazite grains within the matrix are expected to the younger than those in the porphyroblasts. With the notable exception of K53-Mnz8, which lies within the strain shadow of a garnet porphyroblast, the mean dates for all other grains are within the Late Pennsylvanian time window (Fig. 11d). The weighted mean for these grains is 289 ± 5 Ma (MSWD = 1.9), which is not significantly different to the weighted means for either the garnet porphyroblast rim and staurolite inclusions above. However, the weighted means for both the garnet rims, staurolite and matrix grains follow a slight downward progression consistent within the relative timing constraints.

5.8. Mount Mineral Formation summary

Only limited data was obtained for this sample, but it appears as though the monazite inclusions within the garnet porphyroblast rims contain two different ages. The age of younger of the two (poorly defined: ca 290 Ma) would be most representative of the maximum age of the rim growth, if it were better constrained. The older age (ca 310 Ma) must represent an earlier event, but the relationship between this stage of monazite growth and garnet is not known. A third monazite generation must also be present in this formation as both Late Acadian and Late Pennsylvanian monazite ages have previously been obtained (Robinson et al., 1992), although not observed here. If Late Acadian metamorphism affected this sample, the majority of the evidence (apart from the garnet porphyroblast cores, the age of which is unknown) was destroyed during Late Pennsylvanian tectonism.

6. Discussion

6.1. Pattern of metamorphism in central Massachusetts

Regional deformation and metamorphism during the Late Acadian, reached the granulite facies in central Massachusetts, with apparently little or no overprinting from the Late Pennsylvanian event (Robinson et al., 1998). Further west, towards the Mesozoic border fault, overprinting due to later tectonism appears to have either obliterated the majority of earlier textures, or Late Acadian metamorphism was not as widespread as previously thought. Relic high grade (Kfs-Sill-Grt) metamorphism within the Mount Mineral Formation has been dated at 367 ± 3 Ma (Robinson et al., 1992), and evidence in two samples examined here of at least garnet-grade metamorphism, appear to indicate that this Late Acadian metamorphism did indeed effect a wide area. However, in some samples (e.g., K45, K52) monazite and potentially all garnet porphyroblast growth appears to be restricted to the Late Pennsylvanian, implying that the earlier event may only be locally preserved and/or was less intense in the vicinity of the Northfield Syncline. One reason for the apparent lack of Late Acadian monazite ages could be related to the monazite isograd relative to that of garnet. If the Late Acadian history is only preserved in the garnet porphyroblasts within the Northfield Syncline, the lack of monazite inclusions may be restricting the ability to date it. A more thorough investigation of additional samples, or alternative methods would be required test this theory. Metamorphism and deformation during the Late Pennsylvanian was essentially localised around the Pelham Dome, and appears to be responsible for additional garnet plus all staurolite-kyanite growth within the rocks of the Northfield and Wendell synclines.

6.2. Implications for P-T paths

The data presented here gives new insights into P-T paths calculated for this area (e.g., Moecher, 1999; Kim and Bell, 2005). The extent of peak P-T conditions of 800-825° C and 6 ± 1 kbar during Late Acadian metamorphism, obtained from cover sequences above the Pelham Dome (Moecher, 1999), is uncertain as there appears to be no clear evidence for these intense temperatures in the samples examined from the Northfield and Wendell synclines. It would be expected that major cations (such as Mn), would either partially or fully diffuse within pre-existing garnet porphyroblasts, if temperatures of this magnitude were attained (e.g., Tracy, 1982). Diffusional homogenisation occurred in both sample M54, from the Mount Mineral Formation and another (not examined here) from the Wendell Syncline (Kim and Bell, 2005). This supports the interpretation that these temperatures were possible, as long as these porphyroblasts grew during the Late Acadian. This contrasts to chemical maps of other garnet porphyroblasts from the Northfield Syncline, which show that in most cases growth zoning profiles are retained (Kim and Bell, 2005). However, the age of these porphyroblasts is not known, although it is possible (considering the results presented here) that some grew during the Late Pennsylvanian.

Sample K53, in particular, is crucial for understanding the tectonic history of the Northfield Syncline region. It now seems apparent that early garnet porphyroblast growth occurred in this sample in the Late Acadian, although the total amount is uncertain. Porphyroblasts retain a relatively smooth Mn (and Mg) growth zoning profile from core to rim (Fig. 12, see also Kim and Bell, 2005), which contrasts with the far more complex Y-zoning profile obtained here (Fig. 5c). The high-Y "outer core" (also seen in sample K38: Fig. 4b) is not consistent with Mn or Mg, but locally may be similar to that of Ca (Fig. 12e, f). This may be critical in understanding the porphyroblast growth history, because Y diffusivity in garnet is considerably slower than Mn, Fe and Mg, but possibly similar to that of Ca (Pyle and Spear, 1999). One tentative explanation for the Y zoning is that the inner core represents a resorbed relic of Late Acadian growth. In this model, breakdown of garnet would be responsible for releasing Y into the matrix, and potentially enriching the core in Mn through diffusion. This would have occurred sometime prior to new growth (possibly Late Pennsylvanian?), in a higher-Y environment, resulting in the preserved Y and seemingly continuous Mn zoning profiles. However, this scenario is unlikely based on the preserved euhedral inner core, which would not be expected to survive if significant resorption occurred; also microstructural evidence clearly shows that inclusion trails within the inner core are truncated by a subsequent foliation.

A more likely explanation is that the continuous growth of the porphyroblast core during the Late Acadian was stopped by the development of a differentiated crenulation cleavage. Due to the size of the core, intracrystalline variation of Mn and Mg was minimal, although homogenisation of these cations through diffusion cannot be ruled out. The timing of the subsequent stages of growth is uncertain, but equilibrium between the matrix and the core must have been maintained for Mn and Mg, to explain the continuous zoning profiles. This cannot have been the case for Ca and Y. Similar zoning has previously been interpreted to be the result of disequilibrium of certain elements during garnet growth, rather than any major changes in P-T conditions or fluid composition (Chernoff and Carlson, 1999). This is adequate to explain the zoning, but cannot account for the ca. 60 m.y. hiatus in recorded in this sample. If porphyroblast growth was shut down for this length of time, new growth during Late Pennsylvanian tectonism would have to be at approximately the same P-T conditions as that in the Late Acadian to explain the smooth profiles in Mn and Mg. This would only be possible if no deformation partitioned through these rocks between the end of the Acadian and the Late Pennsylvanian. The rock mass must also have remained static within the crust, such that no reactions would have proceeded, and all phases maintained equilibrium until the onset of Late Pennsylvanian metamorphism. The Y profile, with oscillatory zoning seen in two examples shown herein, can then be interpreted to be either the result of open-system behaviour, that did not change Mn and Mg concentrations, or the breakdown of an earlier generation of Y-bearing accessory phase (such as xenotime), subsequent to the growth of the porphyroblast core (e.g., Hickmott et al., 1987).

Whilst the cause of abrupt variation in Y and Ca is uncertain, the preservation of zoning of these elements throughout the garnet porphyroblast indicates that this sample, and potentially others within the Northfield Syncline did not reach temperatures high enough for noticeable intracrystalline diffusion of these elements. Diffusion of Mn and/or Mg could have occurred, but only within the inner core, which would infer that this is the only portion of the garnet porphyroblast in K53 that grew during the Late Acadian. This observation and the lack of relic high grade assemblages, is inconsistent with temperatures over 800° C (Moecher, 1999) being attained during the Late Acadian in the Northfield Syncline.

The recognition of at least two distinct phases of garnet porphyroblast growth, but continuous Mn and Mg zoning profiles and potential for open system behaviour in samples such as K53 has important implications for P-T path calculations (e.g., Tracy et al., 1976; Spear and Selverstone, 1983; Vance and Mahar, 1998). With the data available at the time, P-T paths calculated for sample K53 (Kim and Bell, 2005), were unable to take into account the hiatus of potentially 60 million years between the growth of the core and the rim. Open system behaviour could also have affected certain elements of the garnet-whole rock equilibrium (but not Mn and Mg) that is inferred by intersecting isopleth methods (e.g., Vance and Holland, 1993; Vance and Mahar, 1998; Stowell et al., 2001; Evans, 2004), although this is not obvious in Kim and Bell (2005).

6.3. Tectonic synthesis

Late Acadian deformation, metamorphism and plutonism in central Massachusetts appears to have occurred some 40-50 million years after the Late Silurian-Early Devonian (Acadian) peak recorded elsewhere in northern New England (Robinson et al., 1998). The tectonic setting of this later event is uncertain. Since the bulk of the staurolite, matrix (and kyanite) metamorphic mineral assemblage(s) around the northern margin and within the Pelham Dome are Late Pennsylvanian, previous interpretations of a link between the emplacement of the dome and localised metamorphism seem applicable. Assuming that the Pelham Dome is a fragment of Avalon (Getty and Gromet, 1992), emplacement of this terrain under the Acadian metamorphic belt, must have occurred around 300 Ma. This mid to deep crustal tectonic burial was probably the result of the initial stages of collision with Africa (Alleghanian Orogeny), prior to the “classical Alleghanian” identified within the

Narragansett Basin further east (Cogswell and Mosher, 1994; Robinson et al., 1998). Continued burial and intra-crustal transport resulted in gneissic deformation around 305-290 Ma within the Avalon terrain and the transmission of heat into the overlying rocks. Much of this must have been localised around and into the cover sequences of the present day Pelham Dome, resulting in the staurolite-kyanite grade metamorphism preserved within these rocks. The whole sequence of events culminated in intense top to the south shearing. Locally, this resulted in the emplacement of the Northfield Syncline above the Pelham Dome, with significant shearing and shortening to rotate the syncline into an antiformal structure against the dome (Bell and Kim, 2004). As such, all inclusion trails within porphyroblasts were truncated by the matrix foliation and inferred Late Acadian mineral elongations were rotated about 180° (Robinson et al., 1992).

7. References

Armstrong, J.T., 1988. Quantitative analysis of silicate and oxide materials: Comparison of Monte Carlo, ZAF and Φ (ρz) procedures. In: D.E. Newbury (Editor), Microbeam Analysis. San Francisco Press.

Armstrong, J.T., 1991. Quantitative elemental analysis of individual microparticles with electron beam instruments. In: K.F.J. Heinrich and D.E. Newbury (Editors), Electron Probe Quantitation. Plenum Press.

Armstrong, T.R., Tracy, R.J. and Hames, W.E., 1992. Contrasting styles of Taconian, Eastern Acadian and Western Acadian metamorphism, central and western New England. Journal of Metamorphic Geology, 10, 415-426.

Bell, T.H., Ham, A.P. and Hickey, K.A., 2003. Early formed regional antiforms and synforms that fold younger matrix schistosities: their effect on sites of mineral growth. Tectonophysics, 367, 253-278.

Bell, T.H., Ham, A.P. and Kim, H.S., 2004. Partitioning of deformation along an orogen and its effects on porphyroblast growth during orogenesis. Journal of Structural Geology, 26, 825-845.

Bell, T.H. and Hayward, N., 1991. Episodic metamorphic reactions during orogenesis; the control of deformation partitioning on reaction sites and reaction duration. Journal of Metamorphic Geology, 9, 619-640.

Bell, T.H. and Hickey, K.A., 1999. Complex microstructures preserved in rocks with a simple matrix; significance for deformation and metamorphic processes. Journal of Metamorphic Geology, 17, 521-535.

Bell, T.H., Hickey, K.A. and Upton, G.J.G., 1998. Distinguishing and correlating multiple phases of metamorphism across a multiply deformed region using the axes of spiral, staircase and sigmoidal inclusion trails in garnet. Journal of Metamorphic Geology, 16, 767-794.

Bell, T.H. and Kim, H.S., 2004. Preservation of Acadian deformation and metamorphism through intense Alleghanian shearing. Journal of Structural Geology, 26, 1591-1613.

Bell, T.H., Rubenach, M.J. and Fleming, P.D., 1986. Porphyroblast nucleation, growth and dissolution in regional metamorphic rocks as a function of deformation partitioning during foliation development. Journal of Metamorphic Geology, 4, 37-67.

Bell, T.H. and Welch, P.W., 2002. Prolonged Acadian orogenesis: revelations from foliation intersection axis (FIA) controlled monazite dating of foliations in porphyroblasts and matrix. American Journal of Science, 302, 549-581.

Chernoff, C.B. and Carlson, W.D., 1999. Trace element zoning as a record of chemical disequilibrium during garnet growth. Geology, 27, 555-558.

Cihan, M. and Parsons, A., 2005. The use of porphyroblasts to resolve the history of macro-scale structures: an example from the Robertson River Metamorphics, North-Eastern Australia. Journal of Structural Geology, 27, 1027-1045.

Cocherie, A., Legendre, O., Peucat, J.J. and Kouamelan, A.N., 1998. Geochronology of polygenetic monazites constrained by in situ electron microprobe Th-U-total lead determination: Implications for lead behaviour in monazite. Geochimica et Cosmochimica Acta, 62 (14), 2475-2497.

Cogswell, J.P.M. and Mosher, S., 1994. Late-stage Alleghanian wrenching of the southwestern Narragansett basin, Rhode Island. American Journal of Science, 294, 861-901.

Dahl, P.S., Hamilton, M.A., Jercinovic, M.J., Terry, M.P., Williams, M.L. and Frei, R., 2005. Comparative isotopic and chemical geochronometry of monazite, with implications for U-Th-Pb dating by electron microprobe: An example from metamorphic rocks of the eastern Wyoming Craton (U.S.A.). American Mineralogist, 90, 619-638.

Evans, T.P., 2004. A method for calculating effective bulk composition modification due to crystal fractionation in garnet-bearing schist: implications for isopleth thermobarometry. Journal of Metamorphic Geology, 22, 547-557.

Getty, S.R. and Gromet, L.P., 1992. Geochronological constraints on ductile deformation, crustal extension, and doming about a basement-cover boundary, New England Appalachians. American Journal of Science, 292, 359-397.

Goncalves, P., Nicollet, C. and Montel, J.-M., 2004. Petrology and in situ U-Th-Pb monazite geochronology of ultrahigh-temperature metamorphism from the Andriamena mafic unit, north-central Madagascar. Significance of a petrographical P-T path in a polymetamorphic context. Journal of Petrology, 45 (10), 1923-1957.

Harrison, T.M., Spear, F.S. and Heizler, M.T., 1989. Geochronologic studies in central New England II: Post-Acadian hinged and differential uplift. Geology, 17, 185-189.

Hickmott, D.D., Shimizu, N., Spear, F.S. and Selverstone, J., 1987. Trace-element zoning in a metamorphic garnet. Geology, 15, 573-576.

Horstwood, M.S.A., Foster, G.L., Parrish, R.R., Noble, S.R. and Nowell, G.M., 2003. Common-Pb corrected in situ U-Pb accessory mineral geochronology by LA-MC-ICP-MS. Journal of Atomic Spectrometry, 18, 837-846.

Kim, H.S. and Bell, T.H., 2005. Combining compositional zoning and foliation intersection axes (FIAs) in garnet to quantitatively determine early P-T-t paths in multiply deformed and metamorphosed schists: north central Massachusetts, USA. Contributions to Mineralogy and Petrology, 149, 141-163.

Kohn, M.J. and Malloy, M.A., 2004. Formation of monazite via prograde metamorphic reactions among common silicates: Implications for age determinations. Geochimica et Cosmochimica Acta, 68, 101-113.

Ludwig, K.R., 2003. User's manual for Isoplot 3.0; a geochronological toolkit for Microsoft Excel, Berkeley Geochronology Centre, Special Publication No. 4.

Moecher, D.P., 1999. The distribution, style, and intensity of Alleghanian metamorphism in south-central New England: Petrologic evidence from the Pelham and Willimatic Domes. Journal of Geology, 107, 449-471.

Moecher, D.P. and Wintsch, R.P., 1994. Deformation induced reconstitution and local resetting of mineral equilibria in polymetamorphic gneisses: tectonic and metamorphic implications. Journal of Metamorphic Geology, 12, 523-538.

Montel, J.-M., Foret, S., Veschambre, M., C, N. and Provost, A., 1996. Electron microprobe dating of monazite. Chemical Geology, 131, 37-53.

Peterson, V.L. and Robinson, P., 1993. Progressive evolution from uplift to orogen-parallel transport in a late-Acadian upper amphibolite to granulite facies shear zone, south central Massachusetts. Tectonics, 12, 550-567.

Pyle, J.M. and Spear, F.S., 1999. Yttrium zoning in garnet: Coupling of major and sccessory phases during metamorphic reactions. Geological Materials Research, 1 (6), 1-49.

Pyle, J.M., Spear, F.S., Rudnick, R.L. and McDonough, W.F., 2001. Monazite-xenotime-garnet equilibrium in metapelites and a new monazite-garnet thermometer. Journal of Petrology, 42, 2083-2107.

Pyle, J.M., Spear, F.S. and Wark, D.A., 2002. Electron Microprobe Analysis of REE in Apatite, Monazite and Xenotime: Protocols and Pitfalls. Reviews in Mineralogy and Geochemistry, 48, 337-362.

Pyle, J.M., Spear, F.S., Wark, D.A., Daniel, C.G. and Storm, L.C., 2005. Contributions to the precision and accuracy of chemical ages of monazite. American Mineralogist, 90, 547-577.

Rasband, W.S., 1997-2005. ImageJ. U. S. National Institutes of Health, Bethesda, Maryland, USA, http://rsb.info.nih.gov/ij/.

Robinson, P., Tucker, R.D., Bradley, D., Berry, H.N.I.V., Osberg, P.H., Sundquist, B. and Stephens, M.B. (Editors), 1998. Paleozoic orogens in New England, USA. Geological Society of Sweden, Stockholm, Sweden, 119-148 pp.

Robinson, P., Tucker, R.D., Gromet, L.P., Ashenden, D.D., Williams, M.L., Reed, R. and Peterson, V.L., 1992. The Pelham Dome, central Massachusetts: Stratigraphy, geochronology, structure and metamorphism. In: P. Robinson and J.B. Brady (Editors), Guidebook for Field Trips in the Connecticut Valley

Region of Massachusetts and Adjacent States. New England Intercollegiate Geological Conference, Amherst, Massachusetts, v1, pp. 132-169.
Scherrer, N.C., Engi, M., Gnos, E., Jakob, V. and Liechti, A., 2000. Monazite analysis; from sample preparation to microprobe age dating and REE quantification. Schweizerische Mineralogische und Petrographische Mitteilungen, 80 (1), 93-105.
Siegel, A.F., 1988. Statistics and Data Analysis. John Wiley & Sons, New York.
Snedecor, G.W. and Cochran, W.G., 1989. Statistical Methods, Eighth Edition. Iowa State University Press.
Spear, F.S. and Harrison, T.M., 1989. Geochronologic studies in central New England I: Evidence for pre-Acadian metamorphism in eastern Vermont. Geology, 17, 181-184.
Spear, F.S. and Pyle, J.M., 2002. Apatite, Monazite, and Xenotime in Metamorphic Rocks. Reviews in Mineralogy and Geochemistry, 48, 293-335.
Spear, F.S. and Selverstone, J., 1983. Quantitative P-T path from zoned minerals; theory and tectonic applications. Contributions to Mineralogy and Petrology, 83, 348-357.
Stallard, A.R. and Hickey, K.A., 2001. Shear zone vs folding origin for spiral inclusion trails in the Canton Schist. Journal of Structural Geology, 23 (12), 1845-1864.
Stallard, A.R., Hickey, K.A. and Upton, G.J., 2003. Measurement and correlation of microstructures: the case of foliation intersection axes. Journal of Metamorphic Geology, 21 (3), 241-252.
Stowell, H.H., Taylor, D.L., Tinkham, D.K., Goldberg, S.A. and Ouderkirk, K.A., 2001. Contact metamorphic P-T-t paths from Sm-Nd garnet ages, phase equilibria modeling, and thermobarometry: Garnet Ledge, south-eastern Alaska, USA. 19, 645-660.
Suzuki, K. and Adachi, M., 1991. Precambrian provenance and Silurian metamorphism of the Tsubonosawa paragneiss in the South Kitakami terrane, Northeast Japan, revealed by the chemical Th-U-total Pb isochron ages of monazite, zircon and xenotime. Geochemical Journal, 25, 357-376.
Thomson, J.A., Peterson, V.L., Berry, H.N., IV and Barreiro, B., 1992. Recent studies in the Acadian metamorphic high, south-central Massachusetts. In: P. Robinson and J.B. Brady (Editors), Guidebook for Field Trips in the Connecticut Valley Region of Massachusetts and Adjacent States. New England Intercollegiate Geological Conference, Amherst, Massachusetts, v1, pp. 229-255.
Tracy, R.J., 1982. Compositional zoning and inclusions in metamorphic minerals. Reviews in Mineralogy, 10, 355-397.
Tracy, R.J., Robinson, P. and Thompson, A.B., 1976. Garnet composition and zoning in the determination of temperature and pressure of metamorphism, central Massachusetts. American Mineralogist, 61, 762-775.
Tucker, R.D. and Robinson, P., 1990. Age and setting of the Bronson Hill magmatic arc: A re-evaluation based on U-Pb zircon ages in southern New England. Geological Society of America Bulletin, 102, 1404-1419.
Vance, D. and Holland, T., 1993. A detailed isotopic and petrological study of a single garnet from the Gassetts Schist, Vermont. Contributions to Mineralogy and Petrology, 114, 101-118.
Vance, D. and Mahar, E., 1998. Pressure-temperature paths from P-T psuedosections and zoned garnets: potential, limitations and examples from the Zanskar Himalaya, NW India. Contributions to Mineralogy and Petrology, 132, 225-245.

Williams, M.L., 1994. Sigmoidal inclusion trails, punctuated fabric development and interactions between metamorphism and deformation. Journal of Metamorphic Geology, 12, 1-21.

Williams, M.L., Jercinovic, M.J. and Terry, M.P., 1999. Age mapping and dating of monazite on the electron microprobe: Deconvoluting multistage tectonic histories. Geology, 27 (11), 1023-1026.

Zhu, X.K. and O'Nions, R.K., 1999. Zonation of monazite in metamorphic rocks and its implications for high temperature thermochronology: a case study from the Lewisian terrain. Earth and Planetary Science Letters, 171, 209-220.

THESIS CONCLUSIONS

Conclusions

This thesis has addressed several issues regarding monazite dating, in particular, data handling and the use of compositional variation as an indicator of distinct stages of growth. The data handling sections are EPMA specific. However, compositional variation, microstructural setting of monazite grains and how they both change from event to event, can also be applied to other in-situ dating techniques. Other issues, such as the chemical zoning profiles in garnet relative to inclusion trails and/or monazite grains, plus the role of deformation partitioning in controlling the location and timing of porphyroblast growth, are to metamorphic and structural interpretations of orogenic belts.

The first chapter shows that the use of counting statistics to calculate precision errors on EPMA monazite ages is not a good procedure. Additional sources of non-quantifiable systematic error such spectrometer drift, uncertainty in standard composition, sample damage, pulse shift and electron beam instability, all affect the reproducibility of analyses. Counting statistics, based on the number of counts (x-rays) recorded by the detectors, cannot account for these uncertainties and only provides a minimum estimate of the precision. The recommended way to determine the precision of EPMA monazite dates is by calculating distribution statistics (i.e. mean and confidence intervals) for repeated measurements on a homogeneous domain. This is the most representative method for estimating the reproducibility of an EPMA dataset.

These methods were extended to heterogeneous domains in Chapter 2. Although the underlying distribution of EPMA data from heterogeneous monazite grains can not be automatically regarded as normal (or approximately normal), the use of parametric statistics as in Chapter 1 is still adequate. Non parametric methods such as the bootstrap are not considered necessary, as in all cases the confidence intervals from this procedure are slightly (5-10 %) smaller compared to parametric statistics. This was tested with data from the Murphy Syncline. The samples examined preserve predominately Taconic (ca. 450 Ma) metamorphic textures, with the exception of one from the northwest limb of the syncline, which was subject to staurolite grade overprinting in the Acadian, some 50 million years later. This is explained by Acadian deformation preferentially partitioning along the limb(s), of the fold as well as into rocks further north.

Chapter 3 is a combined microstructural/monazite dating study that dates periods of deformation within garnet porphyroblastic samples preserving a multi-stage foliation development history. The results indicate that a large portion, if not all the metamorphism within the Dahlonega Gold Belt in northern Georgia occurred during the early Alleghanian. These findings show that amphibolite-facies Alleghanian deformation and metamorphism occurred within this belt, with minimal affect on the surrounding rocks, and prior to major thrust sheet movement within the southern Appalachians.

The timing of porphyroblast growth within samples from north central Massachusetts is investigated in Chapter 4. Monazite inclusions within the cores of several garnet porphyroblasts were dated, and where possible correlated to periods of garnet growth using a combination of Yttrium chemical maps and microstructures. Other monazite grains within garnet porphyroblast rims, within staurolite porphyroblasts and within the matrix were also dated. Results show that some samples preserve evidence for an earlier (Late Acadian) event, which is prevalent in central

Massachusetts, but the bulk of metamorphic assemblage relates to localised Late Pennsylvanian (early Alleghanian) tectonism. Continuous zoning profiles of certain major cations (Mn, Mg) in garnet porphyroblasts are compared with discontinuous Y profiles across microstructural truncations of inclusion trails. The data obtained here indicates that smooth zoning in Mn and Mg, can not automatically be assumed to indicate continuous growth. Such zoning could equally could result from a lack of any significant P-T-X change between periods of episodic growth.

Directions for future work

This can be split into two parts; EPMA/monazite dating specific and microstructural/metamorphism specific. With regards to dating on the EPMA, some major issues need addressing, the first being the need for a homogeneous, isotopically dated inter-laboratory monazite age standard. Although we appear to have an adequate standard (Manangotry), we now have reservations regarding the homogeneity of our fragment. It is suspected that there are at least two subtle domains, one with an age equivalent to the published isotopic age (ca. 555 Ma), and another closer to 545 Ma (Kevin Blake, pers. comm.). The precision of monazite dates would also be increased if additional data points could be obtained from individual grains. The first step would be to improve sample preparation/polishing techniques, particularly by using a final collodial silica polish. This potentially would increase the area of grains that can be analysed. Investigating other conductive coating materials, would also be beneficial allowing count times to be increased and the beam diameter to be reduced without having to worry about the effects of sample damage. Some of these issues are currently being examined, and will hopefully be implemented in the near future.

With regard to microstructural and metamorphic issues, further scope exists to investigate garnet zoning patterns with respect to preserved microstructures. The identification of other porphyroblasts similar to those discussed from sample K53 (Chapter 4), could be used to either expand or re-interpret the findings here. This obviously has important implications for P-T-D-t paths. The addition of xenotime analyses would be useful as garnet-xenotime thermometry can be relatively easily integrated with EPMA monazite dates. More thorough studies into the behaviour of monazite during foliation development and fluid saturation, would aid in the understanding of how grains are altered, reset, dissolved and recrystallised. This would improve correlations between ages and periods of deformation and fluid infiltration. In terms of interpreting results with regard to regional scale features, future work should involve more data from an increased number of samples, an aspect of this study that was controlled more by the presence (or lack) of monazite in selected samples than anything else.

Combining microstructural analysis with EPMA monazite geochronology to constrain progressive stages of orogenesis in the Appalachians

Volume II: Tables, Figures and Appendices.

Thesis submitted by

Nicholas John Lisowiec BSc(Hons) *Adelaide*

in December 2005

for the degree of Doctor of Philosophy

in the School of Earth Sciences

James Cook University

TABLE OF CONTENTS: VOLUME II

CHAPTER 1

PRECISION ESTIMATION IN ELECTRON MICROPROBE MONAZITE DATING: REPEATED MEASUREMENTS VERSUS STATISTICAL (POISSON) BASED CALCULATIONS

Table 1. Summary of analytical conditions used for monazite data

Element	X-ray Line	Diffraction Crystal	Spectrometer Number	Standard	Analytical Time (sec) (Pk)	(Bkg)	Std R.S.D.* (1σ)
P	Kα	TAP	1	$CePO_4$	20	10	0.21%
Pb	Mα	PETJ	2	$PbSiO_3$	180	90	0.20%
Dy	Lβ	LIFH	3	$DyPO_4$	40	20	0.23%
U	Mβ	PETJ	4	U (pure)	180	90	0.20%
Th	Mα	PETJ	5	ThO_2	90	45	0.12%
Y	Lα	TAP	1	YPO_4	90	45	0.13%
Gd	Lβ	LIFH	3	$GdPO_4$	40	20	0.32%
Ca	Kα	PETJ	5	$CaSiO_3$	20	10	0.17%
Si	Kα	TAP	1	$PbSiO_3$	20	10	0.13%
Sm	Lβ	LIFH	3	$SmPO_4$	40	20	0.32%
S	Kα	PETJ	5	$BaSO_4$	20	10	0.38%
Nd	Lβ	LIFH	3	$NdPO_4$	10	5	0.33%
Pr	Lβ	LIFH	3	$PrPO_4$	20	10	0.35%
Ce	Lα	LIFH	3	$CePO_4$	10	5	0.34%
La	Lα	LIFH	3	$LaPO_4$	10	5	0.30%

* - Relative standard deviation for standard

Table 2. Pb, U, and Th concentrations and ages, with associated standard errors and confidence intervals for the mean

Analysis No.	Elemental conc. (ppm)			Age	Mean Age[a]	Std Err.	t-value[b]	95% C.I.
	Pb	U	Th	(Ma)	(Ma)			(Ma)
1	2636	1918	102557	538.7	538.7	N/A	N/A	N/A
2	2691	1894	102469	550.7	544.7	5.98	12.706	75.97
3	2689	1752	103524	547.2	545.5	3.55	4.303	15.29
4	2662	1737	102997	544.8	545.3	2.52	3.182	8.02
5	2665	1857	103436	541.2	544.5	2.12	2.776	5.89
6	2720	1881	102733	555.3	546.3	2.50	2.571	6.43
7	2678	1759	102206	551.6	547.1	2.24	2.447	5.49
8	2708	1829	102733	553.8	547.9	2.12	2.365	5.01
9	2612	1695	103085	534.8	546.5	2.37	2.306	5.46
10	2743	1776	102118	564.8	548.3	2.80	2.262	6.34
11	2680	1771	102206	551.8	548.6	2.56	2.228	5.69
12	2718	1862	102733	555.2	549.2	2.40	2.201	5.28
13	2711	1778	101503	561.5	550.1	2.40	2.179	5.23
14	2713	1692	101854	561.5	550.9	2.37	2.160	5.11
15	2726	1767	102294	560.7	551.6	2.30	2.145	4.93
16	2609	1793	101327	541.2	550.9	2.24	2.131	4.78
17	2651	1821	101415	549.0	550.8	2.11	2.120	4.48
18	2599	1809	101415	538.6	550.1	2.10	2.110	4.44
19	2610	1668	102645	537.1	549.5	2.10	2.101	4.42
20	2658	1956	102030	545.0	549.2	2.01	2.093	4.20
21	2683	1876	101679	553.2	549.4	1.92	2.086	4.00
22	2730	1883	103260	554.6	549.7	1.85	2.080	3.84
23	2725	1821	102294	559.6	550.1	1.82	2.074	3.77
24	2655	1788	102469	545.2	549.9	1.75	2.069	3.62
25	2607	1843	103260	530.8	549.1	1.85	2.064	3.81
26	2727	1808	102557	558.8	549.5	1.81	2.060	3.73
27	2665	1941	103524	539.4	549.1	1.78	2.056	3.67
28	2751	1730	103436	560.5	549.5	1.77	2.052	3.62
29	2669	1808	103436	542.8	549.3	1.72	2.048	3.52
30	2608	1743	101854	539.2	549.0	1.69	2.045	3.47
31	2620	1901	103173	532.8	548.4	1.72	2.042	3.51
32	2741	1849	103700	555.2	548.6	1.68	2.040	3.42
33	2679	1822	102821	547.6	548.6	1.63	2.037	3.31
34	2561	1727	102997	524.6	547.9	1.73	2.035	3.52
35	2597	1878	102997	529.3	547.4	1.76	2.032	3.58
36	2740	1900	102909	558.2	547.7	1.74	2.030	3.53
37	2702	1848	103876	546.7	547.7	1.69	2.028	3.43
38	2731	1845	103173	556.0	547.9	1.66	2.026	3.36
39	2742	1732	103876	556.6	548.1	1.63	2.024	3.30
40	2647	1906	103524	536.4	547.8	1.62	2.023	3.27
41	2749	1690	103436	560.7	548.1	1.61	2.021	3.25
42	2636	1769	103788	535.2	547.8	1.60	2.020	3.23
43	2668	1825	103612	541.5	547.7	1.57	2.018	3.17
44	2651	1821	103348	539.4	547.5	1.54	2.017	3.11
45	2690	1827	103524	546.4	547.5	1.51	2.015	3.04
46	2675	1847	103876	541.3	547.3	1.48	2.014	2.99
47	2661	1913	103524	539.1	547.1	1.46	2.013	2.94

Table 2. Continued

Analysis No.	Elemental conc. (ppm)			Age	Mean Age[a]	Std Err.	t-value[b]	95% C.I.
	Pb	U	Th	(Ma)	(Ma)			(Ma)
48	2634	1786	103876	534.0	546.9	1.46	2.012	2.93
49	2744	1783	103348	558.6	547.1	1.45	2.011	2.91
50	2646	1900	103436	536.7	546.9	1.43	2.010	2.88
51	2750	1706	103700	559.3	547.1	1.42	2.009	2.86
52	2796	1756	102821	572.3	547.6	1.48	2.008	2.97
53	2639	1950	103612	533.8	547.4	1.47	2.007	2.96
54	2596	1872	103788	525.6	547.0	1.50	2.006	3.01
55	2669	1720	103260	545.0	546.9	1.47	2.005	2.96
56	2636	1770	103524	536.5	546.7	1.46	2.004	2.92
57	2641	1748	103963	535.6	546.5	1.45	2.003	2.90
58	2609	1783	104051	528.3	546.2	1.46	2.002	2.92
59	2675	1819	103700	542.5	546.2	1.43	2.002	2.87
60	2569	1839	104315	518.2	545.7	1.48	2.001	2.97

[a] Cumulative mean age

[b] Student's t value for probability = 0.05 and n-1 degrees of freedom

Table 3. Pb, U, and Th and ages, with uncertainties calculated using Poisson statistics and Monte Carlo simulation, plus confidences interval from Table 2 (for comparison)

No.	Pb		U		Th		Age	MC Error	Cumulative		
	(ppm)	(1σ)	(ppm)	(1σ)	(ppm)	(1σ)	(Ma)	(95 % C.I.)	Mean Age	MC Error	t x SE
1	2636	46.7	1918	58.0	102557	321.9	538.7	13.53	538.7	13.53	N/A
2	2691	46.9	1894	57.7	102469	321.6	550.7	13.51	544.7	9.56	75.97
3	2689	46.8	1752	56.5	103524	324.9	547.2	13.46	545.5	7.79	15.29
4	2662	46.6	1737	56.2	102997	323.3	544.8	13.51	545.3	6.75	8.02
5	2665	46.9	1857	57.3	103436	324.6	541.2	13.51	544.5	6.04	5.89
6	2720	47.1	1881	57.5	102733	322.4	555.3	13.53	546.3	5.51	6.43
7	2678	46.6	1759	56.7	102206	320.8	551.6	13.54	547.1	5.11	5.49
8	2708	46.9	1829	57.2	102733	322.4	553.8	13.49	547.9	4.78	5.01
9	2612	46.5	1695	56.0	103085	323.5	534.8	13.57	546.5	4.51	5.46
10	2743	46.9	1776	56.8	102118	320.5	564.8	13.53	548.3	4.28	6.34
11	2680	46.9	1771	56.6	102206	320.8	551.8	13.66	548.6	4.08	5.69
12	2718	46.8	1862	57.1	102733	322.4	555.2	13.43	549.2	3.90	5.28
13	2711	46.7	1778	57.0	101503	318.6	561.5	13.55	550.1	3.75	5.23
14	2713	47.0	1692	55.9	101854	319.7	561.5	13.68	550.9	3.62	5.11
15	2726	46.9	1767	56.8	102294	321.0	560.7	13.55	551.6	3.50	4.93
16	2609	46.7	1793	56.9	101327	318.0	541.2	13.80	550.9	3.39	4.78
17	2651	46.7	1821	57.1	101415	318.3	549.0	13.67	550.8	3.29	4.48
18	2599	46.6	1809	56.9	101415	318.3	538.6	13.73	550.1	3.20	4.44
19	2610	46.5	1668	55.6	102645	322.1	537.1	13.63	549.5	3.11	4.42
20	2658	46.5	1956	57.8	102030	320.2	545.0	13.48	549.2	3.03	4.20
21	2683	46.7	1876	57.3	101679	319.1	553.2	13.57	549.4	2.96	4.00
22	2730	46.7	1883	57.0	103260	324.1	554.6	13.32	549.7	2.89	3.84
23	2725	46.9	1821	56.9	102294	321.0	559.6	13.52	550.1	2.83	3.77
24	2655	46.8	1788	56.8	102469	321.6	545.2	13.60	549.9	2.77	3.62
25	2607	46.4	1843	56.9	103260	324.1	530.8	13.47	549.1	2.71	3.81
26	2727	46.4	1808	56.7	102557	321.9	558.8	13.30	549.5	2.66	3.73
27	2665	46.7	1941	57.6	103524	324.9	539.4	13.37	549.1	2.61	3.67
28	2751	47.1	1730	56.2	103436	324.6	560.5	13.47	549.5	2.56	3.62
29	2669	46.5	1808	56.7	103436	324.6	542.8	13.36	549.3	2.51	3.52
30	2608	46.2	1743	56.1	101854	319.7	539.2	13.57	549.0	2.47	3.47
31	2620	46.7	1901	57.4	103173	323.8	532.8	13.51	548.4	2.43	3.51
32	2741	46.6	1849	56.7	103700	315.9	555.2	13.33	548.6	2.39	3.42
33	2679	46.7	1822	57.0	102821	322.7	547.6	13.46	548.6	2.35	3.31
34	2561	46.1	1727	56.1	102997	323.3	524.6	13.52	547.9	2.32	3.52
35	2597	46.3	1878	57.2	102997	323.3	529.3	13.43	547.4	2.28	3.58
36	2740	46.4	1900	57.0	102909	323.0	558.2	13.19	547.7	2.25	3.53
37	2702	46.5	1848	56.8	103876	316.4	546.7	13.34	547.7	2.22	3.43
38	2731	46.5	1845	56.8	103173	323.8	556.0	13.25	547.9	2.19	3.36
39	2742	46.9	1732	56.2	103876	316.4	556.6	13.47	548.1	2.16	3.30
40	2647	46.4	1906	57.3	103524	315.4	536.4	13.39	547.8	2.13	3.27
41	2749	46.8	1690	55.7	103436	315.1	560.7	13.47	548.1	2.11	3.25
42	2636	46.4	1769	56.4	103788	316.2	535.2	13.48	547.8	2.08	3.23
43	2668	46.7	1825	56.7	103612	315.6	541.5	13.53	547.7	2.06	3.17
44	2651	46.7	1821	56.8	103348	324.4	539.4	13.48	547.5	2.03	3.11
45	2690	46.6	1827	56.9	103524	315.4	546.4	13.43	547.5	2.01	3.04
46	2675	46.3	1847	57.0	103876	316.4	541.3	13.31	547.3	1.99	2.99
47	2661	46.3	1913	57.5	103524	315.4	539.1	13.35	547.1	1.97	2.94

Table 3. Continued

No.	Pb		U		Th		Age	MC Error	Cumulative		
	(ppm)	(1σ)	(ppm)	(1σ)	(ppm)	(1σ)	(Ma)	(95 % C.I.)	Mean Age	MC Error	t x SE
48	2634	46.4	1786	56.6	103876	316.4	534.0	13.45	546.9	1.95	2.93
49	2744	46.7	1783	56.5	103348	324.4	558.6	13.31	547.1	1.93	2.91
50	2646	46.6	1900	57.3	103436	315.1	536.7	13.50	546.9	1.91	2.88
51	2750	47.1	1706	55.9	103700	315.9	559.3	13.54	547.1	1.89	2.86
52	2796	46.5	1756	56.0	102821	313.2	572.3	13.29	547.6	1.87	2.97
53	2639	46.5	1950	57.6	103612	315.6	533.8	13.43	547.4	1.85	2.96
54	2596	46.5	1872	57.2	103788	316.2	525.6	13.53	547.0	1.83	3.01
55	2669	46.5	1720	56.0	103260	324.1	545.0	13.42	546.9	1.82	2.96
56	2636	46.4	1770	56.4	103524	315.4	536.5	13.51	546.7	1.80	2.92
57	2641	46.3	1748	56.4	103963	316.7	535.6	13.39	546.5	1.78	2.90
58	2609	46.2	1783	56.3	104051	317.0	528.3	13.42	546.2	1.77	2.92
59	2675	46.6	1819	56.9	103700	315.9	542.5	13.44	546.2	1.75	2.87
60	2569	46.3	1839	56.7	104315	317.8	518.2	13.46	545.7	1.74	2.97

Table 4. Results of changing the measured concentration by adding/subtracting the 2σ counting errors for each element. The changes in Pb, Th and U concentrations and calculated age as a result of imputing these values into the matrix correction are shown.

Element	**1st analysis (wt %)**	**+ 2σ (wt %)**	**- 2σ (wt %)**
SiO_2	2.004	2.5464	1.4615
P_2O_5	27.57	27.6102	27.5297
CaO	0.9062	1.1419	0.6706
La_2O_3	14.52	14.6021	14.438
Ce_2O_3	29.29	29.3437	29.2364
Pr_2O_3	2.99	3.0399	2.9401
Nd_2O_3	9.77	9.9483	9.5918
Sm_2O_3	1.0139	1.0957	0.9321
Gd_2O_3	0.4103	0.4228	0.3978
Dy_2O_3	0.0215	0.1108	-0.0678*
PbO	*0.2839*	*0.2846*	*0.2832*
ThO_2	*11.67*	*11.73*	*11.62*
UO_2	*0.2175*	*0.2179*	*0.2172*
Age (Ma)	538.6	537.3 (- 1.3)	539.5 (+ 1.3)

* - zero was used in matrix correction

Table 5. Difference in concentration calculated from linear trend of 60 analyses

Element*	increase/decrease	
	conc. (wt %)	**% of total**
Pb	- 0.002	- 0.81%
U	+ 0.0002	+ 0.13%
Th	+ 0.165	+ 1.62%
Ca	- 0.006	- 0.64%
Ce	+ 0.047	+ 0.16%
P	- 0.142	- 0.51%
La	- 0.030	- 0.20%
Pr	- 0.018	- 0.59%
Si	- 0.005	- 0.23%
Y	- 0.004	- 2.05%
Sm	+ 0.053	+ 5.73%
Nd	- 0.002	- 0.02%
Gd	- 0.100	- 24.50%
Total wt. %	- 0.100	- 0.10%
Age	N/A	- 2.35%

* - Dy and S omitted as totals were too low to be significant

Table 6. Averages used for generating simulated data

Pb	U	Th
Average concentration		
2673.18	1813.12	103009.93
Average 1σ error		
46.62	56.79	319.95

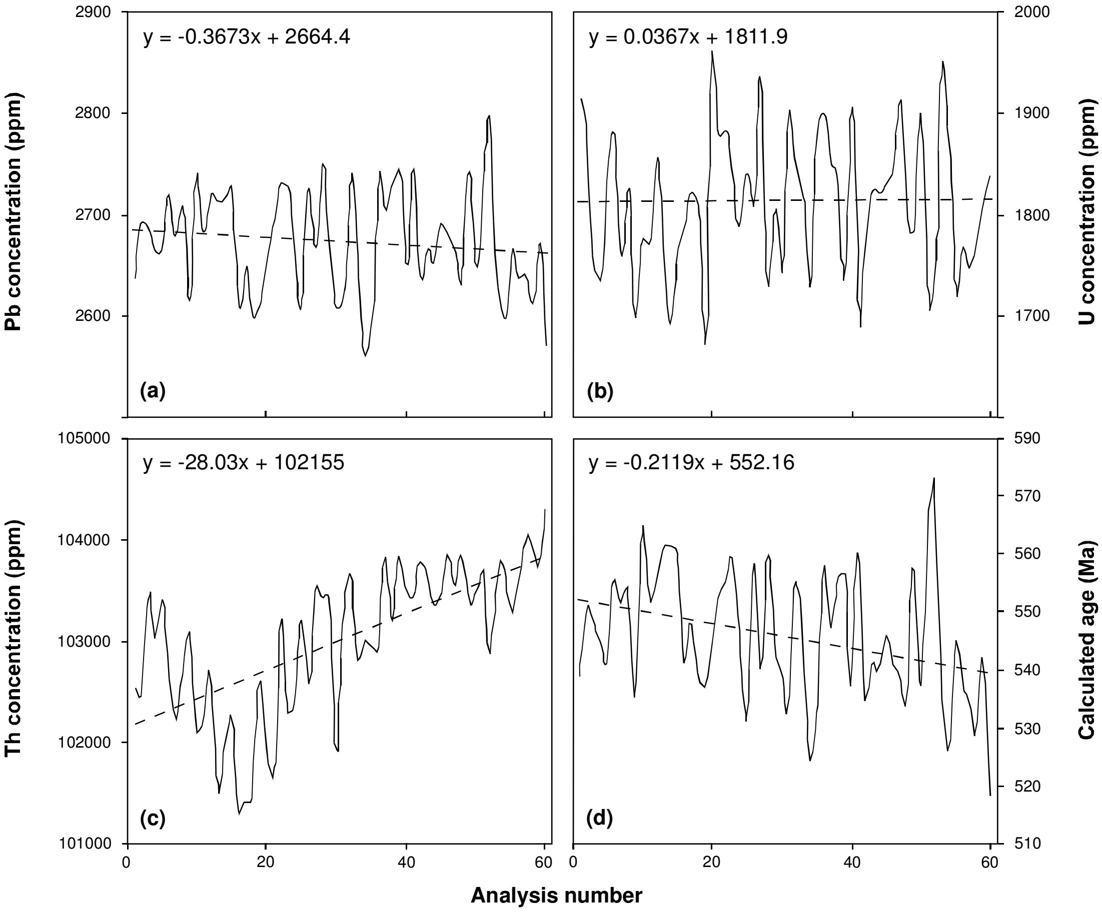

Fig. 1. Plots of measured concentration and calculated age, for increasing numbers of analyses. Pb (a) and U (b) concentration values display minimal systematic change, but Th concentration (c) shows a systematic increase over time (mostly evident after approximately 30 analyses). In response to increasing Th, calculated age (d) gradually decreases. Equations for linear trend lines fitted to the data are shown.

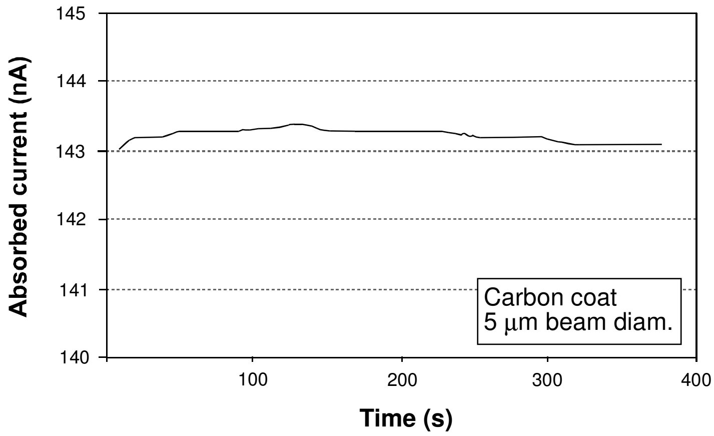

Fig. 2. Absorbed current in monazite as a function of time for a representative analysis from this data set. Sampling period was approximately 1 second.

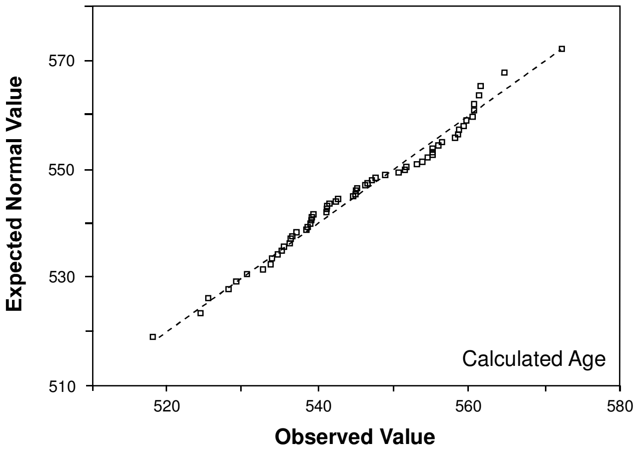

Fig. 3. Quantile-quantile (Q-Q) plot showing the correlation of the calculated ages to a normal (Gaussian) distribution.

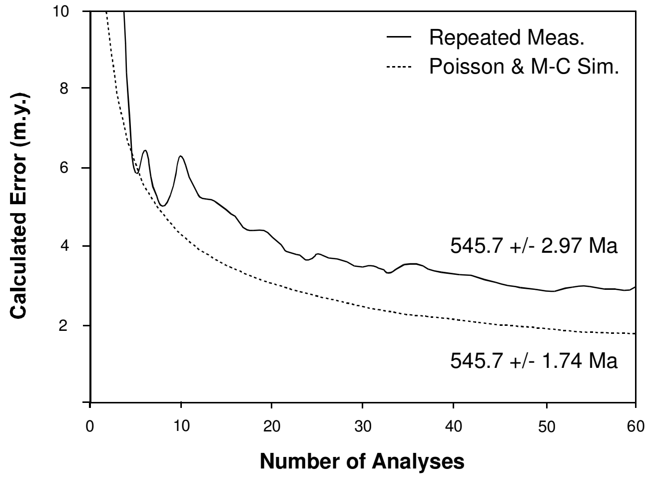

Fig. 4. Progressive age errors (95% C.I.) for both the repeated measures (Standard error multiplied by Students-*t* value) and the Poisson statistics/Monte Carlo (weighted average of simulated age errors) techniques. The final age errors are shown for both.

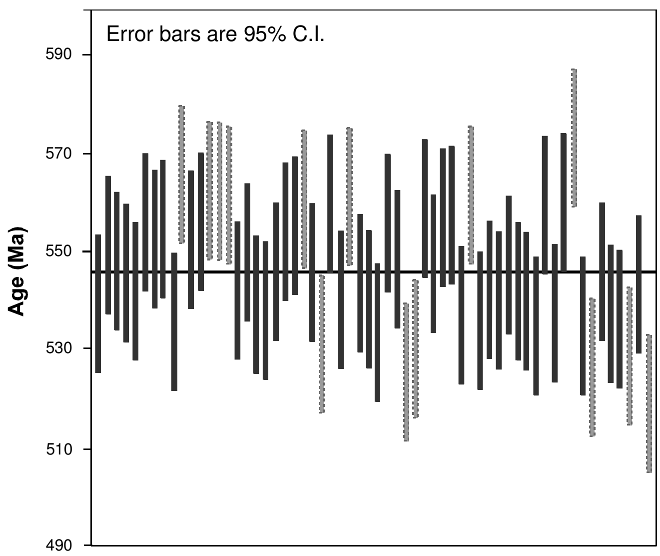

Fig. 5. Individual age measurements (60) with 95% confidence interval error bars calculated via Poisson statistics and Monte Carlo simulation. The grey bars indicate the intervals that do not include the (sample) mean.

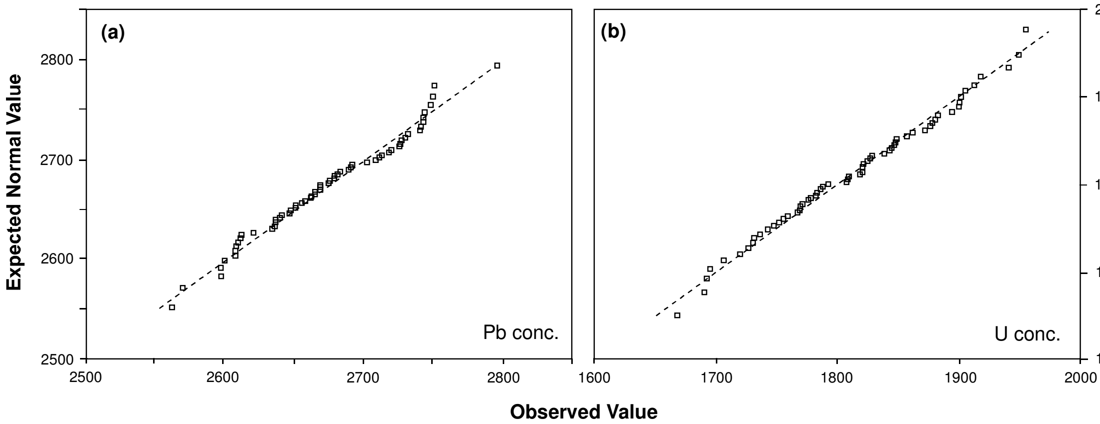

Fig. 6. Quantile-quantile (Q-Q) plot showing the correlation of the measured Pb (a) and U (b) concentrations to a normal (Gaussian) distribution.

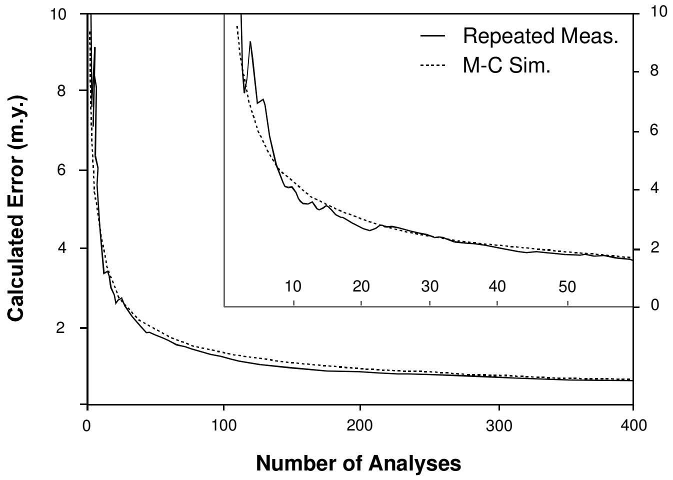

Fig. 7. Progressive age errors (95% C.I.) for both the repeated measures and the Poisson statistics/Monte Carlo techniques using 400 normally-distributed (computer) generated data points. The inset shows the plot on the same scale as the EMP data in Fig. 4.

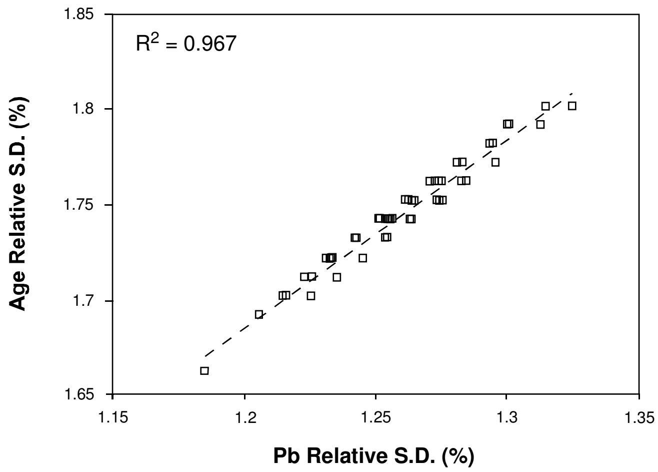

Fig. 8. Scatter plot of calculated age Relative Standard Deviation (R.S.D.) versus Pb concentration R.S.D. Values were calculated using Poisson statistics (plus Monte Carlo simulation for age values) and are at the 1σ level. The R^2 correlation coefficient is shown. Since both values are highly correlated, a reduction in Pb error will lead to a similar reduction in age error.

CHAPTER 2

OVERPRINTING ACADIAN AMPHIBOLITE-GRADE OROGENESIS IN THE TACONIC APPALACHIAN BLUE RIDGE: NEW AGES AND APPROACHES USING MONAZITE

Table 1. Summary of microstructural/textural position of monazites analysed

Monazite grains as inclusions in porphyroblasts

Sample	Surrounding phase (fully enclosed?)	Shape	Relative to Inclusion trails (if applicable)
CH22-			
0-Mnz4	St (no)	rounded	?
140-Mnz1	St (no)	blocky	?
CH35-			
Mnz1	Ky (yes)	rounded/partially elong.	aligned (incl)
Mnz3	Grt (no)	rounded	incl free rim
Mnz4	Ky (no)	rounded	not aligned
Mnz6	St (no)	rounded	N/A
CH62-			
Mnz1	St (yes)	pris./partly elong.	yes
Mnz3	St (no)	blocky/partly elong.	uncertain

Monazite grains in matrix

Sample	Position/ Fabric	Shape	Relative to Fabric
CH22-			
30-Mnz1	S_m	elongate	parallel
30-Mnz2	S_m	elongate	parallel
0-Mnz3	S_m	elongate	parallel
CH27-			
20-Mnz1	S_B (= S_m)*	elongated	parallel
20-Mnz2	S_B? (= S_m)*	blocky	sub-parallel?
50-Mnz2	S_A?*	rounded/partly elong.	uncertain
CH35-			
Mnz2	$S_?$	large/mostly elongate	sub-parallel
Mnz5	$S_?$	elongated	parallel
CH62-			
Mnz2	S_m	blocky/partly elong.	sub-parallel
Mnz4	S_m	elongated	parallel

* - S_A and S_B indicate relative timing of foliations (e.g. S_A predates S_B), S_m = dominant matrix foliation

Table 2. EPMA analytical conditions

Element - Peak	Standard	Crystal - Spectrometer	Background -/+ (mm)	Count time (s) Peak/Bgd
SiKα	[1]$PbSiO_3$	TAP-1	5/3	20/10
PKα	[3]$CePO_4$	TAP-1	3/4	20/10
SKα[#]	[1]$BaSO_4$	PETJ-3*	6/4	30/15
CaKα	[1]$CaSiO_3$	PETJ-5	1.6/1.6	20/10
YLα	[3]YPO_4	TAP-1	1.25/2	90/45
LaLα	[3]$LaPO_4$	LIFH-3*	1.6/1.6	10/5
CeLα	[3]$CePO_4$	LIFH-3*	3.2/3.2	10/5
PrLβ	[3]$PrPO_4$	LIFH-3*	1/1	20/10
NdLβ	[3]$NdPO_4$	LIFH-3*	1/1	10/5
SmLβ	[3]$SmPO_4$	LIFH-3*	1/1	40/20
GdLβ	[3]$GdPO_4$	LIFH-3*	1/1	40/20
DyLβ	[3]$DyPO_4$	LIFH-3*	1/4	40/20
PbMα	[1]$PbSiO_3$	PETJ-2*	4/6	180/90
ThMα	[2]ThO_2	PETJ-5	2.5/3	90/45
UMβ	[1]U	PETJ-4	3.5/2.5	180/90

* - sealed Xe detectors, others are P-10 gas-flow detectors

[#] - S not routinely analysed in this study

Standards: 1 - Astimex, 2 - Taylor, 3 - Pb-free synthetic (J. Pyle, RPI ,USA)

Table 3. Summary of monazite domains, compositions, mean dates and confidence intervals

Sample	Domain	n	Comp range (wt%)		Mean*	95% CI*		Comment
			Th	Y	(Ma)	SE x t	boot.	
CH22-								*Manangotry: 556 ± 11 Ma (n=10)*
30-Mnz1	core	4	2.7-3.3	1.34-1.49	425	33		continuous zoning (minor)
	rim	5	1.7-1.9	1.26-1.30	441	23		
	total	10			**434**	**14**	13	1 additional "mixed" analysis included
30-Mnz2	total	10	1.6-2.2	1.2-1.4	**444**	**16**	15	relatively homogenuous
0-Mnz3	median	5	2.3-2.5	1.35-1.47	456	33		
	total	10	1.5-3.1	1.22-1.47	**457**	**18**	17	complex zoning
140-Mnz1	total	10	2.3-3.8	0.34-0.68	**439**	**19**	18	patchy zoning
0-Mnz4	total	10	1.7-2.9	1.22-1.45	**445**	**24**	23	complex zoning
CH27-								*Manangotry: 556 ± 9 Ma (n=10)*
20-Mnz1	total	7	2.8-3.2	1.2-1.4	**451**	**17**	16	relatively homogenuous
20-Mnz2	total	10	2.5-2.9	1.5-1.8	**443**	**24**	23	relatively homogenuous
50-Mnz2	core	4	3.1-3.2	1.03-1.06	445	11		high U (~ 0.8 wt%)
	rim	10	2.2-3.0	1.13-1.64	440	9	8	complex zoning, U: 0.40-0.52 wt%
	total	14			**442**	**6**	6	core and rim ages indistinguishable
CH35-								*Manangotry: 551 ± 7 Ma (n=10)*
Mnz1	total	10	1.6-5.9	1.53-1.70	**452**	**20**	19	semi-continuous zoning
Mnz2	core	6	4.5-5.1	1.59-1.75	454	11	10	
	total	15	1.4-5.1	1.42-1.75	**464**	**10**	10	semi-continuous, patchy zoning
Mnz3[#]	total	9	1.3-1.6	0.9-2.3	**424**	**34**	32	U: 0.08-0.3 wt%, in assoc. with xen.
Mnz4	core	4	2.5-2.8	1.49-1.55	433	35		relatively homogenuous
	rim	10	1.2-1.8	1.36-1.57	411	25	24	
	total	16			**428**	**24**	23	2 additional analyses included
Mnz5	core	5	1.8-2.4	1.46-1.60	441	58	52	
	rim	5	1.1-1.4	1.37-1.53	438	54	50	
	total	10			**440**	**33**	32	
Mnz6	total	10	1.6-1.8	0.61-1.05	**310**	**25**	24	relatively homog., low U: 0.07-0.1 wt%

Table 3. Continued

Sample	Domain	n	Comp range (wt%)		Mean*	95% CI*		Comment
			Th	Y	(Ma)	SE x t	boot.	
CH62-								*Manangotry: 552 ± 11 Ma (n=10)*
Mnz1	core-A	5	7.4-7.9	0.36-0.47	**451**	**8**	8	core-B not analysed
	rim	7	0.7-2.0	0.06-0.16	**417**	**45**	41	
Mnz2	core-A	1	8.8	0.48	451			only 1 analysis
	core-B	5	4.7-5.7	0.32-0.52	450	22	19	
	core-total	6			**450**	**16**	15	Y-conc and dates indistinguishable
	rim	7	0.7-1.4	0.08-0.12	**398**	**32**	30	
Mnz3	total	7	1.0-3.6	0.1-0.36	**440**	**47**	44	probably mixed
Mnz4	core-A	2	7.2-7.4	0.45-0.48	455			
	core-B	3	4.7-5.6	0.46-0.53	451			
	core-total	5			**453**	**21**	19	Y-conc and dates indistinguishable
	rim	5	1.0-2.0	0.08-0.18	**390**	**31**	28	

* - CI = confidence interval; SE x t = standard error of the mean multiplied by the Student's t value for n-1 degrees of freedom; boot. = results of bootstrap method

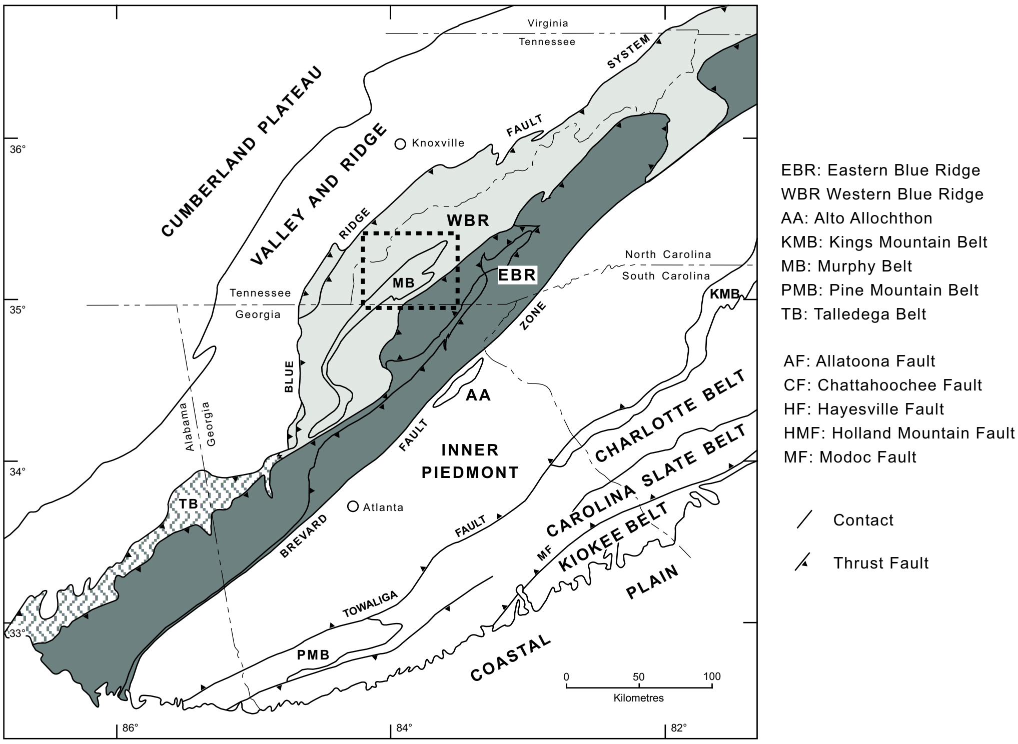

Fig. 1. Regional geology map of the southern Appalachians, showing extent of different lithostratigraphic belts/provinces. The Blue Ridge province is separated from the Valley and Ridge to the northwest by the Blue Ridge fault system (Holston-Iron Mountain, Great Smoky, Cartersville Faults), and from the Inner Piedmont province to the southeast by the Brevard Fault Zone (King, 1955; Hatcher, 1972). The location of the study area is marked. Modified after German (1989).

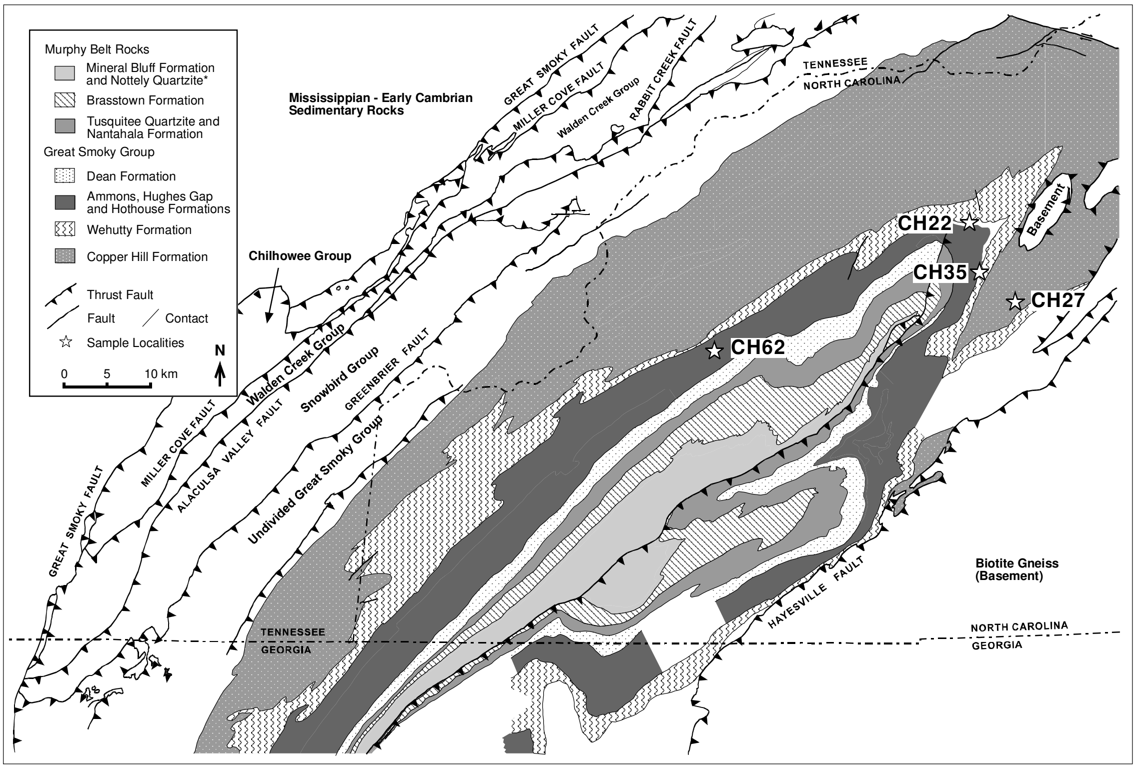

Fig. 2. Map showing the geology and sample localities around the Murphy Syncline, North Carolina and neighbouring Georgia and Tennessee. The syncline is best represented by the trace of the Ammons Creek, Hughes Gap and Hothouse Formations. Modified from Wiener and Merschat (1992). *includes Andrews Formation and Murphy Marble.

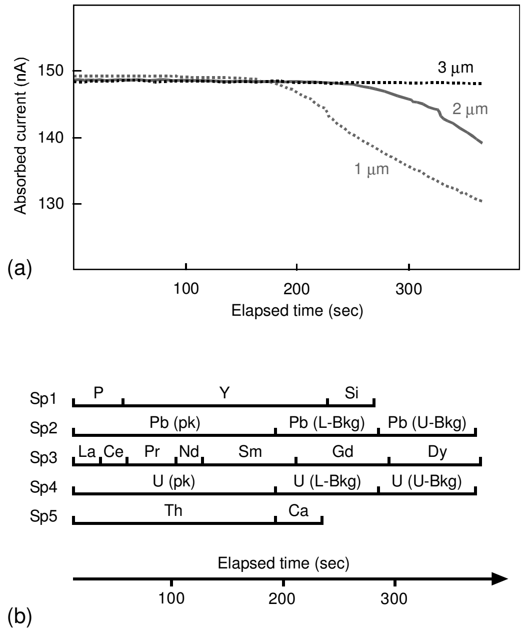

Fig. 3. (a) Measured absorbed current (nA) as a function of time and beam diameter for representative monazite analyses in this study (sample CH35). Sampling period is approximately 1 second. The Carbon coat is approximately 250 Angstroms. (b) The order and duration of measurement for each element in the protocol. Sp = spectrometer.

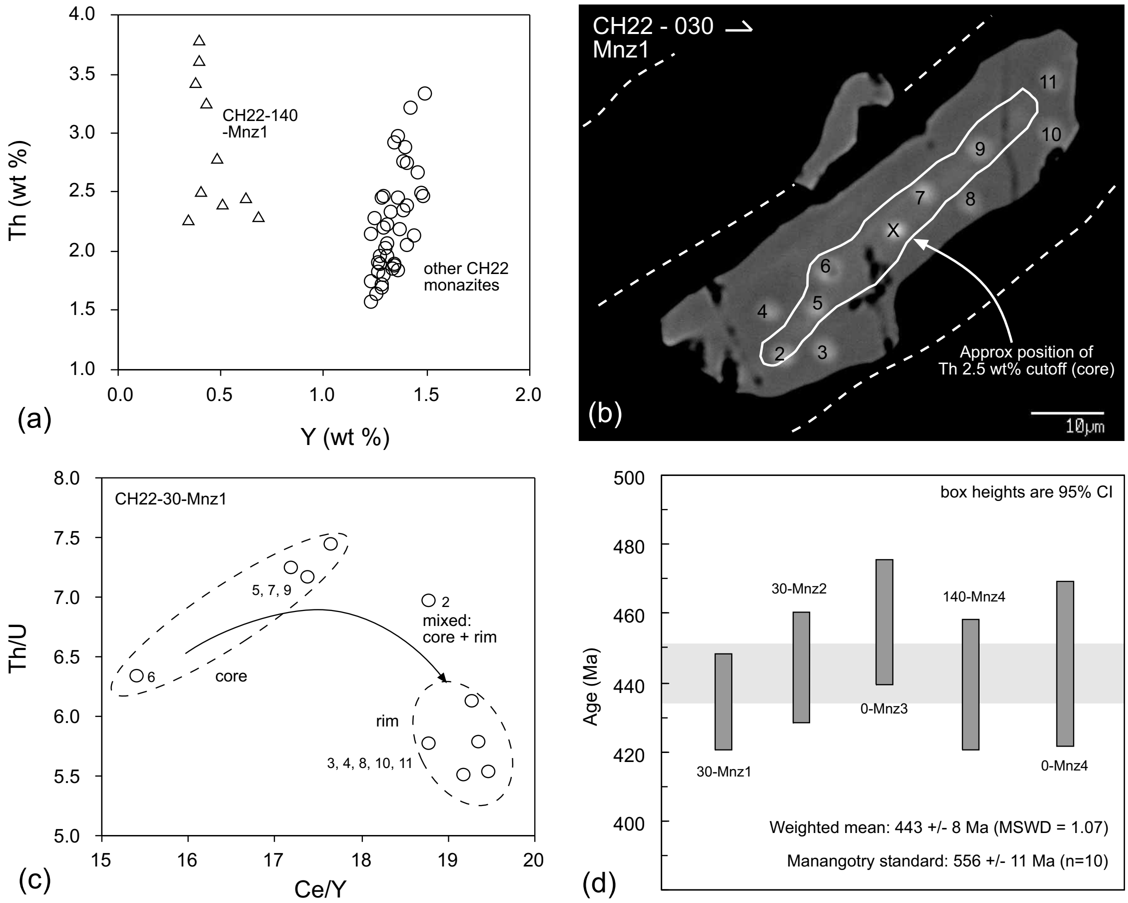

Fig. 4. (a) Plot of Th vs Y concentrations for monazites in sample CH22. Monazite 140-Mnz1 clearly has a lower Y content relative to the other monazites analysed. (b) BSE image of CH22-30-Mnz1, displaying Th variation defining the core and rim. Analytical points are shown (X = reconnaissance spot not included in the results). Dashed line represents trend of matrix foliation, barbed arrow represents strike of section. (c) Plot showing Th/U vs Ce/Y chemical evolution from core to rim for CH22-30-Mnz1. The trend represents Th being replaced by REEs (including Ce) in the monazite structure as the grain grows. Numbers correspond to analytical points shown in (b). (d) Box plot of mean dates and CIs for monazites analysed in sample CH22. The weighted mean is represented by the horizontal shaded box. The results of the Manangotry age standard applicable to this data is shown.

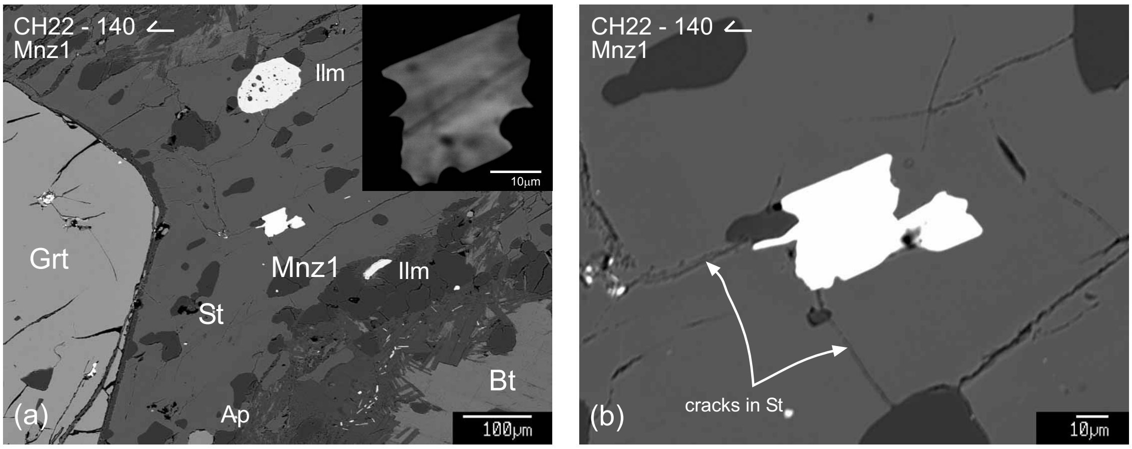

Fig. 5. (a) BSE image showing textural setting of monazite CH22-140-Mnz1. Inset: BSE image of grain. (b) BSE image, with cracks in the surrounding staurolite porphyroblast (indirectly linking monazite with the matrix) labelled.

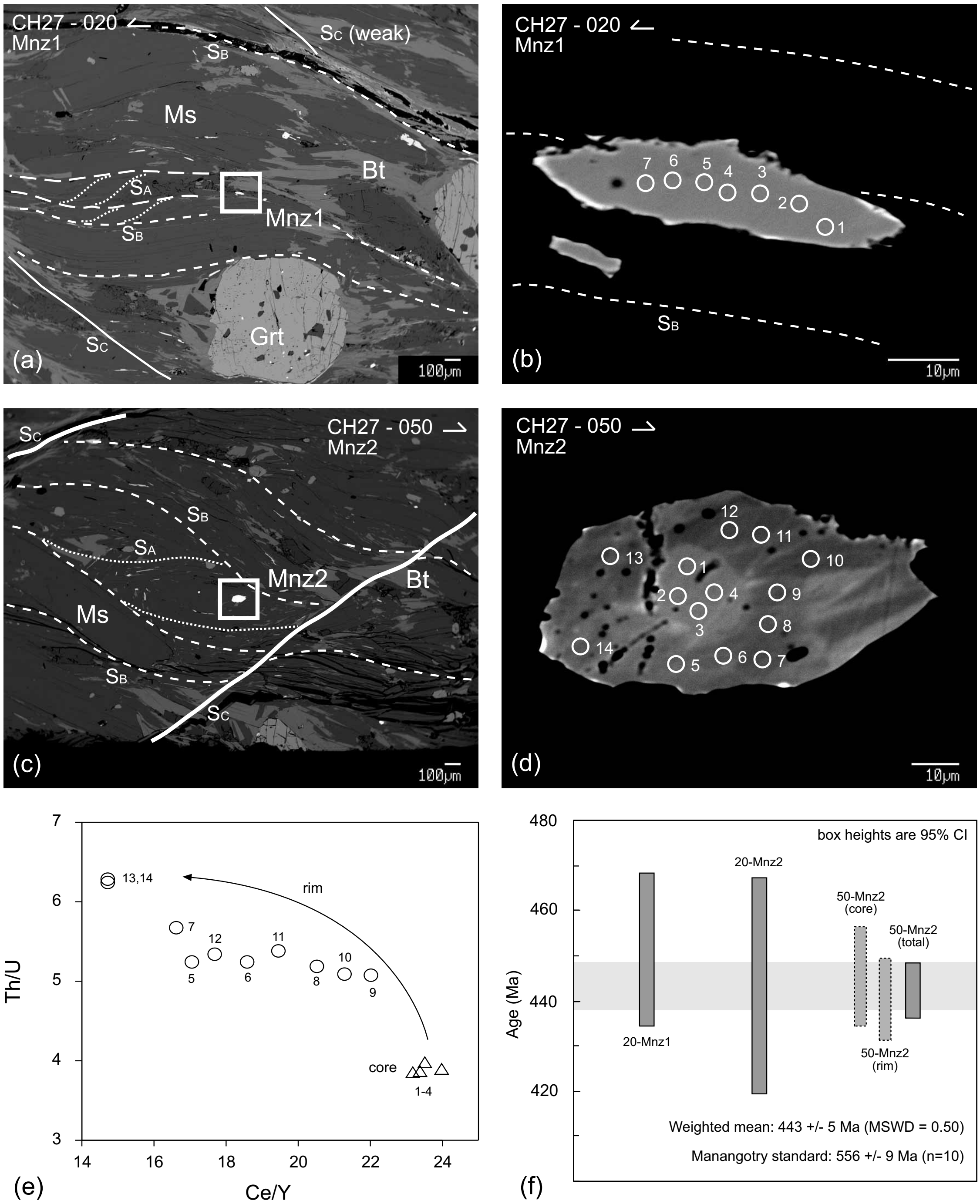
CH27 - 020
Mnz1
Sc (weak)
SB
Ms
Bt
SA
Mnz1
SB
Sc
Grt
(a)
100μm
(b)
10μm
1
2
3
4
5
6
7
CH27 - 050
Mnz2
Sc
SB
SA
Mnz2
Bt
Ms
(c)
(d)
14
13
12
11
10
9
8
Th/U
Ce/Y
13,14
rim
core
1-4
(e)
Age (Ma)
box heights are 95% CI
20-Mnz1
20-Mnz2
50-Mnz2 (core)
50-Mnz2 (total)
50-Mnz2 (rim)
Weighted mean: 443 +/- 5 Ma (MSWD = 0.50)
Manangotry standard: 556 +/- 9 Ma (n=10)
(f)

Fig. 6.

Fig. 6. (a) BSE image showing textural setting of CH27-20-Mnz1. Three generations of foliations preserved within the matrix are marked, in relative order (S_A = oldest recognised). S_B is the dominant matrix foliation, although this is weakly crenulated by S_C. Note: these foliations do not represent all foliations preserved within the sample. (b) BSE image of same monazite grain, with analytical points and matrix foliation trend marked. The grain is relatively homogeneous. (c) BSE image showing textural setting of CH27-50-Mnz2. The three foliations marked correspond to those in (a). (d) BSE image of same grain, displaying high U + Th core and similar contrast zones in small patches in the rim. Analytical spots are marked. (e) Plot of Th/U vs Ce/Y for CH27-50-Mnz2, with reverse trend to that shown in Fig. 4(c). Numbers correspond to analytical points shown in (d). (f) Box plot of mean dates for monazites analysed in sample CH27. The core and rim mean dates of 50-Mnz2 (lighter shade, with dashed outline) were not used to calculate the weighted mean, but are plotted to show they are indistinguishable. The weighted mean of the three grains is represented by the horizontal shaded box. The results of the Manangotry age standard applicable to this data is shown.

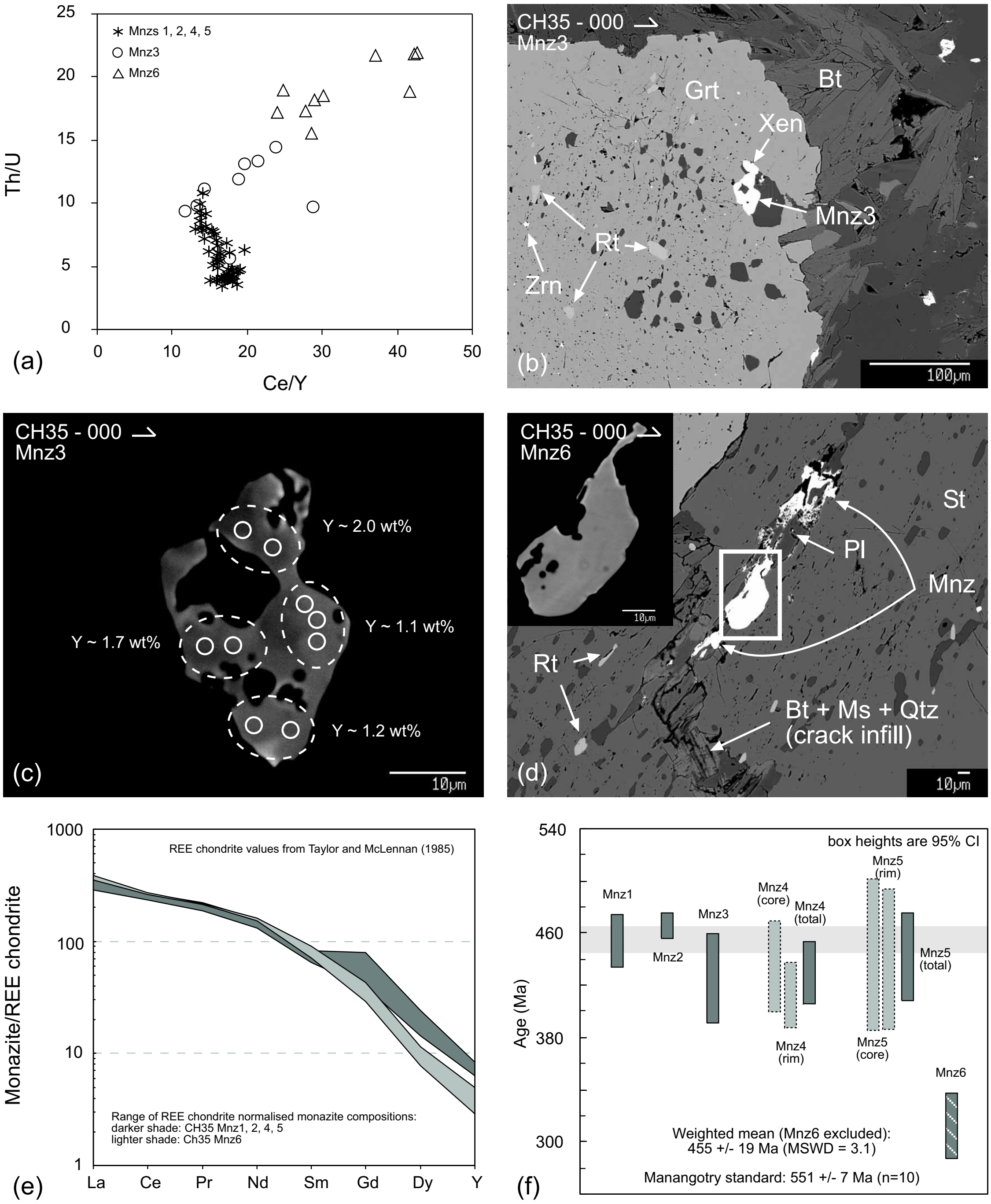

(a)
Th/U
Ce/Y
Mnzs 1, 2, 4, 5
Mnz3
Mnz6
(b)
CH35 - 000
Mnz3
Grt
Bt
Xen
Mnz3
Rt
Zrn
100μm
(c)
CH35 - 000
Mnz3
Y ~ 2.0 wt%
Y ~ 1.7 wt%
Y ~ 1.1 wt%
Y ~ 1.2 wt%
10μm
(d)
CH35 - 000
Mnz6
St
Pl
Mnz
Rt
Bt + Ms + Qtz
(crack infill)
10μm
(e)
Monazite/REE chondrite
REE chondrite values from Taylor and McLennan (1985)
Range of REE chondrite normalised monazite compositions:
darker shade: CH35 Mnz1, 2, 4, 5
lighter shade: Ch35 Mnz6
La Ce Pr Nd Sm Gd Dy Y
(f)
Age (Ma)
box heights are 95% CI
Mnz1
Mnz2
Mnz3
Mnz4 (core)
Mnz4 (total)
Mnz4 (rim)
Mnz5 (rim)
Mnz5 (core)
Mnz5 (total)
Mnz6
Weighted mean (Mnz6 excluded):
455 +/- 19 Ma (MSWD = 3.1)
Manangotry standard: 551 +/- 7 Ma (n=10)

Fig. 7.

Fig. 7. (a) Plot of Th/U vs Ce/Y ratios for monazite grains analysed in sample CH35. Grains Mnz3 (part) and Mnz6 have a distinct composition. (b) BSE image showing textural setting of Mnz3 as an inclusion in garnet, with a xenotime (Xen) inclusion in contact with the top of the grain. (c) BSE image of Mnz3, with average Y concentrations marked. The highest Y values are from the rim in contact with xenotime, although high values were also found on the garnet side of the grain, compared to the quartz side. (d) BSE image showing the textural setting of Mnz6, sitting within a crack in a staurolite porphyroblast. Bright spots in the image above and below the grain are also fragments of monazite. (e) REE chondrite normalised plot displaying the difference in composition between Mnz6 and the other monazites analysed (except Mnz3). The depletion in Y and HREEs is significant. (f) Box plot of mean dates for the monazites analysed in sample CH35. The dashed boxes (lighter shade) and Mnz6 were not used in calculating the weighted mean, but are plotted for comparison. The weighted mean of the five grains is represented by the horizontal shaded box. The results of the Manangotry age standard applicable to this data is shown.

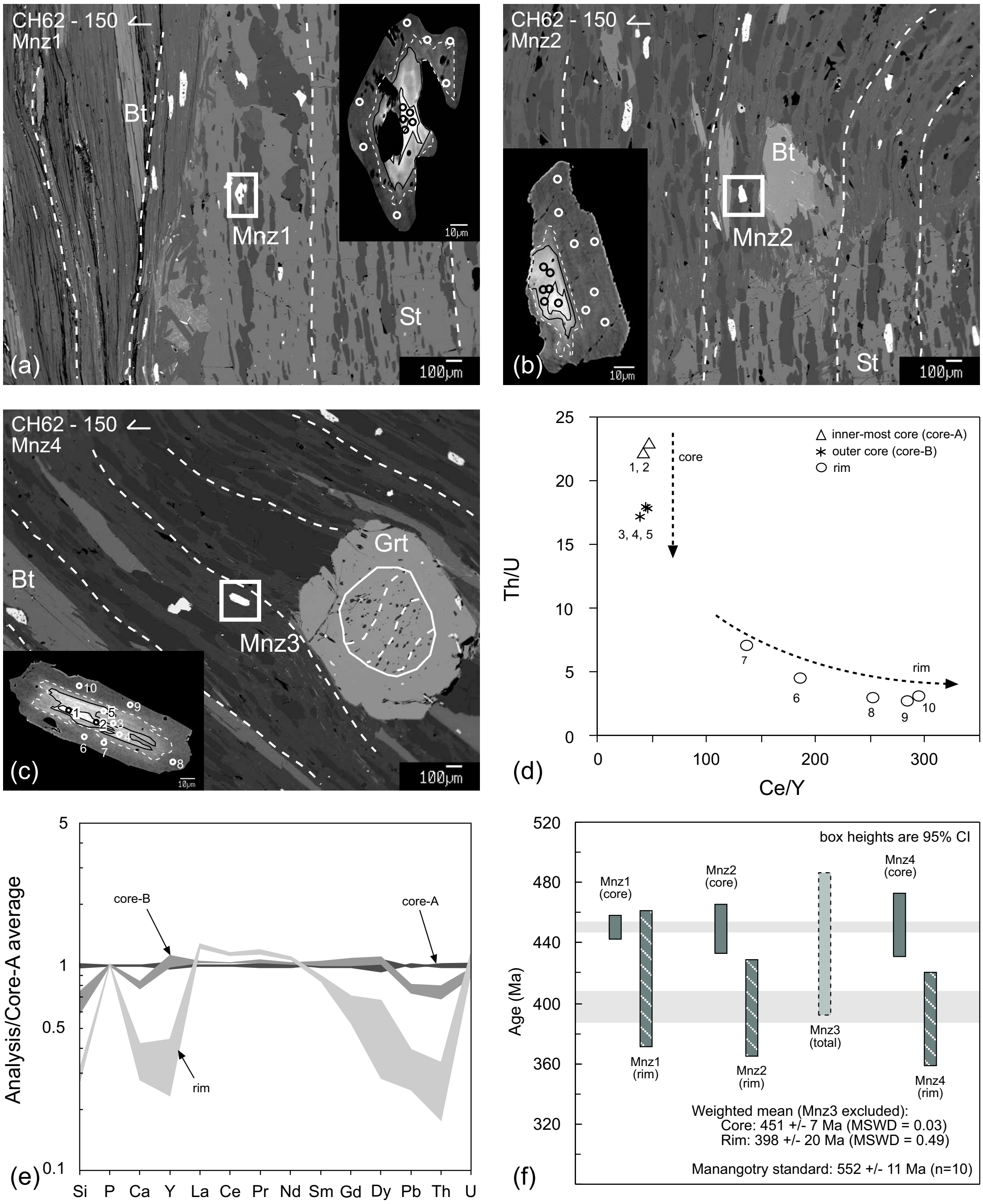
CH62 - 150
Mnz1
Bt
Mnz1
St
(a)
100μm
10μm
CH62 - 150
Mnz2
Bt
Mnz2
St
(b)
100μm
10μm
CH62 - 150
Mnz4
Grt
Bt
Mnz3
(c)
100μm
10μm
inner-most core (core-A)
outer core (core-B)
rim
core
1, 2
3, 4, 5
Th/U
Ce/Y
(d)
core-B
core-A
rim
Analysis/Core-A average
Si P Ca Y La Ce Pr Nd Sm Gd Dy Pb Th U
(e)
box heights are 95% CI
Mnz1 (core)
Mnz2 (core)
Mnz4 (core)
Mnz1 (rim)
Mnz2 (rim)
Mnz3 (total)
Mnz4 (rim)
Age (Ma)
Weighted mean (Mnz3 excluded):
Core: 451 +/- 7 Ma (MSWD = 0.03)
Rim: 398 +/- 20 Ma (MSWD = 0.49)
Manangotry standard: 552 +/- 11 Ma (n=10)
(f)

Fig. 8.

Fig. 8. (a) BSE image showing textural setting of CH62-Mnz1. Inclusion trails in staurolite are sub-parallel to the matrix foliation. Inset: BSE image of grain, with zoning profile and analytical spots marked. (b) BSE image showing textural setting of CH62-Mnz2 and the curvature of the foliation outside the staurolite porphyroblast. Inset: BSE image of grain, with zoning profile and analytical spots marked. (c) BSE image showing textural setting of CH62-Mnz4. The matrix foliation trend is at an angle those marked above due to a weak crenulation. The inclusion trail geometry (including inclusion free rim truncation) is marked on the adjacent garnet. Inset: BSE image of grain, with zoning profile and analytical spots marked. (d) Plot of Th/U vs Ce/Y ratios for Mnz4. The decrease in Th between core-A and core-B is not significantly related to a variation in Ce/Y, unlike the rim where the decrease in Y becomes evident. Numbers correspond to analytical points shown in (c). (e) Spiderplot for the same monazite, with analyses normalised to the average of core-A (i.e. the earliest stage of growth). The plot shows that the chemical variation between core-A and core-B is almost entirely a consequence of the huttonite and brabantite exchanges (decreases in Th, Si, and Ca associated with increases in the REE). The rim however shows Y and the HREEs exchanging with the LREEs (in association with the exchanges described above). (f) Box plot of mean dates for the monazites analysed in sample CH62. Weighted means for core-A and core-B (combined) and the rim analyses are represented by the horizontal shaded boxes. Mnz3 (dashed box in lighter shade) was not used in calculating a weighted mean, as it is considered to be mixed. The results of the Manangotry age standard applicable to this data is shown.

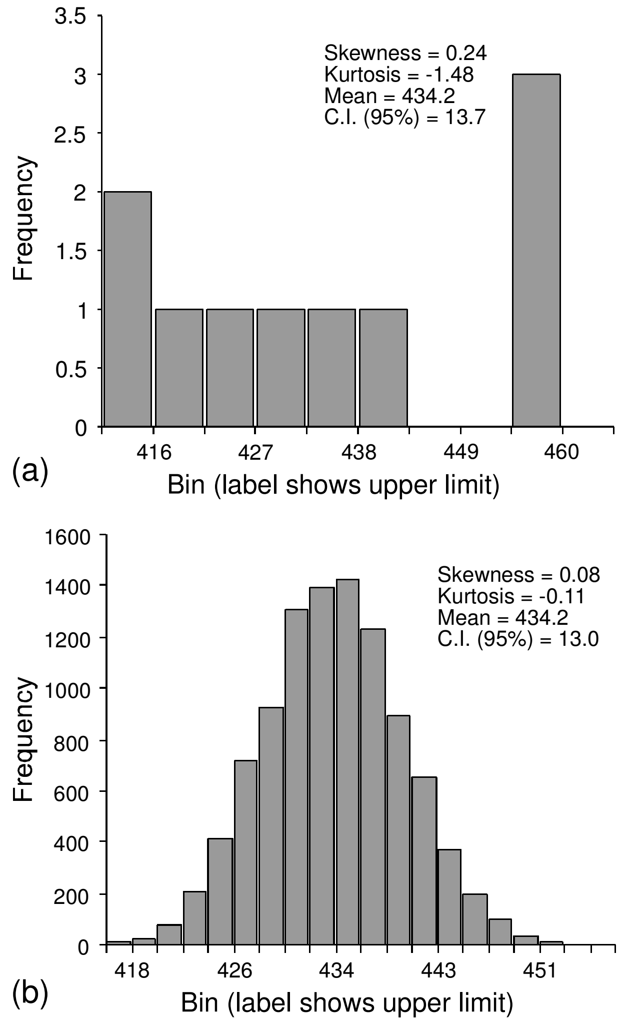

Fig. 9. (a) Histogram of calculated dates from a representative mixed composition monazite in this study (CH22-30-Mnz1), demonstrating difficulties in assuming normality and/or assessing shape of sampling distribution (n=10). (b) Output of bootstrap resampling of data in (a), showing close approximation to normality (n=10000). Differences in calculated CI between the two methods are negligible.

CHAPTER 3

ALLEGHANIAN AMPHIBOLITE FACIES TECTONISM WITHIN THE SOUTHERN BLUE RIDGE APPALACHIANS

Table 1. Summary of samples examined in this study

Sample	Assemblage*	n (t.s.)#	Mnz in Porphyroblasts	Mnz in Matrix
CA1	Grt-Bt-Ms-Qtz-Pl-Chl-Ilm	1	no	yes
CA2	Grt-Bt-Ms-Qtz-Ilm	5	no	yes
CA3	Grt-Bt-Ms-Qtz-Ilm	3	no	yes
CA4	Grt-Qtz-Bt-Ms-Ilm-Pl-Chl	2	1 v. small (Grt)	yes
CA5	Grt-St-Bt-Ms-Qtz-Chl-Py-Ilm	12	7 small (Grt + St)	yes
CA6	Grt-Bt-Ms-Qtz-Chl-Ilm	1	no	uncertain
CA7	Grt-Bt-Ms-Qtz-Chl-Ilm	2	no	yes
CA10	Grt-Bt-Ms-Qtz-Ilm	2	no	uncertain
CA14	Grt-St-Bt-Ms-Qtz-Chl-Ilm	7	3 small (Grt)	yes
CA17a	Grt-St-Bt-Ms-Qtz-Ilm	5	numerous (Grt), 2 (St)	yes
CA19	Grt-St-Bt-Ms-Qtz-Ky-Ilm-Gr	1	no	no
CA20	Grt-St-Bt-Ms-Qtz-Ky-Ilm-Gr	1	no	no
CA23	Grt-St-Bt-Ms-Qtz-Ky-Ilm-Pl-Gr	1	no	no
CA29	Grt-Bt-Ms-Qtz-Chl-Ilm	1	no	yes
CA30	Grt-Bt-Ms-Qtz-Chl-Ru-Ilm	7	numerous, small (Grt)	yes
CA31	Grt-Bt-Ms-Qtz-Pl-Ilm	1	no	yes
CA37	Grt-Bt-Ms-Qtz-Pl-Ilm	1	3 (in altered Grt)	yes
GA13	Grt-St-Bt-Ms-Qtz-Pl-Ilm	2	no	yes
W1	Grt-St-Bt-Ms-Qtz-Chl-Ilm	1	no	yes
W2c	Grt-Bt-Ms-Qtz-Pl-Chl-Ilm	2	no	yes

* mineral abbreviations after Kretz (1983)

number of thins sections examined for monazite using EPMA

Table 2. Description and microstructural setting of monazite grains analysed

Monazite grains in porphyroblasts

Sample	Surrounding phase (fully enclosed?)	Shape	Relative to Inclusion trails (if applicable)	Relationship between incl. trails
CA5-170E-Mnz1	Grt (yes)	elongate	sub parallel (rim)	cont. w/ S_m
CA17a-150A-Mnz1	Grt (no)	mostly elongate	parallel (core)	truncated by rim
CA17a-150A-Mnz2	Grt (yes)	elongate	parallel (rim)	cont. w/ S_m
CA17a-150A-Mnz3	Grt (yes)	elongate	parallel (rim)	cont. w/ S_m
CA17a-150-Mnz4	Grt (no)	elongate	parallel (core)	truncated by rim
CA30-0B-Mnz2	Grt (no)	partly elongate	parallel (core?)	truncated by rim
CA30-0E-Mnz1	Grt (yes)	rounded	N/A (rim)	?
CA30-0G-Mnz1	Grt (yes)	rounded	N/A (rim)	?

Monazite grains in matrix

Sample	Fabric	Shape	Relative to Fabric
CA5-0E-Mnz1	S_m	elongate	parallel
CA5-0E-Mnz2	S_m	blocky	parallel ?
CA5-170E-Mnz2	S_m	elongate	parallel
CA14-0A-Mnz2	S_m	blocky	sub parallel
CA14-0A-Mnz3	S_m	elongate	parallel
CA30-0E-Mnz2	S_m	elongate	parallel
CA30-0G-Mnz2	S_m	elongate	parallel

Table 3. EPMA analytical conditions

Element - Peak	Standard	Crystal - Spectrometer	Background -/+ (mm)	Count time (s) Peak/Bgd
SiKα	[1]$PbSiO_3$	TAP-1	5/3	20/10
PKα	[3]$CePO_4$	TAP-1	3/4	20/10
SKα[#]	[1]$BaSO_4$	PETJ-3*	6/4	30/15
CaKα	[1]$CaSiO_3$	PETJ-5	1.6/1.6	20/10
YLα	[3]YPO_4	TAP-1	1.25/2	90/45
LaLα	[3]$LaPO_4$	LIFH-3*	1.6/1.6	10/5
CeLα	[3]$CePO_4$	LIFH-3*	3.2/3.2	10/5
PrLβ	[3]$PrPO_4$	LIFH-3*	1/1	20/10
NdLβ	[3]$NdPO_4$	LIFH-3*	1/1	10/5
SmLβ	[3]$SmPO_4$	LIFH-3*	1/1	40/20
GdLβ	[3]$GdPO_4$	LIFH-3*	1/1	40/20
DyLβ	[3]$DyPO_4$	LIFH-3*	1/4	40/20
PbMα	[1]$PbSiO_3$	PETJ-2*	4/6	180/90
ThMα	[2]ThO_2	PETJ-5	2.5/3	90/45
UMβ	[1]U	PETJ-4	3.5/2.5	180/90

* - sealed Xe detectors, others are P-10 gas-flow detectors

[#] - S not routinely analysed in this study

Standards: 1 - Astimex, 2 - Taylor, 3 - Pb-free synthetic (J. Pyle, RPI ,USA)

Table 4. Summary of monazite domains, compositions, mean dates and confidence intervals

Sample	Set.	Dom.	n	bd	Comp range (wt%)		Mean	95% CI	Comment
					Th	Y	(Ma)	(SE x t)	
CA5-									Protocol A *Manangotry: 552 ± 9 Ma (n=6)*
0E-Mnz1	Sm	total	9	1	2.0-2.7	0.78-1.69	**312**	**20**	two Th + Y zones
0E-Mnz2	Sm	total	7	1	2.4-3.6	1.50-1.82	**334**	**9**	minor Th + Y zoning across grain
170E-Mnz1	Grt-r	total	4	1	3.0-3.3	0.42-0.58	**327**	**42***	rel. homog., excess Si from Grt
170E-Mnz2	Sm	total	9	1	2.3-2.6	1.61-1.72	**312**	**24**	relatively homogeneous
CA14-									Protocol A *Manangotry: 552 ± 9 Ma (n=6)*
Mnz2	Sm	total	7	1	2.3-3.0	1.43-1.61	**311**	**31**	minor compositional variation
Mnz3	Sm	total	5	1	3.2-3.7	0.94-1.4	**312**	**40**	minor comp. variation, 1 low Y value
CA17a-									Protocol B *Manangotry: 551 ± 6 Ma (n=10)*
150A-Mnz1	Grt-c	total	8	3	4.4-6.4	0.85-1.10	**323**	**7**	Th + Y + U decr. from core-rim
150A-Mnz2	Grt-r	total	8	3	3.1-5.1	1.16-1.35	**315**	**12**	Th + Y + U decr. from core-rim (tips)
150A-Mnz3	Grt-r	total	6	3	3.2-4.6	0.68-1.01	**304**	**23**	Th + Y + U decr. from core-rim (tips)
150-Mnz4	Grt-c	total	10	3	3.2-5.3	0.51-0.85	**309**	**15**	some Th + Y + U variation

Table 4. Continued

Sample	**Set.**	**Dom.**	**n**	**bd**	**Comp range (wt%)**		**Mean**	**95% CI**	**Comment**
					Th	**Y**	**(Ma)**	**(SE x t)**	
CA30-									Protocol A *Manangotry: 548 ± 10 Ma (n=6)*
0B-Mnz2	Grt-c	total	6	1	2.2-2.5	0.23-0.66	**309**	**22**	relatively homog., U: 0.7-0.9 wt%
0E-Mnz1	Grt-r	total	4	1	2.6-2.7	0.7	**318**	**30***	homogeneous, excess Si in 1 analysis
0E-Mnz2	Sm	total	5	1	2.4-2.7	1.49-1.66	**326**	**27**	relatively homogeneous
0G-Mnz1	Grt-r	total	5	1	2.9-3.0	0.83-0.90	**323**	**6***	rel. homog., excess Si in 1 analysis
0G-Mnz2	Sm	total	7	1	1.9-2.6	1.41-1.69	**335**	**23**	minor irregular Th + Y variation

Set. = summary of setting (see Table 2 for more details)

Dom. = domain

n = number of analyses

bd = beam diameter

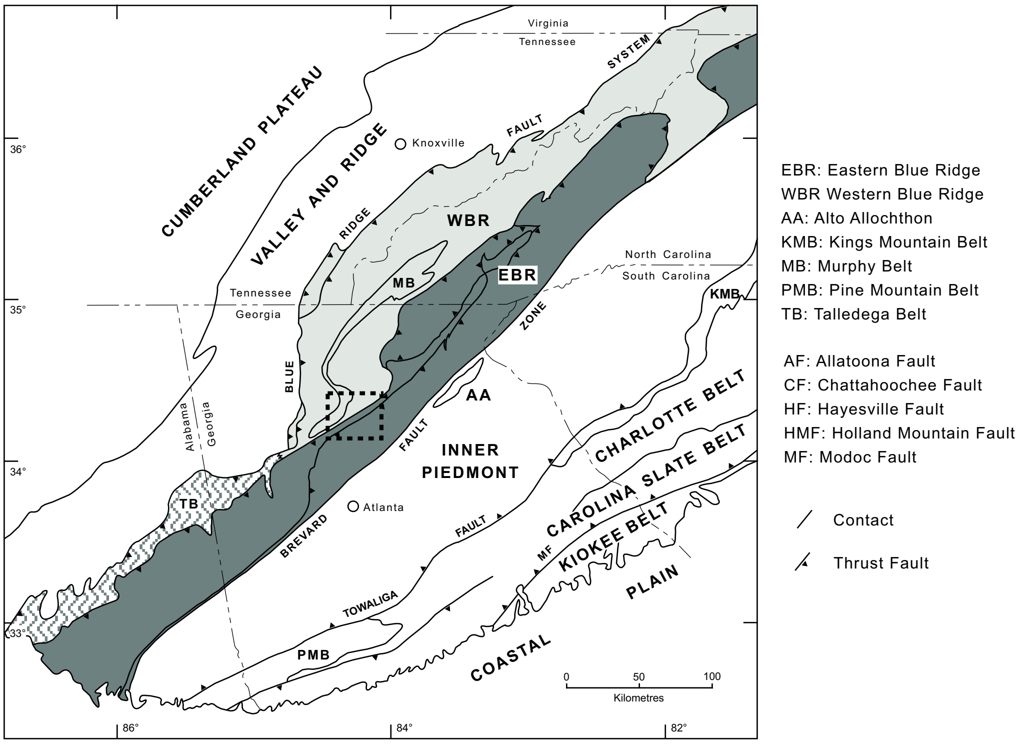

Fig. 1. Regional geology map of the southern Appalachians, showing extent of different lithostratigraphic belts/provinces. The Blue Ridge province is separated from the Valley and Ridge to the northwest by the Blue Ridge fault system (Holston-Iron Mountain, Great Smoky, Cartersville Faults), and from the Inner Piedmont province to the southeast by the Brevard Fault Zone (King, 1955; Hatcher, 1972). The location of the study area is marked. Modified after German (1989).

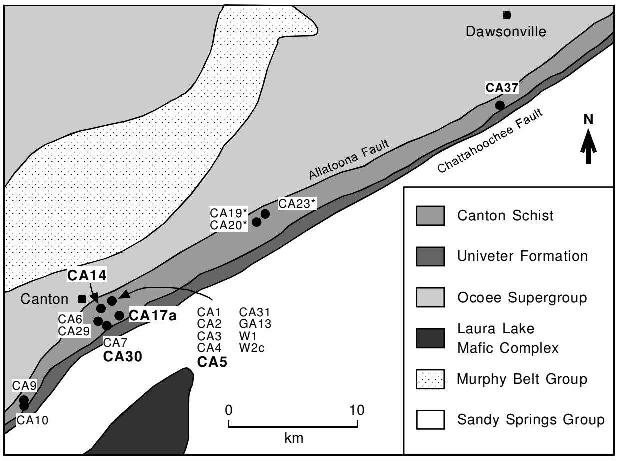

Fig. 2. Simplified geological map showing sample localities. Bold font indicates samples with monazite inclusions (> 5mm) in porphyroblasts, whereas plain font indicates samples with monazite either located exclusively in the matrix or too small to detect as inclusions. No monazite was located in samples indicated with *.

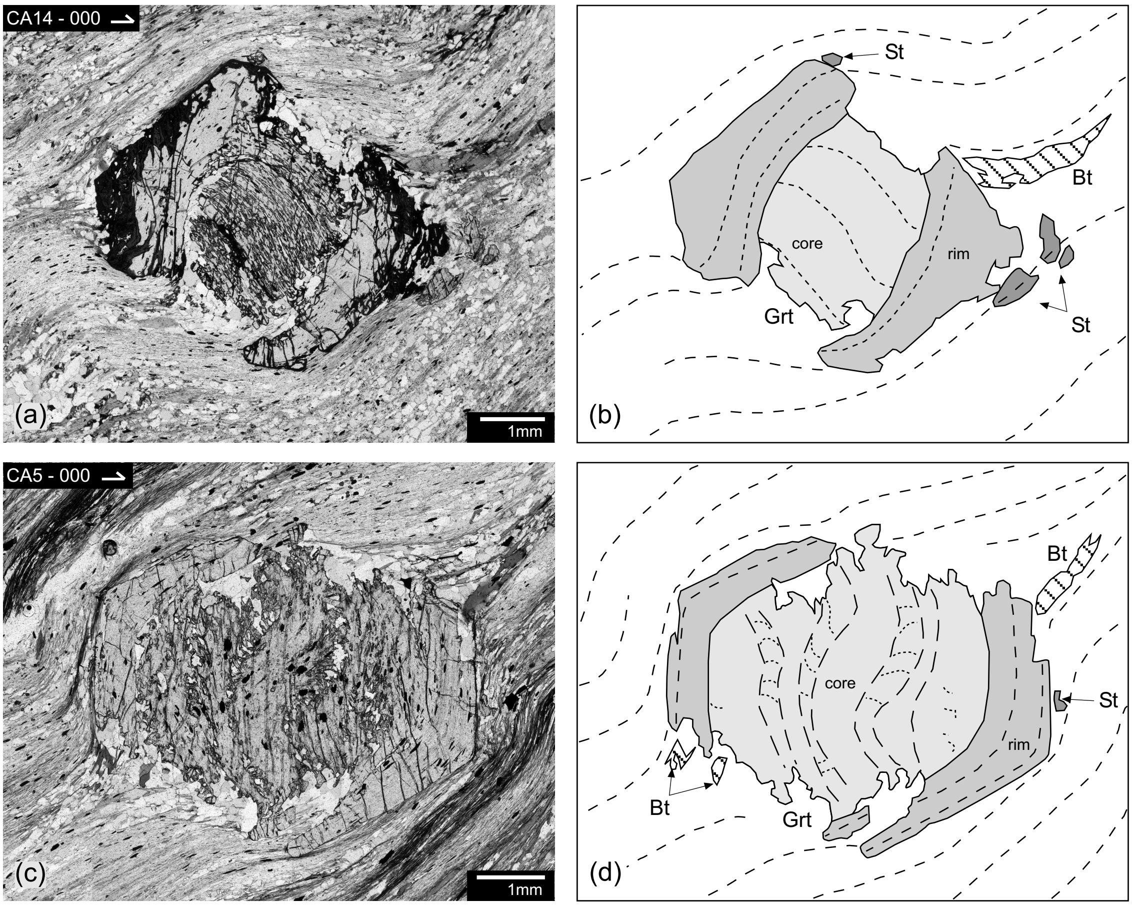

Fig. 3. (a) Photomicrograph and (b) line diagram of a typical garnet porphyroblast from this study showing a clear textural difference between the inclusion-rich core relative to the rim. The core grew during the early stages of development of the differentiated crenulation cleavage present in the rim. The rim grew during the development of a subsequent low angle foliation. Vertical thin section. Strike and way up shown by single barbed arrow. Plane-polarised light. (c) Photomicrograph and (d) line diagram showing a garnet porphyroblast preserving multiple stages of foliation development as inclusion trails. Prior to garnet growth, coaxial deformation resulted in a sub-vertical crenulation cleavage, retaining remnants of the original foliation as crenulation hinges. The bulk of the garnet core subsequently grew during the early stages of development of a sub-horizontal crenulation cleavage. The second stage of the core is weakly preserved, but relates to sub-vertical differentiated crenulation cleavage development, now present in the rim. The rim grew during the development of the approximate 45 degree matrix foliation. Vertical thin section. Strike and way up shown by single barbed arrow. Plane-polarised light.

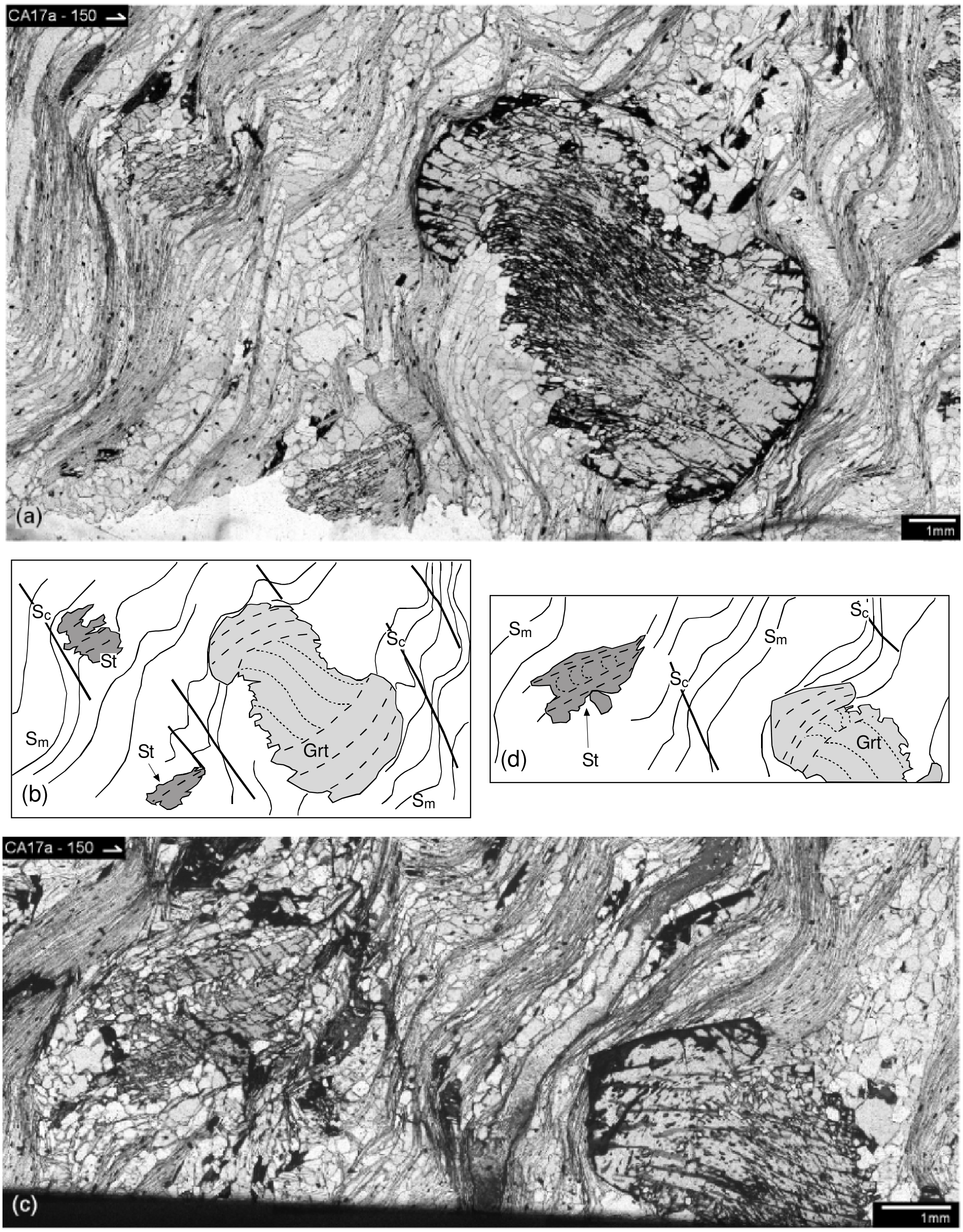
CA17a - 150
(a)
1mm
Sc
St
Sc
Sm
St
Grt
(b)
Sm
Sm
Sc
Sm
St
Grt
(d)
CA17a - 150
(c)
1mm

Fig. 4.

Fig. 4. (a) Photomicrograph and (b) line diagram of sample CA17a showing that staurolite and the rims of a garnet porphyroblasts, overgrew the same foliation (S_m) during the development of a sub-vertical crenulation cleavage (S_c). Vertical thin section. Strike and way up shown by single barbed arrow. Plane-polarised light. (a) Photomicrograph and (b) line diagram from a different section of the same sample in (a), also showing the preservation of the same foliation in staurolite and the rims of garnet porphyroblasts. Relict hinges from the development of the sub-horizontal differentiated crenulation cleavage (S_m), are also preserved in both phases. Vertical thin section. Strike and way up shown by single barbed arrow. Plane-polarised light.

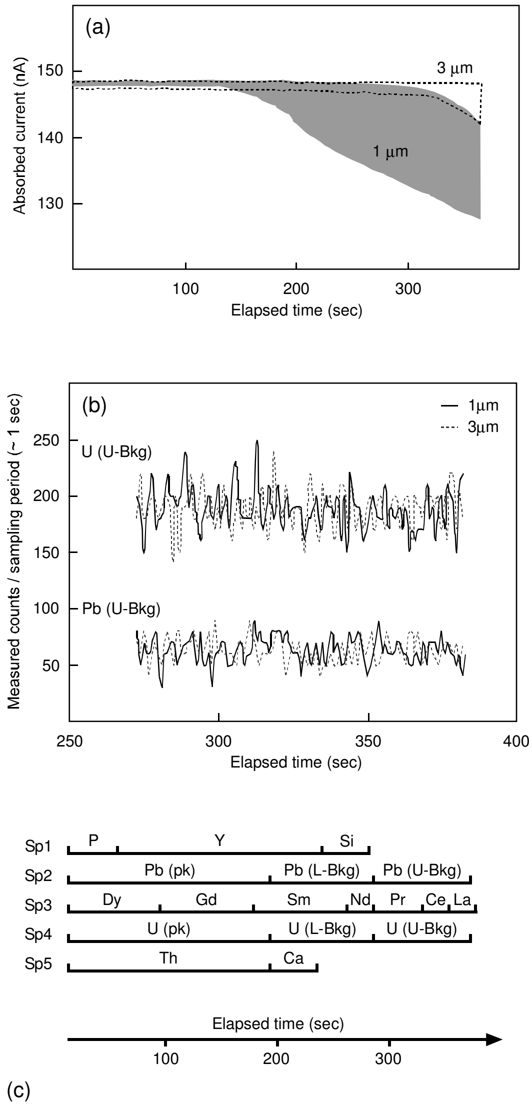

Fig. 5. (a) Range of measured absorbed current (nA) as a function of time and beam diameter for different monazite analyses (1 mm: n = 10, 3 mm: n = 8). Sampling period is approximately 1 second. The Carbon coat is approximately 250 Angstroms. (b) Average recorded counts per sampling period on U and Pb upper background for the 1 and 3 mm (beam diameter) analyses used in (a). No affect on count rate associated with decreasing absorbed current is observed in the final stages of measuring these elements, hence no affect on the calculated date is expected. (c) The order and duration of measurement for each element in Protocol "A". The measurement order on spectrometer 3 is reversed in Protocol "B", such that La is measured first and Dy is measured last. Sp = spectrometer.

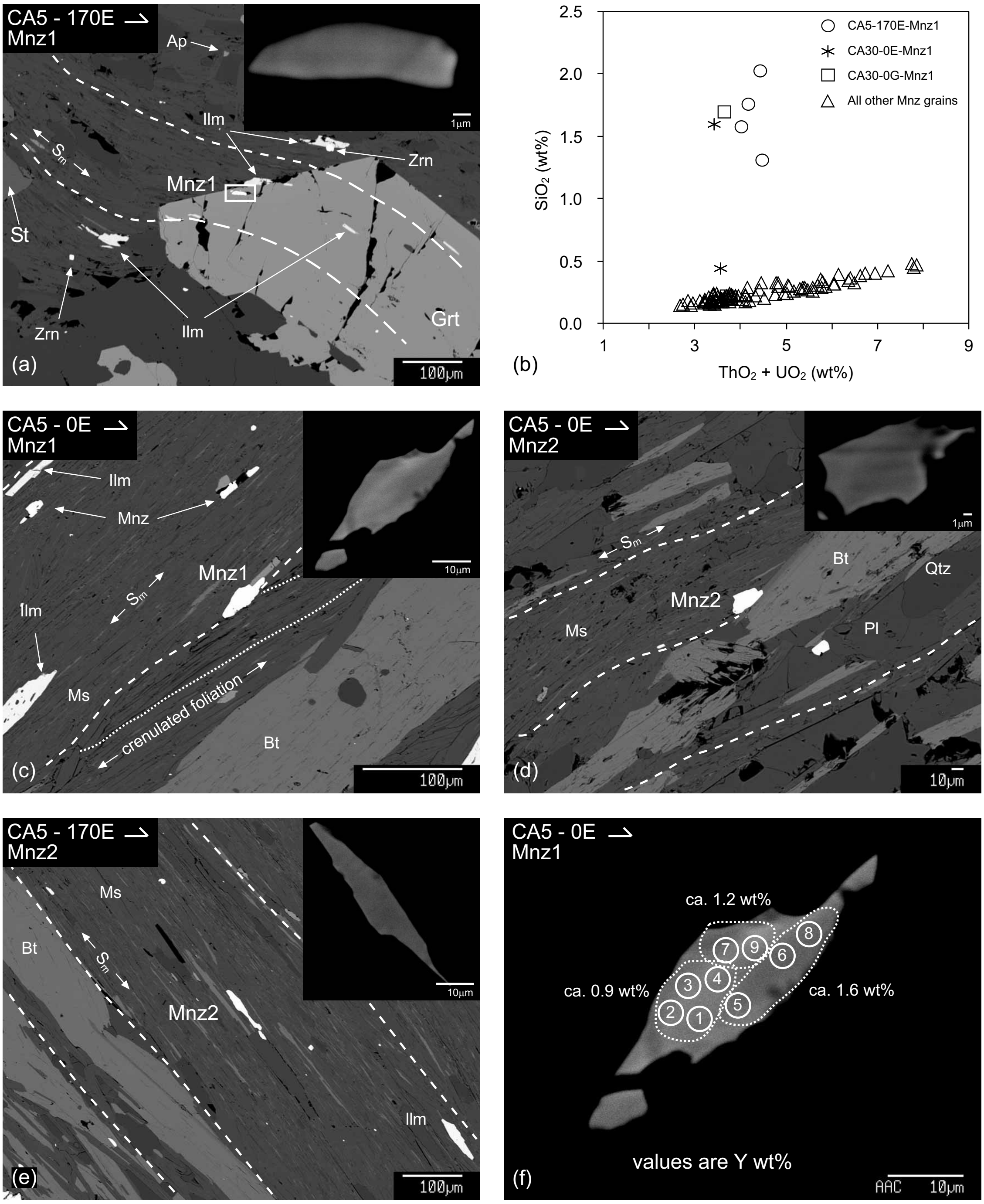
CA5 - 170E
Mnz1
Ap
Ilm
Zrn
Mnz1
St
Zrn
Ilm
Grt
(a)
100μm
1μm
2.5
2.0
1.5
1.0
0.5
0.0
1
3
5
7
9
SiO2 (wt%)
ThO2 + UO2 (wt%)
CA5-170E-Mnz1
CA30-0E-Mnz1
CA30-0G-Mnz1
All other Mnz grains
(b)
CA5 - 0E
Mnz1
Ilm
Mnz
Mnz1
Ilm
Ms
crenulated foliation
Bt
(c)
100μm
10μm
CA5 - 0E
Mnz2
Bt
Qtz
Mnz2
Ms
Pl
(d)
10μm
1μm
CA5 - 170E
Mnz2
Ms
Bt
Mnz2
Ilm
(e)
100μm
10μm
CA5 - 0E
Mnz1
ca. 1.2 wt%
ca. 0.9 wt%
ca. 1.6 wt%
values are Y wt%
(f)
AAC 10μm

Fig. 6.

Fig. 6. (a) BSE images showing location and detail (inset) of monazite grain CA5-170E-Mnz1, in the rim of a garnet porphyroblast. The grain is elongate, parallel to the inclusions trails, which are continuous with, but curve into S_m. (b) Plot of ThO_2 + UO_2 vs SiO_2 for all monazites in this study, showing excess SiO_2 in all analyses of CA5-170E-Mnz1, two from CA30-0E-Mnz1, and one from CA30-0G-Mnz1. All other analyses show correlation between ThO_2 + UO_2 and SiO_2 as expected due to the huttonite exchange in monazite. (c) BSE images showing location and detail (inset) of monazite grain CA5-0E-Mnz1, within S_m. (d) BSE images showing location and detail (inset) of monazite grain CA5-0E-Mnz2, within S_m. (e) BSE images showing location and detail (inset) of monazite grain CA5-170E-Mnz2, lying elongate and parallel to S_m. (f) BSE image of monazite grain CA5-170E-Mnz1, showing analytical spots and average Y concentrations for each "domain". Analyses 7 and 9 are a mixture of the other domains.

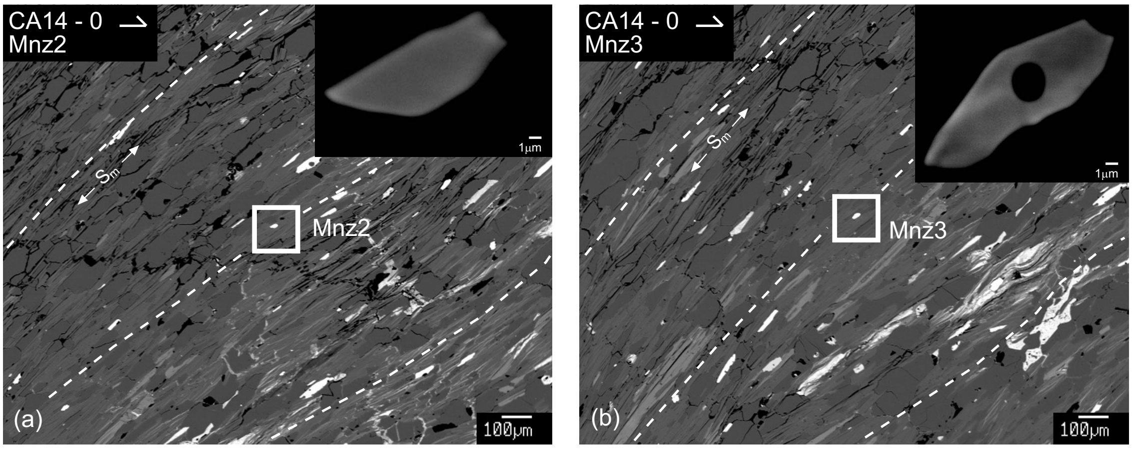

Fig. 7. (a) BSE images showing location and detail (inset) of monazite grain CA14-0-Mnz2, lying partially elongate and sub-parallel to S_m. (b) BSE images showing location and detail (inset) of monazite grain CA14-0-Mnz3, lying elongate and parallel to S_m.

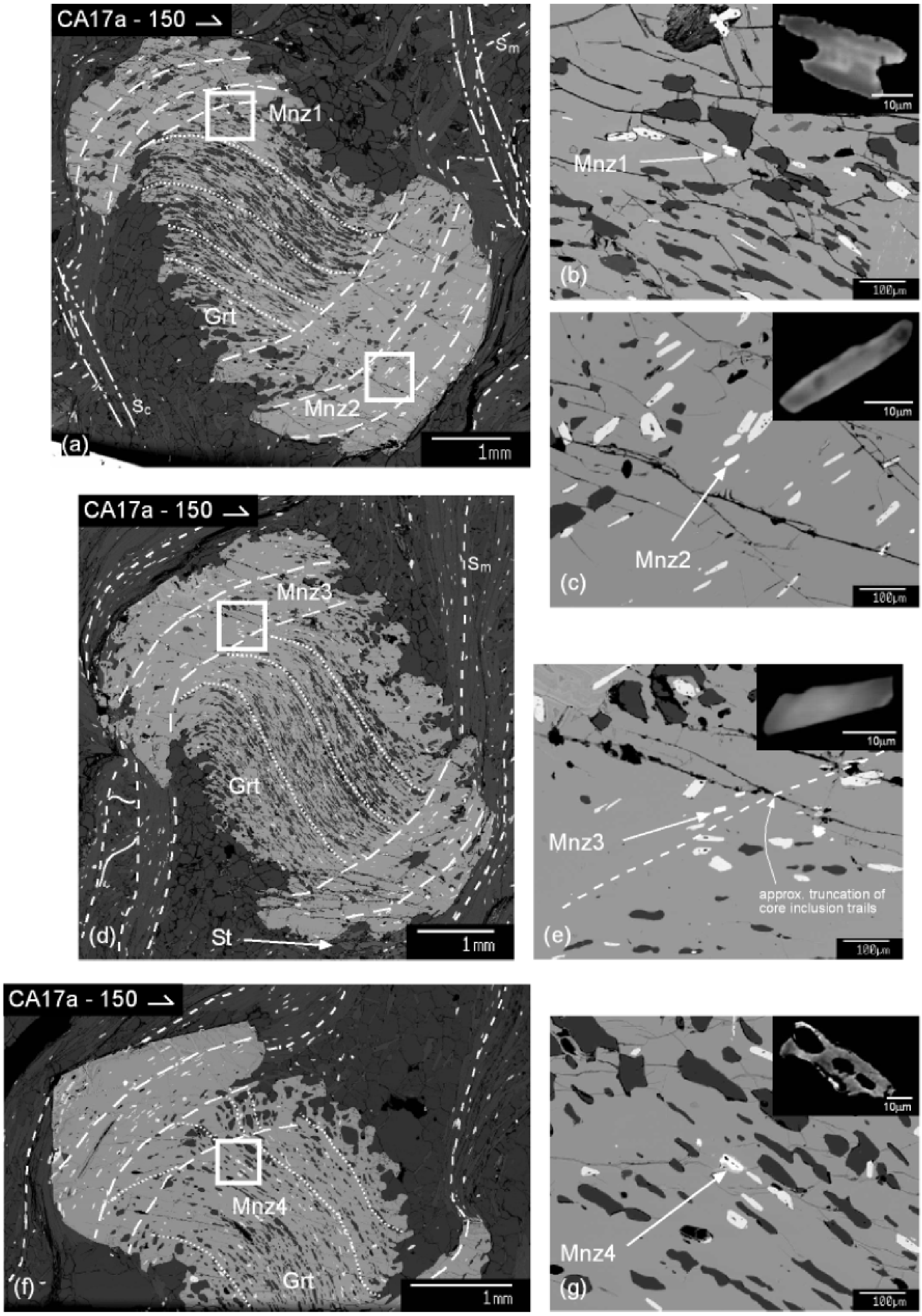
CA17a - 150
Mnz1
Mnz2
Grt
Sm
Sc
(a)
1mm
Mnz1
(b)
10µm
100µm
Mnz2
(c)
10µm
100µm
CA17a - 150
Mnz3
Grt
Sm
St
(d)
1mm
Mnz3
approx. truncation of
core inclusion trails
(e)
10µm
100µm
CA17a - 150
Mnz4
Grt
(f)
1mm
Mnz4
(g)
10µm
100µm

Fig. 8.

Fig. 8. (a) BSE image of garnet porphyroblast showing the locations of monazite inclusions Mnz1 (b) and Mnz2 (c) in sample CA17a. Both grains lie parallel to the inclusion trails in the core and the rim of the porphyroblast respectively. (d) BSE image of garnet porphyroblast showing the location of monazite inclusion Mnz3 (e) in sample CA17a. The grain lies sub-parallel to the inclusion trails in the rim of the porphyroblast, adjacent to the truncation of inclusion trails in the core. (f) BSE image of garnet porphyroblast showing the location of monazite inclusion Mnz4 (g) in sample CA17a. This grain is elongate, parallel to the inclusion trails in the core of the porphyroblast, and contains similarly oriented quartz inclusions.

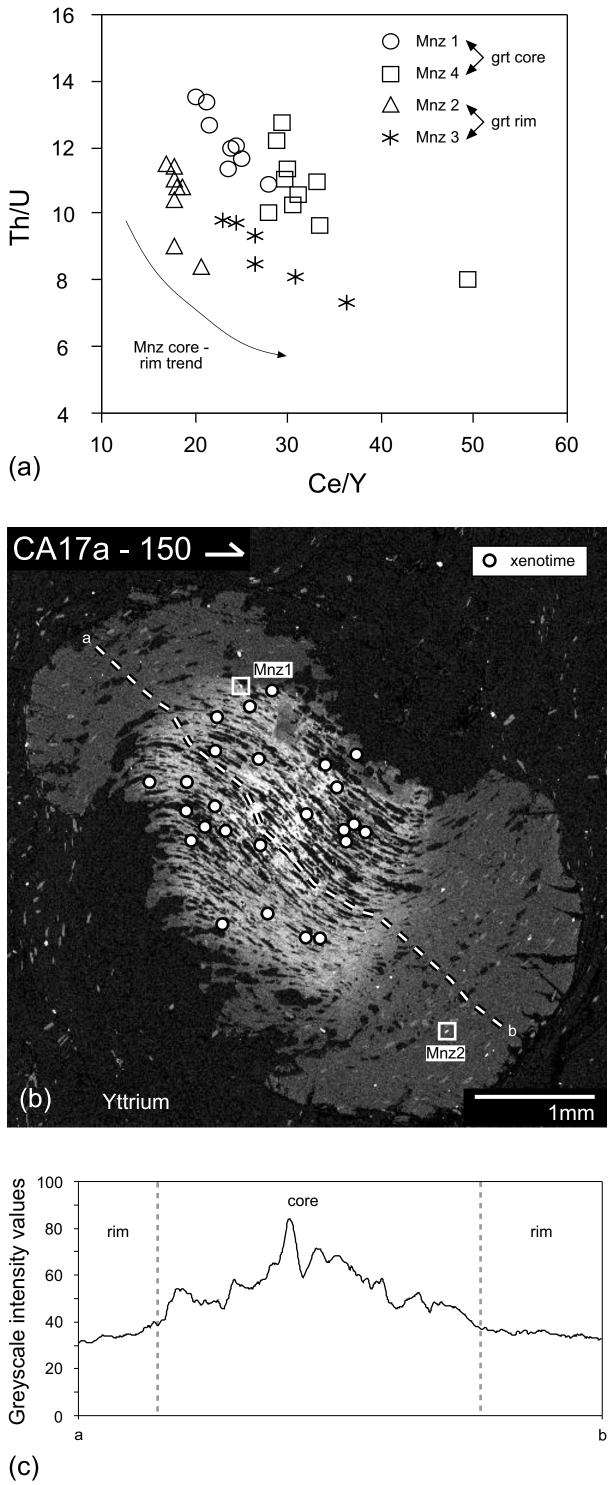
Th/U
Ce/Y
Mnz 1
Mnz 4
grt core
Mnz 2
Mnz 3
grt rim
Mnz core - rim trend
(a)
CA17a - 150
xenotime
Mnz1
Mnz2
a
b
(b)
Yttrium
1mm
Greyscale intensity values
rim
core
rim
(c)

Fig. 9.

Fig. 9. (a) Plot showing Th/U vs Ce/Y chemical trend for 4 monazite inclusions analysed in sample CA17a. The grains preferentially incorporated Th and Y (mostly at the expense on REEs), upon initial crystallisation. Continued growth resulted in more REEs included within the monazite structure, possibly due to decreased availability of Th and Y. Grains located closer to the garnet porphyroblast rims generally have more Y than those closer to the cores. (b) Yttrium chemical map and (c) line profile of the grey scale intensity values (line a-b) of the garnet porphyroblast in sample CA17a containing monazite grains Mnz1 and Mnz2. The profile shows that Y is highest in the core and decreases steadily until the approximate core-rim boundary (marked by dashed line). The rim appears to have a more subtle decrease in Y. The location of xenotime inclusions is marked. The line profile in (c) is a 10-point rolling average of approximately 500 pixel values. Much of the fluctuation is due to the high density of quartz inclusions within the core.

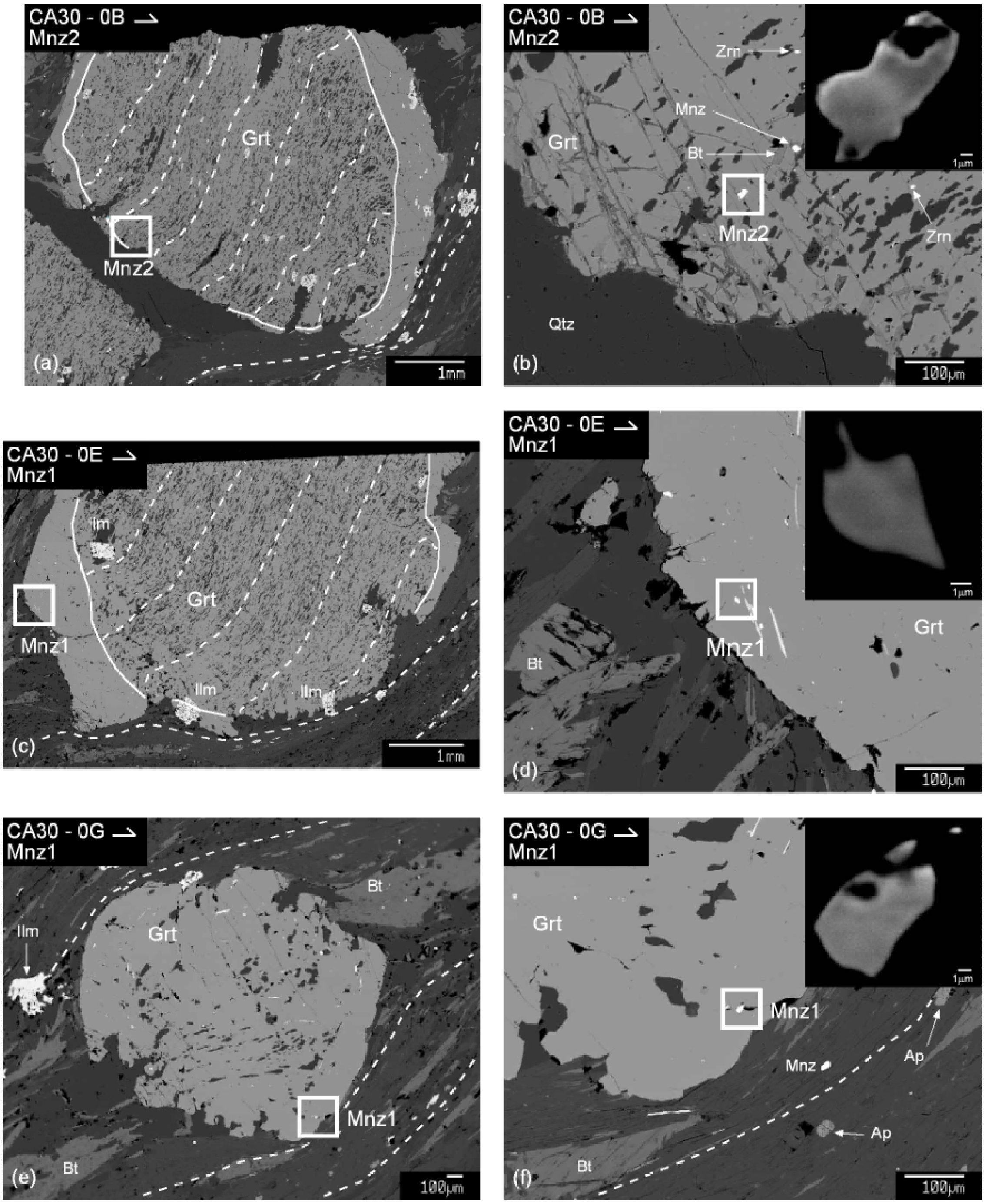
CA30 - 0B
Mnz2
Grt
Mnz2
(a)
1mm
CA30 - 0B
Mnz2
Zrn
Mnz
Grt
Bt
Mnz2
Zrn
Qtz
(b)
100μm
1μm
CA30 - 0E
Mnz1
Ilm
Grt
Mnz1
Ilm
Ilm
(c)
1mm
CA30 - 0E
Mnz1
Grt
Bt
Mnz1
(d)
100μm
1μm
CA30 - 0G
Mnz1
Bt
Ilm
Grt
Mnz1
Bt
(e)
100μm
CA30 - 0G
Mnz1
Grt
Mnz1
Mnz
Ap
Ap
Bt
(f)
100μm
1μm

Fig. 10.

Fig. 10. (a) BSE image showing approximate location of monazite grain CA30-0B-Mnz2, in edge of a garnet porphyroblast core. The inclusion trails within the core are truncated by the inclusion-poor rim. (b) Zoomed BSE image showing location and detail (inset) of grain in (a). The grain is partially elongate, parallel to the inclusions trails. (c) BSE image showing approximate location monazite grain CA30-0E-Mnz1, in a garnet porphyroblast rim. (d) Zoomed BSE image showing location and detail (inset) of grain in (c). (e) BSE image showing approximate location monazite grain CA30-0G-Mnz1, in a garnet porphyroblast rim. (d) Zoomed BSE image showing location and detail (inset) of grain in (e).

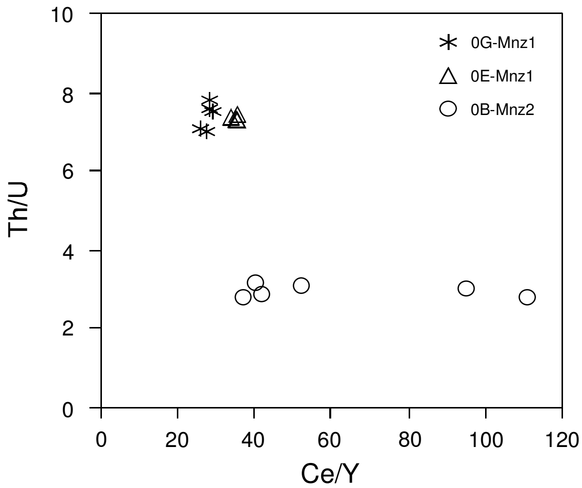

Fig. 11. Plot showing Th/U vs Ce/Y chemical trend for the three monazite inclusions within garnet porphyroblasts analysed in sample CA30. Grains 0G-Mnz1 and 0E-Mnz1, which both lie in the porphyroblast rims have a relatively similar composition, compared to 0B-Mnz2, which lies on the edge of the garnet porphyroblast core and has more U, but less Y.

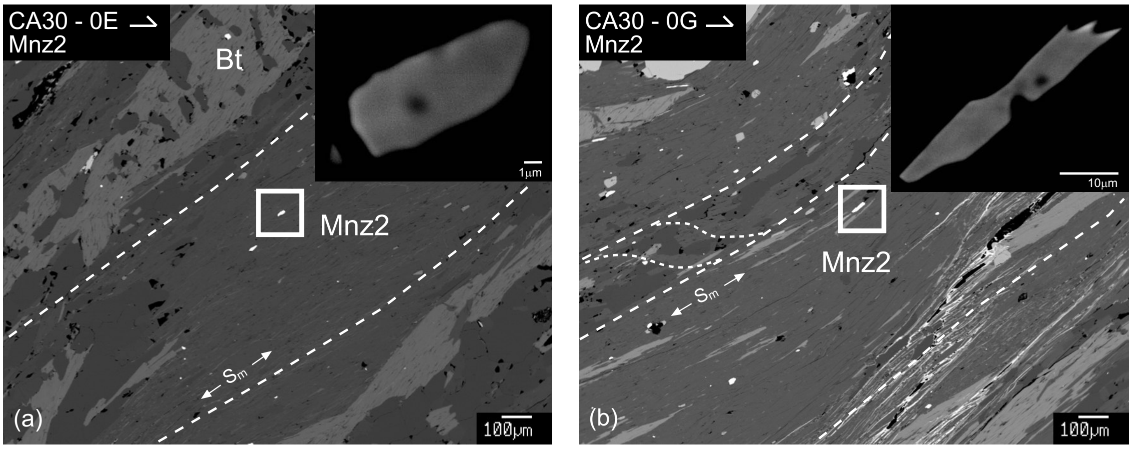

Fig. 12. (a) BSE images showing location and detail (inset) of monazite grain CA30-0E-Mnz2, lying elongate and parallel to S_m. (b) BSE images showing location and detail (inset) of monazite grain CA30-0G-Mnz2, lying elongate and parallel to S_m.

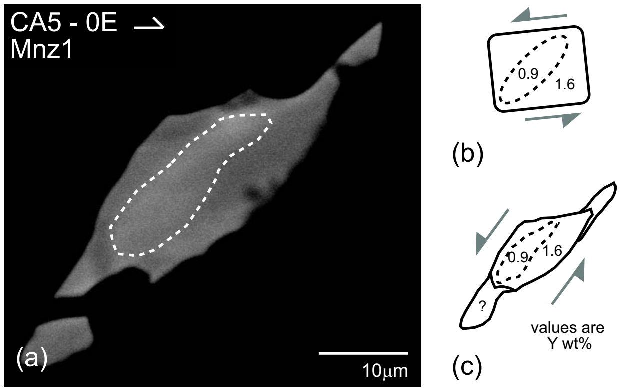

Fig. 13. (a) BSE image showing of monazite grain CA5-0E-Mnz1, with approximate outline of original (Y = 0.9 wt %) core. (b) Sketch showing (sinistral) shear sense required to first grow additional monazite in sub-horizontal direction (b), prior to growth of tails in sub-vertical direction (c). Both flat and steep sinistral shear is preserved in other microstructures within the sample. The composition of the tails is not known.

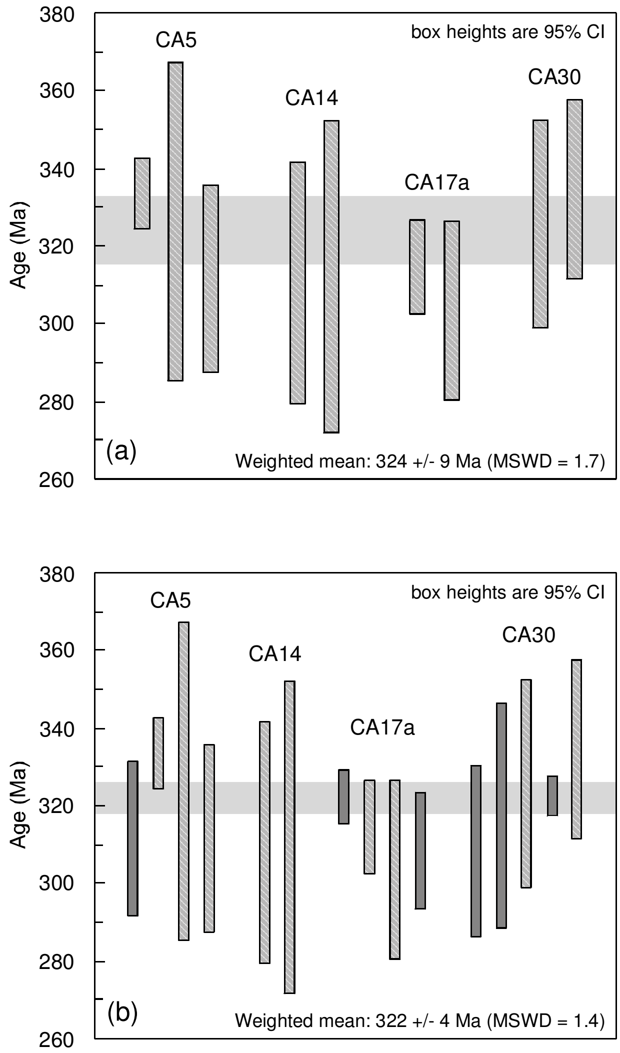

Fig. 14. (a) Box plot of the mean dates and CIs of monazite grains correlated with the development of S_m. The weighted mean (with 95% CI) of these grains is shown by the shaded horizontal bar. (b) Box plot of the mean dates and CIs of all monazite grains analysed in this study. The boxes with the striped/lighter pattern are the same as those in (a). The weighted mean (with 95% CI) of these grains is shown by the shaded horizontal bar.

CHAPTER 4

PRESERVATION OF MULTIPLE STAGES OF PORPHYROBLAST AND MONAZITE GROWTH THROUGH INTENSE ALLEGHANIAN DEFORMATION AND METAMORPHISM

Table 1. Summary of sample lithology, mineralogy and which porphyroblasts monazite grains were located

Sample	Lithology - Locality	Assemblage*	Mnz in Porphyroblasts
K31	LF - NS	Grt-Ms-Bt-Qtz-Pl-Tur	Grt (rims)
K38	LF - NS	Grt-St-Ms-Bt-Qtz-Pl-Ilm-Gr	Grt + St
K45	LF - NS	Grt-St-Ms-Bt-Qtz-Pl-Ilm-Gr	Grt
K52	LF - NS	Grt-St-Ms-Bt-Pl-Tur-Gr	Grt + St
K53	LF - NS	Grt-St-Ky-Ms-Bt-Qtz-Pl-Ilm-Tur	Grt + St
K59	LF - NS	Grt-St-Ms-Bt-Qtz-Pl-Ilm-Chl-Gr	Grt (rims) + St
K63	LF - NS	Grt-St-Ms-Bt-Qtz-Pl-Ilm	Grt + St
K103	LF - WS	Grt-St-Ms-Bt-Qtz-Pl	Grt + St
M54	Mt Min	Grt-St-Ky-Ms-Bt-Qtz-Pl-Ilm-Tur	Grt

* mineral abbreviations after Kretz (1983)

LF = Littleton Formation; Mt Min = Mount Mineral Formation

NS = Northfield Syncline; WS = Wendell Syncline

Table 2. Description and microstructural setting of monazite grains analysed

Monazite grains in garnet porphyroblasts				
Sample	**Shape**	**Fully enclosed?**	**Relative to Inclusion trails (if applicable)**	**Relationship between incl. trails**
K31-0-Mnz1	partially elongate	crack in porph.	N/A (rim of Grt)	N/A
K38-30-Mnz2	blocky	crack in porph.	N/A (rim of Grt)	N/A
K38-30-Mnz6	elongate	adjacent to incl.	parallel to truncated core	predates Grt rim
K45-10-Mnz1	elongate	yes	parallel (core)	truncated by rim
K52-40-Mnz1	"U" shaped (?)	yes	N/A (core of Grt)	truncated by rim
K52-40-Mnz2	elongate	yes	sub-parallel (rim)	truncated by matrix
K52-40-Mnz3	partially elongate	uncertain	sub-parallel (rim)	truncated by matrix
K53-30-Mnz1	elongate	yes	sub-parallel (core)	truncated by median
K53-30-Mnz2	blocky/part elong.	yes	uncertain (core)	truncated by median (?)
K53-30-Mnz4	partially elongate	crack in porph.	N/A (rim of Grt)	truncated by matrix
K53-30-Mnz5	blocky	yes	N/A (rim of Grt)	truncated by matrix
K59-90-Mnz1	blocky	yes	N/A (rim of Grt)	N/A
K59-90-Mnz2	elongate	yes	N/A (rim of Grt)	truncated by matrix (?)
K63-120-Mnz1	partially elongate	yes	N/A (rim of Grt)	N/A
K63-120-Mnz2	fragmented	yes	N/A (core of Grt)	uncertain
K63-120-Mnz3	elongate	yes	N/A (median of Grt)?	uncertain
K103-20-Mnz1	blocky	yes	high angle (core)?	truncated by matrix
K103-20A-Mnz2	blocky	yes	N/A (rim of Grt)	truncated by matrix
M54-83-Mnz1	partially elongate	yes	N/A (rim of Grt)	truncated by matrix
M54-83-Mnz2	blocky	crack in porph.	N/A (rim of Grt)	truncated by matrix
M54-83-Mnz3	blocky/part elong.	yes	sub-parallel (core?)	truncated by rim

Table 2. Continued

Monazite grains in staurolite porphyroblasts

Sample	Shape	Fully enclosed?	Relative to Inclusion trails (if applicable)	Relationship between incl. trails
K38-30-Mnz8	blocky	crack in porph.	high angle	truncated by matrix
K52-40A-Mnz1	blocky/part elong.	yes	ca. 45° (to core trails)	truncated by rim
K53-30-Mnz6	elongated	yes	parallel (core)	truncated by rim
K53-30-Mnz7	partially elongated	yes	parallel (rim?)	cont. w. matrix (?)
K63-120-Mnz4	blocky	crack in porph.	N/A	truncated by matrix

Monazite grains in matrix

Sample	Fabric	Shape	Relative to Fabric
K31-0-Mnz3	Sm	elongate	parallel
K38-30-Mnz5	adjacent to Grt	elongate	N/A
K38-30-Mnz10	Sm	elongate	parallel
K45-10-Mnz2	Sm	elongate	parallel
K52-40-Mnz4	Sm	elongate	parallel
K52-40A-Mnz2	cren. limb	elongate	sub-parallel (Sm)
K53-30-Mnz8	Grt Str. shadow	blocky	N/A
K63-120-Mnz6	Sm	partially elongate	parallel
K103-20-Mnz2	Sm	elongated	parallel
K103-20A-Mnz3	diff. cren. (= Sm)	elongated	parallel (Sm)
M54-83-Mnz4	Sm	partially elongate	sub-parallel

Table 3. EPMA analytical conditions for monazite analysis

Element - Peak	Standard	Crystal - Spectrometer	Back-ground -/+ (mm)	Count time (s) Peak/Bgd	Meas. Order[a] B	C
SiKα	[1]$PbSiO_3$	TAP-1	5/3	20/10	1-3	1-3
PKα	[3]$CePO_4$	TAP-1	3/4	20/10	1-1	1-1
SKα[#]	[1]$BaSO_4$	PETJ-3*	6/4	30/15	5-3	5-3[#]
CaKα	[1]$CaSiO_3$	PETJ-5	1.6/1.6	20/10	5-2	5-2
YLα	[3]YPO_4	TAP-1	1.25/2	90/45[b]	1-2	1-3
LaLα	[3]$LaPO_4$	LIFH-3*	1.6/1.6	10/5	3-7	3-1
CeLα	[3]$CePO_4$	LIFH-3*	3.2/3.2	10/5	3-6	3-2
PrLβ	[3]$PrPO_4$	LIFH-3*	1/1	20/10	3-5	3-3
NdLβ	[3]$NdPO_4$	LIFH-3*	1/1	10/5	3-4	3-4
SmLβ	[3]$SmPO_4$	LIFH-3*	1/1	40/20	3-3	3-5
GdLβ	[3]$GdPO_4$	LIFH-3*	1/1	40/20	3-2	3-6
DyLβ	[3]$DyPO_4$	LIFH-3*	1/4	40/20	3-1	3-7
PbMα	[1]$PbSiO_3$	PETJ-2*	4/6	180/90	2-1	2-1
ThMα	[2]ThO_2	PETJ-5	2.5/3	90/45[b]	5-1	5-1
UMβ	[1]U	PETJ-4	3.5/2.5	180/90	4-1	4-1

* - sealed Xe detectors, others are P-10 gas-flow detectors

- S not analysed for all monazites in this study

a - spectrometer no. - order of measurement (for protocol B and C)

b - count time doubled for Y and Th in protocol "A"

Standards: 1 - Astimex, 2 - Taylor, 3 - Pb-free synthetic (J. Pyle, RPI ,USA)

Table 4. Summary of monazite domains, compositions, mean dates and confidence intervals

Sample	prot.-bd	Set.	Dom.	n	Comp range (wt%) Th	Comp range (wt%) Y	Mean (Ma)	95% CI	Comment
K31-									
Mnz1	B-1	Grt-r	rim	8	3.0-3.5	1.34-1.50	297	11	
			total	10	3.0-5.0	0.40-1.50	**295**	**9**	2 additional analyses from core
Mnz3	B-1	m	total	9	2.5-3.6	0.28-1.46	**289**	**10**	Y + Th + U zoning across grain
K38-									
Mnz2	B-1	Grt-r	total	16	2.2-4.5	0.35-0.74	**300**	**12**	gradual decr. in Y + Th + U towards rim
Mnz5	B-1	m	main	11	1.8-4.8	0.34-0.55	276	11	Th decrease outwards from core
			total	13	1.8-4.9	0.08-0.64	**277**	**11**	2 additional analyses from overgrowth (?)
Mnz6	B-1	Grt-c	main	9	3.4-4.4	0.98-1.14	**350**	**8**	U: 0.28-0.36 wt%
			edge	4	2.9-3.3	0.71-1.0	**305**	**38**	U: 0.09-0.25 wt%
Mnz8	B-1	St	total	16	1.1-3.1	0-1.23	**290**	**15**	complex zoning
Mnz10	B-1	m	total	10	2.5-3.8	0.01-0.58	**282**	**14**	U: 0.33-1.24 wt%, complex zoning
K45-									
Mnz1	B-1	Grt-c	total	8	2.7-3.5	0.91-1.23	**310**	**9**	Y (+ Th) decrease away from Grt core
Mnz2	B-1	m	core	1	4.2	1.23	282	N/A	U: 0.52 wt%
			median	2	4.5-5.1	0.04	294	N/A	U: 0.52-0.57 wt%
			rim	5	3.4-3.8	0.10-0.23	288	10	U: 0.92-1.02 wt%
			total	8			**289**	**6**	three distinct comp. zones
K52-									
40-Mnz1	B-1	Grt-c	total	8	1.3-2.7	1.30-1.57	**287**	**34**	
40-Mnz2	B-1	Grt-r	total	10	1.2-2.1	0.75-1.15	**254**	**31**	minor Y + Th + U variation
40-Mnz3	B-1	Grt-r	zone1	7	9.8-12.8	0.04-0.14	302	5	high Th zone
			total	10	3.5-12.8	0.04-0.36	**300**	**4**	3 additional analyses
40-Mnz4	B-1	m	total	8	2-8	0.13-0.48	**296**	**10**	high Th core - most analyses "mixed"
40A-Mnz1	C-3	St	rim-A	6	2.1-2.4	0.58-0.61	**291**	**17**	high-Th core unable to be analysed
			rim-B	4	1.2-1.5	0.47-0.54	**301**	**21**	rim-A closest to core
			total	10			**297**	**12**	
40A-Mnz2	C-3	m	total	10	3.34-5.05	0.40-0.57	**282**	**11**	

Table 4. Continued

Sample	prot.-b.d.	Set.	Dom.	n	Comp range (wt%) Th	Y	Mean (Ma)	95% CI	Comment
K53-									
Mnz1	A-1	Grt-c	total	12	2.4-9.1	0.94-1.09	**365**	**14**	Th (+ Y) decrease from core to rim
Mnz2	A-1	Grt-c	total	12	1.9-3.7	0.87-1.01	**356**	**24**	mostly rim analyses
Mnz4	A-1	Grt-r	core(?)	3	1.7-1.9	1.51-2.04	296	N/A	U: 1.13-1.54 wt%
			rim(?)	8	2.7-3.5	0.83-1.26	295	11	U: 0.67-1.15 wt%
			total	11			**295**	**8**	negative correlation between Th & Y
Mnz5	A-1	Grt-r	total	9	1.7-2.8	1.03-1.73	**287**	**20**	U: 0.48-0.59 wt%
Mnz6	A-1	St	total	11	3.7-5.5	0.10-0.96	**288**	**9**	higher Th core - most analyses "mixed"
Mnz7	A-1	St	rim	6	3.2-3.4	0.40-0.58	292	14	homogeneous rim
			total	12	2.9-5.5	0.33-1.29	**300**	**15**	additional core (1) and mixed analyses
Mnz8	A-1	m	total	10	1.9-2.7	0.31-1.54	**343**	**24**	U: 0.44-0.63 wt%
K59-									
Mnz1	B-1	Grt-r	zone1	6	1.8-3.0	0.16-0.21	282	26	U: 0.35-0.47 wt%
			zone2	3	3.5-4.2	0.21-0.22	319	N/A	U: 0.55-0.64 wt%
			total	9			**294**	**23**	
Mnz2	B-1	Grt-r	core	7	3.9-6.3	0.12-0.27	274	14	Th decreases across grain
			total	9	3.9-6.4	0.12-2.36	**273**	**10**	includes 2 high Y analyses from rim
K63-									
Mnz1	B-1	Grt-r	total	10	0.9-1.8	0.06-0.16	**271**	**24**	minor variation in Th + Y + U
Mnz2	B-1	Grt-c	total	6	11.0-14.2	1.10-1.26	**334**	**11**	minor variation in Th + U
Mnz3	B-1	Grt-c	total	6	10.1-13.9	1.19-1.57	**337**	**10**	minor variation in Th + U
Mnz4	B-1	St	total	12	1.2-3.5	0.10-0.19	**278**	**23**	majority of analyses from low Th rim
Mnz6	C-3	m	total	11	2.7-3.1	0.14-0.19	**281**	**19**	relatively homogenous

Table 4. Continued

Sample	**prot.-b.d.**	**Set.**	**Dom.**	**n**	**Comp range (wt%) Th**	**Y**	**Mean (Ma)**	**95% CI**	**Comment**
K63-									
Mnz1	B-1	Grt-r	total	10	0.9-1.8	0.06-0.16	**271**	**24**	minor variation in Th + Y + U
Mnz2	B-1	Grt-c	total	6	11.0-14.2	1.10-1.26	**334**	**11**	minor variation in Th + U
Mnz3	B-1	Grt-c	total	6	10.1-13.9	1.19-1.57	**337**	**10**	minor variation in Th + U
Mnz4	B-1	St	total	12	1.2-3.5	0.10-0.19	**278**	**23**	majority of analyses from low Th rim
Mnz6	C-3	m	total	11	2.7-3.1	0.14-0.19	**281**	**19**	relatively homogenous
K103-									
20-Mnz1	B-1	Grt-c	total	4	6.4-7.8	0.51-0.53	**307**	**22**	
20-Mnz2	B-1	m	total	8	2.3-3.7	0.05-0.49	**299**	**9**	variation in Th + Y + U across grain
20A-Mnz2	C-3	Grt-r	total	8	2.3-4.1	0-1.04	**304**	**19**	Y variation related to Grt?
20A-Mnz3	C-3	m	total	10	3.0-4.6	0.05-1.00	**294**	**16**	most analyses "mixed" core +rim
M54-									
Mnz1	B-1	Grt-r	total	13	3.3-3.6	0.70-0.83	**307**	**12**	adjacent section not analysed
Mnz2	B-1	Grt-r	core?	4	6.0-7.3	0.62-0.93	311	20	relationship between high Th zone and
			rim-A	8	3.4-4.8	0.32-0.81	306	14	rim-A is uncertain
			c + r-A	12			**308**	**9**	core (?) + rim-A combined
			rim-B	2	3.8-3.9	1.38-1.39	**294**	**N/A**	rims both high Th and rim-A zones
Mnz3	B-1	Grt-r	core	4	6.4-8.4	1.23-1.39	312	17	relationship between high Th zone and
			rim-A	3	4.3-5.0	0.50-0.99	315	N/A	rim-A is uncertain
			c + r-B	7			**313**	**9**	core (?) + rim-A combined
			rim-B	3	3.3-3.6	1.83-1.95	**285**	**N/A**	similar to rim-B above
Mnz12	B-1	m	core	1	2.7	1.2	**315**	**N/A**	U: 0.4 wt%
			rim	10	3.4-3.7	0.53-0.87	**298**	**11**	U: 0.8-1.2 wt%

prot. = protocol (A, B or C); bd = beam diameter

Set. = summary of setting (see Table 2 for more details)

Dom. = domain

n = number of analyses

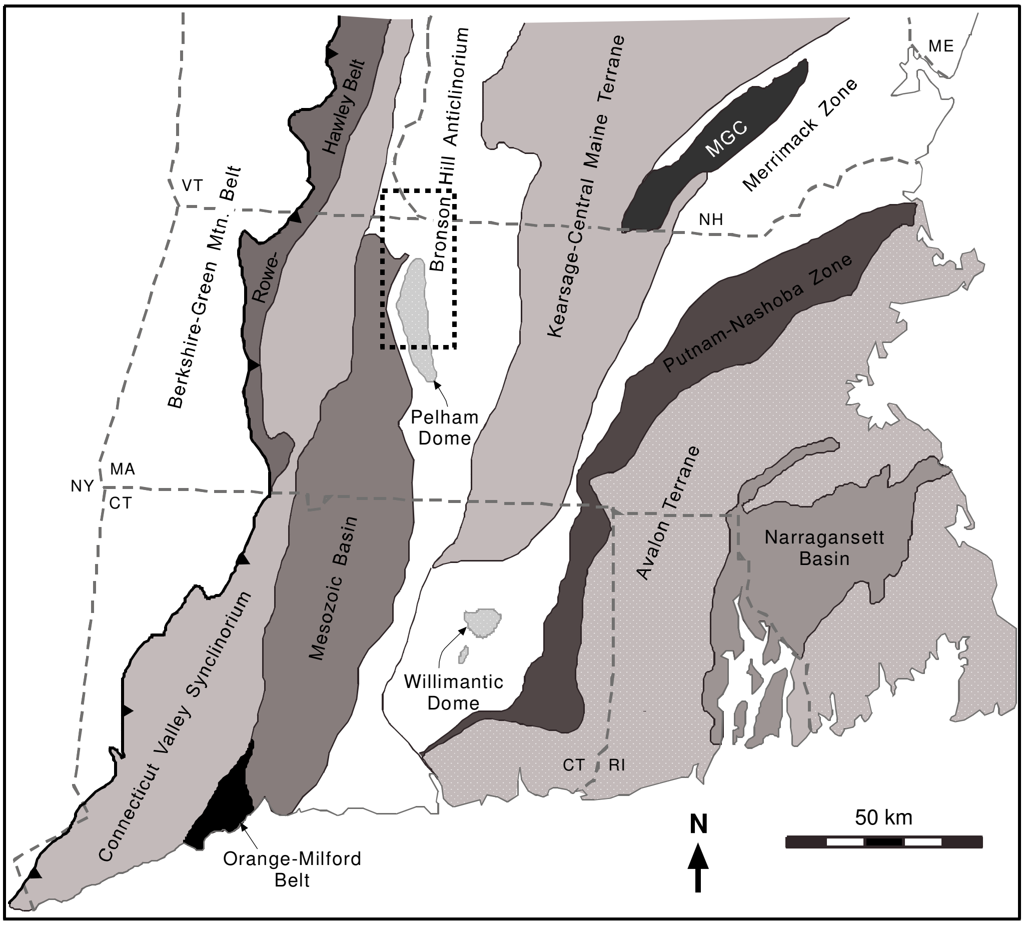

Fig. 1. Regional Tectonic map of the New England Orogenic Belt, illustrating the location of the study area (dashed box) relative to surrounding lithotectonic terranes. Modified from Moecher (1999). MGC - Massabesic Gneiss Complex.

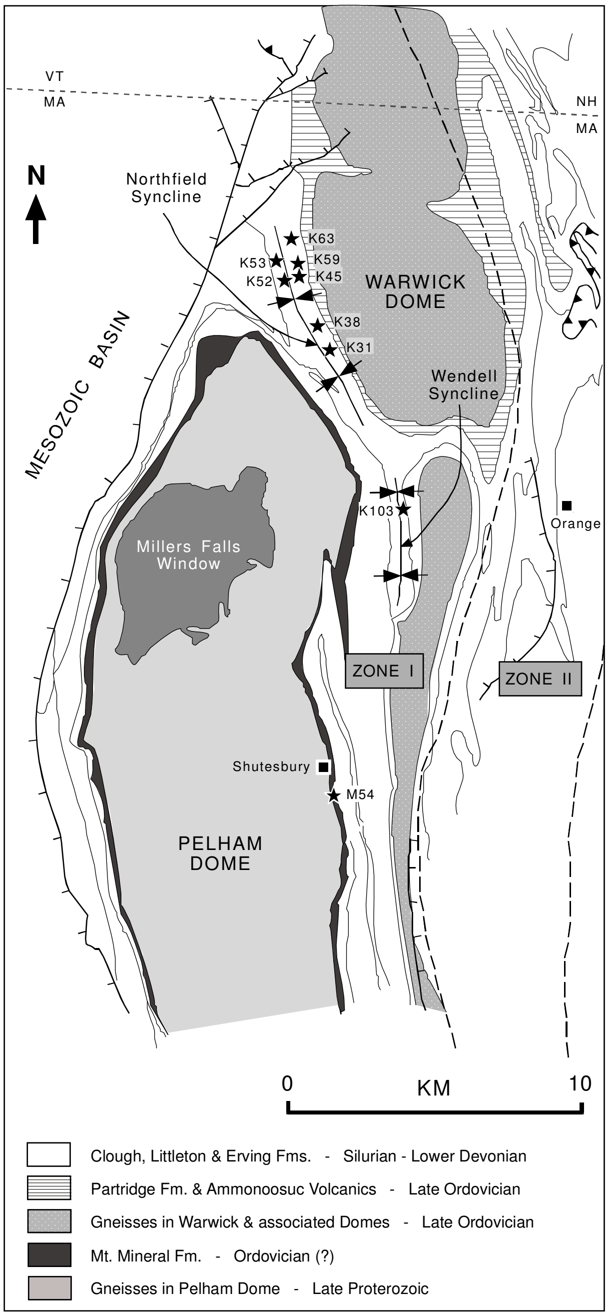

Fig. 2. Generalised geological map of the north eastern flank of the Pelham Dome showing sample locations and metamorphic zones of Tracy et al. (1976). Zone I: Grt + St + Ky + Bt + Ms. Zone II: Grt + St + Sil + Bt + Ms. Modified after Zen et al. (1983).

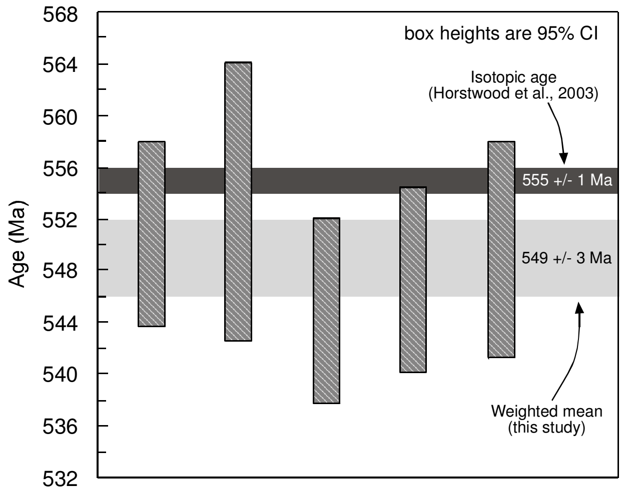

Fig. 3. Results of groups of ten analyses on the Manangotry age standard during the course of the study. The weighted mean of the five groups relative to the isotopic age of Horstwood et al. (2003) is shown.

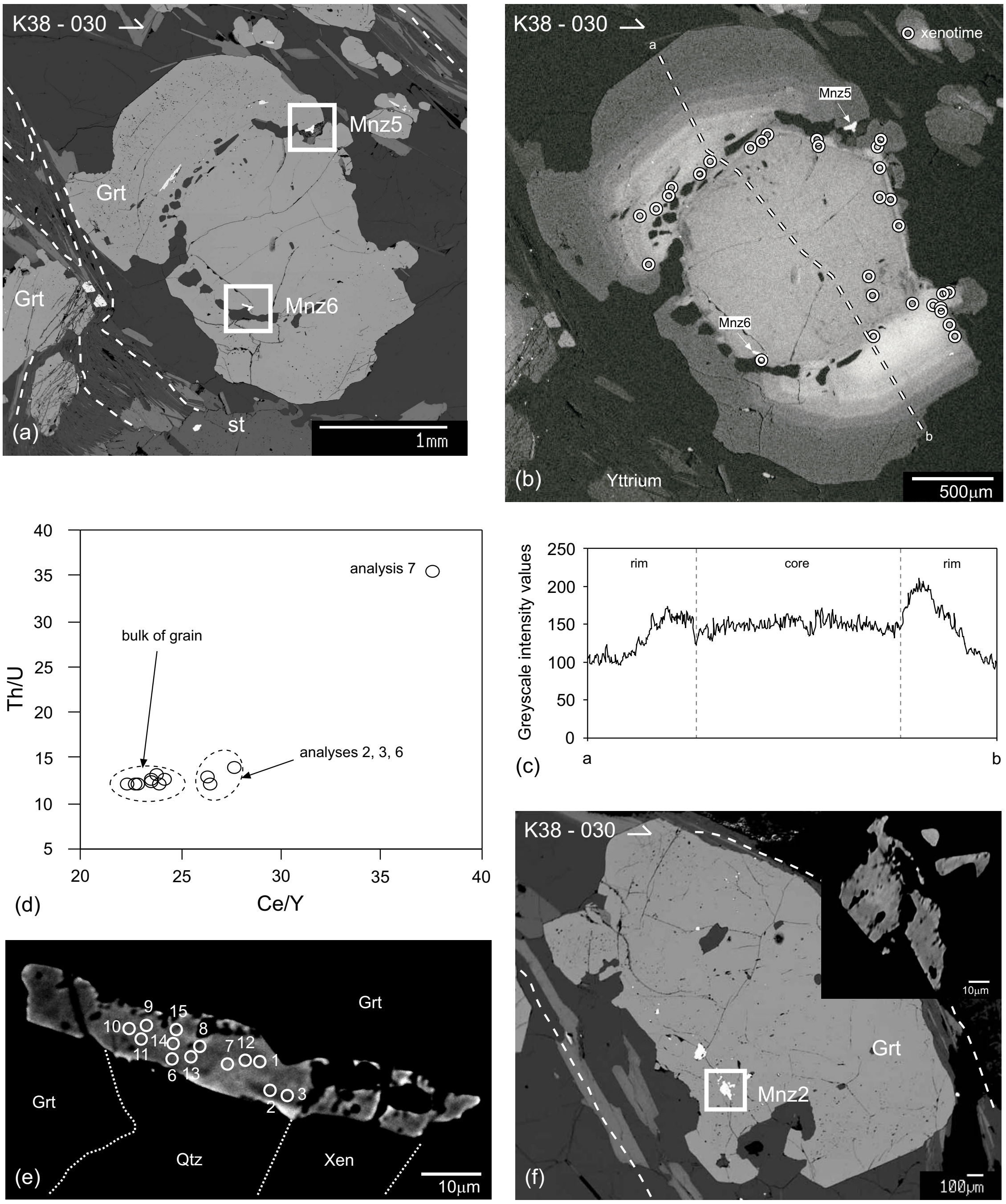
K38 - 030
Mnz5
Grt
Mnz6
Grt
st
(a)
1mm
K38 - 030
xenotime
a
Mnz5
Mnz6
b
(b)
Yttrium
500µm
analysis 7
bulk of grain
Th/U
analyses 2, 3, 6
(d)
Ce/Y
Greyscale intensity values
rim
core
rim
a
b
(c)
K38 - 030
10µm
Grt
Mnz2
(f)
100µm
Grt
Grt
Qtz
Xen
(e)
10µm

Fig. 4.

Fig. 4. (a) BSE image of a garnet porphyroblast in sample K38 showing the location of Mnz6 (within Grt) and Mnz5 (in the matrix adjacent to the porphyroblast). (b) Yttrium map and (c) line profile of greyscale intensity along line (a-b) of the garnet porphyroblast in (a). The Y-profile shows a very slight decrease away from the core and a spike in Y-content at the core-rim boundary. The zoning from this point is oscillatory in parts, before levelling off in the very rim. The location of identified xenotime grains is marked. (d) Plot of Th/U vs Ce/Y and (e) BSE image of Mnz6 showing that the bulk of the grain has a relatively homogeneous composition. Analyses on the qtz inclusion side of the grain have decreased Y and/or U content (most evident in analysis 7). The approximate positions of adjacent/surrounding phases are marked. Xen = xenotime. (f) BSE image of another garnet porphyroblast in sample K38 showing location and detailed view (inset) of Mnz2.

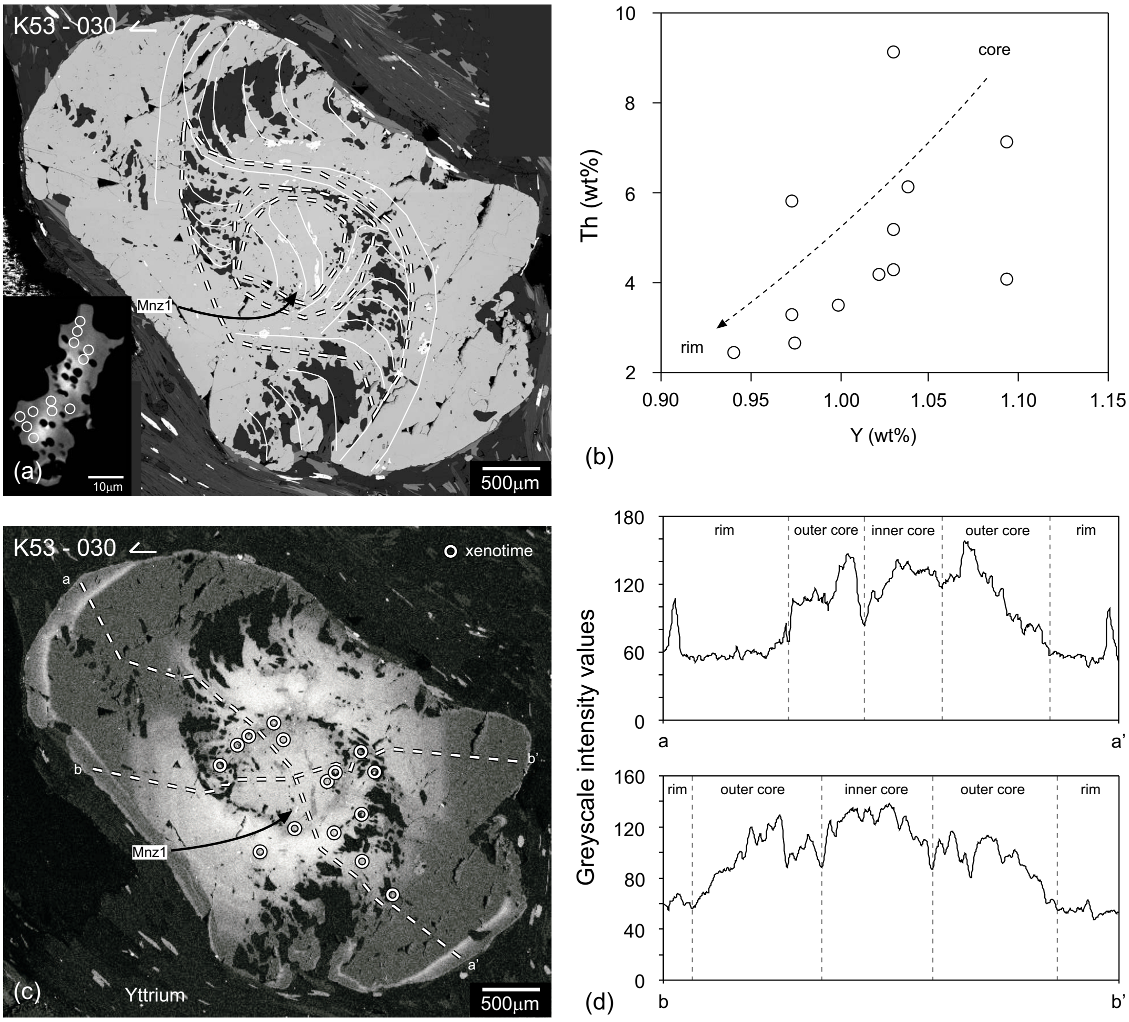

Fig. 5. (a) BSE image of a garnet porphyroblast in sample K53 showing the location and analytical points (inset) of Mnz1. The trace of the inclusions trails in the porphyroblast is marked. (b) Plot of Th vs Y for Mnz1, showing that the strong core-rim decrease in Th is correlative with Y. (c) Yttrium map and (d) line profiles of greyscale intensity values along lines (a-a') and (b-b') for garnet porphyroblast in (a). Yttrium concentration decreases within the inner core, but increases initially in the outer core, before decreasing (with oscillatory zoning in parts) towards the rim. A high Y annulus is present just inside the rim of the porphyroblast. The location of identified xenotime grains is marked and possibly indicates that Mnz1 grew prior to or synchronous with the first appearance of xenotime.

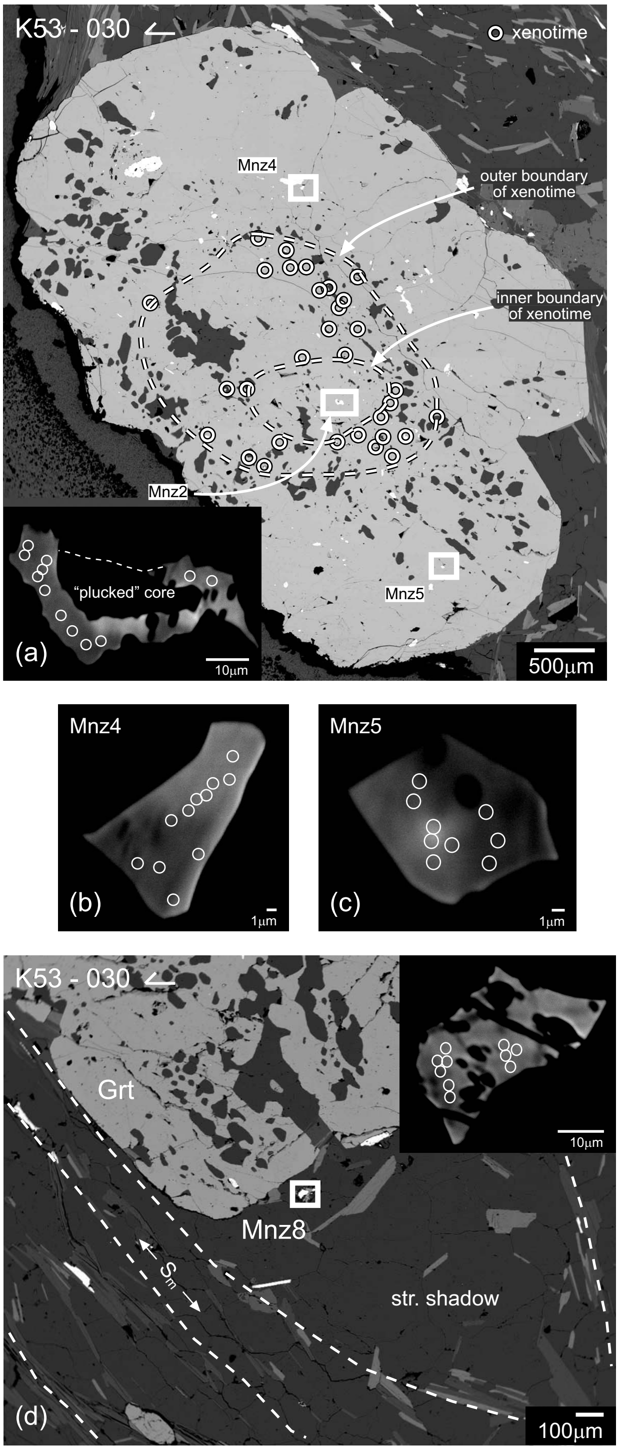
K53 - 030
xenotime
Mnz4
outer boundary of xenotime
inner boundary of xenotime
Mnz2
"plucked" core
Mnz5
(a)
10μm
500μm
Mnz4
(b)
1μm
Mnz5
(c)
1μm
K53 - 030
Grt
Mnz8
Sm
str. shadow
10μm
(d)
100μm

Fig. 6.

Fig. 6. (a) BSE image of a garnet porphyroblast in sample K53, showing the location and analytical points (inset) of Mnz2 and the locations of Mnz4 and Mnz5. The location of identified xenotime grains and the approximate inner (first appearance) and outer (last appearance) boundaries of the phase (relative to garnet) are marked. (b) BSE image of Mnz4, showing zoning and analytical points. (c) BSE image of Mnz5, showing zoning and analytical points. (d) BSE image showing location and analytical points (inset) of Mnz8, within the strain shadow of a garnet porphyroblast.

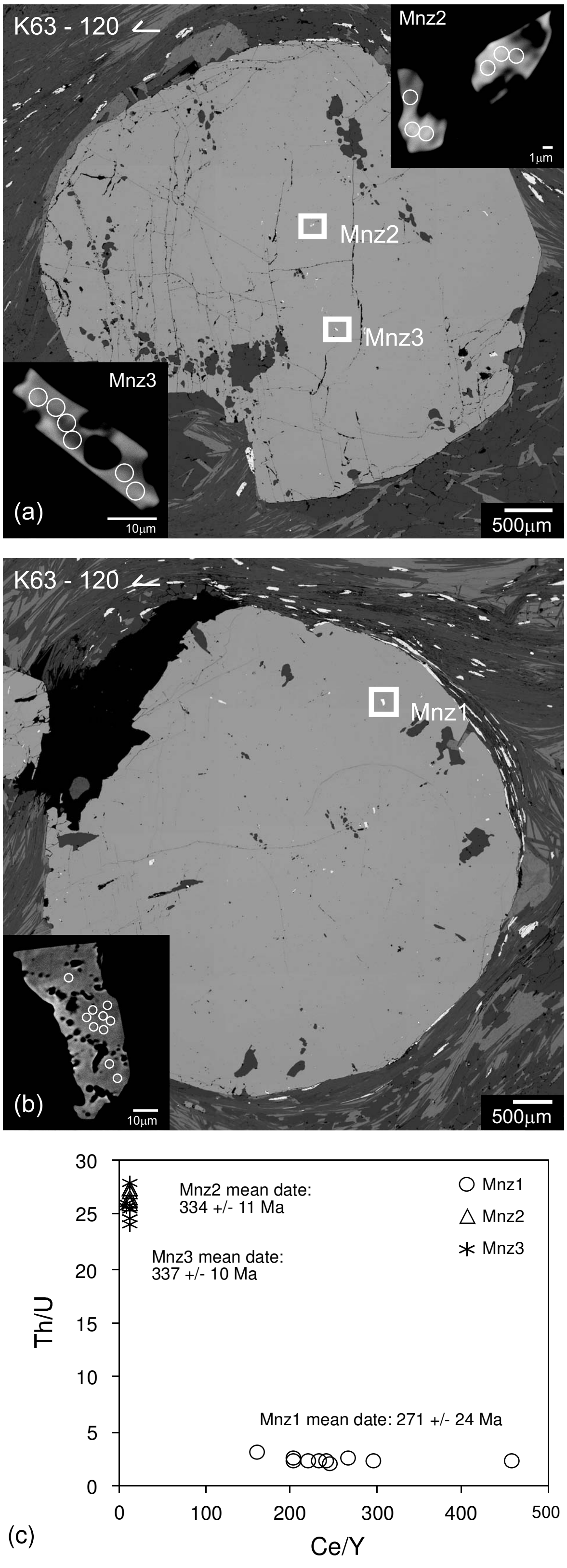
K63 - 120
Mnz2
1µm
Mnz2
Mnz3
Mnz3
(a)
10µm
500µm
K63 - 120
Mnz1
(b)
10µm
500µm
Mnz2 mean date:
334 +/- 11 Ma
Mnz3 mean date:
337 +/- 10 Ma
Mnz1 mean date: 271 +/- 24 Ma
Mnz1
Mnz2
Mnz3
Th/U
Ce/Y
0
5
10
15
20
25
30
0
100
200
300
400
500
(c)

Fig. 7.

Fig. 7. (a) BSE image of a garnet porphyroblast in sample K63, showing the location and analytical points (insets) of Mnz2 and Mnz3. (b) BSE image of another garnet porphyroblast in sample K63, showing the location and analytical points (inset) of Mnz1 (c) Plot of Th/U vs Ce/Y for Mnz1, Mnz2 and Mnz3 in sample K63 showing that the latter grains have a relatively similar composition, but Mnz1 has a distinctly lower Th (thus higher Ce) and Y content.

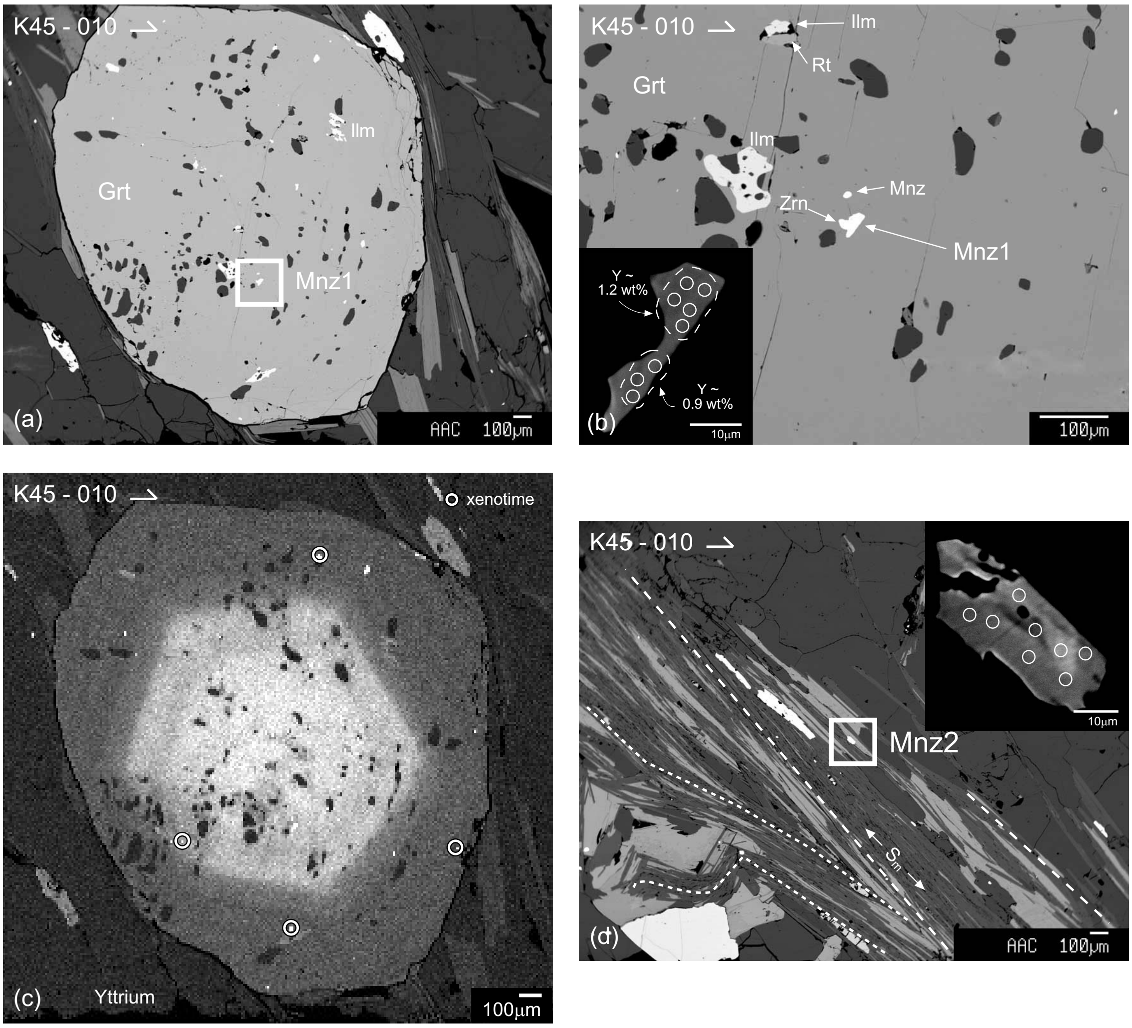

Fig. 8. (a) BSE image of a garnet porphyroblast in sample K45 showing the location of Mnz1. (b) BSE image of the same porphyroblast zoomed in on the location of Mnz1, with detailed image (inset) showing locations of analytical points and averages of Y content in the upper and lower portions of the grain. The Y content correlates to that of Dy. (c) Yttrium map of garnet porphyroblast in (a), showing concentric zoning, with a sharp core-rim decrease in Y content. The location of identified xenotime grains is marked. (d) BSE image showing location and analytical points (inset) of Mnz2, within the matrix.

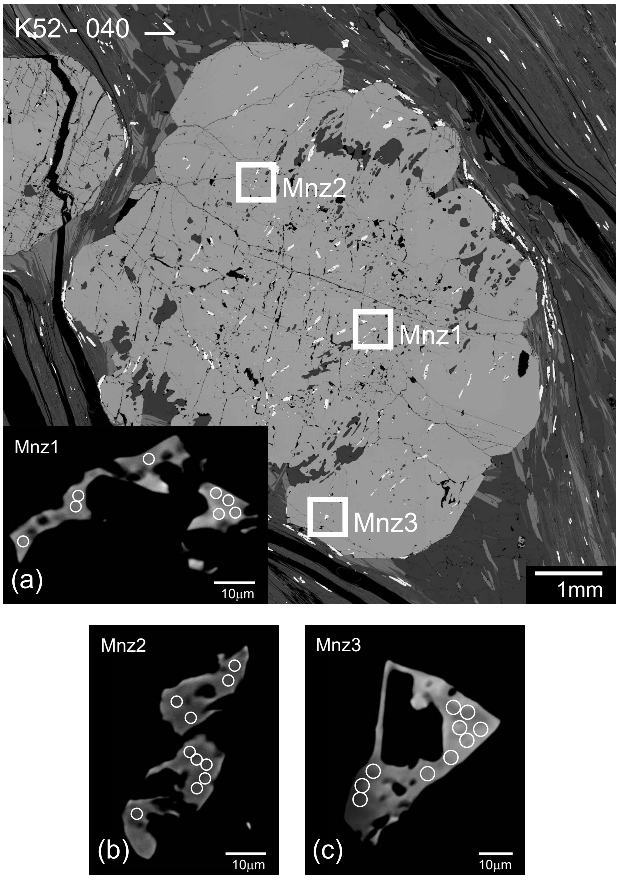

Fig. 9. (a) BSE image of a garnet porphyroblast in sample K52, showing the location and analytical points (inset) of Mnz1 and locations of Mnz2 and Mnz3. (b) BSE image of Mnz2, showing zoning and analytical points. (c) BSE image of Mnz5, showing zoning and analytical points.

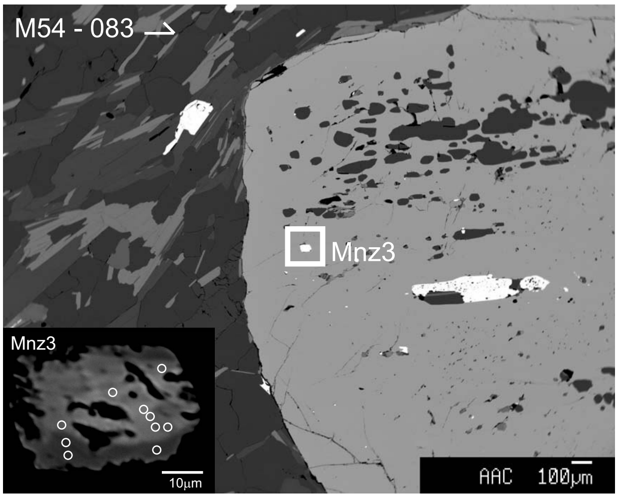

Fig. 10. BSE image of a portion of a garnet porphyroblast in sample M54, showing the location and analytical points (inset) of Mnz3. The darker rim of the monazite grain (inset) is suspected to an overgrowth, which occurred subsequent to the formation of the core.

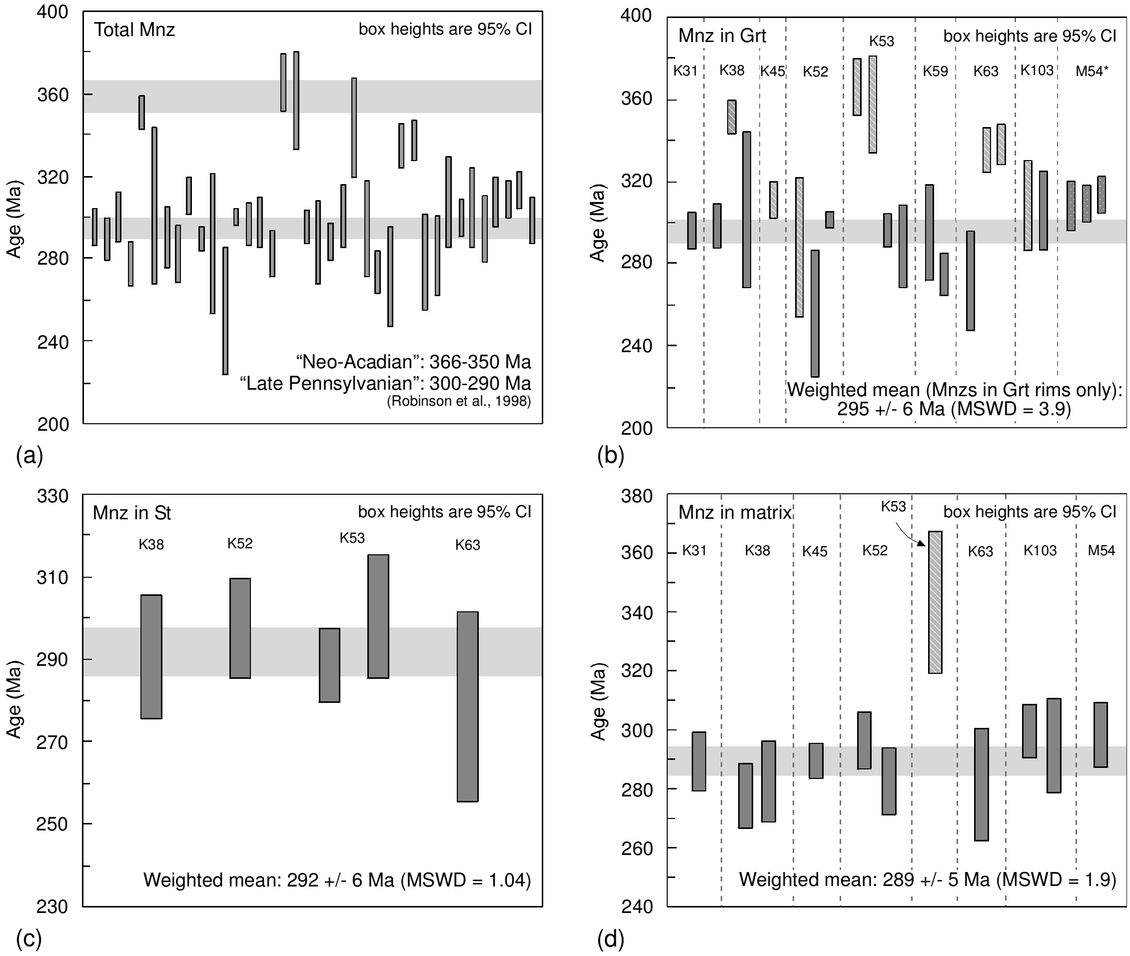

Fig. 11. (a) Box plot of the mean dates and CIs of all monazite grains analysed in this study. The order is equivalent to Table 4. The duration of metamorphism and deformation during both the Late (Neo) Acadian and Late Pennsylvanian, as interpreted by Robinson et al. (1998) are marked by the shaded horizontal bars. (b) Box plot of the mean dates and CIs of all monazite grains analysed within garnet porphyroblasts. Grains within the cores/medians of porphyroblasts have striped/lighter patterns. The weighted mean (with 95% CI) of the grains within the garnet porphyroblast rims (only) is shown by the shaded horizontal bar. * - Analyses from sample M54 were excluded as the bulk of these analyses are potentially from an older generation of monazite growth (see text). (c) Box plot of the mean dates and CIs of all monazite grains analysed within staurolite porphyroblasts. The weighted mean (with 95% CI) of these grains is shown by the shaded horizontal bar. (d) Box plot of the mean dates and CIs of all monazite grains analysed within the matrix. The grain from within a strain shadow in sample K53 is represented by the striped/lighter pattern and was not used to calculate the weighted mean. The weighted mean (with 95% CI) of the other grains is shown by the shaded horizontal bar.

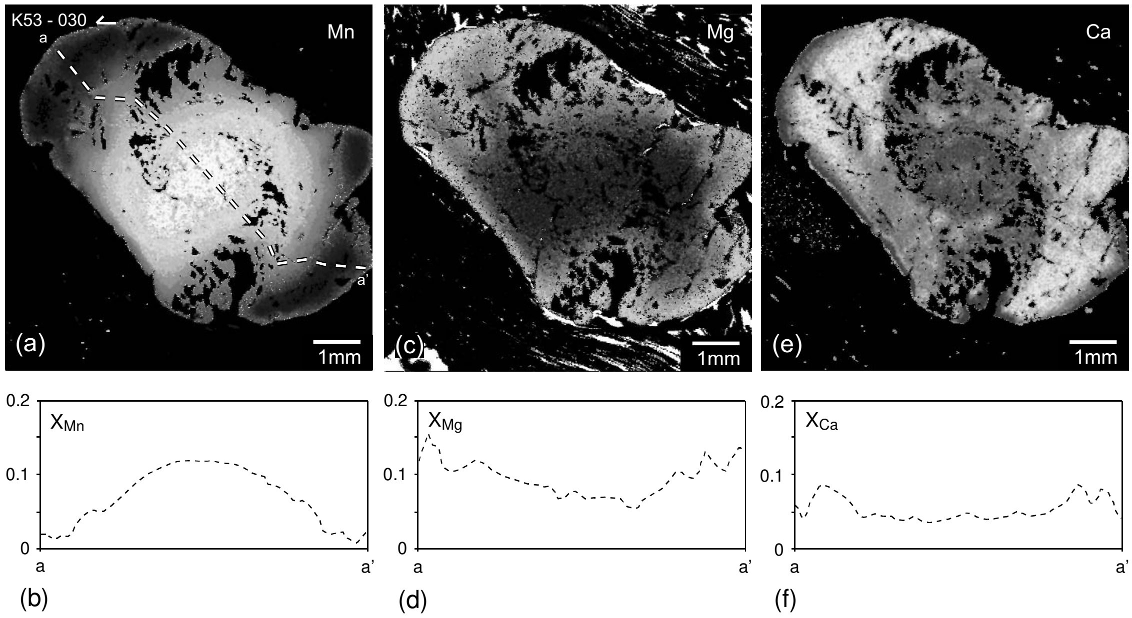

Fig. 12. (a-f) Mn, Mg and Ca maps and compositional profiles along line (a-a') for garnet porphyroblast in sample K53 (Fig. 5.). Modified from Kim and Bell (2005).

APPENDICES

Appendix A. Overview of Monte Carlo error propagation technique

Microsoft Excel® is required to run the whole procedure outlined here, with the addition of the NTRAND add-in (available from: http://www.numtech.com/NtRand/). Since normally distributed "random" numbers are used to estimate the expected concentration distributions, random values for the inverse of the normal cumulative distribution function are required. The following formula is used:

X = NORMINV(NTRAND(n, a, rs1, rs2), MEAN, STDEV) (A-1)

where n is the desired number of sets (e.g. 10000), a is the algorithm used (0 for mt11937), rs1 is random seed 1 (default = 12345), rs2 is random seed 2 (default = 67890), MEAN is the concentration (in ppm), and STDEV is the 1σ error (in ppm) on the concentration (calculated using the equations above). An array of the desired number of sets is then created. Each set is then independently inserted into equation (1) via a Microsoft Visual Basic® for Applications (VBA) macro such that age values can be generated using the "Goal Seek" procedure. The standard deviation of all the computer generated ages will represent an approximate 68% confidence interval on the mean and the 95% confidence interval is calculated by multiplying the standard deviation by 1.96. The process can then be repeated for subsequent analyses.

The choice of the number of randomly generated concentration values is somewhat arbitrary; essentially the quality of the randomly generated population will be offset by the computation time required to both generate and process it. Ideally, the difference between repeated runs (with the same inputs) should be negligible, and the mean of the generated population should be approximately the same (to at least the nearest whole number) to that of the calculated age. Therefore trial and error may be required for different data sets (particularly for large error values), but from experience, when using a robust pseudo-random number generator such as NTRAND, 10000 sets are adequate in all situations encountered thus far.

Note: the spreadsheet is included on the CD that accompanies this thesis.

Appendix B. Monazite compositional data and counting errors for Chapter 1

No.	SiO2	P2O5	SO3	CaO	Y2O3	La2O3	Ce2O3	Pr2O3	Nd2O3	Sm2O3	Gd2O3	Dy2O3	PbO	ThO2	UO2	Total
Concentrations																
1	2.004	27.57	0.0161	0.9062	0.2116	14.52	29.29	2.99	9.77	1.0139	0.4103	0.0215	0.3085	11.67	0.2743	100.9764
2	2.0147	27.6	0	0.9262	0.2049	14.52	28.97	2.99	9.7	0.9764	0.3701	0.0764	0.3144	11.66	0.2716	100.5946
3	2.0307	27.56	0.0038	0.9114	0.1981	14.4	29.01	3.04	9.72	0.9643	0.4371	0.0992	0.3143	11.78	0.256	100.7248
4	2.0075	27.5	0.0096	0.9166	0.2025	14.5	28.89	2.98	9.65	0.9888	0.3757	0.1079	0.3114	11.72	0.254	100.4139
5	2.0085	27.5	0.0189	0.9143	0.1976	14.45	29.14	2.94	9.75	0.938	0.3857	0.0982	0.3117	11.77	0.2679	100.6907
6	2.017	27.55	0.0056	0.9176	0.1981	14.48	29.09	2.98	9.7	0.9532	0.4178	0.0995	0.3175	11.69	0.2702	100.6864
7	2.0089	27.66	0.0147	0.9212	0.202	14.55	29.35	2.98	9.62	0.8553	0.3529	0.0733	0.3129	11.63	0.256	100.7872
8	2.0203	27.64	0.0081	0.9238	0.2083	14.4	29.17	3.01	9.79	0.902	0.3642	0.0668	0.3163	11.69	0.2643	100.774
9	2.0104	27.7	0.0078	0.9251	0.1975	14.52	29.21	3	9.8	0.8716	0.3425	0.1107	0.3059	11.73	0.2493	100.9808
10	1.998	27.6	0.0109	0.9058	0.1947	14.52	29.11	3.03	9.8	0.8269	0.3912	0.09	0.3198	11.62	0.258	100.6752
11	2.0057	27.62	0.007	0.9341	0.1963	14.35	29.17	2.98	9.6	0.8287	0.3125	0.0534	0.3131	11.63	0.2574	100.2581
12	1.9927	27.64	0.0102	0.9239	0.2004	14.55	29	2.97	9.72	0.8596	0.4511	0.1077	0.3173	11.69	0.2681	100.701
13	2.0287	27.65	0.0105	0.9136	0.2039	14.45	29.13	3	9.79	0.9113	0.461	0.0948	0.3163	11.55	0.2578	100.7678
14	2.0381	27.66	0.0133	0.9183	0.1953	14.47	29.06	2.99	9.63	0.9017	0.3785	0.0767	0.3165	11.59	0.2483	100.4867
15	2.0304	27.63	0.005	0.919	0.2051	14.39	29.21	3.05	9.65	0.9062	0.4536	0.0675	0.3181	11.64	0.257	100.7318
16	2.0204	27.6	0.0118	0.9222	0.2028	14.62	29.05	3.05	9.76	0.9147	0.4179	0.1072	0.3052	11.53	0.2594	100.7715
17	2.017	27.61	0.003	0.9199	0.2021	14.44	28.96	3.05	9.81	0.9114	0.4672	0.083	0.3098	11.54	0.2627	100.586
18	2.0101	27.64	0.0055	0.9039	0.1897	14.61	28.94	2.99	9.71	0.8901	0.4779	0.0358	0.3041	11.54	0.2613	100.5084
19	2.0159	27.63	0.0054	0.8839	0.2023	14.51	29.13	3.06	9.78	0.9841	0.471	0.1243	0.3057	11.68	0.246	101.0285
20	2.0201	27.64	0.0053	0.9021	0.1966	14.36	29.13	2.96	9.76	0.9966	0.4853	0.0679	0.3106	11.61	0.2783	100.7227
21	2.0441	27.67	0.0103	0.8907	0.1914	14.48	29.28	3.04	9.84	0.9901	0.4298	0.0191	0.3132	11.57	0.2691	101.0377
22	2.0266	27.59	0.0058	0.9104	0.2041	14.54	29.15	2.98	9.78	0.9816	0.4594	0.1015	0.3187	11.75	0.2707	101.0687
23	1.9972	27.61	0.0089	0.9022	0.2029	14.58	29.24	3.02	9.85	0.9555	0.3882	0.0997	0.318	11.64	0.2631	101.0757
24	1.9996	27.63	0.0056	0.8946	0.1999	14.54	29.14	3.03	9.73	0.9859	0.4265	0.0117	0.3105	11.66	0.2595	100.8237
25	2.0184	27.59	0.002	0.9209	0.1986	14.45	29.18	3.09	9.67	0.9905	0.2893	0.0582	0.3055	11.75	0.2662	100.7795
26	2.0045	27.53	0.015	0.9159	0.1967	14.49	29.06	3.05	9.7	0.965	0.3058	0.0283	0.3182	11.67	0.2619	100.5112
27	1.9863	27.63	0.0157	0.9195	0.1959	14.52	29.12	2.97	9.82	0.9802	0.2518	0.0678	0.3117	11.78	0.2775	100.8464
28	1.9886	27.56	0.0088	0.9239	0.1989	14.47	29.16	2.97	9.71	0.9509	0.3052	0.0463	0.321	11.77	0.2535	100.637

Appendix B. Continued

No.	SiO2	P2O5	SO3	CaO	Y2O3	La2O3	Ce2O3	Pr2O3	Nd2O3	Sm2O3	Gd2O3	Dy2O3	PbO	ThO2	UO2	Total
Concentrations																
28	1.9886	27.56	0.0088	0.9239	0.1989	14.47	29.16	2.97	9.71	0.9509	0.3052	0.0463	0.321	11.77	0.2535	100.637
29	1.9943	27.56	0.0169	0.9084	0.208	14.43	29.09	3.02	9.5	0.9837	0.2603	0.0445	0.3122	11.77	0.2623	100.3605
30	2.0128	27.61	0.0102	0.9087	0.2007	14.41	28.7	2.9	9.68	0.9314	0.3558	0.1399	0.3053	11.59	0.2543	100.009
31	2.0298	27.55	0.0076	0.9276	0.2049	14.52	29.19	3.01	9.8	0.954	0.2995	0.0875	0.3069	11.74	0.2728	100.9005
32	2.0266	27.5	0	0.9167	0.2013	14.56	29.18	3.05	9.92	0.9649	0.3249	0.0852	0.32	11.8	0.2672	101.1168
33	2.0351	27.51	0.0031	0.9184	0.1946	14.59	29.32	3.04	9.72	0.9833	0.32	0.1163	0.3131	11.7	0.2636	101.0274
34	2.0089	27.46	0.0068	0.9123	0.2004	14.54	29.01	2.95	9.74	0.9716	0.3489	0.0754	0.3005	11.72	0.2529	100.4977
35	2.0091	27.45	0.0138	0.9242	0.2014	14.35	29.15	2.94	9.73	0.9848	0.3251	0.0666	0.3043	11.72	0.27	100.4392
36	2.0216	27.5	0.0119	0.9198	0.1932	14.41	28.72	2.94	9.62	0.9906	0.2947	0.0954	0.3198	11.71	0.2728	100.0197
37	2.005	27.59	0.0141	0.9344	0.2035	14.47	29.16	3.04	9.98	0.9967	0.3525	0.0759	0.3159	11.82	0.2671	101.225
38	2.0057	27.57	0.006	0.9178	0.2089	14.57	28.95	2.98	9.8	0.9458	0.3138	0.0561	0.3189	11.74	0.2664	100.6494
39	1.9937	27.6	0.0091	0.9324	0.2002	14.56	29.12	2.99	9.75	0.9539	0.329	0.0822	0.3202	11.82	0.2539	100.9146
40	2.0121	27.48	0.0113	0.9191	0.199	14.56	29.08	3	9.65	0.9711	0.3128	0.1341	0.3098	11.78	0.2735	100.6927
41	1.9821	27.51	0.0013	0.9244	0.206	14.41	29.05	2.97	9.77	1.0024	0.3289	0.0161	0.3208	11.77	0.249	100.5109
42	1.9988	27.47	0.0045	0.9266	0.1947	14.46	29.01	3.01	9.81	0.9263	0.3393	0.052	0.3087	11.81	0.2581	100.5789
43	1.9955	27.48	0	0.926	0.196	14.62	29.11	2.98	9.6	0.9633	0.3117	0	0.3121	11.79	0.2643	100.5488
44	2.0049	27.55	0.0071	0.9042	0.1948	14.54	29.16	2.99	9.62	0.9797	0.3257	0	0.3102	11.76	0.2638	100.6103
45	2.0144	27.55	0.0162	0.9201	0.199	14.42	29.38	3.05	9.53	0.9674	0.3345	0.0226	0.3145	11.78	0.2645	100.7631
46	2.0082	27.48	0.0078	0.9165	0.1928	14.37	29.02	3.1	9.7	0.9774	0.3208	0.036	0.3129	11.82	0.267	100.5294
47	1.9979	27.48	0.0081	0.9291	0.1952	14.49	29.07	2.99	9.5	1.004	0.3787	0.0261	0.3113	11.78	0.2743	100.4346
48	2.0014	27.51	0.0083	0.9282	0.202	14.48	29.28	2.99	9.58	0.9983	0.321	0	0.3085	11.82	0.2601	100.6878
49	2.0181	27.48	0.0114	0.9289	0.1989	14.64	29.26	3.07	9.79	0.984	0.3672	0.0055	0.3202	11.76	0.2595	101.0937
50	2.0101	27.47	0.0117	0.9263	0.1988	14.36	28.97	3.04	9.65	0.9433	0.3367	0.0012	0.3097	11.77	0.2728	100.2705
51	2.0294	27.48	0.0077	0.9225	0.1956	14.61	29.17	3	9.81	0.9687	0.3376	0.0592	0.3209	11.8	0.2509	100.9624
52	2.0297	27.56	0	0.9117	0.1939	14.22	28.84	3.01	9.66	0.9474	0.3655	0	0.3258	11.7	0.2564	100.0203
53	2.0148	27.47	0.015	0.9217	0.1945	14.41	29	2.99	9.75	0.9732	0.3585	0.0064	0.309	11.79	0.2785	100.4815
54	2.0161	27.42	0.0107	0.9024	0.194	14.4	29.13	3.02	9.7	0.9508	0.3006	0	0.3044	11.81	0.2698	100.4287
55	2.0222	27.54	0.0179	0.8744	0.1999	14.58	29.33	2.92	9.68	0.9768	0.315	0.0237	0.3121	11.75	0.2522	100.7942

Appendix B. Continued

No.	SiO2	P2O5	SO3	CaO	Y2O3	La2O3	Ce2O3	Pr2O3	Nd2O3	Sm2O3	Gd2O3	Dy2O3	PbO	ThO2	UO2	Total
Concentrations																
56	2.0006	27.55	0.0036	0.9032	0.2011	14.41	29.15	2.94	9.85	0.9585	0.3258	0.0357	0.3087	11.78	0.258	100.6751
57	2.0144	27.56	0.0049	0.8948	0.1997	14.49	29.26	3.02	9.8	0.9549	0.3506	0	0.3093	11.83	0.2558	100.9443
58	1.9997	27.44	0.0031	0.8991	0.2015	14.41	29.18	2.94	9.78	0.9555	0.3385	0.0062	0.3059	11.84	0.2598	100.5593
59	2.0252	27.51	0.0148	0.9055	0.1915	14.42	29.24	2.92	9.81	0.9588	0.3078	0.0315	0.3128	11.8	0.2637	100.7115
60	2.0064	27.52	0.0057	0.8857	0.1996	14.49	29.26	2.96	9.79	0.937	0.3283	0.0591	0.3016	11.87	0.2663	100.8796

No.	SiO2	P2O5	SO3	CaO	Y2O3	La2O3	Ce2O3	Pr2O3	Nd2O3	Sm2O3	Gd2O3	Dy2O3	PbO	ThO2	UO2
Counting error (1σ %)															
1	0.48	0.12	38.94	0.81	2.25	0.55	0.34	1.34	0.78	2.4	6.39	151.18	1.76	0.29	3.02
2	0.48	0.12	100	0.8	2.32	0.54	0.34	1.34	0.79	2.49	7.1	42.43	1.73	0.29	3.04
3	0.48	0.12	160.4	0.81	2.41	0.55	0.34	1.31	0.79	2.52	6.03	32.55	1.73	0.29	3.22
4	0.48	0.12	64.85	0.8	2.34	0.55	0.34	1.34	0.79	2.46	6.98	30.03	1.74	0.29	3.23
5	0.48	0.12	32.86	0.81	2.41	0.55	0.34	1.36	0.79	2.59	6.81	32.91	1.75	0.29	3.08
6	0.48	0.12	113.14	0.81	2.41	0.54	0.34	1.34	0.79	2.56	6.3	32.5	1.72	0.29	3.05
7	0.48	0.12	42.29	0.81	2.35	0.54	0.34	1.35	0.8	2.82	7.46	44.25	1.73	0.29	3.22
8	0.48	0.12	76.63	0.8	2.29	0.55	0.34	1.33	0.78	2.68	7.23	48.39	1.72	0.29	3.12
9	0.48	0.12	79.98	0.8	2.41	0.54	0.34	1.33	0.78	2.77	7.7	29.4	1.77	0.29	3.3
10	0.49	0.12	55.48	0.82	2.45	0.54	0.34	1.32	0.78	2.91	6.7	35.91	1.7	0.29	3.19
11	0.48	0.12	88.7	0.8	2.43	0.55	0.34	1.34	0.79	2.91	8.43	60.62	1.74	0.29	3.19
12	0.49	0.12	61.51	0.8	2.38	0.54	0.34	1.34	0.79	2.81	5.82	29.92	1.71	0.29	3.06
13	0.48	0.12	58.54	0.81	2.34	0.55	0.34	1.33	0.78	2.64	5.71	34.09	1.71	0.29	3.2
14	0.48	0.12	46.98	0.81	2.44	0.54	0.34	1.34	0.79	2.68	6.96	42.16	1.72	0.29	3.3
15	0.48	0.12	125.59	0.81	2.33	0.55	0.34	1.31	0.79	2.68	5.81	48.24	1.71	0.29	3.21
16	0.48	0.12	51.59	0.8	2.36	0.54	0.34	1.32	0.79	2.65	6.28	30.16	1.78	0.29	3.17
17	0.48	0.12	201.46	0.8	2.36	0.54	0.34	1.31	0.78	2.66	5.63	38.93	1.75	0.29	3.13
18	0.48	0.12	111.07	0.81	2.53	0.54	0.34	1.33	0.79	2.71	5.51	90.42	1.78	0.29	3.14
19	0.48	0.12	114.02	0.83	2.36	0.54	0.34	1.31	0.78	2.46	5.6	25.99	1.77	0.29	3.33

Appendix B. Continued

No.	SiO2	P2O5	SO3	CaO	Y2O3	La2O3	Ce2O3	Pr2O3	Nd2O3	Sm2O3	Gd2O3	Dy2O3	PbO	ThO2	UO2
Counting error (1σ %)															
20	0.48	0.12	117.06	0.81	2.43	0.55	0.34	1.35	0.78	2.43	5.42	47.69	1.74	0.29	2.95
21	0.48	0.12	59.32	0.82	2.51	0.54	0.34	1.32	0.78	2.45	6.11	169.33	1.73	0.29	3.05
22	0.48	0.12	106.65	0.81	2.35	0.54	0.34	1.34	0.78	2.48	5.73	31.73	1.7	0.29	3.02
23	0.49	0.12	70.58	0.81	2.37	0.54	0.34	1.32	0.78	2.54	6.79	32.31	1.71	0.29	3.12
24	0.49	0.12	110.88	0.82	2.4	0.54	0.34	1.32	0.79	2.47	6.15	275.76	1.75	0.29	3.17
25	0.48	0.12	313.37	0.8	2.41	0.55	0.34	1.3	0.79	2.46	8.99	55.44	1.77	0.29	3.08
26	0.48	0.12	41.22	0.81	2.43	0.54	0.34	1.31	0.79	2.52	8.55	114.23	1.69	0.29	3.13
27	0.49	0.12	39.83	0.8	2.45	0.54	0.34	1.34	0.78	2.49	10.38	47.65	1.74	0.29	2.96
28	0.49	0.12	68.96	0.8	2.41	0.54	0.34	1.34	0.78	2.55	8.53	69.85	1.7	0.29	3.24
29	0.49	0.12	36.2	0.81	2.3	0.54	0.34	1.32	0.8	2.48	9.99	72.62	1.73	0.29	3.13
30	0.49	0.12	60.7	0.81	2.41	0.54	0.34	1.36	0.78	2.57	7.26	22.83	1.76	0.29	3.21
31	0.48	0.12	80.73	0.8	2.34	0.54	0.34	1.33	0.78	2.54	8.69	37	1.77	0.29	3.01
32	0.48	0.12	100	0.81	2.39	0.54	0.34	1.31	0.78	2.51	7.98	37.87	1.69	0.28	3.06
33	0.48	0.12	193.18	0.8	2.47	0.54	0.33	1.32	0.79	2.46	8.15	27.71	1.73	0.29	3.12
34	0.48	0.12	88.75	0.81	2.4	0.54	0.34	1.34	0.78	2.49	7.47	42.84	1.79	0.29	3.24
35	0.48	0.12	44.36	0.8	2.39	0.55	0.34	1.35	0.78	2.46	8	48.46	1.77	0.29	3.04
36	0.49	0.12	51.25	0.8	2.5	0.54	0.34	1.34	0.79	2.42	8.76	33.65	1.68	0.29	2.99
37	0.48	0.12	43.45	0.79	2.37	0.54	0.34	1.31	0.77	2.42	7.37	42.58	1.71	0.28	3.07
38	0.48	0.12	104.08	0.8	2.3	0.54	0.34	1.34	0.78	2.57	8.26	57.71	1.69	0.29	3.07
39	0.49	0.12	69.11	0.8	2.4	0.54	0.34	1.33	0.79	2.54	7.93	39.25	1.7	0.28	3.24
40	0.48	0.12	54.45	0.81	2.42	0.54	0.34	1.32	0.79	2.49	8.31	24.08	1.74	0.28	3
41	0.49	0.12	486.71	0.8	2.33	0.54	0.34	1.33	0.78	2.41	7.95	201.22	1.69	0.28	3.29
42	0.48	0.12	134.51	0.8	2.46	0.54	0.34	1.32	0.78	2.61	7.67	62.05	1.75	0.28	3.18
43	0.49	0.12	100	0.8	2.44	0.54	0.34	1.34	0.79	2.51	8.34	100	1.74	0.28	3.1
44	0.48	0.12	87.79	0.82	2.47	0.54	0.34	1.33	0.79	2.47	7.98	100	1.75	0.29	3.11
45	0.48	0.12	38.13	0.8	2.42	0.54	0.33	1.31	0.79	2.5	7.8	143.35	1.72	0.28	3.11
46	0.48	0.12	79.22	0.81	2.49	0.54	0.34	1.29	0.78	2.48	8.1	89.42	1.72	0.28	3.08
47	0.48	0.12	75.83	0.8	2.45	0.54	0.34	1.34	0.8	2.41	6.9	123.9	1.73	0.28	3

Appendix B. Continued

No.	SiO2	P2O5	SO3	CaO	Y2O3	La2O3	Ce2O3	Pr2O3	Nd2O3	Sm2O3	Gd2O3	Dy2O3	PbO	ThO2	UO2
Counting error (1σ %)															
48	0.48	0.12	74.96	0.8	2.38	0.54	0.34	1.33	0.79	2.44	8.13	100	1.75	0.28	3.16
49	0.48	0.12	52.99	0.79	2.42	0.54	0.34	1.3	0.78	2.46	7.1	586.35	1.69	0.29	3.16
50	0.48	0.12	52.08	0.8	2.41	0.55	0.34	1.31	0.79	2.56	7.71	2578.6	1.75	0.28	3.01
51	0.48	0.12	82.6	0.8	2.46	0.54	0.34	1.32	0.78	2.5	7.76	54.47	1.7	0.28	3.27
52	0.48	0.12	100	0.81	2.5	0.55	0.34	1.32	0.78	2.53	7.06	100	1.65	0.28	3.18
53	0.48	0.12	40.52	0.8	2.48	0.54	0.34	1.32	0.78	2.48	7.28	510.37	1.75	0.28	2.95
54	0.48	0.12	57.93	0.82	2.48	0.54	0.34	1.32	0.79	2.53	8.63	100	1.78	0.28	3.05
55	0.48	0.12	35.09	0.83	2.41	0.54	0.33	1.36	0.78	2.48	8.24	136.13	1.73	0.29	3.25
56	0.48	0.12	171.5	0.81	2.39	0.54	0.34	1.35	0.78	2.53	8.01	90.46	1.75	0.28	3.18
57	0.48	0.12	124.72	0.82	2.41	0.54	0.34	1.32	0.78	2.54	7.42	100	1.74	0.28	3.22
58	0.48	0.12	193.16	0.82	2.38	0.54	0.34	1.35	0.78	2.55	7.71	521.63	1.76	0.28	3.15
59	0.48	0.12	41.7	0.81	2.51	0.54	0.34	1.37	0.78	2.52	8.44	102.46	1.73	0.28	3.12
60	0.48	0.12	107.28	0.82	2.41	0.54	0.33	1.34	0.78	2.59	7.92	54.6	1.79	0.28	3.08

Appendix C. Compositional data, k-ratio errors, calculated dates and Monte Carlo CIs for analyses in Chapter 2

Sample	SiO2	P2O5	CaO	Y2O3	La2O3	Ce2O3	Pr2O3	Nd2O3	Sm2O3	Gd2O3	Dy2O3	PbO	ThO2	UO2	Total	Date (Ma)	95% CI
Concentrations																	
CH22-30-mz1-2	0.1564	30.75	0.5805	1.63	15.04	28.21	3.42	13.05	2.14	1.82	0.5688	0.0754	2.78	0.3987	100.6545	435.6	35.8
CH22-30-mz1-3	0.1348	30.93	0.479	1.61	15.15	28.6	3.59	13.51	2.23	1.69	0.5993	0.0628	2.2	0.3594	101.1701	439	41.9
CH22-30-mz1-4	0.1102	30.87	0.4306	1.62	15.31	28.64	3.62	13.62	2.17	1.7	0.6459	0.0597	1.92	0.3492	101.0885	459.7	45.5
CH22-30-mz1-5	0.1764	30.73	0.681	1.7	14.76	27.64	3.34	13.09	2.25	1.84	0.6419	0.0825	3.3	0.443	100.7074	410.1	31.3
CH22-30-mz1-6	0.1876	30.78	0.7991	1.89	14.38	26.81	3.26	12.84	2.24	1.96	0.7224	0.11	3.76	0.5933	100.3694	454.9	26.3
CH22-30-mz1-7	0.176	30.69	0.6649	1.72	14.64	27.55	3.36	13.34	2.21	1.89	0.6044	0.0854	3.36	0.4691	100.8031	411.9	30.6
CH22-30-mz1-8	0.1511	30.89	0.4243	1.6	15.27	28.69	3.42	13.38	2.14	1.68	0.5812	0.0595	2.05	0.3704	100.7458	430.5	43.5
CH22-30-mz1-9	0.159	30.82	0.6218	1.75	14.76	27.72	3.34	13.34	2.22	1.79	0.6111	0.0808	3.11	0.4294	100.7866	422.3	32.5
CH22-30-mz1-10	0.1439	30.9	0.4563	1.65	15.01	28.53	3.52	13.56	2.22	1.67	0.5913	0.061	2.2	0.3815	100.9329	417.7	41.3
CH22-30-mz1-11	0.1289	30.88	0.463	1.6	15.47	28.53	3.56	13.24	2.08	1.6	0.5461	0.0655	2.14	0.3704	100.6981	460.2	42.4
CH22-30-mz2-4	0.1293	30.14	0.4453	1.59	15.28	28.18	3.51	13.17	2.15	1.81	0.6346	0.0589	1.83	0.3721	99.3225	455.6	46.6
CH22-30-mz2-6	0.1287	30.13	0.47	1.61	15.26	28	3.4	12.98	2.17	1.92	0.5711	0.0601	2.12	0.3932	99.2375	416.6	42.4
CH22-30-mz2-8	0.1286	30.16	0.4737	1.69	14.97	28.09	3.48	13.06	2.32	2.03	0.6237	0.0655	2.08	0.3948	99.591	457.8	42
CH22-30-mz2-12	0.154	30.71	0.4956	1.72	14.56	28.21	3.42	13.59	2.35	2.22	0.6561	0.0662	2.07	0.4042	100.6505	460.1	41.5
CH22-30-mz2-13	0.1476	30.72	0.5438	1.73	14.72	28.08	3.29	13.4	2.37	2.17	0.6767	0.0763	2.46	0.4501	100.8615	457.6	36.6
CH22-30-mz2-14	0.1439	30.74	0.5259	1.77	14.44	27.97	3.31	13.37	2.37	2.35	0.7175	0.0746	2.3	0.4457	100.5538	467.4	37.5
CH22-30-mz2-15	0.1364	30.81	0.4922	1.7	14.7	28.44	3.41	13.18	2.34	2.22	0.6664	0.0679	2.13	0.4103	100.728	461	40.8
CH22-30-mz2-16	0.1557	30.67	0.5309	1.65	14.73	28.08	3.46	13.41	2.18	1.86	0.5714	0.066	2.32	0.3922	100.1018	432.4	39.7
CH22-30-mz2-17	0.1502	30.77	0.4861	1.7	14.69	28.39	3.47	13.44	2.35	2.17	0.6977	0.0592	2.11	0.4123	100.92	404.5	41
CH22-30-mz2-18	0.1567	30.8	0.5546	1.82	14.37	27.85	3.35	13.41	2.42	2.39	0.7047	0.0687	2.39	0.4385	100.7503	424.1	37.4
CH22-0-mz3-1	0.1379	30.81	0.4164	1.55	15.35	29.02	3.6	13.63	2.07	1.62	0.6091	0.0581	1.76	0.35	101.0027	471.3	47.2
CH22-0-mz3-2	0.149	30.84	0.5487	1.63	14.93	28.5	3.57	13.4	2.2	1.8	0.6331	0.0676	2.47	0.3809	101.1459	429.6	38.4
CH22-0-mz3-3	0.1678	30.79	0.6049	1.72	15.04	28.27	3.41	13.29	2.2	1.84	0.5841	0.0847	2.76	0.4419	101.2323	474	33.9
CH22-0-mz3-4	0.1524	30.77	0.6316	1.87	14.52	28	3.36	13.33	2.22	1.95	0.7083	0.0853	2.78	0.5217	100.9294	448.5	32.1
CH22-0-mz3-5	0.1632	30.71	0.6217	1.86	14.57	27.92	3.46	13.43	2.29	1.89	0.6589	0.0892	2.8	0.4988	100.9918	473.9	32.2
CH22-0-mz3-6	0.1439	30.74	0.5973	1.75	14.87	28.41	3.5	13.24	2.17	1.84	0.6146	0.0842	2.64	0.4809	101.1092	470.5	34
CH22-0-mz3-7	0.1583	30.79	0.6163	1.78	14.94	28.47	3.45	13.35	2.19	1.8	0.7048	0.0751	2.69	0.4934	101.5368	412.2	33.8

CH22-0-mz3-8	0.1904	30.69	0.8072	1.8	14.33	27.59	3.43	13.02	2.22	1.91	0.7313	0.1137	3.62	0.5522	101.0399	492.9	26.7
CH22-0-mz3-9	0.1148	30.78	0.4828	1.63	15.16	28.93	3.48	13.38	2.13	1.64	0.6322	0.0595	2.01	0.3662	100.8189	437.9	43.5
CH22-0-mz3-10	0.1249	30.76	0.4531	1.62	15.11	28.86	3.63	13.7	2.14	1.72	0.6129	0.059	1.89	0.3413	101.0438	462.6	45.5
CH22-14-mz1-1	0.1978	30.41	0.6472	0.5052	14.91	28.26	3.41	14.04	2.47	2.13	0.3108	0.078	2.83	0.5262	100.7468	405.2	35.7
CH22-14-mz1-2	0.1922	30.54	0.7448	0.6062	14.44	28.02	3.42	13.77	2.6	2.2	0.3578	0.109	3.16	0.6873	100.8717	474.5	29.4
CH22-14-mz1-3	0.239	30.48	0.8282	0.5432	14.69	27.52	3.38	13.42	2.5	2.12	0.321	0.1199	3.69	0.7106	100.5894	469.5	26.7
CH22-14-mz1-4	0.2399	30.49	0.8357	0.4722	14.98	27.71	3.26	13.52	2.43	1.99	0.279	0.1102	3.89	0.6408	100.8763	434.3	27.2
CH22-14-mz1-5	0.1763	30.56	0.5699	0.4337	15	28.5	3.51	13.58	2.34	1.95	0.3002	0.0731	2.57	0.4676	100.0502	420.8	39.8
CH22-14-mz1-7	0.2403	30.44	0.9538	0.498	14.39	27	3.23	13.34	2.43	2.09	0.3365	0.1246	4.3	0.6764	100.0808	450.9	24.9
CH22-14-mz1-8	0.1973	30.55	0.6235	0.6406	14.37	28.24	3.46	13.63	2.49	2.14	0.3499	0.0796	2.72	0.5294	100.042	422.1	36.3
CH22-14-mz1-9	0.1973	30.56	0.6517	0.7866	14	27.93	3.36	13.51	2.47	2.2	0.3624	0.0922	2.77	0.551	99.4645	474.9	34.1
CH22-14-mz1-10	0.1665	30.57	0.6107	0.8679	13.9	28.03	3.38	13.54	2.49	2.34	0.4424	0.0761	2.59	0.5402	99.5662	412.4	36.6
CH22-14-mz1-6	0.2314	30.45	0.9144	0.4943	14.6	27.04	3.23	13.26	2.35	2.08	0.2716	0.1136	4.1	0.664	99.8295	427.7	26.1
CH22-0-mz4-1	0.1504	30.94	0.576	1.68	14.42	27.61	3.43	13.31	2.26	2.03	0.727	0.0699	2.62	0.3819	100.233	426.6	37.7
CH22-0-mz4-2	0.1437	30.76	0.5882	1.58	14.78	28.17	3.33	13.01	2.2	1.96	0.6577	0.0655	2.56	0.3796	100.2115	407	38.2
CH22-0-mz4-3	0.1485	30.79	0.5555	1.65	14.4	27.77	3.48	13.24	2.25	1.96	0.6914	0.0777	2.51	0.3649	99.9149	493.2	38
CH22-0-mz4-4	0.1316	30.83	0.5413	1.55	14.72	28.11	3.43	13.04	2.17	1.96	0.6421	0.0729	2.41	0.3565	99.99	479.8	39.3
CH22-0-mz4-5	0.1852	30.8	0.6834	1.76	14.19	27.45	3.36	13.09	2.25	2.13	0.7304	0.0803	3.25	0.4463	100.438	402.8	31.2
CH22-0-mz4-6	0.1618	30.88	0.6693	1.84	14.15	27.4	3.38	13.22	2.31	2.12	0.6911	0.0836	3.01	0.4727	100.4198	432.9	31.8
CH22-0-mz4-7	0.1933	30.88	0.6827	1.77	14.4	27.4	3.45	12.9	2.15	1.85	0.6621	0.0883	3.1	0.4694	100.0273	448.9	31.6
CH22-0-mz4-8	0.1313	30.92	0.4464	1.55	14.98	28.63	3.61	13.46	2.09	1.73	0.6063	0.0609	1.96	0.3228	100.5203	475.7	46
CH22-0-mz4-9	0.1462	31.04	0.5043	1.64	14.44	27.94	3.45	13.36	2.19	1.91	0.645	0.0598	2.28	0.3616	99.9924	408.1	40.7
CH22-0-mz4-10	0.1758	30.91	0.5965	1.62	14.76	28.08	3.51	13.05	2.12	1.81	0.6371	0.0814	2.76	0.3883	100.5274	475.4	35.8
ch27-2-mz1-1	0.2133	30.39	0.666	1.5	13.34	28.81	3.3	12.73	2.12	1.79	0.6538	0.0963	3.19	0.6262	99.456	433.7	28.9
ch27-2-mz1-2	0.2318	29.09	0.6835	1.65	13.35	28.73	3.26	12.79	2.09	1.79	0.6576	0.1029	3.54	0.6326	98.6353	432.9	26.8
ch27-2-mz1-3	0.2305	30.26	0.6954	1.76	13.06	28.07	3.22	12.78	2.12	1.88	0.6843	0.1102	3.67	0.596	99.19	462	26.5
ch27-2-mz1-4	0.2244	30.31	0.6871	1.73	13.05	28.04	3.19	12.74	2.1	1.95	0.7559	0.1052	3.6	0.5568	99.0902	457.3	27.4
ch27-2-mz1-5	0.2166	30.3	0.655	1.59	13.28	28.64	3.29	12.6	2.07	1.79	0.6691	0.0933	3.38	0.5337	99.1565	429.7	29.4
ch27-2-mz1-6	0.2027	30.29	0.6545	1.55	13.59	29.16	3.3	12.74	2.13	1.74	0.5974	0.1038	3.34	0.5737	100.0218	468.5	28.6
ch27-2-mz1-7	0.2245	30.28	0.654	1.54	13.46	28.89	3.28	12.57	2.16	1.82	0.7076	0.1037	3.34	0.5522	99.6172	474.6	29
ch27-2-mz2-1	0.1802	30.56	0.6247	2.07	13.3	27.53	3.17	13.19	2.29	2.17	0.7539	0.0847	3.01	0.5817	99.5481	407.7	29.8
ch27-2-mz2-2	0.1951	30.59	0.6523	1.96	13.31	28	3.22	12.82	2.23	2.04	0.7826	0.0811	3.2	0.5059	99.6205	394.8	29.9

ch27-2-mz2-3	0.1718	30.52	0.6181	2.03	13.24	27.44	3.28	13.17	2.35	2.14	0.7318	0.087	2.98	0.5448	99.336	431.4	30.3
ch27-2-mz2-4	0.1872	30.53	0.6469	2.06	13.03	27.92	3.23	13.26	2.31	2.14	0.7567	0.0919	3.07	0.5381	99.8041	448.5	29.8
ch27-2-mz2-5	0.1727	30.61	0.6685	2.22	13.23	27.22	3.22	13.18	2.34	2.23	0.8196	0.0992	3.08	0.6547	99.7792	448	27.7
ch27-2-mz2-6	0.2188	30.58	0.6737	1.97	13.03	27.9	3.22	12.84	2.25	2.08	0.763	0.0872	3.32	0.5187	99.4858	410.7	29.3
ch27-2-mz2-7	0.1918	30.62	0.7114	2.25	12.85	27.13	3.15	13.22	2.42	2.36	0.7865	0.102	3.28	0.6426	99.7502	446.8	26.9
ch27-2-mz2-8	0.1749	30.51	0.6154	2.04	13.09	27.67	3.25	13.25	2.31	2.19	0.7199	0.0932	2.97	0.5379	99.4538	464.4	30.2
ch27-2-mz2-9	0.2098	30.6	0.6725	2.04	13.07	27.84	3.27	12.86	2.27	2.14	0.7879	0.1042	3.32	0.5472	99.7664	479.9	28.3
ch27-2-mz2-10	0.1704	30.57	0.6243	2.02	13.47	27.52	3.25	13.12	2.37	2.15	0.7592	0.1001	2.9	0.5462	99.6022	502.3	30.1
ch27-5-mz2-1	0.162	30.6	0.8638	1.33	13.75	28.81	3.31	12.18	1.91	1.65	0.6383	0.1259	3.59	0.903	99.8551	453.7	24
ch27-5-mz2-2	0.156	30.62	0.8728	1.35	13.65	28.8	3.32	12.69	1.98	1.72	0.6259	0.1255	3.63	0.9436	100.5162	440.9	23.6
ch27-5-mz2-3	0.1514	30.63	0.8486	1.31	13.78	28.93	3.22	12.5	1.88	1.64	0.6607	0.1194	3.49	0.8972	100.0885	438.6	24.5
ch27-5-mz2-4	0.1451	30.59	0.8458	1.34	13.66	28.84	3.31	12.38	1.91	1.67	0.6186	0.1227	3.5	0.9075	99.8713	447.5	24.1
ch27-5-mz2-5	0.1856	30.62	0.6718	1.81	13.2	28.48	3.37	13	2.22	1.98	0.6447	0.0927	3.11	0.5927	100.0094	433.5	29.4
ch27-5-mz2-6	0.1659	30.62	0.6407	1.68	13.66	28.83	3.26	12.62	2.08	1.81	0.5974	0.0903	2.95	0.5615	99.596	445	30.9
ch27-5-mz2-7	0.1553	30.69	0.5759	1.89	13.92	29	3.32	12.68	2.05	1.78	0.625	0.0803	2.66	0.4682	99.9242	451.9	34.2
ch27-5-mz2-8	0.1483	30.6	0.5664	1.53	14.17	28.97	3.33	12.74	2	1.78	0.6186	0.0778	2.66	0.5124	99.7306	423.5	34.3
ch27-5-mz2-9	0.1475	30.58	0.5723	1.43	14.22	29.05	3.25	13.04	2.12	1.76	0.5052	0.0802	2.59	0.509	99.8804	444.7	35.1
ch27-5-mz2-10	0.1499	30.45	0.5582	1.48	14.32	29.07	3.35	12.92	2.06	1.76	0.5799	0.0785	2.55	0.4996	99.8522	442.5	35.4
ch27-5-mz2-11	0.158	30.47	0.6105	1.6	13.8	28.74	3.35	12.83	2.09	1.85	0.5357	0.0838	2.83	0.5243	99.501	435	32.7
ch27-5-mz2-12	0.1717	30.56	0.6705	1.74	13.37	28.43	3.4	13.05	2.11	1.85	0.6806	0.0891	3.09	0.5775	99.8208	422.5	30
ch27-5-mz2-13	0.2055	30.65	0.7033	2.06	13.36	27.97	3.37	12.82	2.12	1.92	0.7303	0.0997	3.46	0.553	100.0575	446.3	27.8
ch27-5-mz2-14	0.245	30.64	0.6969	2.08	13.11	28.23	3.33	12.71	2.14	1.89	0.7487	0.1014	3.42	0.543	99.9208	459.9	27.9
CH35-0-mz1-2	0.1152	30.94	0.4798	1.94	14.96	29.78	3.38	12.72	1.99	1.77	0.8796	0.0679	1.8	0.4847	101.3312	472.2	40.9
CH35-0-mz1-3	0.1859	30.74	0.7764	2.08	13.52	28.14	3.26	12.45	2.14	2.27	0.9931	0.0943	3.5	0.5867	100.7728	411.1	27.5
CH35-0-mz1-4	0.1095	30.77	0.4872	2.05	14.45	29.58	3.34	12.88	2.06	1.83	0.8802	0.0793	1.98	0.5479	101.074	494.6	37
CH35-0-mz1-5	0.1237	30.82	0.5714	2.13	14.07	29.24	3.4	12.83	2.13	2.01	0.9341	0.0817	2.25	0.6239	101.2431	449	33.4
CH35-0-mz1-6	0.4249	30.45	1.3046	2.16	13.37	26.78	2.99	10.95	1.75	2.54	0.9411	0.1679	6.73	0.689	101.3143	440.6	17.3
CH35-0-mz1-7	0.3062	30.73	1.0558	2.16	12.93	27.22	3.15	11.88	2.07	2.72	1.0626	0.1406	5.23	0.5911	101.2949	462.2	21.2
CH35-0-mz1-8	0.1532	30.9	0.6196	1.99	13.86	29.03	3.34	12.76	2.14	2.24	0.956	0.0861	2.64	0.5224	101.2688	466.3	33
CH35-0-mz1-9	0.4135	30.49	1.2273	2.1	12.61	26.75	3.07	11.76	2	2.59	0.9938	0.1487	6.5	0.6144	101.3329	412.4	18.3
CH35-0-mz1-10	0.2279	30.66	0.8785	1.96	13.08	27.89	3.22	12.27	2.16	2.5	0.9929	0.1118	4.21	0.5778	100.7927	432.5	24.8
CH35-0-mz1-11	0.2445	30.8	0.9384	2.12	12.97	27.39	3.18	12.52	2.21	2.69	1.0559	0.1305	4.37	0.6283	101.2933	478.1	23.1

CH35-0-mz2-2	0.298	30.82	0.957	1.98	13.53	27.83	3.1	12.19	2.2	2.66	1.0053	0.1179	4.09	0.5456	101.3737	472.4	24.8
CH35-0-mz2-3	0.1182	31.01	0.4546	1.85	14.51	29.8	3.49	12.71	2	1.8	0.8135	0.0711	1.89	0.4632	101.0112	491.4	40.3
CH35-0-mz2-4	0.2105	30.91	0.7422	1.94	13.58	28.37	3.26	12.77	2.19	2.38	0.94	0.1128	3.47	0.5449	101.4635	505	27.3
CH35-0-mz2-5	0.1369	30.93	0.507	1.82	14.49	30.06	3.4	12.72	1.96	1.8	0.8146	0.0709	2.09	0.5061	101.3308	446.6	37.6
CH35-0-mz2-6	0.2161	30.91	0.8437	1.95	13.72	28.32	3.21	12.15	2.13	2.53	0.942	0.1117	3.87	0.5642	101.5193	460.4	26
CH35-0-mz2-8	0.2846	30.79	1.0626	2.16	12.84	27.09	3.09	12.04	2.15	2.68	0.9862	0.1398	5.1	0.6468	101.1077	456.6	20.8
CH35-0-mz2-9	0.2708	30.73	0.9512	1.97	12.88	27.53	3.19	12.4	2.17	2.56	0.9918	0.128	4.57	0.5978	100.9922	462.3	22.9
CH35-0-mz2-10	0.169	30.96	0.6334	1.95	13.84	28.87	3.36	12.71	2.14	2.21	0.9292	0.0858	2.76	0.5292	101.1771	450.3	31.9
CH35-0-mz2-7	0.3815	30.65	1.1602	2.12	12.27	26.56	3.12	12.21	2.19	2.81	0.9756	0.1515	5.76	0.6267	101.041	457.1	19.4
CH35-0-mz2-11	0.2751	30.91	0.9581	2.14	12.93	27.46	3.18	12.16	2.1	2.75	0.9696	0.1226	4.53	0.5945	101.1271	446.5	23
CH35-0-mz2-12	0.3128	30.25	1.123	2.22	12.81	26.35	3.02	11.76	2.1	2.74	1.0203	0.1502	5.26	0.68	99.8465	472.6	19.9
CH35-0-mz2-13	0.2804	30.26	0.9816	2.06	12.94	26.97	3.24	12.35	2.22	2.79	1.0378	0.127	4.62	0.5796	100.5009	459.3	23
CH35-0-mz2-14	0.3438	30.26	1.0872	2.12	12.77	26.55	3.13	11.84	2.03	2.7	0.9542	0.1365	5.13	0.6112	99.7115	451.4	21
CH35-0-mz2-15	0.3338	30.19	1.0752	2.01	12.8	26.62	3.06	12.03	2.17	2.72	0.9528	0.1346	5.27	0.5891	100.0043	440.8	21.1
CH35-0-mz2-17	0.1105	30.37	0.4093	1.8	15.08	29.77	3.47	12.73	2	1.59	0.7664	0.0635	1.61	0.4501	100.2418	484.9	45.2
CH35-0-mz3-2	0.1901	30.9	0.3567	1.7	15.78	30.43	3.45	13.13	2.03	1.34	0.588	0.036	1.48	0.1149	101.5479	456.7	65.7
CH35-0-mz3-3	0.1218	31.02	0.3292	1.38	15.74	30.13	3.48	13.49	2.29	1.35	0.5246	0.0304	1.44	0.1007	101.4447	405.1	71.7
CH35-0-mz3-4	0.1559	30.83	0.3225	1.1699	16.07	30.76	3.44	13.2	1.98	1.16	0.404	0.0392	1.59	0.1668	101.3071	433.5	63.7
CH35-0-mz3-5	0.0879	31.21	0.4865	2.49	15.27	29.85	3.42	12.7	1.91	1.38	0.6312	0.0438	1.76	0.1834	101.4615	437.5	49.6
CH35-0-mz3-6	0.1363	31.07	0.4558	1.88	15.5	30.17	3.41	12.83	1.85	1.32	0.536	0.0603	1.84	0.342	101.4245	479.7	45
CH35-0-mz3-7	0.0986	31.18	0.4203	1.51	15.09	29.66	3.4	13.46	2.36	1.52	0.5355	0.0361	1.7	0.1294	101.1207	401.7	60.7
CH35-0-mz3-8	0.1511	31.08	0.4059	1.73	15.43	29.85	3.42	13.12	2.27	1.46	0.6149	0.0338	1.7	0.145	101.4327	367.4	57
CH35-0-mz3-9	0.1168	31.26	0.3754	2.32	15.6	29.94	3.43	12.76	1.95	1.37	0.6296	0.0431	1.64	0.1505	101.6135	475.8	54.7
CH35-0-mz3-10	0.0757	31.41	0.4624	2.86	15.05	30.18	3.37	12.46	1.76	1.33	0.7364	0.0299	1.47	0.1607	101.3831	354.4	50.8
CH35-0-mz4-1	0.1493	30.79	0.6536	1.93	14.01	28.42	3.3	12.57	2.06	2.12	0.8801	0.0929	2.93	0.5475	100.4854	463.5	31
CH35-0-mz4-2	0.1049	30.82	0.509	1.99	14.57	28.98	3.46	12.72	2.01	1.84	0.8921	0.0716	1.99	0.5321	100.5155	452.7	37.8
CH35-0-mz4-3	0.0883	30.84	0.4325	1.86	14.86	29.62	3.53	12.71	1.92	1.69	0.7833	0.054	1.72	0.4435	100.5748	402.7	44.1
CH35-0-mz4-4	0.1736	30.67	0.6973	1.93	13.88	28.45	3.32	12.48	2.03	2.13	0.8919	0.0895	3.22	0.554	100.5503	420.2	29.5
CH35-0-mz4-5	0.1554	30.63	0.6723	1.89	13.83	28.37	3.37	12.62	2.08	2.24	0.9427	0.0842	3.06	0.5322	100.5095	414.4	30.5
CH35-0-mz4-6	0.1455	30.69	0.6528	1.97	13.96	28.64	3.28	12.64	2.1	2.13	0.8795	0.0842	2.82	0.535	100.5584	434.6	31.9
CH35-0-mz4-7	0.1115	30.72	0.5287	1.9	14.83	29.21	3.39	12.59	1.96	1.73	0.8131	0.0661	2.01	0.5233	100.4082	419.6	38.4
CH35-0-mz4-8	0.0744	30.74	0.4416	1.89	15.4	29.85	3.3	12.59	1.95	1.56	0.7691	0.0455	1.6	0.4015	100.6346	370.5	46.9
CH35-0-mz4-9	0.0854	30.7	0.4003	1.76	15.6	29.94	3.36	12.49	1.87	1.41	0.6893	0.0448	1.52	0.3414	100.2323	401.4	51.2

CH35-0-mz4-10	0.1049	30.59	0.457	1.84	14.97	29.67	3.37	12.6	1.94	1.53	0.7323	0.0606	1.76	0.4364	100.0845	448.5	44.1
CH35-0-mz4-11	0.0972	30.73	0.4618	1.85	15.06	29.67	3.36	12.54	1.94	1.61	0.7386	0.0555	1.81	0.4578	100.4045	396.8	42.8
CH35-0-mz4-12	0.1098	30.79	0.5225	1.81	14.92	29.49	3.41	12.25	1.9	1.76	0.7468	0.0556	2.13	0.4876	100.4081	353.8	38.8
CH35-0-mz4-13	0.0705	30.77	0.3459	1.73	15.75	30.13	3.4	12.69	1.96	1.41	0.6245	0.0462	1.37	0.3046	100.6216	459.6	56.6
CH35-0-mz4-14	0.0846	30.8	0.3829	1.67	15.8	29.99	3.37	12.62	1.96	1.38	0.6316	0.0476	1.59	0.2601	100.6078	459.8	55.2
CH35-0-mz4-15	0.1015	30.81	0.4554	1.89	14.89	29.52	3.39	12.69	1.97	1.68	0.74	0.0585	1.79	0.4861	100.4952	409.1	42.3
CH35-0-mz4-16	0.0758	30.9	0.3448	1.83	15.12	29.6	3.37	12.91	2.04	1.48	0.6708	0.0497	1.36	0.2323	100.0039	550.3	59.3
CH35-0-mz5-1	0.1271	30.46	0.5212	1.87	14.58	29.4	3.43	12.62	2	1.89	0.84	0.0671	2.09	0.5361	100.4573	412.8	37.6
CH35-0-mz5-2	0.1516	30.34	0.6184	1.96	14.25	28.79	3.35	12.59	2.09	2.11	0.9257	0.0686	2.54	0.5457	100.3595	375.8	34.1
CH35-0-mz5-3	0.1605	30.33	0.6525	2.03	13.93	28.49	3.31	12.66	2.12	2.16	0.9373	0.0916	2.72	0.5664	100.1894	471.9	31.7
CH35-0-mz5-4	0.1419	30.33	0.5728	1.85	14.38	29.28	3.41	12.72	2.04	1.98	0.8438	0.0785	2.37	0.5272	100.5519	452.3	35.4
CH35-0-mz5-5	0.1141	30.32	0.4924	1.87	14.39	29.31	3.36	12.68	1.99	1.82	0.811	0.0765	1.99	0.5101	99.7592	491.6	38.8
CH35-0-mz5-6	0.1029	30.45	0.3621	1.8	15.52	30.1	3.43	12.94	2.01	1.5	0.7151	0.0403	1.35	0.3445	100.6851	384.9	53.9
CH35-0-mz5-7	0.0969	30.6	0.3455	1.8	15.21	29.76	3.44	12.9	2.02	1.45	0.659	0.0435	1.34	0.3069	99.9919	437.7	55.9
CH35-0-mz5-8	0.1163	30.36	0.4036	1.82	15.26	29.82	3.44	12.85	1.97	1.53	0.6951	0.0645	1.5	0.4083	100.2591	533.8	47.4
CH35-0-mz5-9	0.1116	30.28	0.4402	1.94	14.8	29.36	3.39	12.84	2	1.73	0.8485	0.0529	1.59	0.494	99.9	390.7	43.6
CH35-0-mz5-10	0.1025	30.36	0.3836	1.89	15.01	29.59	3.47	13.09	2.12	1.48	0.7451	0.0471	1.56	0.2344	100.1049	476.1	55.5
CH35-0-mz5-11	0.1098	30.29	0.3533	1.77	15.43	30	3.44	12.82	1.97	1.51	0.6916	0.0512	1.3	0.3897	100.1454	468.7	52.7
CH35-0-mz5-12	0.1154	30.33	0.345	1.74	15.44	29.83	3.44	12.89	1.95	1.42	0.6932	0.0378	1.37	0.3072	99.9287	376.7	56.2
CH35-0-mz6-1	0.1146	30.09	0.3937	0.7768	16.56	30.47	3.4	12.58	1.9	1.0311	0.3396	0.0324	1.87	0.0858	99.6618	356.4	67.9
CH35-0-mz6-2	0.1268	30.03	0.4143	0.7811	16.13	30.27	3.46	12.86	2.22	1.22	0.3905	0.0231	1.89	0.0871	99.9208	251.6	64.9
CH35-0-mz6-3	0.1502	29.87	0.4017	0.7857	16.09	30.1	3.41	12.79	2.2	1.18	0.374	0.0282	1.89	0.1014	99.3892	301.1	65
CH35-0-mz6-4	0.1164	29.92	0.3798	1.1265	15.14	29.42	3.42	13.42	2.42	1.52	0.4355	0.0289	1.81	0.1182	99.2946	311.4	62.2
CH35-0-mz6-5	0.0981	29.98	0.4073	1.0622	15.54	29.32	3.43	13.27	2.37	1.38	0.4451	0.033	1.87	0.1021	99.3272	354.2	63
CH35-0-mz6-6	0.0831	30	0.4073	0.8838	16.34	30.08	3.46	12.73	2.07	1.19	0.3954	0.0233	1.78	0.0827	99.5434	269.1	67.4
CH35-0-mz6-7	0.0679	29.99	0.387	1.1609	15.37	29.53	3.49	13.31	2.32	1.39	0.472	0.0262	1.83	0.1065	99.4703	285.3	61.8
CH35-0-mz6-8	0.1212	29.9	0.4084	1.33	15.19	29.29	3.5	13.31	2.41	1.49	0.5008	0.0301	1.9	0.1114	99.5131	314.5	59
CH35-0-mz6-9	0.0907	29.98	0.4397	1.3	15.2	29.4	3.46	13.02	2.24	1.42	0.3869	0.0324	2.07	0.1105	99.1724	315.1	55.5
CH35-0-mz6-10	0.1055	29.98	0.4032	1.1282	15.59	29.85	3.48	13	2.09	1.22	0.4033	0.0337	1.97	0.1095	99.3839	342.3	59.8
CH62-15-mz1-1	0.6681	29.49	1.58	0.5425	11.86	24.15	3.01	12.36	2.55	2.61	0.4147	0.1974	9.03	0.4026	98.9284	449.5	15.7
CH62-15-mz1-2	0.6066	29.49	1.52	0.5991	12.06	24.21	3.01	12.39	2.58	2.76	0.5	0.1861	8.58	0.4167	98.9688	441.1	16.2
CH62-15-mz1-3	0.786	29.21	1.41	0.5031	12.1	24.37	3.02	12.5	2.52	2.6	0.4318	0.1921	8.73	0.3845	98.8183	453.2	16.2

CH62-15-mz1-4	0.779	29.2	1.3529	0.4919	12.22	24.66	3.11	12.51	2.54	2.6	0.3835	0.1828	8.36	0.3705	98.8188	449.9	17
CH62-15-mz1-5	0.6587	29.41	1.51	0.4576	12.19	24.57	2.99	12.4	2.4	2.49	0.3427	0.1946	8.7	0.3863	98.7602	459.9	16.3
CH62-15-mz1-6	0.2187	30.24	0.4965	0.1992	15.68	28.23	3.61	13.5	2.3	1.87	0.2645	0.0602	2.27	0.3386	99.2939	420.8	48.9
CH62-15-mz1-7	0.1696	30.23	0.375	0.1492	16.09	28.94	3.65	13.76	2.13	1.52	0.1606	0.0497	1.61	0.3595	99.2052	421.5	59.4
CH62-15-mz1-8	0.2003	30.12	0.5105	0.1824	15.81	28.24	3.6	13.57	2.2	1.73	0.2129	0.065	2.24	0.3888	99.0857	436.5	46.5
CH62-15-mz1-9	0.1579	30.3	0.2514	0.0839	16.58	29.41	3.79	14.05	2.11	1.2	0.0841	0.0347	0.9176	0.379	99.3552	381.3	79.6
CH62-15-mz1-10	0.1696	30.08	0.3405	0.0822	16.49	29.12	3.69	13.98	2.07	1.21	0.1105	0.0491	1.26	0.4645	99.1252	417.5	61.3
CH62-15-mz1-11	0.1705	30.16	0.2499	0.0869	16.54	29.65	3.78	14.15	2.09	1.26	0.0658	0.0432	0.7981	0.3784	99.4287	498.8	79.9
CH62-15-mz1-12	0.1587	30.2	0.3146	0.1068	16.51	29.31	3.79	13.92	2.04	1.32	0.132	0.0373	1.28	0.3987	99.5272	342.7	67
CH62-15-mz2-1	0.4763	29.86	1.0387	0.4092	13.61	25.61	3.25	12.75	2.41	2.51	0.4238	0.1345	5.83	0.3759	98.7294	449	22.9
CH62-15-mz2-2	0.5545	29.72	1.1261	0.4732	13.41	25.09	3.21	12.67	2.46	2.64	0.4451	0.1393	6.49	0.3832	98.857	424.2	21
CH62-15-mz2-3	0.3854	29.99	0.9973	0.5813	13.14	25.5	3.24	12.78	2.62	2.81	0.4988	0.1226	5.4	0.3341	98.4387	445.1	24.7
CH62-15-mz2-4	0.7738	29.29	1.67	0.6128	11.69	23.38	2.96	11.99	2.51	2.72	0.4437	0.2158	9.96	0.4002	98.686	451.2	14.2
CH62-15-mz2-5	0.4798	29.81	1.1648	0.6609	12.63	24.64	3.22	12.64	2.65	2.98	0.5609	0.1514	6.35	0.4069	98.3907	464.3	20.7
CH62-15-mz2-6	0.176	30.27	0.2598	0.0961	16.56	28.94	3.79	13.98	2.14	1.21	0.159	0.0383	0.8761	0.4347	98.9364	394.8	74.3
CH62-15-mz2-7	0.1636	30.29	0.3219	0.1107	16.56	29.02	3.81	13.55	2.05	1.32	0.1594	0.0459	1.21	0.3695	98.9897	447.6	68.1
CH62-15-mz2-8	0.1745	30.27	0.2562	0.1036	16.46	28.94	3.77	14.03	2.11	1.22	0.1549	0.031	0.8382	0.3709	98.7355	359.1	83.9
CH62-15-mz2-9	0.144	30.26	0.3293	0.1218	16.55	28.84	3.7	13.77	2.11	1.39	0.0961	0.0437	1.28	0.391	99.035	404	66
CH62-15-mz2-10	0.1371	30.19	0.381	0.1328	16.26	28.57	3.69	13.75	2.08	1.49	0.2228	0.0466	1.58	0.4228	98.9643	372.5	57.3
CH62-15-mz2-11	0.1448	30.25	0.3227	0.1266	16.41	28.86	3.75	13.84	2.1	1.43	0.1296	0.038	1.22	0.3757	99.0061	367.8	69.1
CH62-15-mz2-12	0.1489	30.2	0.3485	0.157	15.96	28.54	3.79	14.02	2.24	1.62	0.2122	0.0491	1.47	0.3617	99.1281	437	61.5
CH62-15-mz2-13	0.3969	30.26	1.0177	0.5839	13.57	25.81	3.33	12.88	2.66	2.89	0.5046	0.1298	5.43	0.3392	99.8415	467.5	24.2
CH62-15-mz3-1	0.225	29.86	0.574	0.2806	14.87	27.69	3.55	13.74	2.46	2.28	0.3657	0.0739	2.65	0.3136	98.952	473.3	43.3
CH62-15-mz3-2	0.1714	30.01	0.4026	0.176	15.7	28.07	3.71	13.95	2.3	1.77	0.1817	0.0593	1.7	0.3091	98.5224	513.8	58.3
CH62-15-mz3-3	0.3086	29.91	0.8108	0.4567	13.52	26.21	3.44	13.66	2.67	2.86	0.4829	0.0977	4.1	0.3304	98.8869	444.5	30.6
CH62-15-mz3-4	0.2088	29.94	0.571	0.2633	14.62	27.4	3.61	13.93	2.57	2.29	0.3139	0.0715	2.67	0.3004	98.7781	460.9	44
CH62-15-mz3-5	0.2413	30.06	0.6303	0.3272	14.51	27.25	3.44	13.88	2.61	2.46	0.3853	0.0732	3.08	0.3239	99.2935	417.4	39.3
CH62-15-mz3-6	0.1385	30.07	0.299	0.1232	15.94	28.63	3.8	14.34	2.25	1.44	0.1619	0.0344	1.16	0.3495	98.745	354.4	74.1
CH62-15-mz3-7	0.1846	30.08	0.4348	0.1872	15.52	28.08	3.72	14.01	2.32	1.89	0.2213	0.0523	1.92	0.3184	98.9523	417.2	55.4
CH62-15-mz4-1	0.8035	29.28	1.3909	0.566	12.29	24.53	3.15	12.75	2.62	2.86	0.4715	0.1873	8.24	0.3603	99.5574	468.3	16.9
CH62-15-mz4-2	0.7791	29.16	1.3854	0.6145	12.13	24.07	3.03	12.45	2.7	3.02	0.5445	0.1809	8.4	0.38	98.9036	442.2	16.6
CH62-15-mz4-3	0.4223	29.73	1.0224	0.6737	12.69	25.27	3.35	13.11	2.84	3.23	0.5571	0.1279	5.37	0.3148	98.7477	470.5	24.5
CH62-15-mz4-4	0.4956	29.54	1.0919	0.6057	12.94	25.08	3.2	12.97	2.68	2.94	0.5711	0.1324	6.11	0.3414	98.7422	432.1	22.3

CH62-15-mz4-5	0.5564	29.43	1.1311	0.5806	12.91	25.12	3.22	12.84	2.69	2.97	0.5172	0.1434	6.32	0.3568	98.8308	451.3	21.2
CH62-15-mz4-6	0.1713	30.03	0.3685	0.1634	15.56	28.04	3.75	13.91	2.3	1.77	0.2221	0.0435	1.55	0.3544	98.2445	380.5	61.7
CH62-15-mz4-7	0.2048	30.04	0.4908	0.2228	15.23	28.01	3.63	13.64	2.33	1.97	0.3239	0.0614	2.32	0.3327	98.823	424.9	47.7
CH62-15-mz4-8	0.1724	30.02	0.3065	0.1223	16.2	28.39	3.74	13.98	2.25	1.49	0.141	0.036	1.0968	0.3911	98.3442	359.8	72.6
CH62-15-mz4-9	0.1752	30.06	0.309	0.1096	16.03	28.64	3.83	14.02	2.16	1.48	0.1153	0.0397	1.0875	0.4276	98.4918	378.8	68.8
CH62-15-mz4-10	0.1927	30.06	0.3088	0.1062	16.16	28.81	3.72	13.92	2.2	1.38	0.14	0.0425	1.17	0.4022	98.6207	404.5	68

Sample	**Si**	**P**	**Ca**	**Y**	**La**	**Ce**	**Pr**	**Nd**	**Sm**	**Gd**	**Dy**	**Pb**	**Th**	**U**
k-ratio errors (1σ %)														
CH22-30-mz1-2	3.44	0.25	1.10	0.43	0.61	0.44	1.23	0.73	1.29	1.61	5.86	5.39	0.67	2.07
CH22-30-mz1-3	3.91	0.25	1.25	0.44	0.61	0.44	1.18	0.72	1.24	1.72	5.51	6.27	0.77	2.28
CH22-30-mz1-4	4.72	0.25	1.35	0.44	0.61	0.44	1.18	0.72	1.27	1.71	5.13	6.57	0.85	2.35
CH22-30-mz1-5	3.08	0.25	0.99	0.42	0.62	0.45	1.24	0.72	1.24	1.60	5.17	4.95	0.60	1.87
CH22-30-mz1-6	2.90	0.25	0.90	0.39	0.63	0.45	1.27	0.73	1.24	1.51	4.61	3.88	0.56	1.45
CH22-30-mz1-7	3.06	0.25	1.00	0.42	0.62	0.45	1.23	0.72	1.25	1.56	5.49	4.82	0.59	1.78
CH22-30-mz1-8	3.55	0.25	1.37	0.44	0.61	0.44	1.23	0.72	1.28	1.73	5.67	6.59	0.81	2.22
CH22-30-mz1-9	3.37	0.25	1.05	0.41	0.62	0.45	1.25	0.72	1.25	1.64	5.44	5.03	0.62	1.93
CH22-30-mz1-10	3.69	0.25	1.29	0.43	0.61	0.44	1.20	0.72	1.25	1.74	5.58	6.42	0.77	2.16
CH22-30-mz1-11	4.08	0.25	1.28	0.44	0.61	0.44	1.19	0.72	1.32	1.80	6.03	6.11	0.79	2.22
CH22-30-mz2-4	4.03	0.24	1.30	0.44	0.61	0.43	1.20	0.72	1.29	1.64	5.21	6.76	0.89	2.22
CH22-30-mz2-6	4.06	0.24	1.26	0.43	0.61	0.43	1.24	0.73	1.29	1.56	5.80	6.60	0.82	2.11
CH22-30-mz2-8	4.08	0.24	1.25	0.42	0.62	0.43	1.21	0.72	1.21	1.48	5.28	6.10	0.83	2.10
CH22-30-mz2-12	3.41	0.25	1.18	0.41	0.63	0.52	1.23	0.72	1.19	1.37	5.14	6.01	0.82	2.06
CH22-30-mz2-13	3.56	0.25	1.11	0.41	0.62	0.52	1.27	0.72	1.18	1.40	4.95	5.34	0.74	1.86
CH22-30-mz2-14	3.66	0.25	1.14	0.40	0.63	0.53	1.25	0.72	1.18	1.31	4.65	5.39	0.77	1.88
CH22-30-mz2-15	3.84	0.25	1.18	0.41	0.62	0.52	1.23	0.73	1.19	1.37	5.03	5.90	0.81	2.03
CH22-30-mz2-16	3.41	0.25	1.12	0.42	0.62	0.52	1.22	0.72	1.26	1.57	5.80	6.03	0.77	2.10
CH22-30-mz2-17	3.54	0.25	1.20	0.41	0.62	0.52	1.20	0.72	1.19	1.40	4.81	6.56	0.81	2.02
CH22-30-mz2-18	3.35	0.25	1.09	0.39	0.63	0.53	1.25	0.72	1.17	1.29	4.77	5.77	0.75	1.90
CH22-0-mz3-1	3.78	0.25	1.33	0.44	0.61	0.52	1.18	0.71	1.32	1.77	5.43	6.70	0.91	2.33
CH22-0-mz3-2	3.51	0.25	1.10	0.43	0.62	0.52	1.19	0.72	1.25	1.63	5.22	5.87	0.74	2.15

CH22-0-mz3-3	3.20	0.25	1.03	0.41	0.62	0.52	1.24	0.72	1.25	1.59	5.70	4.83	0.70	1.88
CH22-0-mz3-4	3.47	0.25	1.00	0.39	0.63	0.52	1.25	0.72	1.25	1.52	4.68	4.78	0.70	1.62
CH22-0-mz3-5	3.24	0.25	1.01	0.39	0.62	0.53	1.22	0.72	1.22	1.57	5.04	4.61	0.69	1.70
CH22-0-mz3-6	3.66	0.25	1.04	0.41	0.62	0.52	1.21	0.73	1.27	1.59	5.43	4.87	0.72	1.74
CH22-0-mz3-7	3.36	0.25	1.01	0.40	0.62	0.52	1.22	0.72	1.25	1.62	4.70	5.35	0.71	1.71
CH22-0-mz3-8	2.85	0.25	0.86	0.40	0.63	0.53	1.22	0.73	1.24	1.55	4.56	3.74	0.60	1.54
CH22-0-mz3-9	4.50	0.25	1.20	0.43	0.61	0.52	1.21	0.72	1.29	1.77	5.20	6.54	0.84	2.24
CH22-0-mz3-10	4.16	0.25	1.26	0.43	0.61	0.52	1.17	0.71	1.29	1.68	5.38	6.56	0.87	2.39
CH22-14-mz1-1	2.78	0.25	0.99	1.05	0.62	0.52	1.23	0.70	1.15	1.42	10.55	5.62	0.69	1.62
CH22-14-mz1-2	2.82	0.25	0.91	0.90	0.63	0.53	1.24	0.71	1.11	1.38	9.16	4.16	0.65	1.29
CH22-14-mz1-3	2.34	0.25	0.85	0.99	0.63	0.53	1.24	0.72	1.14	1.42	10.26	3.82	0.60	1.25
CH22-14-mz1-4	2.32	0.25	0.85	1.12	0.62	0.53	1.27	0.72	1.16	1.51	11.76	4.12	0.59	1.36
CH22-14-mz1-5	3.05	0.25	1.08	1.20	0.62	0.52	1.20	0.72	1.20	1.53	10.94	6.05	0.72	1.80
CH22-14-mz1-7	2.33	0.25	0.78	1.07	0.63	0.53	1.29	0.72	1.16	1.44	9.76	3.69	0.56	1.29
CH22-14-mz1-8	2.75	0.25	1.01	0.86	0.63	0.52	1.22	0.72	1.15	1.42	9.42	5.54	0.71	1.61
CH22-14-mz1-9	2.76	0.25	0.99	0.73	0.64	0.53	1.25	0.72	1.16	1.38	9.13	4.79	0.70	1.56
CH22-14-mz1-10	3.20	0.25	1.02	0.67	0.64	0.53	1.24	0.72	1.15	1.31	7.48	5.70	0.72	1.58
CH22-14-mz1-6	2.39	0.25	0.80	1.07	0.63	0.53	1.29	0.73	1.20	1.45	12.12	4.00	0.57	1.32
CH22-0-mz4-1	3.53	0.25	1.07	0.42	0.63	0.53	1.23	0.73	1.23	1.49	4.64	5.78	0.72	2.17
CH22-0-mz4-2	3.66	0.25	1.05	0.44	0.62	0.52	1.25	0.73	1.26	1.53	5.08	6.08	0.73	2.16
CH22-0-mz4-3	3.55	0.25	1.09	0.42	0.63	0.53	1.21	0.73	1.24	1.53	4.83	5.24	0.73	2.25
CH22-0-mz4-4	3.95	0.25	1.12	0.44	0.62	0.52	1.22	0.73	1.27	1.53	5.20	5.53	0.75	2.29
CH22-0-mz4-5	2.92	0.25	0.97	0.41	0.63	0.53	1.24	0.73	1.24	1.42	4.57	5.04	0.64	1.86
CH22-0-mz4-6	3.27	0.25	0.97	0.39	0.64	0.53	1.24	0.73	1.21	1.43	4.86	4.87	0.67	1.78
CH22-0-mz4-7	2.79	0.25	0.96	0.40	0.63	0.53	1.22	0.74	1.29	1.59	5.05	4.70	0.66	1.79
CH22-0-mz4-8	4.02	0.25	1.28	0.45	0.62	0.52	1.18	0.72	1.31	1.69	5.49	6.48	0.86	2.51
CH22-0-mz4-9	3.64	0.25	1.16	0.43	0.63	0.53	1.21	0.72	1.26	1.55	5.13	6.46	0.78	2.25
CH22-0-mz4-10	3.08	0.25	1.04	0.43	0.62	0.53	1.20	0.74	1.30	1.62	5.21	5.07	0.70	2.11
ch27-2-mz1-1	2.54	0.25	0.97	0.45	0.65	0.52	1.27	0.74	1.28	1.62	5.05	4.43	0.66	1.40
ch27-2-mz1-2	2.36	0.25	0.96	0.42	0.65	0.52	1.28	0.74	1.31	1.63	5.01	4.13	0.63	1.38
ch27-2-mz1-3	2.37	0.25	0.95	0.40	0.66	0.53	1.29	0.74	1.29	1.56	4.85	3.91	0.62	1.45
ch27-2-mz1-4	2.43	0.25	0.96	0.40	0.66	0.53	1.29	0.74	1.30	1.51	4.38	4.05	0.62	1.54

ch27-2-mz1-5	2.50	0.25	0.97	0.43	0.66	0.52	1.26	0.75	1.31	1.62	4.93	4.52	0.64	1.60
ch27-2-mz1-6	2.67	0.25	0.98	0.44	0.65	0.52	1.27	0.74	1.28	1.66	5.53	4.14	0.64	1.50
ch27-2-mz1-7	2.43	0.25	0.98	0.44	0.65	0.52	1.27	0.75	1.27	1.60	4.63	4.15	0.64	1.56
ch27-2-mz2-1	2.95	0.25	1.01	0.36	0.65	0.53	1.29	0.72	1.21	1.39	4.42	4.79	0.67	1.48
ch27-2-mz2-2	2.74	0.25	0.98	0.37	0.65	0.52	1.28	0.74	1.23	1.45	4.24	4.93	0.65	1.67
ch27-2-mz2-3	3.06	0.25	1.02	0.36	0.65	0.53	1.26	0.73	1.18	1.41	4.55	4.67	0.68	1.57
ch27-2-mz2-4	2.83	0.25	0.97	0.36	0.66	0.53	1.28	0.72	1.19	1.40	4.40	4.47	0.67	1.59
ch27-2-mz2-5	3.07	0.25	0.97	0.35	0.65	0.53	1.27	0.73	1.18	1.35	4.05	4.18	0.67	1.34
ch27-2-mz2-6	2.48	0.25	0.96	0.37	0.66	0.53	1.28	0.74	1.22	1.43	4.35	4.68	0.64	1.63
ch27-2-mz2-7	2.80	0.25	0.93	0.35	0.66	0.53	1.31	0.72	1.16	1.29	4.26	4.07	0.64	1.36
ch27-2-mz2-8	3.04	0.25	1.01	0.36	0.66	0.53	1.27	0.72	1.20	1.38	4.65	4.41	0.68	1.59
ch27-2-mz2-9	2.58	0.25	0.97	0.36	0.66	0.53	1.26	0.74	1.22	1.40	4.24	4.04	0.64	1.56
ch27-2-mz2-10	3.11	0.25	1.01	0.36	0.65	0.53	1.27	0.73	1.17	1.40	4.38	4.16	0.69	1.57
ch27-5-mz2-1	3.23	0.25	0.83	0.49	0.64	0.52	1.25	0.76	1.40	1.75	5.21	3.58	0.62	1.04
ch27-5-mz2-2	3.37	0.25	0.82	0.48	0.65	0.52	1.25	0.74	1.35	1.69	5.30	3.60	0.62	0.99
ch27-5-mz2-3	3.45	0.25	0.83	0.49	0.64	0.52	1.28	0.75	1.42	1.76	5.02	3.74	0.63	1.04
ch27-5-mz2-4	3.59	0.25	0.84	0.48	0.65	0.52	1.26	0.75	1.40	1.74	5.39	3.64	0.63	1.03
ch27-5-mz2-5	2.88	0.25	0.97	0.39	0.66	0.52	1.24	0.73	1.24	1.51	5.19	4.50	0.66	1.46
ch27-5-mz2-6	3.18	0.25	0.99	0.41	0.65	0.52	1.27	0.75	1.31	1.61	5.56	4.63	0.68	1.53
ch27-5-mz2-7	3.38	0.25	1.06	0.38	0.64	0.52	1.25	0.74	1.32	1.64	5.34	5.06	0.73	1.80
ch27-5-mz2-8	3.53	0.25	1.08	0.44	0.63	0.52	1.25	0.74	1.35	1.64	5.35	5.31	0.73	1.66
ch27-5-mz2-9	3.54	0.25	1.07	0.46	0.63	0.52	1.28	0.73	1.29	1.66	6.54	5.22	0.74	1.68
ch27-5-mz2-10	3.48	0.25	1.08	0.45	0.63	0.52	1.24	0.74	1.32	1.65	5.72	5.29	0.75	1.71
ch27-5-mz2-11	3.34	0.25	1.02	0.43	0.64	0.52	1.24	0.74	1.30	1.59	6.20	4.97	0.70	1.63
ch27-5-mz2-12	3.09	0.25	0.97	0.40	0.65	0.52	1.23	0.73	1.29	1.59	4.89	4.68	0.67	1.50
ch27-5-mz2-13	2.63	0.25	0.95	0.36	0.65	0.53	1.24	0.74	1.28	1.55	4.60	4.19	0.63	1.56
ch27-5-mz2-14	2.28	0.25	0.94	0.36	0.66	0.52	1.26	0.74	1.28	1.57	4.50	4.12	0.64	1.57
CH35-0-mz1-2	4.53	0.25	1.31	0.38	0.61	0.43	1.24	0.74	1.37	1.66	3.83	5.83	1.75	0.9
CH35-0-mz1-3	2.92	0.25	0.98	0.37	0.65	0.44	1.27	0.74	1.30	1.36	3.43	4.38	1.47	0.6
CH35-0-mz1-4	4.74	0.25	1.30	0.37	0.63	0.43	1.24	0.73	1.33	1.61	3.85	5.11	1.57	0.84
CH35-0-mz1-5	4.20	0.25	1.16	0.36	0.63	0.44	1.23	0.73	1.30	1.49	3.63	4.96	1.41	0.78
CH35-0-mz1-6	1.46	0.25	0.75	0.35	0.65	0.45	1.35	0.81	1.53	1.24	3.63	2.67	1.26	0.44

CH35-0-mz1-7	1.90	0.25	0.83	0.36	0.66	0.45	1.29	0.77	1.33	1.17	3.22	3.13	1.44	0.49
CH35-0-mz1-8	3.51	0.25	1.11	0.38	0.64	0.44	1.23	0.74	1.29	1.37	3.55	4.76	1.63	0.71
CH35-0-mz1-9	1.50	0.25	0.77	0.36	0.67	0.45	1.33	0.77	1.37	1.22	3.41	2.96	1.39	0.45
CH35-0-mz1-10	2.46	0.25	0.91	0.38	0.66	0.44	1.28	0.75	1.28	1.25	3.43	3.80	1.47	0.55
CH35-0-mz1-11	2.31	0.25	0.88	0.36	0.66	0.45	1.29	0.74	1.26	1.17	3.23	3.32	1.37	0.54
CH35-0-mz2-2	1.92	0.25	0.86	0.37	0.64	0.44	1.30	0.75	1.24	1.17	3.31	3.58	1.53	0.55
CH35-0-mz2-3	4.39	0.25	1.33	0.39	0.62	0.43	1.20	0.73	1.35	1.61	4.11	5.57	1.80	0.85
CH35-0-mz2-4	2.58	0.25	0.99	0.38	0.64	0.44	1.25	0.73	1.25	1.28	3.55	3.74	1.54	0.6
CH35-0-mz2-5	3.80	0.25	1.23	0.39	0.62	0.43	1.22	0.73	1.37	1.61	4.08	5.58	1.65	0.81
CH35-0-mz2-6	2.54	0.25	0.92	0.38	0.63	0.44	1.27	0.75	1.28	1.22	3.55	3.79	1.48	0.57
CH35-0-mz2-8	2.02	0.25	0.81	0.35	0.66	0.45	1.30	0.75	1.27	1.17	3.42	3.09	1.32	0.49
CH35-0-mz2-9	2.10	0.25	0.87	0.37	0.65	0.44	1.27	0.74	1.27	1.21	3.38	3.36	1.42	0.52
CH35-0-mz2-10	3.16	0.25	1.08	0.38	0.63	0.43	1.23	0.73	1.28	1.36	3.59	4.72	1.59	0.68
CH35-0-mz2-7	1.58	0.25	0.78	0.36	0.67	0.45	1.30	0.74	1.26	1.12	3.44	2.89	1.35	0.47
CH35-0-mz2-11	2.07	0.25	0.86	0.35	0.65	0.44	1.27	0.75	1.30	1.14	3.45	3.46	1.43	0.52
CH35-0-mz2-12	1.86	0.24	0.72	0.35	0.66	0.45	1.35	0.77	1.33	1.17	3.35	2.95	0.52	1.3
CH35-0-mz2-13	2.06	0.24	0.79	0.37	0.66	0.44	1.28	0.75	1.26	1.16	3.27	3.43	0.55	1.48
CH35-0-mz2-14	1.73	0.24	0.74	0.36	0.66	0.44	1.31	0.77	1.36	1.19	3.55	3.19	0.52	1.4
CH35-0-mz2-15	1.80	0.24	0.74	0.37	0.66	0.44	1.33	0.76	1.28	1.17	3.55	3.25	0.51	1.44
CH35-0-mz2-17	4.71	0.24	1.40	0.40	0.62	0.43	1.22	0.73	1.36	1.84	4.37	6.30	0.98	1.88
CH35-0-mz3-2	2.84	0.25	1.57	0.41	0.60	0.43	1.21	0.72	1.33	2.08	5.55	9.55	6.45	1.01
CH35-0-mz3-3	4.29	0.25	1.67	0.48	0.60	0.43	1.20	0.71	1.21	2.07	6.22	11.32	7.3	1.03
CH35-0-mz3-4	3.37	0.25	1.68	0.53	0.60	0.43	1.21	0.72	1.35	2.38	8.08	9.48	4.56	0.95
CH35-0-mz3-5	5.81	0.25	1.27	0.32	0.61	0.43	1.22	0.73	1.39	2.04	5.22	7.60	4.17	0.89
CH35-0-mz3-6	3.81	0.25	1.33	0.39	0.61	0.43	1.22	0.72	1.42	2.11	6.15	6.33	2.35	0.87
CH35-0-mz3-7	5.19	0.25	1.40	0.45	0.61	0.43	1.23	0.71	1.17	1.86	6.10	9.68	5.71	0.92
CH35-0-mz3-8	3.47	0.25	1.44	0.41	0.61	0.43	1.22	0.72	1.21	1.93	5.32	9.85	5.19	0.92
CH35-0-mz3-9	4.39	0.25	1.52	0.34	0.60	0.43	1.21	0.73	1.38	2.04	5.24	7.84	5.02	0.94
CH35-0-mz3-10	6.62	0.25	1.32	0.30	0.61	0.43	1.23	0.74	1.48	2.09	4.48	9.38	4.73	1.01
CH35-0-mz4-1	3.55	0.24	1.02	0.38	0.64	0.43	1.27	0.74	1.33	1.45	3.84	4.51	0.68	1.56
CH35-0-mz4-2	4.91	0.24	1.19	0.37	0.63	0.43	1.22	0.73	1.36	1.62	3.77	5.58	0.85	1.62
CH35-0-mz4-3	5.74	0.24	1.34	0.39	0.62	0.43	1.20	0.74	1.40	1.74	4.27	7.09	0.94	1.9
CH35-0-mz4-4	3.10	0.24	0.98	0.38	0.64	0.43	1.26	0.74	1.36	1.44	3.78	4.63	0.64	1.55

CH35-0-mz4-5	3.44	0.24	0.99	0.39	0.64	0.43	1.25	0.74	1.33	1.38	3.57	4.84	0.67	1.6
CH35-0-mz4-6	3.61	0.24	1.02	0.38	0.64	0.43	1.28	0.74	1.31	1.44	3.83	4.87	0.7	1.61
CH35-0-mz4-7	4.60	0.24	1.15	0.39	0.62	0.43	1.24	0.74	1.39	1.71	4.12	5.99	0.85	1.64
CH35-0-mz4-8	6.78	0.24	1.31	0.39	0.61	0.43	1.27	0.74	1.39	1.86	4.35	8.06	0.98	2.09
CH35-0-mz4-9	5.92	0.24	1.41	0.41	0.61	0.43	1.25	0.74	1.44	2.05	4.82	8.24	1.01	2.41
CH35-0-mz4-10	4.90	0.24	1.29	0.40	0.62	0.43	1.25	0.74	1.39	1.90	4.58	6.51	0.92	1.94
CH35-0-mz4-11	5.30	0.24	1.28	0.39	0.62	0.43	1.25	0.74	1.40	1.82	4.53	6.95	0.91	1.85
CH35-0-mz4-12	4.71	0.24	1.17	0.40	0.62	0.43	1.23	0.75	1.42	1.69	4.49	6.91	0.81	1.75
CH35-0-mz4-13	7.16	0.24	1.59	0.41	0.61	0.43	1.24	0.74	1.39	2.05	5.31	8.18	1.08	2.67
CH35-0-mz4-14	5.95	0.24	1.46	0.42	0.60	0.43	1.25	0.74	1.39	2.08	5.23	7.97	0.98	3.08
CH35-0-mz4-15	5.03	0.24	1.29	0.39	0.62	0.43	1.25	0.74	1.39	1.76	4.53	6.70	0.92	1.75
CH35-0-mz4-16	6.79	0.24	1.57	0.40	0.61	0.43	1.24	0.73	1.33	1.93	4.91	7.57	1.08	3.43
CH35-0-mz5-1	4.14	0.24	1.17	0.39	0.63	0.43	1.23	0.74	1.37	1.58	4.01	5.93	0.82	1.6
CH35-0-mz5-2	3.50	0.24	1.05	0.38	0.64	0.43	1.25	0.74	1.33	1.45	3.67	5.80	0.74	1.58
CH35-0-mz5-3	3.34	0.24	1.01	0.37	0.64	0.43	1.27	0.74	1.31	1.43	3.63	4.55	0.71	1.53
CH35-0-mz5-4	3.74	0.24	1.11	0.40	0.63	0.43	1.24	0.74	1.35	1.53	4.00	5.22	0.77	1.62
CH35-0-mz5-5	4.61	0.24	1.22	0.39	0.63	0.43	1.26	0.74	1.38	1.64	4.15	5.37	0.85	1.68
CH35-0-mz5-6	5.03	0.24	1.52	0.40	0.61	0.43	1.23	0.73	1.36	1.92	4.67	8.97	1.09	2.39
CH35-0-mz5-7	5.43	0.24	1.57	0.41	0.61	0.43	1.22	0.73	1.35	1.98	5.06	8.42	1.09	2.64
CH35-0-mz5-8	4.49	0.24	1.40	0.40	0.62	0.43	1.22	0.73	1.38	1.91	4.84	6.18	1.02	2.06
CH35-0-mz5-9	4.68	0.24	1.33	0.38	0.62	0.43	1.25	0.73	1.37	1.70	3.94	7.18	0.98	1.73
CH35-0-mz5-10	5.00	0.24	1.46	0.39	0.62	0.43	1.22	0.73	1.30	1.97	4.47	7.86	0.99	3.4
CH35-0-mz5-11	4.71	0.24	1.56	0.41	0.61	0.43	1.23	0.73	1.39	1.92	4.84	7.52	1.12	2.15
CH35-0-mz5-12	4.53	0.24	1.58	0.41	0.61	0.43	1.23	0.73	1.39	2.03	4.81	9.50	1.08	2.65
CH35-0-mz6-1	4.58	0.24	1.43	0.75	0.59	0.43	1.24	0.74	1.42	2.70	9.59	11.67	0.88	8.37
CH35-0-mz6-2	4.14	0.24	1.36	0.74	0.60	0.43	1.22	0.73	1.25	2.30	8.33	15.08	0.88	8.24
CH35-0-mz6-3	3.54	0.24	1.41	0.74	0.60	0.43	1.23	0.73	1.26	2.39	8.71	12.91	0.88	7.15
CH35-0-mz6-4	4.44	0.24	1.46	0.57	0.62	0.43	1.23	0.72	1.17	1.90	7.51	12.13	0.91	6.29
CH35-0-mz6-5	5.25	0.24	1.39	0.58	0.61	0.43	1.23	0.72	1.19	2.08	7.36	10.99	0.88	7.15
CH35-0-mz6-6	6.17	0.24	1.39	0.67	0.59	0.43	1.21	0.74	1.32	2.36	8.26	14.79	0.91	8.68
CH35-0-mz6-7	7.44	0.24	1.45	0.55	0.61	0.43	1.21	0.72	1.21	2.06	6.97	12.98	0.90	6.9
CH35-0-mz6-8	4.28	0.24	1.39	0.50	0.61	0.43	1.20	0.72	1.18	1.95	6.58	11.45	0.87	6.61
CH35-0-mz6-9	5.62	0.24	1.32	0.51	0.62	0.43	1.22	0.73	1.25	2.03	8.55	10.75	0.83	6.62

CH35-0-mz6-10	4.88	0.24	1.40	0.56	0.61	0.43	1.22	0.73	1.32	2.33	8.16	10.76	0.86	6.69
CH62-15-mz1-1	1.02	0.25	0.59	0.99	0.69	0.55	1.36	0.76	1.13	1.22	8.02	2.42	1.95	0.38
CH62-15-mz1-2	1.10	0.25	0.59	0.90	0.68	0.55	1.35	0.76	1.12	1.16	6.63	2.53	1.89	0.39
CH62-15-mz1-3	0.91	0.25	0.62	1.05	0.68	0.55	1.35	0.76	1.14	1.22	7.69	2.47	2.02	0.38
CH62-15-mz1-4	0.92	0.25	0.64	1.07	0.68	0.54	1.32	0.75	1.13	1.22	8.60	2.59	2.09	0.39
CH62-15-mz1-5	1.03	0.25	0.59	1.14	0.68	0.54	1.36	0.76	1.17	1.25	9.61	2.45	2.01	0.38
CH62-15-mz1-6	2.54	0.25	1.18	2.43	0.61	0.53	1.19	0.72	1.21	1.57	12.28	7.35	2.41	0.76
CH62-15-mz1-7	3.13	0.25	1.44	3.17	0.61	0.52	1.17	0.71	1.28	1.89	20.20	8.87	2.28	0.95
CH62-15-mz1-8	2.71	0.25	1.15	2.62	0.61	0.52	1.18	0.72	1.24	1.68	15.21	6.82	2.11	0.77
CH62-15-mz1-9	3.36	0.25	1.96	5.51	0.60	0.52	1.14	0.70	1.29	2.30	38.16	12.77	2.20	1.41
CH62-15-mz1-10	3.14	0.25	1.53	5.60	0.60	0.52	1.16	0.71	1.31	2.29	29.25	9.19	1.83	1.12
CH62-15-mz1-11	3.11	0.25	1.96	5.34	0.60	0.52	1.14	0.70	1.30	2.19	49.00	10.40	2.20	1.57
CH62-15-mz1-12	3.33	0.25	1.63	4.38	0.60	0.52	1.14	0.71	1.33	2.13	24.45	11.78	2.09	1.12
CH62-15-mz2-1	1.33	0.25	0.74	1.25	0.65	0.54	1.28	0.75	1.18	1.24	7.73	3.42	2.11	0.46
CH62-15-mz2-2	1.17	0.25	0.70	1.11	0.65	0.54	1.29	0.75	1.16	1.20	7.42	3.29	2.06	0.43
CH62-15-mz2-3	1.57	0.25	0.76	0.93	0.66	0.54	1.28	0.74	1.10	1.14	6.65	3.68	2.33	0.48
CH62-15-mz2-4	0.92	0.25	0.57	0.88	0.69	0.55	1.37	0.76	1.14	1.17	7.45	2.21	1.92	0.36
CH62-15-mz2-5	1.32	0.25	0.69	0.83	0.67	0.54	1.28	0.75	1.10	1.09	5.89	3.04	1.95	0.44
CH62-15-mz2-6	3.01	0.25	1.90	4.82	0.60	0.52	1.14	0.70	1.27	2.28	20.06	11.59	1.93	1.45
CH62-15-mz2-7	3.27	0.25	1.60	4.21	0.60	0.52	1.14	0.72	1.32	2.13	20.10	9.66	2.23	1.15
CH62-15-mz2-8	3.06	0.25	1.91	4.50	0.60	0.52	1.14	0.70	1.28	2.26	20.57	14.12	2.22	1.50
CH62-15-mz2-9	3.66	0.25	1.58	3.85	0.60	0.52	1.15	0.71	1.29	2.01	33.43	10.15	2.12	1.11
CH62-15-mz2-10	3.81	0.25	1.42	3.54	0.60	0.52	1.16	0.71	1.30	1.89	14.36	9.44	1.97	0.96
CH62-15-mz2-11	3.61	0.25	1.61	3.71	0.60	0.52	1.14	0.71	1.29	1.97	24.84	11.46	2.19	1.15
CH62-15-mz2-12	3.52	0.25	1.51	3.02	0.61	0.52	1.14	0.70	1.22	1.76	15.06	8.92	2.26	1.00
CH62-15-mz2-13	1.53	0.25	0.75	0.93	0.65	0.54	1.26	0.74	1.09	1.12	6.60	3.50	2.31	0.47
CH62-15-mz3-1	2.44	0.25	1.07	1.76	0.62	0.53	1.19	0.71	1.16	1.34	8.94	5.99	2.55	0.70
CH62-15-mz3-2	3.13	0.25	1.37	2.73	0.61	0.53	1.16	0.71	1.21	1.65	17.94	7.50	2.62	0.92
CH62-15-mz3-3	1.88	0.25	0.86	1.15	0.65	0.54	1.23	0.71	1.09	1.13	6.85	4.52	2.40	0.54
CH62-15-mz3-4	2.64	0.25	1.07	1.88	0.63	0.53	1.18	0.71	1.11	1.33	10.48	6.20	2.66	0.70
CH62-15-mz3-5	2.31	0.25	1.00	1.54	0.63	0.53	1.23	0.71	1.11	1.26	8.56	6.01	2.48	0.64
CH62-15-mz3-6	3.80	0.25	1.70	3.82	0.61	0.52	1.14	0.69	1.23	1.98	20.01	12.64	2.36	1.19
CH62-15-mz3-7	2.92	0.25	1.29	2.57	0.61	0.52	1.15	0.70	1.20	1.57	14.70	8.36	2.54	0.85

CH62-15-mz4-1	0.90	0.25	0.62	0.95	0.68	0.54	1.31	0.74	1.11	1.13	7.06	2.51	2.12	0.39
CH62-15-mz4-2	0.91	0.25	0.62	0.89	0.68	0.54	1.34	0.75	1.08	1.08	6.12	2.58	2.04	0.39
CH62-15-mz4-3	1.46	0.25	0.74	0.83	0.67	0.54	1.24	0.73	1.04	1.02	5.99	3.53	2.46	0.48
CH62-15-mz4-4	1.29	0.25	0.72	0.90	0.66	0.54	1.29	0.74	1.09	1.10	5.82	3.43	2.28	0.44
CH62-15-mz4-5	1.18	0.25	0.70	0.94	0.66	0.54	1.28	0.74	1.08	1.09	6.44	3.18	2.19	0.44
CH62-15-mz4-6	3.11	0.25	1.45	2.94	0.61	0.52	1.14	0.71	1.20	1.65	14.72	9.99	2.31	0.97
CH62-15-mz4-7	2.66	0.25	1.19	2.18	0.61	0.52	1.17	0.71	1.20	1.52	10.10	7.14	2.43	0.75
CH62-15-mz4-8	3.09	0.25	1.67	3.86	0.60	0.52	1.15	0.70	1.23	1.92	22.95	12.23	2.13	1.23
CH62-15-mz4-9	3.05	0.25	1.65	4.29	0.61	0.52	1.14	0.70	1.27	1.92	28.08	11.14	1.97	1.25
CH62-15-mz4-10	2.82	0.25	1.65	4.41	0.60	0.52	1.15	0.71	1.25	2.05	23.05	10.43	2.08	1.17

Appendix D. Compositional data, k-ratio errors, calculated dates and Monte Carlo CIs for analyses in Chapter 3

Sample	SiO2	P2O5	CaO	Y2O3	La2O3	Ce2O3	Pr2O3	Nd2O3	Sm2O3	Gd2O3	Dy2O3	PbO	ThO2	UO2	Total	Date (Ma)	95% CI
Concentrations																	
CA5.0E-mz1-1	0.1215	30.65	0.5723	1.0736	15.32	30.6	3.61	13.87	2.25	1.67	0.4344	0.0574	2.23	0.6066	103.0883	323.589	36.8978
CA5.0E-mz1-2	0.1444	30.6	0.648	0.9943	15.69	30.18	3.6	13.77	2.28	1.65	0.3808	0.0655	2.45	0.7879	103.2694	310.282	31.6282
CA5.0E-mz1-3	0.1464	30.7	0.6308	1.1714	14.98	29.97	3.67	13.81	2.29	1.65	0.4331	0.0478	2.52	0.6149	102.6643	251.42	33.6868
CA5.0E-mz1-4	0.1456	30.57	0.6607	1.2052	15.21	30.17	3.63	13.77	2.23	1.72	0.4056	0.0622	2.71	0.6331	103.1546	309.066	32.2009
CA5.0E-mz1-5	0.1435	30.73	0.6623	2.01	14.86	29.44	3.61	13.71	2.3	1.8	0.6653	0.0589	2.76	0.5486	103.3324	307.291	30.9871
CA5.0E-mz1-6	0.153	30.81	0.7231	2.15	14.56	29.12	3.59	13.43	2.29	1.89	0.6762	0.0635	2.97	0.5591	103.0195	314.188	29.1105
CA5.0E-mz1-7	0.1735	30.75	0.6957	1.55	14.74	29.49	3.58	13.74	2.34	1.77	0.5165	0.0689	2.93	0.5751	102.9502	339.812	30.8867
CA5.0E-mz1-8	0.1667	30.82	0.7631	1.99	14.69	29.51	3.57	13.39	2.3	1.84	0.6734	0.0674	3	0.5308	103.3454	337.737	29.9158
CA5.0E-mz1-9	0.1566	30.67	0.7288	1.59	14.92	29.77	3.63	13.56	2.28	1.81	0.547	0.0662	3.08	0.6053	103.4459	311.007	29.2641
CA5.0E-mz2-1	0.1702	30.88	0.7666	2.11	14.17	28.78	3.5	13.24	2.29	1.97	0.8046	0.0754	3.29	0.5779	102.6702	344.863	27.432
CA5.0E-mz2-2	0.2068	30.81	0.9076	2.22	14.18	28.11	3.4	12.99	2.2	1.97	0.7124	0.0845	4.07	0.6224	102.5294	328.419	23.464
CA5.0E-mz2-3	0.1826	30.79	0.8644	2.31	14.03	28.12	3.37	13.05	2.2	2.01	0.7394	0.0859	3.78	0.6681	102.2455	341.329	24.088
CA5.0E-mz2-4	0.1356	30.75	0.6743	1.98	14.4	28.79	3.47	13.31	2.35	2.03	0.7238	0.0646	2.71	0.5481	101.9732	340.152	31.3928
CA5.0E-mz2-5	0.1307	30.84	0.686	1.9	14.33	28.61	3.43	13.46	2.35	2.02	0.7755	0.0668	2.79	0.5702	101.9911	340.478	30.5241
CA5.0E-mz2-6	0.1704	30.85	0.7138	2.1	14.41	28.57	3.49	13.24	2.34	2.02	0.7625	0.065	2.9	0.5931	102.2588	318.921	28.9673
CA5.0E-mz2-7	0.2059	30.77	0.7665	2.15	14.26	28.38	3.38	13.04	2.25	1.94	0.7772	0.074	3.43	0.6094	102.0709	323.851	26.3199
CA5.170E-mz1-1	1.9994	30.29	0.8816	0.5365	14.57	28.73	3.37	13.08	2.13	1.32	0.2094	0.0859	3.69	0.6763	101.603	345.26	27.5559
CA5.170E-mz1-2	1.2915	30.12	0.8901	0.5966	14.79	29.28	3.43	13.29	2.17	1.32	0.2107	0.0813	3.77	0.6315	101.9142	330.444	27.7223
CA5.170E-mz1-3	1.7395	29.87	0.858	0.6711	14.48	28.93	3.42	13.22	2.2	1.3	0.2279	0.0656	3.53	0.5687	101.1101	289.376	29.8198
CA5.170E-mz1-4	1.5522	29.92	0.8247	0.7399	14.8	29.32	3.37	13.11	2.17	1.4	0.2343	0.0767	3.36	0.5962	101.5042	342.522	29.8332
CA5.170E-mz2-1	0.1459	30.56	0.6096	2.15	14.56	29.42	3.59	13.29	2.24	1.86	0.7238	0.0693	2.63	0.6061	102.4999	356.048	30.222
CA5.170E-mz2-2	0.1508	30.41	0.616	2.18	14.73	29.35	3.55	13.21	2.23	1.86	0.6919	0.0572	2.67	0.6129	102.3567	291.116	29.6965
CA5.170E-mz2-3	0.1542	30.59	0.594	2.05	14.96	29.73	3.46	13.39	2.19	1.78	0.6583	0.0597	2.57	0.5548	102.7781	323.356	31.9136
CA5.170E-mz2-4	0.1512	30.41	0.5954	2.06	14.7	29.6	3.53	13.39	2.25	1.8	0.647	0.0509	2.6	0.5465	102.3669	276.159	31.1944
CA5.170E-mz2-5	0.1586	30.59	0.6316	2.09	14.71	29.29	3.48	13.23	2.18	1.85	0.6923	0.0632	2.8	0.5898	102.3933	317.41	29.8732
CA5.170E-mz2-6	0.1619	30.33	0.6334	2.08	14.83	29.44	3.4	13.29	2.2	1.86	0.6961	0.0584	2.8	0.5747	102.3891	296.739	29.758
CA5.170E-mz2-7	0.1668	30.52	0.6385	2.04	14.48	29.36	3.48	13.17	2.2	1.82	0.7068	0.0711	2.86	0.5396	102.093	363.984	30.3714

CA5.170E-mz2-8	0.1763	30.49	0.6426	2.08	14.6	29.17	3.51	13.37	2.27	1.87	0.7462	0.0593	2.9	0.6038	102.5218	289.293	28.8022
CA5.170E-mz2-9	0.1526	30.09	0.6243	2.11	14.54	29.03	3.51	13.41	2.23	1.85	0.7339	0.0593	2.9	0.5849	101.8589	292.948	28.7673
CA14.0a-mz2-1	0.1721	30.53	0.4817	1.81	14.86	29.7	3.4	12.85	2.06	1.47	0.6466	0.0671	2.64	0.5011	101.2243	371.517	33.8989
CA14.0a-mz2-2	0.1925	30.6	0.4976	1.86	14.85	30.06	3.52	13.14	2.06	1.48	0.6537	0.0503	2.7	0.527	102.2226	270.491	32.5091
CA14.0a-mz2-3	0.176	30.78	0.5199	1.99	14.56	30.17	3.45	13.28	2.09	1.51	0.6947	0.0538	2.83	0.5571	102.6946	275.225	30.6436
CA14.0a-mz2-4	0.2006	30.6	0.596	1.94	14.18	29.56	3.44	12.96	2.09	1.54	0.6758	0.0728	3.37	0.6714	101.9381	310.773	26.9592
CA14.0a-mz2-5	0.1677	30.79	0.5503	2.05	14.5	29.98	3.56	13.21	2.13	1.56	0.6581	0.0682	3.01	0.6186	102.8877	321.839	29.215
CA14.0a-mz2-6	0.1842	30.41	0.5283	2.05	14.35	29.55	3.44	13.22	2.07	1.55	0.678	0.0643	3.05	0.6005	101.7813	304.981	29.1668
CA14.0a-mz2-7	0.1754	30.5	0.5162	1.97	14.48	29.98	3.61	13.32	2.15	1.55	0.7276	0.0622	2.87	0.5308	102.4754	320.755	31.4815
CA14.0a-mz3-7	0.3058	30.38	0.6367	1.76	13.85	28.31	3.37	12.61	2.01	1.43	0.6555	0.0785	3.87	0.505	99.8106	336.953	27.1681
CA14.0a-mz3-2	0.2689	30.47	0.5923	1.78	13.86	28.48	3.39	13.17	2.08	1.5	0.6688	0.0666	3.6	0.4787	100.4464	306.053	28.8086
CA14.0a-mz3-3	0.3019	30.52	0.6489	1.1961	14.34	28.99	3.37	12.34	1.8	1.18	0.4394	0.0862	4.21	0.549	100.0159	340.229	26.3022
CA14.0a-mz3-4	0.307	30.64	0.6597	1.71	13.77	28.33	3.33	12.51	1.95	1.41	0.5666	0.079	4.17	0.5397	100.0129	315.777	25.6984
CA14.0a-mz3-5	0.2514	30.39	0.6174	1.57	14.46	28.9	3.3	12.56	1.94	1.33	0.5849	0.0607	3.79	0.5387	100.3393	260.172	27.2602
CA17a-150A-mz1-1	0.2355	30.37	0.9616	1.0812	13.24	27.73	3.18	11.98	2.13	2.02	0.5332	0.0914	5.04	0.4643	99.0991	330.224	23.8245
CA17a-150A-mz1-2	0.3013	30.41	1.1389	1.2487	12.81	27.09	3.15	11.92	2.24	2.27	0.6008	0.1056	5.89	0.5215	99.7455	329.22	20.5927
CA17a-150A-mz1-3	0.3782	30.35	1.1738	1.1636	12.6	26.78	3.14	11.83	2.17	2.17	0.5945	0.1086	6.34	0.5448	99.3948	316.955	19.3939
CA17a-150A-mz1-4	0.3972	30.23	1.2074	1.2078	12.25	26.42	3.15	11.9	2.28	2.32	0.6347	0.1185	6.6	0.553	99.3221	333.712	18.6342
CA17a-150A-mz1-5	0.4482	30.29	1.2909	1.32	12.06	26.3	3.07	11.88	2.26	2.41	0.7195	0.1261	7.22	0.5715	100.0246	328.415	17.4137
CA17a-150A-mz1-6	0.4339	30.26	1.3048	1.4	12.06	25.97	3.01	11.73	2.2	2.32	0.6183	0.1156	7.19	0.5321	99.2036	306.783	17.4944
CA17a-150A-mz1-7	0.3811	30.28	1.1373	1.1947	12.36	26.87	3.11	12.08	2.32	2.31	0.6226	0.1054	6.15	0.5115	99.4827	319.12	20.0012
CA17a-150A-mz1-8	0.4589	30.02	1.2821	1.33	12.13	25.95	3.1	11.69	2.23	2.32	0.6029	0.121	7.14	0.5341	98.9672	322.573	17.5208
CA17a-150A-mz2-1	0.1681	30.13	0.7207	1.47	12.82	27.9	3.32	12.74	2.27	2.06	0.6748	0.063	3.54	0.4248	98.3349	303.073	30.531
CA17a-150A-mz2-2	0.248	30.39	0.9486	1.58	12.52	27.13	3.24	12.39	2.33	2.46	0.7194	0.0893	4.83	0.4498	99.3683	335.552	24.1753
CA17a-150A-mz2-3	0.265	30.43	0.9597	1.63	12.69	27.2	3.26	12.37	2.26	2.4	0.6854	0.0852	4.88	0.4541	99.6135	317.329	24.0159
CA17a-150A-	0.2904	30.4	0.9864	1.65	12.52	27.11	3.23	12.44	2.27	2.38	0.7007	0.0907	5.15	0.4694	99.7336	321.374	23.1971

mz2-4																	
CA17a-150A-mz2-5	0.3131	30.42	1.0151	1.65	12.4	27	3.16	12.19	2.28	2.51	0.7379	0.0847	5.23	0.5021	99.5394	292.348	22.4519
CA17a-150A-mz2-6	0.3413	30.37	1.116	1.71	12.45	26.7	3.23	12.13	2.3	2.47	0.6917	0.1074	5.83	0.5086	100.0061	339.305	20.58
CA17a-150A-mz2-7	0.2995	30.41	1.0702	1.64	12.48	26.71	3.18	11.82	2.21	2.33	0.6987	0.0886	5.5	0.4826	98.9679	296.936	21.7123
CA17a-150A-mz2-8	0.2725	30.53	0.9246	1.67	12.24	27.24	3.2	12.41	2.33	2.43	0.7777	0.0805	4.48	0.498	99.1247	312.408	25.1172
CA17a-150A-mz3-1	0.2002	30.64	0.7904	1.004	13.3	28.47	3.21	12.4	2.2	1.71	0.4694	0.0714	3.77	0.4702	98.738	318.856	29.9033
CA17a-150A-mz3-2	0.2183	30.58	0.893	1.151	12.82	28.01	3.38	12.34	2.27	1.94	0.5455	0.0825	4.47	0.4828	99.2213	323.125	26.1474
CA17a-150A-mz3-3	0.2458	30.59	0.9751	1.2166	12.74	27.5	3.25	12.36	2.29	2.1	0.5797	0.0765	4.9	0.5045	99.3698	277.434	24.09
CA17a-150A-mz3-4	0.2695	30.49	1.0266	1.28	12.41	27.13	3.23	12.22	2.28	2.21	0.6506	0.0922	5.18	0.5302	99.0431	316.209	22.8067
CA17a-150A-mz3-5	0.2116	30.65	0.8651	1.1348	12.77	27.85	3.33	12.42	2.25	1.92	0.5418	0.0763	4.18	0.4971	98.7327	311.674	27.1714
CA17a-150A-mz3-6	0.1659	30.75	0.8004	0.8675	13.67	28.98	3.33	12.38	2.18	1.64	0.4522	0.061	3.63	0.4998	99.4374	275.357	30.5617
CA17a-150-mz4-1	0.3733	30.77	1.1038	1.0396	12.8	27.59	3.23	12.51	2.26	2.24	0.4885	0.0846	5.62	0.462	100.6172	281.328	21.9744
CA17a-150-mz4-2	0.3625	30.28	1.1501	1.0099	12.71	27.47	3.23	12.54	2.22	2.2	0.4963	0.0947	6.07	0.4764	100.3584	294.23	20.7564
CA17a-150-mz4-3	0.2633	30.58	0.9385	1.0155	14.46	27.98	3.11	12.29	1.99	1.98	0.4235	0.0749	4.87	0.4315	100.4473	282.988	25.0863
CA17a-150-mz4-4	0.2392	30.62	0.9765	0.9816	12.97	28.09	3.23	12.59	2.36	2.28	0.4412	0.0836	4.66	0.4425	100.003	324.304	25.8463
CA17a-150-mz4-5	0.2185	30.87	0.8943	0.9176	12.69	28.17	3.43	13.29	2.46	2.19	0.5055	0.0867	4.41	0.4595	100.6283	347.243	26.7337
CA17a-150-mz4-6	0.2774	30.44	1.077	0.9026	12.45	27.51	3.3	12.96	2.39	2.33	0.502	0.0885	5.3	0.4861	100.0559	304.565	23.1269
CA17a-150-mz4-7	0.1563	31.01	0.787	0.6421	13.56	29.17	3.46	13.22	2.25	1.7	0.286	0.0641	3.59	0.45	100.3743	300.376	31.6332
CA17a-150-mz4-8	0.264	30.98	1.0274	1.0133	13.04	27.65	3.22	12.35	2.24	2.3	0.4834	0.0853	4.85	0.4412	99.9846	321.148	24.9698
CA17a-150-mz4-9	0.2716	30.66	1.0544	0.9788	12.59	27.66	3.29	12.82	2.46	2.47	0.5499	0.0859	5.02	0.4898	100.4412	307.734	24.2136
CA17a-150-mz4-10	0.2547	31.18	0.9846	1.0839	13.72	27.99	3.22	12.61	2.09	2.1	0.4694	0.0861	4.74	0.4757	101.0439	323.992	25.2049
CA30.0B-mz2-1	0.2013	29.98	0.7558	0.3405	14.93	30.04	3.46	13.32	2.25	1.38	0.1353	0.069	2.74	0.9309	100.5562	284.464	29.909
CA30.0B-mz2-2	0.2007	30.31	0.858	0.8432	14.68	29.15	3.35	13.26	2.26	1.6	0.3034	0.0826	2.8	1.014	100.737	321.197	26.9945

CA30.0B-mz2-3	0.1967	30.28	0.865	0.2904	15.13	29.75	3.48	13.21	2.25	1.35	0.1725	0.0775	2.75	1.0006	100.8277	306.499	28.6705
CA30.0B-mz2-4	0.224	30.34	0.8381	0.7503	14.79	29.27	3.4	13.09	2.29	1.57	0.3194	0.0742	2.72	0.9725	100.6835	299.739	28.1723
CA30.0B-mz2-5	0.2057	30.26	0.7154	0.6154	15.01	29.92	3.45	13.1	2.19	1.46	0.2825	0.0752	2.5	0.8201	100.6291	344.389	31.7036
CA30.0B-mz2-6	0.2067	30.34	0.7267	0.7986	14.95	29.9	3.45	13.21	2.19	1.53	0.2972	0.0645	2.53	0.8159	101.0377	295.625	31.2672
CA30.0E-mz1-1	1.5825	30.53	0.7826	0.8854	14.19	28.72	3.42	12.97	2.24	1.71	0.437	0.0645	3.08	0.4198	101.0635	343.021	34.3093
CA30.0E-mz1-2	0.2151	30.55	0.7254	0.8885	14.78	29.99	3.47	13.42	2.28	1.73	0.4308	0.0582	3.01	0.4039	101.9831	318.702	35.5945
CA30.0E-mz1-3	0.2178	30.76	0.7051	0.8864	14.86	30.11	3.52	13.5	2.28	1.77	0.4019	0.0554	2.94	0.4046	102.4376	308.583	36.1078
CA30.0E-mz1-4	0.4185	30.41	0.7441	0.8899	14.71	29.77	3.55	13.49	2.26	1.69	0.3785	0.0567	3.08	0.4222	101.9028	301.88	34.5103
CA30.0G-mz1-1	1.7194	30.5	0.8038	1.1384	14.2	28.82	3.36	12.96	2.25	1.75	0.4564	0.0632	3.24	0.4506	101.7461	318.157	32.0905
CA30.0G-mz1-2	0.2091	30.45	0.7546	1.0555	14.61	29.91	3.52	13.22	2.28	1.68	0.4513	0.0649	3.29	0.4309	101.9564	327.603	32.3309
CA30.0G-mz1-3	0.1824	30.52	0.763	1.1267	14.49	29.95	3.55	13.59	2.29	1.78	0.4507	0.0655	3.27	0.4592	102.5202	325.659	31.8937
CA30.0G-mz1-4	0.197	30.38	0.7826	1.0882	14.68	29.9	3.48	13.49	2.31	1.74	0.4522	0.0661	3.44	0.4458	102.4902	320.212	31.1861
CA30.0G-mz1-5	0.2031	30.12	0.784	1.0777	14.17	29.48	3.51	13.35	2.24	1.78	0.4609	0.065	3.39	0.427	101.0904	321.948	31.6089
CA30.0G-mz2-1	0.174	30.86	0.6931	2.14	13.99	29.01	3.43	13.26	2.34	1.94	0.6633	0.0585	2.93	0.4512	101.9813	315.183	31.1238
CA30.0G-mz2-2	0.158	31	0.6461	2.06	14.26	29.2	3.49	13.52	2.32	1.96	0.7201	0.0533	2.62	0.4245	102.47	315.563	34.0058
CA30.0G-mz2-3	0.1288	30.9	0.532	1.93	14.44	29.8	3.51	13.64	2.41	1.94	0.7409	0.0468	2.23	0.3723	102.655	322.252	38.2638
CA30.0G-mz2-4	0.1578	30.92	0.5647	1.98	14.27	29.39	3.54	13.53	2.39	2	0.7153	0.0536	2.34	0.4267	102.3148	340.524	36.5591
CA30.0G-mz2-5	0.1368	30.78	0.533	1.79	14.52	29.71	3.45	13.63	2.37	1.99	0.5756	0.0643	2.12	0.5566	102.2526	386.54	35.681
CA30.0G-mz2-6	0.1419	30.77	0.5865	1.95	14.35	29.49	3.62	13.41	2.37	2	0.6465	0.0574	2.34	0.544	102.3052	331.056	33.6682
CA30.0G-mz2-7	0.1632	31	0.6567	2.15	14.13	29.33	3.5	13.33	2.3	1.98	0.7396	0.0612	2.85	0.4637	102.6944	332.323	31.6211
CA30.0E-mz2-1	0.185	30.68	0.7489	2.03	14.5	29.23	3.42	12.89	2.14	1.75	0.6691	0.076	3.05	0.6055	102.009	358.092	28.5217
CA30.0E-mz2-2	0.1921	30.64	0.6865	2.02	14.31	29.2	3.49	13.29	2.22	1.85	0.677	0.0621	2.91	0.5245	102.1177	318.835	30.2167
CA30.0E-mz2-3	0.1831	30.75	0.6613	1.89	14.95	29.78	3.41	12.74	2.05	1.68	0.639	0.0587	2.78	0.5152	102.1189	312.393	31.7856
CA30.0E-mz2-4	0.1927	30.81	0.7199	1.96	14.66	29.66	3.43	12.64	2.13	1.74	0.6399	0.07	2.98	0.5933	102.2761	337.641	29.3432
CA30.0E-mz2-5	0.2024	30.7	0.7223	2.11	14.22	29.06	3.45	12.9	2.21	1.89	0.6754	0.0626	3.07	0.5501	101.8639	305.36	28.7188

Sample	**Si**	**P**	**Ca**	**Y**	**La**	**Ce**	**Pr**	**Nd**	**Sm**	**Gd**	**Dy**	**Pb**	**Th**	**U**
k-ratio errors (1σ %)														
CA5.0E-mz1-1	4.26	0.24	1.09	0.56	0.61	0.43	1.20	0.71	1.24	1.77	7.47	7.00	0.77	1.43
CA5.0E-mz1-2	3.61	0.24	0.99	0.59	0.61	0.43	1.19	0.71	1.22	1.79	8.55	6.23	0.73	1.13
CA5.0E-mz1-3	3.57	0.24	1.01	0.52	0.61	0.43	1.17	0.71	1.22	1.80	7.53	7.94	0.71	1.4

CA5.0E-mz1-4	3.58	0.24	0.98	0.51	0.61	0.43	1.19	0.71	1.24	1.72	8.06	6.38	0.68	1.37
CA5.0E-mz1-5	3.66	0.24	0.98	0.37	0.61	0.43	1.19	0.71	1.21	1.65	4.95	6.24	0.68	1.54
CA5.0E-mz1-6	3.43	0.24	0.92	0.35	0.62	0.43	1.19	0.72	1.21	1.58	4.88	5.78	0.65	1.52
CA5.0E-mz1-7	3.04	0.24	0.95	0.43	0.61	0.43	1.20	0.71	1.19	1.67	6.36	5.69	0.65	1.48
CA5.0E-mz1-8	3.17	0.24	0.89	0.37	0.62	0.43	1.19	0.72	1.21	1.62	4.91	5.58	0.65	1.59
CA5.0E-mz1-9	3.37	0.24	0.92	0.42	0.61	0.43	1.18	0.71	1.22	1.64	6.00	5.81	0.64	1.41
CA5.0E-mz2-1	3.06	0.24	0.89	0.35	0.63	0.43	1.21	0.72	1.21	1.53	4.12	5.05	0.62	1.47
CA5.0E-mz2-2	2.60	0.24	0.80	0.34	0.63	0.44	1.23	0.73	1.25	1.54	4.66	4.52	0.55	1.37
CA5.0E-mz2-3	2.90	0.24	0.83	0.33	0.63	0.44	1.25	0.73	1.25	1.50	4.49	4.49	0.57	1.29
CA5.0E-mz2-4	3.79	0.24	0.97	0.37	0.62	0.43	1.22	0.72	1.19	1.49	4.57	5.81	0.68	1.54
CA5.0E-mz2-5	3.93	0.24	0.96	0.38	0.62	0.44	1.23	0.71	1.19	1.50	4.27	5.65	0.67	1.49
CA5.0E-mz2-6	3.05	0.24	0.93	0.35	0.62	0.44	1.21	0.72	1.19	1.50	4.34	5.68	0.66	1.44
CA5.0E-mz2-7	2.61	0.24	0.89	0.35	0.62	0.44	1.24	0.73	1.22	1.55	4.25	5.10	0.60	1.4
CA5.170E-mz1-1	0.49	0.24	0.82	0.97	0.62	0.44	1.24	0.73	1.28	2.16	15.44	4.98	0.58	1.28
CA5.170E-mz1-2	0.64	0.24	0.81	0.89	0.61	0.43	1.23	0.72	1.27	2.17	15.27	5.19	0.57	1.35
CA5.170E-mz1-3	0.53	0.24	0.83	0.80	0.62	0.43	1.23	0.72	1.24	2.19	14.07	6.22	0.59	1.48
CA5.170E-mz1-4	0.57	0.24	0.85	0.74	0.61	0.43	1.25	0.73	1.27	2.05	13.75	5.42	0.61	1.42
CA5.170E-mz2-1	3.54	0.24	1.04	0.35	0.62	0.43	1.19	0.72	1.23	1.59	4.55	5.42	0.70	1.42
CA5.170E-mz2-2	3.45	0.24	1.03	0.35	0.61	0.43	1.19	0.72	1.24	1.60	4.77	6.28	0.69	1.41
CA5.170E-mz2-3	3.38	0.24	1.05	0.36	0.61	0.43	1.22	0.72	1.26	1.66	5.01	6.16	0.70	1.53
CA5.170E-mz2-4	3.41	0.24	1.05	0.36	0.61	0.43	1.20	0.72	1.23	1.65	5.09	6.89	0.70	1.56
CA5.170E-mz2-5	3.27	0.24	1.01	0.36	0.61	0.43	1.21	0.72	1.27	1.61	4.76	5.87	0.67	1.46
CA5.170E-mz2-6	3.21	0.24	1.01	0.36	0.61	0.43	1.24	0.72	1.25	1.60	4.74	6.19	0.67	1.49
CA5.170E-mz2-7	3.12	0.24	1.00	0.36	0.62	0.43	1.22	0.72	1.25	1.63	4.66	5.34	0.66	1.57
CA5.170E-mz2-8	2.96	0.24	1.00	0.36	0.62	0.43	1.21	0.72	1.22	1.59	4.42	6.12	0.66	1.42
CA5.170E-mz2-9	3.38	0.24	1.01	0.35	0.61	0.43	1.19	0.71	1.23	1.59	4.45	6.05	0.65	1.45
CA14.0a-mz2-1	3.17	0.24	1.25	0.40	0.63	0.44	1.28	0.76	1.36	2.04	5.25	5.83	0.71	1.71
CA14.0a-mz2-2	2.85	0.24	1.23	0.39	0.63	0.44	1.25	0.75	1.37	2.03	5.22	7.27	0.70	1.63
CA14.0a-mz2-3	3.08	0.24	1.18	0.38	0.64	0.44	1.27	0.74	1.35	2.00	4.93	6.77	0.68	1.54
CA14.0a-mz2-4	2.72	0.24	1.09	0.38	0.64	0.44	1.27	0.75	1.35	1.96	5.02	5.38	0.61	1.31
CA14.0a-mz2-5	3.21	0.24	1.14	0.37	0.64	0.44	1.23	0.75	1.33	1.94	5.19	5.66	0.65	1.41
CA14.0a-mz2-6	2.91	0.24	1.17	0.37	0.64	0.44	1.27	0.74	1.36	1.94	5.01	5.91	0.65	1.44

CA14.0a-mz2-7	3.09	0.24	1.18	0.38	0.64	0.44	1.22	0.74	1.32	1.95	4.68	6.11	0.67	1.62
CA14.0a-mz3-7	1.91	0.24	1.04	0.41	0.65	0.45	1.27	0.76	1.38	2.07	5.17	5.06	0.57	1.65
CA14.0a-mz3-2	2.12	0.24	1.09	0.40	0.65	0.45	1.27	0.74	1.34	1.99	5.08	5.80	0.59	1.73
CA14.0a-mz3-3	1.95	0.24	1.02	0.54	0.64	0.44	1.27	0.76	1.50	2.45	7.56	4.84	0.55	1.53
CA14.0a-mz3-4	1.92	0.24	1.01	0.42	0.65	0.45	1.28	0.76	1.41	2.09	5.90	5.05	0.55	1.55
CA14.0a-mz3-5	2.24	0.24	1.06	0.44	0.64	0.44	1.30	0.76	1.42	2.21	5.75	6.29	0.58	1.56
CA17a-150A-mz1-1	2.33	0.24	0.79	0.57	0.64	0.43	1.30	0.76	1.29	1.49	6.18	4.53	0.52	1.76
CA17a-150A-mz1-2	1.90	0.24	0.71	0.51	0.65	0.44	1.30	0.76	1.24	1.36	5.49	3.97	0.49	1.59
CA17a-150A-mz1-3	1.57	0.24	0.70	0.54	0.66	0.44	1.30	0.76	1.28	1.42	5.53	3.87	0.48	1.52
CA17a-150A-mz1-4	1.52	0.24	0.69	0.52	0.67	0.44	1.30	0.76	1.23	1.34	5.24	3.58	0.47	1.50
CA17a-150A-mz1-5	1.39	0.24	0.66	0.49	0.67	0.44	1.32	0.76	1.24	1.30	4.62	3.40	0.45	1.45
CA17a-150A-mz1-6	1.41	0.24	0.66	0.47	0.67	0.45	1.35	0.77	1.26	1.34	5.34	3.61	0.45	1.54
CA17a-150A-mz1-7	1.58	0.24	0.71	0.53	0.67	0.44	1.31	0.75	1.21	1.34	5.32	3.96	0.48	1.61
CA17a-150A-mz1-8	1.35	0.24	0.66	0.48	0.67	0.44	1.31	0.76	1.23	1.33	5.45	3.47	0.45	1.52
CA17a-150A-mz2-1	3.16	0.24	0.96	0.46	0.66	0.43	1.26	0.74	1.24	1.48	4.94	6.19	0.62	1.94
CA17a-150A-mz2-2	2.28	0.24	0.80	0.44	0.67	0.44	1.28	0.75	1.22	1.29	4.69	4.56	0.54	1.84
CA17a-150A-mz2-3	2.14	0.24	0.80	0.43	0.66	0.44	1.28	0.76	1.25	1.32	4.94	4.74	0.54	1.82
CA17a-150A-mz2-4	1.98	0.24	0.79	0.43	0.67	0.44	1.29	0.75	1.25	1.33	4.84	4.53	0.52	1.77
CA17a-150A-mz2-5	1.86	0.24	0.77	0.42	0.67	0.44	1.31	0.76	1.24	1.27	4.59	4.75	0.52	1.66
CA17a-150A-mz2-6	1.73	0.24	0.73	0.41	0.67	0.44	1.29	0.76	1.24	1.29	4.93	3.89	0.49	1.65
CA17a-150A-mz2-7	1.93	0.24	0.75	0.42	0.67	0.45	1.30	0.77	1.28	1.36	4.86	4.55	0.51	1.73
CA17a-150A-mz2-8	2.08	0.24	0.82	0.42	0.68	0.44	1.30	0.75	1.22	1.31	4.38	5.01	0.55	1.70
CA17a-150A-mz3-1	2.71	0.24	0.90	0.60	0.65	0.43	1.31	0.75	1.27	1.75	7.08	5.79	0.60	1.79
CA17a-150A-mz3-2	2.53	0.24	0.84	0.55	0.66	0.44	1.24	0.76	1.24	1.56	6.14	5.04	0.55	1.73
CA17a-150A-mz3-3	2.27	0.24	0.79	0.53	0.66	0.44	1.29	0.75	1.24	1.48	5.81	5.29	0.53	1.67
CA17a-150A-mz3-4	2.10	0.24	0.77	0.51	0.67	0.44	1.29	0.76	1.24	1.41	5.16	4.51	0.52	1.59
CA17a-150A-mz3-5	2.58	0.24	0.85	0.56	0.66	0.44	1.26	0.75	1.26	1.57	6.15	5.39	0.57	1.70
CA17a-150A-mz3-6	3.21	0.24	0.89	0.68	0.64	0.43	1.27	0.75	1.28	1.80	7.32	6.68	0.62	1.70
CA17a-150-mz4-1	1.63	0.24	0.73	0.59	0.66	0.44	1.29	0.74	1.24	1.38	6.76	4.79	0.50	1.76
CA17a-150-mz4-2	1.66	0.24	0.71	0.60	0.66	0.44	1.28	0.74	1.26	1.41	6.66	4.37	0.49	1.72
CA17a-150-mz4-3	2.17	0.24	0.81	0.60	0.63	0.43	1.31	0.75	1.38	1.52	7.81	5.40	0.53	1.89
CA17a-150-mz4-4	2.35	0.24	0.78	0.61	0.65	0.43	1.29	0.74	1.20	1.37	7.54	4.97	0.55	1.86

CA17a-150-mz4-5	2.55	0.24	0.83	0.65	0.66	0.43	1.23	0.72	1.16	1.42	6.57	4.85	0.55	1.80
CA17a-150-mz4-6	2.06	0.24	0.74	0.66	0.67	0.44	1.27	0.73	1.19	1.35	6.65	4.70	0.51	1.70
CA17a-150-mz4-7	3.45	0.24	0.90	0.88	0.64	0.43	1.22	0.72	1.24	1.74	11.49	6.41	0.62	1.84
CA17a-150-mz4-8	2.18	0.24	0.75	0.61	0.65	0.43	1.28	0.75	1.25	1.35	6.84	4.84	0.53	1.84
CA17a-150-mz4-9	2.10	0.24	0.75	0.62	0.66	0.44	1.28	0.73	1.16	1.28	6.09	4.87	0.53	1.70
CA17a-150-mz4-10	2.27	0.24	0.78	0.57	0.64	0.43	1.29	0.74	1.33	1.47	7.03	4.85	0.54	1.74
CA30.0B-mz2-1	2.66	0.24	0.90	1.43	0.61	0.43	1.22	0.72	1.22	2.08	23.80	6.30	0.68	0.99
CA30.0B-mz2-2	2.65	0.24	0.83	0.67	0.62	0.43	1.26	0.72	1.22	1.82	10.64	5.18	0.67	0.92
CA30.0B-mz2-3	2.72	0.24	0.82	1.64	0.61	0.43	1.22	0.73	1.23	2.11	18.57	5.68	0.68	0.93
CA30.0B-mz2-4	2.44	0.24	0.84	0.74	0.61	0.43	1.24	0.73	1.21	1.86	10.09	5.71	0.68	0.95
CA30.0B-mz2-5	2.61	0.24	0.93	0.86	0.61	0.43	1.22	0.73	1.25	1.97	11.38	5.71	0.72	1.1
CA30.0B-mz2-6	2.60	0.24	0.92	0.70	0.61	0.43	1.22	0.72	1.25	1.89	10.85	6.40	0.71	1.1
CA30.0E-mz1-1	0.57	0.24	0.88	0.64	0.63	0.44	1.23	0.73	1.23	1.73	7.47	6.21	0.64	1.93
CA30.0E-mz1-2	2.53	0.24	0.92	0.64	0.61	0.43	1.23	0.72	1.22	1.71	7.57	6.83	0.65	2
CA30.0E-mz1-3	2.49	0.24	0.94	0.64	0.61	0.43	1.21	0.72	1.23	1.68	8.14	7.12	0.65	2.01
CA30.0E-mz1-4	1.44	0.24	0.91	0.64	0.61	0.43	1.20	0.72	1.23	1.74	8.60	6.94	0.64	1.93
CA30.0G-mz1-1	0.54	0.24	0.86	0.53	0.63	0.44	1.24	0.73	1.23	1.68	7.18	6.20	0.62	1.8
CA30.0G-mz1-2	2.55	0.24	0.90	0.56	0.62	0.43	1.20	0.72	1.21	1.75	7.23	6.10	0.62	1.89
CA30.0G-mz1-3	2.90	0.24	0.89	0.53	0.62	0.43	1.20	0.71	1.22	1.66	7.25	6.05	0.62	1.79
CA30.0G-mz1-4	2.68	0.24	0.88	0.55	0.62	0.43	1.22	0.72	1.20	1.69	7.23	6.00	0.60	1.84
CA30.0G-mz1-5	2.61	0.24	0.88	0.55	0.63	0.43	1.20	0.72	1.23	1.67	7.12	6.06	0.61	1.91
CA30.0G-mz2-1	3.01	0.24	0.95	0.35	0.63	0.43	1.23	0.72	1.19	1.56	5.00	6.15	0.65	1.82
CA30.0G-mz2-2	3.30	0.24	0.99	0.36	0.62	0.43	1.22	0.71	1.20	1.54	4.59	6.70	0.70	1.93
CA30.0G-mz2-3	3.94	0.24	1.13	0.37	0.62	0.43	1.21	0.71	1.16	1.56	4.47	7.41	0.77	2.18
CA30.0G-mz2-4	3.28	0.24	1.09	0.37	0.62	0.43	1.20	0.71	1.17	1.52	4.63	6.75	0.75	1.92
CA30.0G-mz2-5	3.75	0.24	1.13	0.39	0.62	0.43	1.23	0.71	1.18	1.52	5.69	5.94	0.80	1.52
CA30.0G-mz2-6	3.65	0.24	1.06	0.37	0.62	0.43	1.18	0.72	1.18	1.51	5.09	6.37	0.74	1.56
CA30.0G-mz2-7	3.22	0.24	0.99	0.35	0.63	0.43	1.21	0.72	1.21	1.53	4.47	5.98	0.66	1.79
CA30.0E-mz2-1	2.87	0.24	0.90	0.36	0.62	0.43	1.23	0.73	1.28	1.68	4.92	5.08	0.65	1.41
CA30.0E-mz2-2	2.77	0.24	0.96	0.36	0.62	0.43	1.21	0.72	1.24	1.61	4.88	5.92	0.66	1.61
CA30.0E-mz2-3	2.90	0.24	0.98	0.38	0.61	0.43	1.24	0.74	1.32	1.75	5.16	6.30	0.67	1.63
CA30.0E-mz2-4	2.75	0.24	0.93	0.37	0.61	0.43	1.24	0.74	1.29	1.70	5.14	5.47	0.65	1.44

CA30.0E-mz2-5	2.64	0.24	0.93	0.35	0.62	0.43	1.22	0.73	1.25	1.57	4.91	5.84	0.65	1.54

Appendix E. Compositional data, k-ratio errors, calculated dates and Monte Carlo CIs for analyses in Chapter 4

Sample	SiO2	P2O5	CaO	Y2O3	La2O3	Ce2O3	Pr2O3	Nd2O3	Sm2O3	Gd2O3	Dy2O3	PbO	ThO2	UO2	Total	Date (Ma)	95% CI
Concentrations																	
K31.0-mz1-1	0.0557	30.41	0.7571	1.73	14.16	28.63	3.08	11.67	1.85	1.51	0.6599	0.0838	3.52	0.8625	99.0227	314.3	24.1
K31.0-mz1-2	0.0562	30.45	0.7264	1.72	13.83	28.15	3.06	11.85	1.9	1.61	0.6495	0.076	3.36	0.8292	98.3027	297.9	25.2
K31.0-mz1-3	0.0523	30.42	0.7315	1.7	13.91	28.67	3.16	11.78	1.95	1.65	0.6842	0.07	3.38	0.8164	99.0096	275.5	25.2
K31.0-mz1-4	0.0713	30.55	0.7805	1.7	13.77	27.85	3.06	11.35	1.83	1.51	0.6698	0.0841	3.64	0.9052	97.811	303.2	23.7
K31.0-mz1-5	0.1326	29.68	0.8191	1.81	13.52	28.02	3.2	11.89	1.98	1.68	0.7024	0.0858	3.63	0.9288	98.1203	305.9	22.8
K31.0-mz1-6	0.0587	30.64	0.7788	1.9	13.69	28.18	3.15	11.98	1.95	1.68	0.7238	0.0825	3.47	0.9169	99.2432	303.6	23.7
K31.0-mz1-7	0.1753	30.1	0.9621	0.8929	13.71	27.63	3.04	11.62	2.1	1.18	0.3105	0.0912	5.65	0.5099	98.0264	295.8	21.8
K31.0-mz1-8	0.0667	30.39	0.8936	0.5119	14.72	29.33	3.13	11.52	1.64	0.9701	0.2016	0.0871	3.92	1.0771	98.4964	279	23.2
K31.0-mz1-9	0.0698	30.38	0.8238	1.81	13.76	28.04	3.16	11.76	1.89	1.59	0.7251	0.0889	3.96	0.9959	99.096	293.1	21.6
K31.0-mz1-10	0.0648	30.71	0.7749	1.88	13.78	28.6	3.21	11.9	1.94	1.61	0.6821	0.076	3.42	0.9228	99.6075	281.3	24.1
K31.0-mz3-1	0.0752	30.22	0.7193	0.996	14.5	29.16	3.11	12.06	1.94	1.3	0.413	0.0714	3.35	0.9026	98.8496	270.2	26
K31.0-mz3-2	0.1072	30.03	0.5689	0.3558	14.75	30.03	3.27	12.6	2.01	0.9858	0.1778	0.0556	2.87	0.5683	98.4047	279.8	35.2
K31.0-mz3-3	0.0656	30.23	0.8051	0.695	14.58	29.61	3.17	12.03	1.85	1.0545	0.2764	0.0894	3.43	1.091	99.006	304.1	24.2
K31.0-mz3-4	0.0668	30.23	0.6897	1.0299	14.68	29.21	3.21	11.99	1.95	1.3	0.4427	0.0684	3.11	0.8337	98.8463	279.2	27.7
K31.0-mz3-5	0.0678	30.31	0.903	1.86	13.71	28.04	3.1	11.66	1.86	1.5	0.6837	0.0956	4.13	1.016	98.9839	305.1	20.8
K31.0-mz3-6	0.0676	30.24	0.7944	1.7	14.05	28.59	3.09	11.6	1.79	1.51	0.6927	0.076	3.62	0.8936	98.7569	276.6	23.4
K31.0-mz3-7	0.0879	30.27	0.7635	1.68	13.93	28.6	3.12	11.8	1.96	1.57	0.6597	0.0755	3.49	0.8351	98.8859	288.8	24.7
K31.0-mz3-8	0.1209	30.05	0.6956	0.6315	14.5	29.56	3.29	12.2	2.01	1.21	0.276	0.0773	3.55	0.7654	98.9662	303.6	27.4
K31.0-mz3-9	0.1193	30.05	0.6343	0.6676	14.48	29.46	3.26	12.26	1.96	1.17	0.3196	0.0662	3.28	0.6466	98.4073	291.8	30.1
k38-30-mz2-1	0.169	29.48	0.721	0.808	15.2	30.95	3.25	12.1	1.96	1.55	0.414	0.0569	3.37	0.4302	100.49	282.9	32.7
k38-30-mz2-2	0.171	29.69	0.697	0.86	14.83	30.85	3.28	12.53	2.11	1.71	0.483	0.0635	3.39	0.4001	101.095	320.6	33
k38-30-mz2-3	0.187	29.92	0.838	0.939	14.17	29.61	3.16	12.13	2.09	1.77	0.567	0.0627	3.58	0.5171	99.572	282.6	29.5
k38-30-mz2-4	0.194	29.67	0.918	0.922	14.67	30.05	3.29	12.43	2.13	1.77	0.465	0.0746	4.26	0.6085	101.494	283.5	25.2
k38-30-mz2-5	0.188	29.69	0.851	0.902	14.68	29.96	3.12	12.16	2.07	1.73	0.568	0.0801	4.04	0.5797	100.652	320.1	26.2
k38-30-mz2-6	0.216	29.57	0.923	0.889	14.8	30.11	3.22	12.18	2.03	1.74	0.541	0.0806	4.36	0.525	101.223	314.5	25.8
k38-30-mz2-7	0.224	29.57	0.971	0.9	14.67	29.81	3.13	12	2.07	1.76	0.604	0.0807	4.81	0.5476	101.19	290.1	23.7

k38-30-mz2-8	0.242	29.55	1.045	0.939	14.55	29.58	3.1	12.06	2.08	1.82	0.524	0.0779	5.12	0.574	101.308	264.5	22.4
k38-30-mz2-9	0.207	29.6	0.999	0.945	14.44	29.22	3.17	11.94	2.11	1.78	0.568	0.0876	4.72	0.6561	100.483	302.8	23.2
k38-30-mz2-10	0.121	29.76	0.546	0.443	15.39	31.68	3.38	12.92	2.08	1.58	0.297	0.0527	2.52	0.3567	101.152	338.9	42.4
k38-30-mz2-11	0.217	29.31	0.821	0.823	14.6	30.33	3.18	12.19	2.07	1.75	0.546	0.0697	4.54	0.43	100.92	278.1	26.6
k38-30-mz2-12	0.201	29.38	0.937	0.941	14.51	29.81	3.1	11.99	2.07	1.78	0.573	0.076	4.5	0.5702	100.485	283.6	24.6
k38-30-mz2-13	0.135	29.24	0.648	0.873	14.79	31.01	3.25	12.47	2.15	1.77	0.469	0.0584	2.87	0.4729	100.232	313.9	34.6
k38-30-mz2-14	0.146	29.53	0.582	0.762	14.96	31.3	3.24	12.38	1.98	1.56	0.461	0.0541	2.87	0.3549	100.206	318.2	37.9
k38-30-mz2-15	0.162	29.56	0.656	0.869	14.78	30.84	3.35	12.81	2.11	1.63	0.546	0.052	3.13	0.3995	100.924	278.3	34.7
k38-30-mz2-16	0.151	29.35	0.606	0.814	15.13	31.25	3.34	12.55	2.08	1.61	0.488	0.0577	2.93	0.3546	100.737	334.2	36.8
k38-30-mz5-1	0.318	28.77	1.025	0.68	13.97	29.18	3.09	11.88	1.94	1.52	0.349	0.0898	5.48	0.619	98.954	284.2	21.2
k38-30-mz5-2	0.066	29.92	1.236	0.118	14.98	30.6	3.16	11.86	1.75	0.826	0.105	0.1195	4.29	1.5673	100.63	302.3	18.6
k38-30-mz5-3	0.178	29.75	0.788	0.81	14.74	29.93	3.21	12.27	2.05	1.69	0.498	0.0649	3.9	0.4524	100.375	286.5	29
k38-30-mz5-4	0.161	29.8	0.687	0.612	15.03	30.65	3.15	12.14	2.06	1.6	0.422	0.0612	3.31	0.4745	100.194	299	32.5
k38-30-mz5-5	0.208	29.69	0.851	0.592	14.67	30.25	3.2	12.17	2.02	1.56	0.439	0.0715	4.3	0.4943	100.558	287.1	26.9
k38-30-mz5-6	0.182	29.85	0.776	0.616	14.84	30.69	3.25	12.27	2.07	1.72	0.363	0.0643	3.78	0.494	100.999	283.3	29.4
k38-30-mz5-7	0.185	29.86	0.737	0.56	14.99	30.78	3.33	12.44	1.99	1.56	0.287	0.0569	3.69	0.3896	100.891	272.1	32.4
k38-30-mz5-8	0.169	29.9	0.655	0.535	15.11	31.01	3.29	12.52	1.99	1.56	0.371	0.0508	3.26	0.3868	100.836	266.9	34.8
k38-30-mz5-9	0.115	30.02	0.571	0.78	15.47	31.08	3.29	12.26	2.13	1.66	0.466	0.043	2.32	0.6098	100.842	237.9	36
k38-30-mz5-10	0.122	29.91	0.508	0.452	15.39	31.8	3.28	12.73	2.15	1.49	0.276	0.0405	2.05	0.4662	100.682	270	45
k38-30-mz5-11	0.155	29.77	0.725	0.705	14.94	30.39	3.19	12.18	2.08	1.67	0.45	0.0605	3.38	0.4932	100.218	288	31.5
k38-30-mz5-12	0.162	29.37	0.715	0.105	15.47	31.44	3.3	12.8	2.06	1.18	0.128	0.0504	3.3	0.4236	100.535	255.8	35.3
k38-30-mz5-13	0.109	29.57	0.57	0.741	15.08	30.82	3.3	12.62	2.17	1.65	0.462	0.0479	2.5	0.5619	100.224	263.2	35.9
k38-30-mz6-1	0.221	29.88	0.797	1.38	14.14	30.11	3.27	12.48	2.17	1.81	0.634	0.0721	4.01	0.3199	101.336	337.7	29.2
k38-30-mz6-2	0.193	29.95	0.643	1.27	14.83	31.01	3.35	12.96	2.08	1.38	0.486	0.0601	3.33	0.2785	101.858	335.4	34.4
k38-30-mz6-3	0.198	29.78	0.699	1.27	14.85	30.92	3.37	12.65	2.04	1.38	0.592	0.0584	3.68	0.2846	101.81	300.4	31.6
k38-30-mz6-6	0.277	30.28	0.685	1.209	14.82	30.89	3.28	12.67	2.14	1.31	0.524	0.0588	3.69	0.2646	102.142	305.9	32
k38-30-mz6-7	0.573	29.84	0.334	0.903	15.08	31.38	3.36	12.95	2.16	1.58	0.493	0.0477	3.73	0.1053	102.568	277	36.4
k38-30-mz6-8	0.226	30.02	0.808	1.37	14.5	30.35	3.32	12.48	2.04	1.43	0.558	0.0759	4.19	0.3509	101.771	336.5	27.9
k38-30-mz6-9	0.199	29.42	0.776	1.249	14.64	30.63	3.25	12.7	2.07	1.39	0.47	0.0743	3.82	0.3569	101.087	352.7	29.7
k38-30-mz6-10	0.224	29.99	0.878	1.39	14.53	30.24	3.27	12.72	2.01	1.37	0.517	0.0863	4.44	0.3596	102.074	363.2	26.6
k38-30-mz6-11	0.229	30.07	0.92	1.43	14.35	30.08	3.21	12.5	2.04	1.42	0.563	0.0865	4.7	0.3872	102.033	343.3	25.2
k38-30-mz6-12	0.24	29.84	0.854	1.36	14.16	29.91	3.25	12.58	2.26	1.88	0.618	0.0787	4.33	0.3342	101.74	343.5	27.4
k38-30-mz6-13	0.213	30.49	0.801	1.38	14.75	30.89	3.34	12.61	2.08	1.51	0.608	0.0809	4.17	0.335	103.296	363.2	28.1

k38-30-mz6-14	0.232	30.01	0.85	1.43	14.51	30.26	3.28	12.53	2.05	1.44	0.563	0.0841	4.45	0.3705	102.101	351.2	26.3
k38-30-mz6-15	0.247	29.8	0.975	1.45	14.15	29.88	3.19	12.5	2.09	1.43	0.588	0.0959	4.99	0.4137	101.849	357.6	23.6
k38-30-mz8-1	0.079	30.06	0.414	1.266	15.2	31.28	3.36	12.65	2.06	1.69	0.627	0.0381	1.69	0.5161	100.96	269.1	42.1
k38-30-mz8-2	0.094	30.07	0.465	1.37	15.09	31.11	3.33	12.65	2.1	1.73	0.702	0.0428	2.09	0.391	101.26	301.6	41.9
k38-30-mz8-3	0.061	29.99	0.326	1.194	15.09	31.49	3.37	12.86	2.2	1.72	0.595	0.0314	1.22	0.4356	100.598	283.3	53.1
k38-30-mz8-4	0.1	29.82	0.488	0.419	15.48	32.07	3.4	12.82	2.15	1.55	0.251	0.0502	2.35	0.3826	101.356	330.5	44.2
k38-30-mz8-5	0.165	29.81	0.703	0.068	15.37	31.64	3.27	12.81	2	1.043	0.169	0.0483	3.46	0.3567	100.94	248.4	36.1
k38-30-mz8-6	0.062	29.87	0.363	1.081	15.21	31.17	3.41	12.64	2.16	1.66	0.649	0.0368	1.41	0.4346	100.175	309.1	50.2
k38-30-mz8-7	0.108	30.01	0.546	1.48	14.48	30.49	3.27	12.68	2.14	1.75	0.75	0.0447	2.31	0.4549	100.539	279.9	37.2
k38-30-mz8-8	0.122	29.98	0.631	1.55	14.61	30.42	3.26	12.76	2.09	1.8	0.7	0.0623	2.82	0.4592	101.301	341.7	33
k38-30-mz8-9	0.143	29.96	0.74	1.56	14.35	30.18	3.24	12.71	2.13	1.78	0.711	0.0602	3.37	0.5113	101.48	284	28.8
k38-30-mz8-10	0.156	29.78	0.73	0.082	15.4	31.68	3.35	12.72	2.03	1.126	0.049	0.0551	3.53	0.3543	101.068	279.1	35.1
k38-30-mz8-11	0.181	29.76	0.705	0	16.32	32.6	3.42	12.68	1.74	0.549	0.019	0.0458	3.46	0.2727	101.777	250	38.8
k38-30-mz8-12	0.152	29.73	0.719	0.2	15.53	31.78	3.36	12.71	1.99	1.19	0.139	0.0497	3.37	0.3472	101.292	262	36.3
k38-30-mz8-13	0.101	30	0.571	0.831	14.97	31.21	3.36	12.75	2.18	1.71	0.514	0.0516	2.38	0.4135	101.068	327.8	41.1
k38-30-mz8-14	0.116	29.85	0.539	1.38	14.8	31.32	3.28	12.86	2.15	1.75	0.738	0.0468	2.57	0.3575	101.788	297.1	37.9
k38-30-mz8-15	0.105	29.85	0.469	1.161	15.21	31.53	3.41	12.82	2.08	1.65	0.679	0.0402	2	0.3945	101.425	290.6	44
k38-30-mz8-16	0.133	29.79	0.741	0.807	15.15	31.45	3.26	12.7	1.95	1.22	0.371	0.0569	3.38	0.4571	101.494	277.3	32.1
k38-30-mz10-1	0.03	30.02	1.192	0.57	14.7	30.17	3.17	12.18	1.92	1.17	0.308	0.1008	4.19	1.2779	101.046	287.1	20.3
k38-30-mz10-2	0.042	29.99	1.166	0.731	14.37	30.1	3.24	12.52	1.99	1.38	0.305	0.089	4.09	1.2584	101.315	259	20.4
k38-30-mz10-3	0.033	29.99	1.236	0.44	14.8	30.16	3.14	11.72	1.81	1.084	0.224	0.1074	4.31	1.3672	100.462	291.5	19.3
k38-30-mz10-4	0.036	29.99	1.186	0.183	15.22	31.03	3.23	11.78	1.7	0.843	0.165	0.1037	3.95	1.4091	100.857	288.9	20.3
k38-30-mz10-5	0.083	29.94	1.041	0.061	15.6	31.65	3.28	12.09	1.76	0.707	0.087	0.0825	3.93	1.0502	101.401	267.1	23.8
k38-30-mz10-6	0.146	29.72	0.82	0.008	15.69	32.2	3.29	12.53	1.74	0.464	0.057	0.0672	3.74	0.4762	100.975	301	31.5
k38-30-mz10-7	0.125	29.85	0.656	0.587	14.9	30.83	3.23	12.65	2.13	1.61	0.323	0.0553	2.83	0.5711	100.376	279.9	34.3
k38-30-mz10-8	0.161	29.76	0.755	0.017	16.13	32.11	3.3	12.35	1.8	0.717	0.012	0.0503	3.64	0.3797	101.218	245.1	34
k38-30-mz10-9	0.037	30	1.16	0.696	14.79	30.09	3.18	11.85	1.94	1.37	0.343	0.0992	4.14	1.1782	100.906	295.4	20.7
k38-30-mz10-10	0.099	30.06	0.781	0.217	15.15	31.12	3.15	12.3	1.91	1.038	0.104	0.075	3.14	0.8173	99.985	306.7	28.9
K45.10-mz1-1	0.1942	30.71	0.8095	1.56	14.41	29.46	3.26	12.46	2.14	1.75	0.6739	0.0749	3.95	0.4955	101.7546	319	26.5
K45.10-mz1-2	0.167	30.89	0.6517	1.42	14.8	30.16	3.31	12.7	2.13	1.74	0.6663	0.058	3.12	0.4062	102.0616	309.5	32.6
K45.10-mz1-3	0.1799	30.8	0.7187	1.51	14.5	29.66	3.29	12.51	2.11	1.75	0.6833	0.065	3.56	0.4489	101.6151	306.5	28.9
K45.10-mz1-4	0.1893	30.75	0.7636	1.52	14.43	29.55	3.29	12.52	2.11	1.79	0.6617	0.0648	3.73	0.4543	101.6368	295.1	28.2

K45.10-mz1-5	0.1887	30.8	0.7743	1.5	14.57	29.51	3.28	12.58	2.16	1.76	0.6389	0.0688	3.71	0.5054	101.8646	304.7	27.7
K45.10-mz1-6	0.1844	30.81	0.7085	1.2386	14.78	30.13	3.37	12.49	2.14	1.86	0.6211	0.0709	3.32	0.5392	102.083	330.8	29.8
K45.10-mz1-7	0.1777	30.53	0.6556	1.1609	14.86	30.24	3.42	12.66	2.18	1.87	0.5253	0.0605	3.11	0.4507	101.7318	313.4	32.8
K45.10-mz1-8	0.1913	30.59	0.6946	1.1685	14.96	30.11	3.4	12.52	2.15	1.84	0.5378	0.0628	3.32	0.4879	101.8479	303.6	30.8
K45.10-mz2-1	0.0497	30.62	1.0364	0.2891	14.86	30.54	3.4	12.68	2.08	1.35	0.1934	0.0879	3.87	1.0933	102.1068	281.4	23.2
K45.10-mz2-2	0.3367	30.17	1.0898	0.0513	15.02	30.38	3.27	12.46	2	1.19	0.0652	0.0974	5.8	0.6424	102.2434	292.7	21.4
K45.10-mz2-3	0.2179	30.5	0.9638	1.56	14.27	28.83	3.26	12.24	2.11	1.91	0.7382	0.0798	4.79	0.5928	101.8456	281.7	22.4
K45.10-mz2-4	0.0441	30.66	1.0782	0.2157	14.96	30.22	3.36	12.61	2.04	1.29	0.1255	0.0941	4.02	1.1595	101.834	287	22
K45.10-mz2-5	0.0918	30.56	1.0565	0.1225	14.95	30.54	3.41	12.65	2.07	1.21	0.1285	0.0925	4.17	1.1387	102.1051	279.2	22.1
K45.10-mz2-6	0.0926	30.55	1.076	0.1359	15.09	30.36	3.37	12.68	2.06	1.26	0.1096	0.0973	4.32	1.0492	102.158	298.6	22.1
K45.10-mz2-7	0.0641	30.68	1.078	0.1683	15.12	30.41	3.42	12.6	2.01	1.2	0.0829	0.0963	4.1	1.1491	102.1146	291.9	22
K45.10-mz2-8	0.2643	30.26	0.9752	0.0505	15.16	30.37	3.32	12.41	1.96	1.1468	0	0.0867	5.06	0.5858	101.3975	295.2	24.1
K52.40-mz1-1	0.099	30.81	0.4938	1.67	15.58	31.81	3.46	12.71	1.75	1.08	0.3629	0.0366	2.19	0.2505	102.3289	288.9	43.1
K52.40-mz1-2	0.105	30.96	0.4413	1.66	15.6	31.61	3.44	12.63	1.77	1.1439	0.4296	0.0354	2.07	0.2144	102.1348	303.1	46
K52.40-mz1-3	0.1608	30.94	0.594	1.99	15.17	30.28	3.38	12.49	2.02	1.6	0.693	0.0495	3.06	0.3059	102.7676	289.1	32.8
K52.40-mz1-4	0.1033	30.68	0.3555	1.72	15.21	31.19	3.58	13.08	2.15	1.61	0.5529	0.0325	1.7	0.121	102.1122	366.8	57.7
K52.40-mz1-5	0.1072	30.77	0.3445	1.82	15.3	31.32	3.48	13.05	2.19	1.61	0.5529	0.0222	1.5	0.1614	102.2535	260	54.6
K52.40-mz1-6	0.1243	31.06	0.5226	1.92	15.34	30.78	3.43	12.57	2.05	1.63	0.6251	0.0352	2.59	0.1337	102.8436	275.8	40.9
K52.40-mz1-7	0.1033	30.79	0.3793	1.69	15.63	31.57	3.47	12.62	2.03	1.47	0.6034	0.0282	1.8	0.1587	102.377	288.6	51.6
K52.40-mz1-8	0.1047	30.69	0.4712	1.65	15.71	31.94	3.58	12.77	1.67	1.0104	0.3971	0.0265	2.06	0.2267	102.332	225.3	43.3
K52.40-mz2-1	0.1453	30.86	0.284	1.31	15.89	31.88	3.53	13.15	2.15	1.7	0.6247	0.0219	1.47	0.2237	103.2583	236.8	56.7
K52.40-mz2-2	0.0728	31.06	0.4879	1.46	15.15	30.89	3.46	12.87	2.24	1.73	0.6797	0.0323	1.96	0.4321	102.5478	228.4	40.4
K52.40-mz2-3	0.1571	30.57	0.27	1.1374	15.84	32.03	3.43	13.04	2.12	1.57	0.5559	0.0241	1.52	0.1753	102.4629	273.7	61.9
K52.40-mz2-4	0.1606	30.74	0.2804	1.0752	15.91	31.98	3.48	13.17	2.1	1.55	0.5003	0.0151	1.53	0.2078	102.7265	163.2	53.5
K52.40-mz2-5	0.1734	30.83	0.2475	0.9496	15.93	31.95	3.46	13.19	2.16	1.6	0.5455	0.0236	1.49	0.1316	102.6976	291.3	69
K52.40-mz2-6	0.0947	30.84	0.4218	1.1716	15.65	31.56	3.52	13.18	2.11	1.6	0.6463	0.0283	1.8	0.3174	102.9656	237.9	48.3
K52.40-mz2-7	0.1793	30.6	0.4096	1.2327	15.57	31.18	3.46	12.84	2.12	1.62	0.5769	0.0328	2.09	0.276	102.2171	260.4	45.8
K52.40-mz2-8	0.1708	30.91	0.3895	1.1564	15.4	31.23	3.53	12.99	2.25	1.57	0.5377	0.0347	1.94	0.2583	102.3887	296.1	50.3
K52.40-mz2-9	0.0953	31.01	0.6197	1.36	15.17	30.76	3.41	12.79	2.11	1.67	0.6162	0.0536	2.37	0.5085	102.5737	315.5	36.6
K52.40-mz2-10	0.1429	30.53	0.2587	1.093	15.79	31.85	3.56	13.46	2.16	1.57	0.6412	0.0184	1.36	0.1412	102.6025	240.8	67.6
K52.40-mz3-1	0.7946	29.72	1.83	0.0694	13.68	26.6	2.85	10.48	1.39	0.7064	0.0414	0.166	11.17	0.4767	100.0671	308.7	13
K52.40-mz3-2	1.4249	28.93	2.15	0.0712	13.36	26.06	2.75	10.17	1.4	0.6844	0	0.2093	14.46	0.5603	102.3403	304.1	10.2

K52.40-mz3-3	1.2858	29.09	2.2	0.0452	13.42	25.83	2.75	9.99	1.28	0.5393	0.0278	0.2096	14.58	0.5353	101.9075	303.9	10.1
K52.40-mz3-4	0.8846	29.75	2.01	0.0527	13.89	26.87	2.87	10.3	1.31	0.558	0.0239	0.1763	12.35	0.5145	101.6513	297.4	11.8
K52.40-mz3-5	0.9562	29.51	2.17	0.0687	12.89	25.28	2.88	10.37	1.35	0.6129	0.0122	0.1956	13.38	0.5533	100.3403	304.9	11
K52.40-mz3-6	0.7286	29.78	1.97	0.1735	12.98	26.05	2.94	10.98	1.72	1.0672	0.1241	0.1645	11.35	0.6214	100.7409	291.2	12.4
K52.40-mz3-7	0.3787	30.17	1.41	0.3476	13.92	28.6	3.18	12.18	2.07	1.41	0.252	0.1205	7.38	0.6853	102.1644	297.1	17
K52.40-mz3-8	0.2052	30.42	0.8388	0.4579	14.75	29.88	3.42	12.79	2.19	1.64	0.3368	0.0781	4.02	0.7212	101.7849	291	25.8
K52.40-mz3-9	1.0593	29.33	2.39	0.1225	12.42	24.99	2.76	10.19	1.55	0.9212	0.1089	0.214	14.43	0.6598	101.261	305.4	10
K52.40-mz3-10	0.5129	29.87	1.68	0.2758	13.51	27.36	3.02	11.54	1.9	1.32	0.2241	0.1444	9.25	0.6677	101.3428	299.4	14.5
K52.40-mz4-1	0.1342	30.43	0.4441	0.6106	15.21	31.38	3.47	12.93	2.12	1.56	0.4448	0.0554	2.24	0.6188	101.6689	309.3	38.7
K52.40-mz4-2	0.2222	30.17	0.7007	0.5868	14.7	29.91	3.33	12.47	2.1	1.5	0.4403	0.0735	4.12	0.615	100.9757	284.8	27
K52.40-mz4-3	0.3704	30.04	1.0779	0.326	14.37	29.11	3.22	12.08	1.84	1.16	0.2517	0.1032	6.83	0.48	101.3148	291.3	19.8
K52.40-mz4-4	0.2379	30.3	0.7223	0.5826	14.75	30.07	3.36	12.48	2.08	1.52	0.4188	0.0754	4.09	0.6239	101.3559	292.4	27.2
K52.40-mz4-5	0.5624	29.84	1.395	0.4107	13.42	27.31	3.04	11.75	2	1.31	0.3054	0.1396	9.1	0.6382	101.2934	295.7	15
K52.40-mz4-6	0.147	30.45	0.7432	0.4457	14.71	30.35	3.37	12.62	2.04	1.38	0.2588	0.086	3.5	0.9217	101.05	314	26.2
K52.40-mz4-7	0.198	30.4	0.7423	0.5557	14.82	30	3.29	12.42	2.01	1.51	0.3189	0.0722	4.17	0.596	101.1362	280.3	27.2
K52.40-mz4-8	0.0958	30.54	0.874	0.1601	15.37	30.71	3.32	11.79	1.76	1.0702	0.1816	0.0928	3.86	1.0903	100.9433	297.6	23.8
K52-40A-mz1-1	0.0945	30.43	0.3732	0.6318	15.01	30.25	3.4	12.44	2.09	1.56	0.4367	0.0395	1.42	0.5256	98.7149	299.6	51.8
K52-40A-mz1-2	0.0865	30.61	0.3788	0.5946	15.18	30.45	3.47	12.61	2.06	1.56	0.4216	0.0421	1.4	0.5441	99.4211	315.5	51.1
K52-40A-mz1-3	0.104	30.59	0.4665	0.6435	14.86	29.95	3.37	12.31	2.06	1.57	0.4397	0.0459	1.75	0.6829	98.8585	275	41.9
K52-40A-mz1-4	0.1014	30.68	0.3755	0.684	14.84	30.46	3.28	12.9	2.06	1.58	0.4532	0.0392	1.4	0.5585	99.4257	289.7	50.4
K52-40A-mz1-5	0.0911	30.71	0.3855	0.6555	14.85	30.69	3.44	12.76	2.16	1.64	0.4128	0.0407	1.44	0.569	99.8586	293.8	49.6
K52-40A-mz1-6	0.1071	30.67	0.3968	0.6229	14.95	30.42	3.4	12.78	2.11	1.56	0.3932	0.0461	1.51	0.5532	99.5337	330.4	49.1
K52-40A-mz1-7	0.1257	30.39	0.5976	0.7758	14.24	29.42	3.35	12.67	2.24	1.76	0.4791	0.0621	2.4	0.7576	99.2894	303	33.7
K52-40A-mz1-8	0.1306	30.38	0.6059	0.7357	14.25	29.38	3.34	12.75	2.14	1.68	0.4432	0.0553	2.47	0.6764	99.0588	281.4	34.7
K52-40A-mz1-9	0.1221	30.51	0.5997	0.7599	14.51	29.53	3.32	12.57	2.17	1.66	0.4237	0.0611	2.45	0.7454	99.4536	297.6	33.7
K52-40A-mz1-10	0.1425	30.49	0.6525	0.7427	14.48	29.32	3.37	12.51	2.16	1.66	0.4862	0.0604	2.75	0.7172	99.5653	282.5	32.2
K52-40A-mz2-1	0.2441	30.56	1.0659	0.6544	13.83	28.16	3.16	12.1	2.1	1.59	0.4218	0.0973	5.02	0.8291	99.8717	298.9	21.5
K52-40A-mz2-2	0.3287	30.36	1.1052	0.5134	13.83	28.42	3.23	12.01	1.98	1.45	0.4162	0.0911	5.75	0.6187	100.1467	278.5	21.3
K52-40A-mz2-3	0.2889	30.4	1.0026	0.5451	14.09	28.61	3.18	12.13	2.01	1.53	0.3724	0.0775	5.09	0.6455	100.0107	256	23.1
K52-40A-mz2-4	0.3191	30.4	1.0225	0.5192	14.05	28.54	3.19	12.15	2.05	1.48	0.341	0.0816	5.31	0.6047	100.0983	266	22.6
K52-40A-mz2-5	0.2115	30.49	1.0379	0.6438	14.51	28.64	3.15	11.74	1.95	1.54	0.4806	0.0855	4.61	0.9221	100.0474	267.1	22.1
K52-40A-mz2-6	0.1836	30.55	0.9399	0.6692	14.3	28.9	3.11	12.18	2.06	1.63	0.3981	0.0879	4.09	0.9005	100.0317	297.1	23.7

K52-40A-mz2-7	0.258	30.46	1.1168	0.576	14.19	28.25	3.1	11.84	2.02	1.47	0.3762	0.0956	5.49	0.7653	100.0498	284.3	20.9
K52-40A-mz2-8	0.2438	30.52	1.0678	0.7251	13.86	28.16	3.15	12.3	2.14	1.71	0.4153	0.0919	4.87	0.8371	100.1293	287.1	21.8
K52-40A-mz2-9	0.251	30.44	0.9331	0.5439	14.23	29.07	3.18	12.27	2.08	1.54	0.3706	0.0763	4.56	0.6171	100.1971	275.8	25.1
K52-40A-mz2-10	0.1942	30.59	0.8095	0.5395	14.43	29.55	3.25	12.38	2.02	1.57	0.403	0.0737	3.8	0.5994	100.239	303.9	28.5
K53-30-mz1-1	0.176	30.5	0.685	1.237	14.5	30	3.4	12.5	2.2	1.49	0.51	0.074	3.71	0.2748	101.2924	379.6	32.8
K53-30-mz1-2	0.33	30.5	1	1.3	14.6	29.9	3.2	11.6	1.9	1.1	0.5	0.0904	4.7	0.302	101.0659	375.7	26.7
K53-30-mz1-3	0.37	30.2	1	1.32	13.3	28	3.2	11.5	1.9	1.7	0.6	0.1212	6.92	0.3389	100.5305	356.7	19.6
K53-30-mz1-4	0.37	30.2	1	1.31	13.3	28	3.2	11.5	1.9	1.7	0.6	0.1024	5.84	0.3279	99.4026	350.4	22.4
K53-30-mz1-5	0.37	30.2	1	1.2385	13.3	28	3.2	11.5	1.9	1.7	0.6	0.1168	6.59	0.3379	100.1106	358.7	20.3
K53-30-mz1-6	0.4	30	1	1.39	13.3	27.7	3.2	11.5	1.9	1.5	0.6	0.1512	8.1	0.3758	101.1868	382.6	16.9
K53-30-mz1-7	0.4	29.8	1.1	1.31	13.1	27.5	3.2	11.4	1.8	1.5	0.6	0.1863	10.37	0.3573	102.7104	381.1	13.4
K53-30-mz1-8	0.33	30.5	1	1.39	14.6	29.9	3.2	11.6	1.9	1.1	0.5	0.0772	4.62	0.2994	101.0601	326.5	27
K53-30-mz1-9	0.176	30.5	0.685	1.27	14.5	30	3.4	12.5	2.2	1.49	0.51	0.0728	3.96	0.2883	101.5898	351.4	30.6
K53-30-mz1-10	0.176	30.5	0.685	1.1965	14.5	30	3.4	12.5	2.2	1.49	0.51	0.0529	2.76	0.2752	100.2737	342	39.9
K53-30-mz1-11	0.33	30.5	1	1.31	14.6	29.9	3.2	11.6	1.9	1.1	0.5	0.0911	4.84	0.297	101.2128	370.4	25.5
K53-30-mz1-12	0.176	30.5	0.685	1.2405	14.5	30	3.4	12.5	2.2	1.49	0.51	0.0686	3	0.296	100.5965	408.3	37.1
K53-30-mz2-1	0.176	30.5	0.685	1.1708	14.5	30	3.4	12.5	2.2	1.49	0.51	0.075	3.48	0.3673	101.0875	378.7	32.3
K53-30-mz2-2	0.176	30.5	0.685	1.151	14.5	30	3.4	12.5	2.2	1.49	0.51	0.0583	3.05	0.3611	100.6115	326.6	35.5
K53-30-mz2-3	0.176	30.5	0.685	1.1131	14.5	30	3.4	12.5	2.2	1.49	0.51	0.0561	2.62	0.3142	100.0911	364.2	40.5
K53-30-mz2-4	0.176	30.5	0.685	1.1089	14.5	30	3.4	12.5	2.2	1.49	0.51	0.0619	2.71	0.3256	100.1947	387.7	39.2
K53-30-mz2-5	0.176	30.5	0.685	1.1367	14.5	30	3.4	12.5	2.2	1.49	0.51	0.0533	2.52	0.3226	100.0196	352.9	41.2
K53-30-mz2-6	0.12	30.5	0.71	1.1343	14.8	31	3.4	11.4	1.5	1.1	0.59	0.0494	2.27	0.2795	98.8775	367.4	45.4
K53-30-mz2-7	0.33	30.5	1	1.28	14.6	29.9	3.2	11.6	1.9	1.1	0.5	0.0759	4.15	0.3982	100.5733	329.8	27.6
K53-30-mz2-8	0.33	30.5	1	1.181	14.6	29.9	3.2	11.6	1.9	1.1	0.5	0.086	4.19	0.3608	100.4866	378.3	28
K53-30-mz2-11	0.176	30.5	0.685	1.1351	14.5	30	3.4	12.5	2.2	1.49	0.51	0.066	2.66	0.3442	100.1935	411.8	39.3
K53-30-mz2-13	0.12	30.5	0.71	1.206	14.8	31	3.4	11.4	1.5	1.1	0.59	0.0397	2.18	0.3255	98.8954	291	44.5
K53-30-mz2-14	0.12	30.5	0.71	1.2346	14.8	31	3.4	11.4	1.5	1.1	0.59	0.0577	2.46	0.3344	99.2332	384.1	40.8
K53-30-mz2-15	0.12	30.5	0.71	1.1043	14.8	31	3.4	11.4	1.5	1.1	0.59	0.0445	2.57	0.2932	99.1583	299	41.4
K53-30-mz4-1	0.176	30.5	0.685	1.0482	14.5	30	3.4	12.5	2.2	1.49	0.51	0.075	3.79	0.7657	101.6749	283.4	25.2
K53-30-mz4-2	0.176	30.5	0.685	1.185	14.5	30	3.4	12.5	2.2	1.49	0.51	0.0965	3.76	1.1787	102.217	301.8	21.2
K53-30-mz4-3	0.176	30.5	0.685	1.46	14.5	30	3.4	12.5	2.2	1.49	0.51	0.0899	3.18	1.2421	101.9661	296	22.1

K53-30-mz4-4	0.12	30.5	0.71	1.92	14.8	31	3.4	11.4	1.5	1.1	0.59	0.0811	2.11	1.2781	100.5373	307.6	24.6
K53-30-mz4-5	0.12	30.5	0.71	2.57	14.8	31	3.4	11.4	1.5	1.1	0.59	0.0907	1.88	1.7494	101.4406	285.3	20.2
K53-30-mz4-6	0.176	30.5	0.685	1.1407	14.5	30	3.4	12.5	2.2	1.49	0.51	0.0918	3.97	1.0389	102.2394	296.7	21.8
K53-30-mz4-7	0.176	30.5	0.685	1.1492	14.5	30	3.4	12.5	2.2	1.49	0.51	0.0921	3.99	1.1774	102.407	280.1	20.9
K53-30-mz4-8	0.176	30.5	0.685	1.6	14.5	30	3.4	12.5	2.2	1.49	0.51	0.0952	3.1	1.3025	102.0921	308.2	21.8
K53-30-mz4-9	0.12	30.5	0.71	2.59	14.8	31	3.4	11.4	1.5	1.1	0.59	0.0945	2.02	1.7287	101.5848	294.2	20.1
K53-30-mz4-10	0.176	30.5	0.685	1.2277	14.5	30	3.4	12.5	2.2	1.49	0.51	0.0859	3.15	1.0166	101.4725	315.7	25
K53-30-mz4-11	0.176	30.5	0.685	1.35	14.5	30	3.4	12.5	2.2	1.49	0.51	0.0871	3.52	1.1902	102.1431	280.1	21.8
K53-30-mz5-1	0.176	30.5	0.685	1.38	14.5	30	3.4	12.5	2.2	1.49	0.51	0.057	2.85	0.5934	100.8716	283	31.1
K53-30-mz5-2	0.176	30.5	0.685	1.4	14.5	30	3.4	12.5	2.2	1.49	0.51	0.0521	2.91	0.6179	100.9717	252.1	30.3
K53-30-mz5-3	0.176	30.5	0.685	1.52	14.5	30	3.4	12.5	2.2	1.49	0.51	0.0606	2.82	0.6503	101.0426	291.3	30
K53-30-mz5-4	0.12	30.5	0.71	1.86	14.8	31	3.4	11.4	1.5	1.1	0.59	0.0393	1.98	0.5496	99.5757	248.5	35.4
K53-30-mz5-5	0.12	30.5	0.71	2.2	14.8	31	3.4	11.4	1.5	1.1	0.59	0.0506	2.31	0.6677	100.3796	268.5	30.3
K53-30-mz5-6	0.176	30.5	0.685	1.45	14.5	30	3.4	12.5	2.2	1.49	0.51	0.0592	2.52	0.5507	100.5689	325.1	33.9
K53-30-mz5-7	0.176	30.5	0.685	1.37	14.5	30	3.4	12.5	2.2	1.49	0.51	0.0638	2.93	0.6068	100.9622	308.7	30.8
K53-30-mz5-8	0.176	30.5	0.685	1.31	14.5	30	3.4	12.5	2.2	1.49	0.51	0.0658	3.16	0.6465	101.1752	296.6	29.1
K53-30-mz5-9	0.12	30.5	0.71	2.11	14.8	31	3.4	11.4	1.5	1.1	0.59	0.0557	2.27	0.6121	100.1983	310.1	32.1
K53-30-mz6-1	0.33	30.5	1	0.3119	14.6	29.9	3.2	11.6	1.9	1.1	0.5	0.0771	4.23	0.4785	99.7613	315.4	28.4
K53-30-mz6-2	0.37	30.2	1	0.1208	13.3	28	3.2	11.5	1.9	1.7	0.6	0.1033	6.27	0.6366	98.9486	293.5	20
K53-30-mz6-3	0.37	30.2	1	0.3057	13.3	28	3.2	11.5	1.9	1.7	0.6	0.0966	5.68	0.7503	98.6473	282.3	20.6
K53-30-mz6-4	0.33	30.5	1	1.1506	14.6	29.9	3.2	11.6	1.9	1.1	0.5	0.095	4.98	0.6934	101.5937	310.9	21.9
K53-30-mz6-5	0.33	30.5	1	0.9727	14.6	29.9	3.2	11.6	1.9	1.1	0.5	0.0867	4.54	0.6202	100.8898	313.4	23.9
K53-30-mz6-6	0.33	30.5	1	1.2242	14.6	29.9	3.2	11.6	1.9	1.1	0.5	0.0841	4.56	0.6952	101.2355	292.3	22.9
K53-30-mz6-7	0.33	30.5	1	0.9309	14.6	29.9	3.2	11.6	1.9	1.1	0.5	0.1007	5.16	0.777	101.6433	310.5	20.8
K53-30-mz6-8	0.33	30.5	1	1.0882	14.6	29.9	3.2	11.6	1.9	1.1	0.5	0.0946	4.89	0.7362	101.4826	307.9	21.6
K53-30-mz6-9	0.33	30.5	1	1.0684	14.6	29.9	3.2	11.6	1.9	1.1	0.5	0.089	4.83	0.7462	101.4066	290.8	21.9
K53-30-mz6-10	0.33	30.5	1	0.7116	14.6	29.9	3.2	11.6	1.9	1.1	0.5	0.0857	4.94	0.6899	101.0988	282.9	22.4
K53-30-mz6-11	0.33	30.5	1	0.476	14.6	29.9	3.2	11.6	1.9	1.1	0.5	0.0908	5.29	0.7177	101.2473	282.6	21.6
K53-30-mz7-1	0.176	30.5	0.685	0.5746	14.5	30	3.4	12.5	2.2	1.49	0.51	0.0809	3.77	0.8655	101.2838	291.5	25.2
K53-30-mz7-2	0.176	30.5	0.685	0.5111	14.5	30	3.4	12.5	2.2	1.49	0.51	0.0802	3.81	0.8568	101.2508	288.6	25.2
K53-30-mz7-3	0.176	30.5	0.685	0.5163	14.5	30	3.4	12.5	2.2	1.49	0.51	0.0761	3.77	0.8697	101.2246	274.1	25.2
K53-30-mz7-4	0.176	30.5	0.685	0.7369	14.5	30	3.4	12.5	2.2	1.49	0.51	0.0765	3.69	0.8358	101.3326	283.4	25.5
K53-30-mz7-5	0.176	30.5	0.685	1.64	14.5	30	3.4	12.5	2.2	1.49	0.51	0.0732	3.25	0.522	101.4809	349.8	29.4

K53-30-mz7-6	0.33	30.5	1	0.8039	14.6	29.9	3.2	11.6	1.9	1.1	0.5	0.0888	5.15	0.5871	101.3035	298.1	22.7
K53-30-mz7-7	0.176	30.5	0.685	0.6111	14.5	30	3.4	12.5	2.2	1.49	0.51	0.0819	3.67	0.8366	101.1919	304	25.8
K53-30-mz7-8	0.176	30.5	0.685	0.57	14.5	30	3.4	12.5	2.2	1.49	0.51	0.0868	3.77	0.885	101.3046	309.6	24.9
K53-30-mz7-9	0.33	30.5	1	0.6405	14.6	29.9	3.2	11.6	1.9	1.1	0.5	0.074	4.13	0.6325	100.1419	283.6	26.1
K53-30-mz7-10	0.37	30.2	1	0.4244	13.3	28	3.2	11.5	1.9	1.7	0.6	0.1007	6.28	0.4922	99.1171	302.4	20.7
K53-30-mz7-11	0.33	30.5	1	0.849	14.6	29.9	3.2	11.6	1.9	1.1	0.5	0.0886	4.4	0.5488	100.5547	338.9	25.6
K53-30-mz7-12	0.176	30.5	0.685	1.0987	14.5	30	3.4	12.5	2.2	1.49	0.51	0.0571	3.61	0.4316	101.1924	270.2	30.3
K53-30-mz8-1	0.12	30.5	0.71	0.4137	14.8	31	3.4	11.4	1.5	1.1	0.59	0.0495	2.19	0.5037	98.2961	306.8	42.8
K53-30-mz8-2	0.176	30.5	0.685	0.4404	14.5	30	3.4	12.5	2.2	1.49	0.51	0.0705	2.86	0.547	99.9032	359.4	35.8
K53-30-mz8-3	0.176	30.5	0.685	0.9689	14.5	30	3.4	12.5	2.2	1.49	0.51	0.0813	2.85	0.641	100.5297	389.1	31.6
K53-30-mz8-4	0.176	30.5	0.685	1.54	14.5	30	3.4	12.5	2.2	1.49	0.51	0.0707	2.55	0.6326	100.7831	363	32.4
K53-30-mz8-5	0.176	30.5	0.685	1.95	14.5	30	3.4	12.5	2.2	1.49	0.51	0.0618	2.48	0.6142	101.0979	327.1	31.9
K53-30-mz8-6	0.12	30.5	0.71	0.3961	14.8	31	3.4	11.4	1.5	1.1	0.59	0.0623	2.21	0.5408	98.3484	370.9	40.9
K53-30-mz8-7	0.176	30.5	0.685	0.3907	14.5	30	3.4	12.5	2.2	1.49	0.51	0.0714	3.04	0.6099	100.0983	336.4	32.7
K53-30-mz8-8	0.176	30.5	0.685	0.8059	14.5	30	3.4	12.5	2.2	1.49	0.51	0.0665	2.99	0.7161	100.567	296.9	30.7
K53-30-mz8-9	0.176	30.5	0.685	0.9399	14.5	30	3.4	12.5	2.2	1.49	0.51	0.0624	2.78	0.6363	100.4063	305	32.8
K53-30-mz8-10	0.176	30.5	0.685	1.48	14.5	30	3.4	12.5	2.2	1.49	0.51	0.0826	2.89	0.7101	101.1547	375.2	28.9
K59.90-mz1-1	0.2084	30.41	0.836	0.2807	14.96	30.36	3.36	12.65	2.15	1.52	0.273	0.0879	4.01	0.6239	101.5294	344.4	26.9
K59.90-mz1-2	0.2269	30.41	0.892	0.2697	14.69	30.07	3.33	12.59	2.19	1.55	0.2315	0.0882	4.4	0.6729	101.3904	317.1	25.2
K59.90-mz1-3	0.1433	30.6	0.5725	0.2343	16.06	31.69	3.41	12.76	2.06	1.37	0.1899	0.0443	2.57	0.499	102.0601	251.4	39.5
K59.90-mz1-4	0.1293	30.67	0.4606	0.1988	16.08	32.07	3.49	13.04	2.07	1.36	0.2091	0.0422	2.01	0.398	102.0987	302.8	50
K59.90-mz1-5	0.1315	30.68	0.5098	0.2172	16.03	31.78	3.45	12.84	2.03	1.35	0.2027	0.0447	2.16	0.5018	101.806	279.8	44
K59.90-mz1-6	0.2691	30.42	0.9648	0.2777	14.55	29.72	3.33	12.59	2.09	1.53	0.2561	0.0893	4.82	0.7284	101.3682	294.6	23.2
K59.90-mz1-7	0.1357	30.68	0.5184	0.2435	15.92	31.78	3.5	12.84	2	1.36	0.2053	0.0407	2.37	0.4416	101.9036	254.2	43.2
K59.90-mz1-8	0.1669	30.61	0.6907	0.2647	15.55	31.3	3.39	12.75	2.1	1.49	0.2434	0.0661	3.27	0.5344	102.2778	312.9	32.8
K59.90-mz1-9	0.1753	30.59	0.6611	0.2604	15.45	30.88	3.4	12.69	2.02	1.45	0.1928	0.0623	3.44	0.5171	101.6181	288.5	33
K59.90-mz2-1	0.3307	30.18	0.9242	0.1619	14.68	30.05	3.35	12.68	2.07	1.38	0.1066	0.0848	5.54	0.5336	101.7411	276.3	23.5
K59.90-mz2-2	0.2504	30.39	0.7798	0.1637	15.14	30.7	3.37	12.65	2.03	1.38	0.1414	0.0661	4.39	0.5151	101.7204	258.9	28.2
K59.90-mz2-3	0.3799	30.12	1.012	0.1583	14.5	29.65	3.31	12.47	2.02	1.31	0.1342	0.0877	6.12	0.5868	101.4965	259.3	21.3
K59.90-mz2-4	0.1197	30.89	0.9531	2.98	13.83	27.73	2.99	11.47	1.96	2.34	1.25	0.0745	4.76	0.5649	101.7936	267.9	20.8
K59.90-mz2-5	0.1532	30.82	0.9327	2.25	14.24	28.56	3.16	11.78	2.04	2.04	0.9387	0.0743	4.82	0.5235	102.1898	270.3	22.1
K59.90-mz2-6	0.4576	30.04	1.1582	0.1723	14.16	29.06	3.24	12.41	2.02	1.4	0.0729	0.0979	7.11	0.5891	101.5363	257.2	19

K59.90-mz2-7	0.4368	30.02	1.1254	0.1568	14.1	28.84	3.21	12.09	2.05	1.38	0.1135	0.1064	6.91	0.5581	100.6673	288.9	19.4
K59.90-mz2-8	0.2674	30.2	0.8337	0.1604	15.11	30.39	3.34	12.44	2.06	1.42	0.1037	0.0783	4.7	0.5506	101.3918	285.9	26.3
K59.90-mz2-9	0.4198	30.05	1.1247	0.3457	14.46	29.02	3.25	12.22	2.02	1.44	0.1835	0.1104	6.99	0.6064	101.8206	291.7	18.8
K63.120-mz1-1	0.0946	30.29	0.4562	0.1648	15.66	31.5	3.5	13.09	2.12	1.34	0.2073	0.0456	1.77	0.7267	100.9788	262.7	42.4
K63.120-mz1-2	0.0644	30.22	0.3315	0.1377	16.03	32.01	3.5	13.33	2.16	1.3	0.1028	0.0275	1.19	0.5964	101.0131	210.4	56.5
K63.120-mz1-3	0.0864	30.21	0.4484	0.1641	15.6	31.3	3.48	12.9	2.15	1.32	0.1286	0.0503	1.72	0.7807	100.3596	281	40.9
K63.120-mz1-4	0.0775	30.23	0.4114	0.1522	15.77	31.47	3.45	12.64	2.09	1.29	0.1431	0.0455	1.56	0.7676	100.1166	267.2	43.2
K63.120-mz1-5	0.0707	30.32	0.3871	0.1145	15.97	31.98	3.54	13.06	2.11	1.19	0.0204	0.0375	1.44	0.6503	100.9013	251.3	49.6
K63.120-mz1-6	0.0641	30.3	0.3089	0.0766	16.65	32.58	3.47	12.84	1.97	1.092	0.0398	0.0299	1.0382	0.4695	100.9395	277.7	67.9
K63.120-mz1-7	0.0908	30.2	0.4875	0.2022	15.73	31.16	3.32	12.58	2	1.27	0.1894	0.0556	2.03	0.6809	100.0178	311	39.6
K63.120-mz1-8	0.0856	30.24	0.3676	0.1469	15.85	31.97	3.46	13.14	2.17	1.27	0.1034	0.0499	1.43	0.6519	100.9463	333.1	48.2
K63.120-mz1-9	0.084	30.33	0.4169	0.1394	15.66	31.5	3.44	13.15	2.15	1.32	0.0381	0.0419	1.57	0.7121	100.5665	256.8	45.2
K63.120-mz1-10	0.0804	30.28	0.3511	0.1264	15.76	31.86	3.41	12.72	2.1	1.2	0.034	0.0387	1.47	0.6309	100.0728	261.6	50.9
K63.120-mz2-1	1.404	28.73	2.3	1.45	12.82	22.53	2.16	8.1	1.35	2	0.5925	0.2557	15.66	0.5709	100.056	344.8	9.2
K63.120-mz2-2	1.4654	28.33	2.2	1.4	12.83	22.85	2.28	8.05	1.43	1.94	0.6215	0.249	15.25	0.5555	99.582	344.8	9.4
K63.120-mz2-3	1.1153	28.87	2.23	1.46	13.08	23.45	2.31	8.25	1.4	2.01	0.6929	0.2181	14.03	0.5378	99.7741	326.7	10.1
K63.120-mz2a-1	1.3934	28.31	2.47	1.49	12.45	22.15	2.28	8.01	1.41	2	0.6051	0.2622	16.23	0.6136	99.8162	339.9	8.8
K63.120-mz2a-2	1.295	28.76	2.47	1.6	12.47	22.28	2.29	8.12	1.46	2.08	0.705	0.2387	15.49	0.5881	99.9781	324.2	9.3
K63.120-mz2a-3	1.0319	29.11	1.97	1.46	13.66	24.52	2.47	8.81	1.54	2.15	0.6796	0.1917	12.49	0.4603	100.6444	324	11.4
K63.120-mz3-1	1.4071	29.03	2.44	1.68	12.08	21.39	2.17	7.71	1.35	2.01	0.6697	0.2579	15.84	0.617	98.79	341.4	9
K63.120-mz3-2	1.2422	28.91	2.13	1.53	13.21	23.02	2.32	7.99	1.36	1.95	0.6526	0.2334	14.28	0.5096	99.4577	346	10
K63.120-mz3-3	1.0485	29.05	2	1.51	13.71	24.07	2.35	8.47	1.45	2.1	0.6819	0.2063	12.87	0.5057	100.1364	335.9	11
K63.120-mz3-4	1.4731	28.51	2.23	1.99	12.01	21.96	2.21	8.09	1.42	2.13	0.8358	0.2415	15.35	0.593	99.1814	330.4	9.2
K63.120-mz3-5	1.109	29.02	2.02	1.7	13	23.46	2.31	8.65	1.54	2.12	0.7767	0.2161	13	0.5289	99.5599	346.9	10.7
K63.120-mz3-6	0.8616	29.15	1.81	1.53	13.98	24.57	2.43	8.65	1.52	2.12	0.7335	0.1776	11.51	0.4791	99.6282	321.3	12.1
K63.120-mz4-1	0.0802	30.39	0.3118	0.1721	15.67	31.72	3.49	13.04	2.1	1.28	0.1896	0.0315	1.59	0.4984	100.5782	234.1	54.2
K63.120-mz4-2	0.0836	29.95	0.3568	0.1923	15.7	31.8	3.49	13.19	2.1	1.32	0.1589	0.0358	1.56	0.5092	100.4588	264.6	54
K63.120-mz4-3	0.0914	30.05	0.349	0.1693	15.72	31.77	3.54	13.21	2.16	1.31	0.1758	0.0371	1.49	0.5904	100.6825	259.5	51.4
K63.120-mz4-4	0.1133	29.95	0.4478	0.2056	15.63	31.34	3.48	12.91	2.05	1.33	0.1988	0.0377	2.24	0.5395	100.4945	225.1	43
K63.120-mz4-5	0.0842	30.13	0.3454	0.1391	15.77	31.84	3.54	13.18	2.11	1.18	0.138	0.0387	1.57	0.5425	100.6294	276	52.5
K63.120-mz4-6	0.1809	29.92	0.6941	0.2196	15.3	30.82	3.43	12.83	1.98	1.28	0.1635	0.0691	3.99	0.5283	101.416	287	29.6
K63.120-mz4-7	0.0946	30.12	0.4411	0.2351	15.45	31.32	3.53	13.1	2.1	1.33	0.1596	0.0462	1.98	0.5743	100.492	285	44.8

K63.120-mz4-8	0.0716	30.07	0.3724	0.2139	15.56	31.66	3.54	13.29	2.08	1.26	0.198	0.042	1.71	0.5226	100.583	292.7	50.4
K63.120-mz4-9	0.1157	30.06	0.5113	0.2139	15.1	31.22	3.49	13	2.05	1.25	0.1727	0.0666	2.58	0.5503	100.384	360.4	38.4
K63.120-mz4-10	0.0801	30.15	0.3481	0.2017	15.63	31.69	3.54	13.28	2.1	1.29	0.1644	0.0353	1.58	0.5274	100.615	254.8	53.1
K63.120-mz4-11	0.0761	30.04	0.3245	0.1266	15.83	31.79	3.48	13.1	2.07	1.23	0.1526	0.0423	1.39	0.5841	100.191	305.7	53.6
K63.120-mz4-12	0.0799	30.15	0.3697	0.2221	15.61	31.75	3.49	13.1	2.07	1.28	0.1724	0.0426	1.66	0.5508	100.537	293	50.2
K63-120-mz6-1	0.0551	30.65	1.0324	0.1926	14.52	29.09	3.29	12.06	1.87	1.1067	0.0469	0.0926	3.3	1.314	98.6445	290.6	23.4
K63-120-mz6-2	0.0471	30.85	1.0323	0.226	14.44	29.37	3.22	11.88	1.86	1.1421	0.1214	0.0893	3.5	1.2331	99.037	282.6	23.6
K63-120-mz6-3	0.0423	30.7	0.9705	0.1802	14.55	29.44	3.21	12.05	1.88	1.0747	0.0805	0.0719	3.07	1.2751	98.6178	237.8	24.9
K63-120-mz6-4	0.0484	30.75	1.0463	0.2039	14.66	29.29	3.15	11.93	1.86	1.11	0.1051	0.0874	3.49	1.2131	98.9699	279.5	23.5
K63-120-mz6-5	0.0388	30.68	0.9653	0.1893	14.71	29.69	3.17	12.26	1.86	1.1002	0.1749	0.0771	3.07	1.2151	99.2234	261.5	25.4
K63-120-mz6-6	0.0428	30.73	0.9487	0.2023	14.77	29.48	3.26	12.03	1.94	1.18	0.0949	0.0798	3.03	1.2554	99.0663	267.1	25.1
K63-120-mz6-7	0.0373	30.65	0.9763	0.1825	14.74	29.52	3.27	12.12	1.94	1.089	0.0684	0.0813	3.09	1.2451	99.0325	271	24.8
K63-120-mz6-8	0.0379	30.75	0.965	0.1981	14.74	29.35	3.22	12.15	1.93	1.1251	0.0664	0.0868	3.12	1.2449	99.0073	288	24.7
K63-120-mz6-9	0.0356	30.75	0.962	0.1984	14.87	29.43	3.23	12.04	1.91	1.18	0.0973	0.1055	3.09	1.2451	99.1667	349.9	24.2
K63-120-mz6-10	0.0381	30.73	0.9808	0.2406	14.94	29.37	3.22	11.93	1.92	1.16	0.1364	0.0861	3.29	1.154	99.2206	290.5	24.8
K63-120-mz6-11	0.0482	30.71	1.0174	0.2059	14.47	29.5	3.3	12.08	1.94	1.16	0.1194	0.086	3.26	1.3342	99.2552	269.4	23.5
K103.20-mz1-1	0.5568	29.96	1.62	0.6696	13.36	27.25	3.01	11.44	1.96	1.64	0.3926	0.1313	8.89	0.5963	101.5544	287.2	15
K103.20-mz1-2	0.4885	30.18	1.3461	0.6419	14.05	28.37	3.18	11.78	1.96	1.67	0.3197	0.1153	7.34	0.471	101.9758	307.6	18
K103.20-mz1-3	0.5167	30.14	1.5	0.6596	13.62	27.63	3.13	11.54	1.98	1.65	0.3938	0.1298	8.07	0.5339	101.5557	313.2	16.3
K103.20-mz1-4	0.4644	30.09	1.3773	0.6478	14	28.25	3.16	11.89	1.96	1.62	0.306	0.1204	7.33	0.4832	101.7591	319.9	17.9
K103.20-mz2-1	0.0828	30.42	0.9221	0.2229	14.93	30.12	3.39	12.39	1.95	1.092	0.1728	0.0989	3.49	1.2522	100.5637	310.5	22.7
K103.20-mz2-2	0.1043	30.39	1.1425	0.0578	15.46	30.24	3.18	11.71	1.72	0.8924	0.0688	0.1157	4.24	1.4984	100.8559	301.4	19.2
K103.20-mz2-3	0.0903	30.53	1.0049	0.0642	15.71	30.9	3.31	11.88	1.76	0.8263	0.0519	0.096	3.79	1.2707	101.3145	288.1	22.1
K103.20-mz2-4	0.1636	30.36	0.7242	0.2684	15.43	31.09	3.38	12.64	1.93	1.16	0.1905	0.0673	3.3	0.5946	101.3287	305	31.6
K103.20-mz2-5	0.1445	30.34	0.8216	0.1481	15.7	30.99	3.35	12.26	1.79	0.9442	0.0898	0.0821	3.48	0.8283	100.9942	315.4	27.3
K103.20-mz2-6	0.1659	30.43	0.5376	0.5823	15.39	31.12	3.38	12.72	2.03	1.34	0.2546	0.0478	2.56	0.3944	100.9798	295.2	40.6
K103.20-mz2-7	0.1539	30.35	0.5491	0.4747	15.64	31.17	3.42	12.54	2.02	1.29	0.2422	0.0486	2.58	0.4093	100.9142	294.5	40.6
K103.20-mz2-8	0.1907	30.38	0.5344	0.6164	15.48	30.87	3.43	12.72	2.01	1.37	0.3325	0.0477	2.58	0.4297	101.0223	284.4	39.4
K103-20A-mz2-1	0.1695	30.71	0.8202	0	15.41	30.71	3.35	12.08	1.79	0.7096	0.0534	0.0641	3.74	0.5163	100.1491	280.6	32
K103-20A-mz2-2	0.2123	30.63	0.9467	0.0257	15.38	30.36	3.26	11.72	1.75	0.7707	0.0209	0.0887	4.26	0.5307	99.9858	350.4	28.2
K103-20A-mz2-	0.1426	30.74	0.8719	0.1828	15.16	30.59	3.34	12.08	1.78	0.8848	0.0548	0.0724	3.89	0.4797	100.2973	314.4	30.5

3																	
K103-20A-mz2-4	0.1521	30.76	0.6708	0.2912	15.34	30.67	3.36	12.76	1.96	1.22	0.1813	0.0546	3.14	0.3875	100.9711	294.2	37.7
K103-20A-mz2-5	0.2266	30.69	0.9965	0.1869	15.28	30.11	3.29	12.03	1.74	0.7402	0.0685	0.0809	4.62	0.4383	100.5312	316.6	27.6
K103-20A-mz2-6	0.2077	30.71	0.8799	1.32	14.01	28.82	3.17	12.2	2.08	1.86	0.5895	0.0703	4.27	0.4118	100.6368	296.8	27.4
K103-20A-mz2-7	0.1224	30.82	0.5885	0.5675	14.94	30.79	3.44	12.65	2.02	1.41	0.286	0.0467	2.6	0.3758	100.6784	290	41.9
K103-20A-mz2-8	0.1671	30.65	0.7907	0.3154	15.65	30.62	3.33	12.12	1.81	0.9703	0.2098	0.0617	3.79	0.3937	100.9071	288.3	32.4
K103-20A-mz3-1	0.1525	30.56	0.9453	0.106	14.89	30.05	3.29	12.22	1.91	0.9438	0.0986	0.0756	3.97	0.7462	99.9866	280.7	26.6
K103-20A-mz3-2	0.1634	30.43	0.9591	0.1617	15.05	30.07	3.22	12.18	1.83	0.968	0.1252	0.0871	4.08	0.7932	100.1472	310	25.6
K103-20A-mz3-3	0.1763	30.56	0.7478	1.1343	14.45	29.42	3.27	12.12	2.05	1.63	0.5037	0.0631	3.41	0.4978	100.0637	297.6	30.6
K103-20A-mz3-4	0.1438	30.58	0.9361	0.0653	15.37	30.46	3.39	12.11	1.79	0.8106	0.0787	0.0812	3.91	0.7553	100.5086	302.6	26.8
K103-20A-mz3-5	0.2427	30.49	0.9596	1.2665	14.08	28.35	3.18	11.78	2	1.73	0.7237	0.0727	4.71	0.4751	100.1009	275.7	24.5
K103-20A-mz3-6	0.1358	30.66	1.256	0.491	14.59	29.19	3.11	11.32	1.69	1.0797	0.2082	0.0929	5.18	0.9138	99.9567	270.7	20.7
K103-20A-mz3-7	0.0572	30.77	1.2017	0.135	14.85	29.67	3.29	11.67	1.64	0.8242	0.0609	0.0978	4.61	1.0348	99.9447	291.1	21.5
K103-20A-mz3-8	0.2356	30.5	0.9984	1.1081	14.2	28.52	3.21	11.82	1.97	1.67	0.482	0.0955	4.9	0.491	100.2414	347.4	24
K103-20A-mz3-9	0.1252	30.59	1.0114	0.0635	15.32	30.25	3.34	12.02	1.73	0.8024	0.0369	0.084	4.1	0.8745	100.3769	287.3	25.1
K103-20A-mz3-10	0.129	30.73	1.0602	0.7491	14.44	28.93	3.21	11.92	1.86	1.27	0.3558	0.0809	4.41	0.8123	99.9926	272.4	23.2
m54-83-mz1-1	0.015	29.8	1.023	0.89	14.83	29.86	3.23	12.26	1.97	1.37	0.304	0.0935	4	0.9204	100.601	316.8	27.7
m54-83-mz1-2	0.019	30	1.046	0.905	14.84	29.66	3.25	12.1	2	1.43	0.318	0.0922	4.08	0.9229	100.704	308.8	27.5
m54-83-mz1-3	0.029	29.9	1.029	0.905	14.57	29.78	3.23	12.41	2.04	1.43	0.313	0.0983	4.05	0.9251	100.744	329.8	28.3
m54-83-mz1-4	0.027	29.82	1.031	0.905	14.66	29.83	3.24	12.07	2.03	1.35	0.299	0.0873	4.05	0.9151	100.354	294.8	27.4
m54-83-mz1-5	0.027	29.86	1.016	0.928	14.8	29.76	3.21	12.32	2.04	1.4	0.343	0.0884	3.89	0.877	100.602	311	28.7
m54-83-mz1-6	0.026	29.83	1.028	0.943	14.61	29.86	3.25	12.3	1.99	1.41	0.363	0.0923	3.93	0.8908	100.558	320.3	28.3
m54-83-mz1-7	0.022	29.83	1.024	0.957	14.73	29.96	3.3	12.4	2.02	1.38	0.292	0.0871	3.96	0.8986	100.902	300.3	28
m54-83-mz1-8	0.021	29.85	1.009	0.938	14.8	30.01	3.23	12.25	2.01	1.42	0.321	0.0944	3.89	0.883	100.766	330.6	28.8
m54-83-mz1-9	0.027	29.87	1.033	1.034	14.6	29.76	3.24	12.14	1.99	1.45	0.347	0.1005	4.02	0.9353	100.583	337	27.6

m54-83-mz1-10	0.02	29.79	1.022	0.945	14.65	29.78	3.31	12.29	1.98	1.37	0.324	0.0793	3.92	0.8998	100.421	275.1	27.7
m54-83-mz1-11	0.027	29.84	1.04	1.059	14.75	29.68	3.15	12.23	2.04	1.46	0.307	0.0863	4.05	0.8931	100.654	294.4	27.7
m54-83-mz1-12	0.022	29.72	0.998	0.946	14.69	29.89	3.3	12.38	2.06	1.4	0.267	0.0813	3.89	0.883	100.564	285.6	28.4
m54-83-mz1-13	0.022	29.67	1.001	0.924	14.8	29.92	3.23	12.34	2.04	1.38	0.387	0.0807	3.78	0.8795	100.488	288.5	28.9
m54-83-mz2-1	0.502	29.02	1.5	1.122	12.5	26.45	2.89	11.13	1.96	1.82	0.629	0.1417	8.25	0.7352	98.729	315.1	18.7
m54-83-mz2-2	0.495	29.39	1.51	1.184	13.09	27.3	2.97	11.3	1.96	1.92	0.627	0.1332	8.29	0.75	100.994	294	18.4
m54-83-mz2-3	0.419	29.33	1.323	0.919	13.12	27.96	3.11	11.79	2.01	1.73	0.506	0.1244	7.03	0.6339	100.069	323.7	22.1
m54-83-mz2-4	0.054	29.96	0.998	1.76	14.01	29.27	3.14	12.17	2.07	1.34	0.487	0.0752	4.28	0.4729	100.14	306.1	30.2
m54-83-mz2-5	0.05	30.06	1.046	1.75	13.93	29.26	3.19	12.26	2.06	1.39	0.409	0.071	4.4	0.4853	100.407	281.7	29.4
m54-83-mz2-6	0.209	29.5	0.823	0.41	14.5	30.19	3.3	12.49	2.12	1.35	0.209	0.0732	4.24	0.5021	99.95	295.3	33.1
m54-83-mz2-7	0.376	29.24	1.176	0.79	13.48	28.8	3.15	12.03	2	1.62	0.392	0.1167	6.79	0.6331	100.658	312.3	22.2
m54-83-mz2-8	0.199	29.55	0.894	0.462	14.25	29.88	3.26	12.47	2.17	1.4	0.281	0.0845	4.4	0.6552	99.994	306.7	30.5
m54-83-mz2-9	0.232	29.34	1.035	0.932	13.68	29	3.25	12.36	2.14	1.73	0.517	0.1011	5.12	0.6803	100.162	326.2	26.5
m54-83-mz2-10	0.241	29.36	1.097	1.013	13.73	28.8	3.1	11.91	2.06	1.78	0.57	0.1048	5.49	0.7003	100.003	319.4	25.5
m54-83-mz2-11	0.205	29.54	0.958	0.685	13.99	29.62	3.19	12.2	2.17	1.49	0.318	0.0847	4.58	0.6273	99.704	303.3	29.3
m54-83-mz2-12	0.204	29.48	0.889	1.033	14.15	29.96	3.24	12.41	2.12	1.86	0.5	0.0898	4.9	0.6025	101.48	310.2	28.3
m54-83-mz2-13	0.19	29.42	0.896	0.651	14.29	29.86	3.25	12.55	2.12	1.37	0.351	0.0845	4.3	0.6278	100.006	315.6	30.6
m54-83-mz2-14	0.174	29.34	0.779	0.813	14.19	29.93	3.3	12.54	2.15	1.69	0.447	0.0653	3.85	0.5572	99.865	273.7	33.1
m54-83-mz3-1	0.262	29.55	1.135	1.258	13.47	27.95	3.02	11.77	2	1.86	0.644	0.1038	5.66	0.7114	99.447	308.5	24.2
m54-83-mz3-2	0.376	29.39	1.64	1.64	12.32	26.11	2.82	11.05	1.99	2.13	0.689	0.1589	8.43	1.0443	99.864	318.1	17
m54-83-mz3-3	0.399	29.35	1.6	1.65	12.31	26.24	2.84	10.94	1.99	2.17	0.646	0.1548	8.41	0.9584	99.738	318	17.3
m54-83-mz3-4	0.242	29.28	0.962	0.637	13.79	29.16	3.19	12.22	2.03	1.43	0.349	0.0912	5.03	0.6028	99.056	308.9	28.2
m54-83-mz3-5	0.031	29.78	0.949	2.47	13.64	28.17	3.02	11.73	2.08	1.87	0.876	0.0661	4	0.5535	99.281	270.3	28.7
m54-83-mz3-6	0.446	29.49	1.82	1.76	11.91	25.16	2.78	10.92	1.94	2.18	0.732	0.174	9.5	1.1082	100.007	314.3	15.4
m54-83-mz3-7	0.224	29.51	1	1.128	13.83	28.9	3.19	12.09	2.02	1.84	0.531	0.0941	4.92	0.5794	99.901	327.4	28.1
m54-83-mz3-8	0.04	29.92	0.913	2.32	14	28.87	3.05	11.89	2.06	1.78	0.7	0.0694	3.8	0.5296	99.987	297.9	30.5
m54-83-mz3-9	0.039	29.73	0.963	2.36	13.7	28.36	2.97	11.85	2.07	1.85	0.789	0.0717	4.05	0.5742	99.425	287.3	28.2
m54-83-mz3-10	0.338	29.29	1.42	1.56	12.71	26.96	2.93	11.49	2.03	2.12	0.697	0.1277	7.28	0.9056	99.924	295.9	19.4
m54-83-mz12-1	0.051	29.63	1.003	0.796	14.16	28.41	3.12	11.83	1.99	1.58	0.425	0.0881	4.01	1.0133	98.144	286.3	26.8
m54-83-mz12-2	0.036	29.7	1.008	0.811	14.15	28.77	3.15	11.93	1.97	1.6	0.409	0.096	4.01	1.0143	98.693	311.4	26.9
m54-83-mz12-3	0.034	29.68	1.031	0.761	14.22	28.48	3.16	11.95	2.06	1.66	0.365	0.1003	4.04	1.1182	98.697	309.8	26.1
m54-83-mz12-4	0.043	29.72	1.013	0.679	14.33	28.72	3.08	11.82	1.94	1.58	0.371	0.0845	4.2	0.8933	98.509	282.3	27.6
m54-83-mz12-5	0.035	29.68	1.05	0.715	14.18	28.58	3.09	11.96	1.99	1.65	0.327	0.0992	4.24	0.9901	98.628	315.2	26.8

m54-83-mz12-6	0.037	29.73	0.992	0.746	14.39	28.89	3.12	11.72	2.02	1.56	0.429	0.0894	4.03	0.9972	98.787	291.7	27.4
m54-83-mz12-7	0.047	29.6	1.021	0.693	14.58	28.79	3.14	11.84	1.9	1.46	0.39	0.0945	4.12	0.9427	98.656	311.9	27.2
m54-83-mz12-8	0.051	29.74	0.994	0.892	14.49	28.7	3.04	11.63	1.99	1.45	0.428	0.1007	3.9	1.1289	98.572	315.3	26.1
m54-83-mz12-9	0.106	29.74	0.638	1.53	14.38	29.02	3.12	11.99	1.87	1.71	0.64	0.0601	3.06	0.4745	98.372	309.3	38.8
m54-83-mz12-10	0.037	29.82	1.002	0.758	14.68	28.78	3.09	11.63	1.97	1.58	0.496	0.0866	3.87	1.0291	98.864	285	27.6
m54-83-mz12-11	0.049	29.82	1.058	1.109	13.9	28.37	3.12	11.98	2	1.61	0.39	0.0961	3.95	1.3387	98.827	275.3	23.6

Sample	**Si**	**P**	**Ca**	**Y**	**La**	**Ce**	**Pr**	**Nd**	**Sm**	**Gd**	**Dy**	**Pb**	**Th**	**U**
k-ratio errors (1σ %)														
K31.0-mz1-1	8.77	0.24	0.92	0.40	0.64	0.44	1.35	0.78	1.46	1.96	5.08	4.78	0.59	1.05
K31.0-mz1-2	8.63	0.24	0.94	0.40	0.64	0.45	1.36	0.77	1.43	1.84	5.16	5.20	0.60	1.08
K31.0-mz1-3	9.35	0.24	0.93	0.41	0.64	0.44	1.33	0.77	1.40	1.80	4.90	5.56	0.60	1.10
K31.0-mz1-4	6.89	0.24	0.89	0.41	0.65	0.45	1.36	0.79	1.47	1.95	5.02	4.82	0.59	1.00
K31.0-mz1-5	3.84	0.24	0.87	0.39	0.65	0.45	1.31	0.77	1.39	1.77	4.76	4.64	0.59	0.99
K31.0-mz1-6	8.39	0.24	0.90	0.38	0.65	0.45	1.33	0.76	1.40	1.78	4.67	4.83	0.59	1.00
K31.0-mz1-7	3.01	0.24	0.78	0.65	0.65	0.45	1.37	0.78	1.31	2.41	10.64	4.53	0.47	1.60
K31.0-mz1-8	7.34	0.24	0.82	1.02	0.63	0.44	1.33	0.78	1.61	2.89	16.18	5.02	0.56	0.87
K31.0-mz1-9	7.03	0.24	0.87	0.39	0.65	0.45	1.32	0.77	1.44	1.86	4.62	4.55	0.56	0.93
K31.0-mz1-10	7.65	0.24	0.90	0.38	0.65	0.44	1.31	0.77	1.41	1.84	4.94	5.22	0.60	0.99
K31.0-mz2-1	1.63	0.24	0.73	1.11	0.65	0.45	1.40	0.81	1.36	1.55	11.22	4.19	0.46	1.29
K31.0-mz2-2	6.62	0.24	0.88	2.16	0.63	0.44	1.29	0.76	1.44	2.72	24.26	6.00	0.59	0.96
K31.0-mz3-1	6.51	0.24	0.94	0.60	0.63	0.44	1.34	0.76	1.41	2.21	7.98	5.77	0.60	1.00
K31.0-mz3-2	4.74	0.24	1.09	1.40	0.62	0.43	1.30	0.75	1.36	2.84	18.25	7.50	0.66	1.49
K31.0-mz3-3	7.41	0.24	0.87	0.80	0.63	0.44	1.32	0.76	1.46	2.68	11.78	4.86	0.60	0.86
K31.0-mz3-4	7.37	0.24	0.97	0.59	0.62	0.44	1.31	0.76	1.39	2.21	7.46	5.97	0.63	1.07
K31.0-mz3-5	7.15	0.24	0.82	0.38	0.65	0.45	1.35	0.78	1.46	1.97	4.89	4.24	0.55	0.91
K31.0-mz3-6	7.21	0.24	0.89	0.41	0.64	0.44	1.34	0.78	1.49	1.94	4.83	5.16	0.59	1.02
K31.0-mz3-7	5.67	0.24	0.91	0.41	0.64	0.44	1.33	0.77	1.40	1.88	5.07	5.23	0.59	1.08
K31.0-mz3-8	4.23	0.24	0.96	0.87	0.63	0.44	1.28	0.76	1.37	2.35	11.85	5.49	0.59	1.16
K31.0-mz3-9	4.27	0.24	1.02	0.83	0.63	0.44	1.29	0.76	1.39	2.42	10.27	6.23	0.61	1.33

k38-30-mz2-1	1.82	0.32	0.91	0.72	0.65	0.49	1.34	0.84	1.49	2.03	8.75	6.97	0.60	1.96
k38-30-mz2-2	1.81	0.24	0.95	0.69	0.6	0.42	1.33	0.76	1.42	1.87	7.51	6.33	0.61	2.10
k38-30-mz2-3	1.66	0.24	0.84	0.64	0.61	0.43	1.37	0.77	1.43	1.81	6.44	6.32	0.59	1.67
k38-30-mz2-4	1.62	0.24	0.8	0.65	0.6	0.43	1.33	0.76	1.41	1.82	7.84	5.4	0.54	1.45
k38-30-mz2-5	1.66	0.24	0.83	0.66	0.6	0.43	1.38	0.77	1.44	1.84	6.37	5.08	0.56	1.51
k38-30-mz2-6	1.47	0.24	0.79	0.67	0.6	0.42	1.36	0.77	1.47	1.85	6.72	5.07	0.53	1.64
k38-30-mz2-7	1.42	0.24	0.77	0.66	0.6	0.43	1.38	0.78	1.45	1.81	6	5	0.51	1.57
k38-30-mz2-8	1.32	0.24	0.74	0.64	0.6	0.43	1.39	0.78	1.44	1.77	6.94	5.12	0.49	1.51
k38-30-mz2-9	1.51	0.24	0.75	0.64	0.61	0.43	1.37	0.78	1.42	1.79	6.4	4.72	0.51	1.35
k38-30-mz2-10	2.47	0.24	1.1	1.19	0.59	0.42	1.3	0.75	1.44	1.99	12.04	7.69	0.72	2.34
k38-30-mz2-11	1.45	0.24	0.85	0.71	0.6	0.42	1.37	0.77	1.44	1.82	6.64	5.77	0.52	1.94
k38-30-mz2-12	1.56	0.24	0.79	0.64	0.6	0.43	1.38	0.78	1.44	1.8	6.34	5.27	0.52	1.52
k38-30-mz2-13	2.23	0.24	1	0.68	0.6	0.42	1.34	0.76	1.39	1.8	7.69	6.76	0.67	1.82
k38-30-mz2-14	2.09	0.24	1.07	0.76	0.6	0.42	1.34	0.76	1.48	2.01	7.81	7.29	0.67	2.33
k38-30-mz2-15	1.89	0.24	0.99	0.68	0.6	0.42	1.31	0.76	1.41	1.95	6.63	7.49	0.63	2.11
k38-30-mz2-16	2.01	0.24	1.04	0.72	0.59	0.42	1.31	0.76	1.44	1.97	7.43	6.82	0.66	2.35
k38-30-mz5-1	1.05	0.24	0.74	0.83	0.61	0.43	1.38	0.78	1.51	2.06	10.24	4.55	0.47	1.40
k38-30-mz5-2	4.36	0.24	0.66	4.05	0.6	0.42	1.37	0.78	1.65	3.63	33.71	3.79	0.54	0.67
k38-30-mz5-3	1.74	0.24	0.88	0.72	0.6	0.43	1.35	0.76	1.45	1.88	7.25	6.13	0.57	1.87
k38-30-mz5-4	1.9	0.24	0.96	0.91	0.59	0.42	1.37	0.77	1.44	1.98	8.52	6.59	0.61	1.79
k38-30-mz5-5	1.52	0.24	0.83	0.94	0.6	0.42	1.36	0.77	1.46	2.02	8.16	5.69	0.54	1.72
k38-30-mz5-6	1.71	0.24	0.89	0.91	0.6	0.42	1.34	0.77	1.44	1.85	9.94	6.26	0.58	1.73
k38-30-mz5-7	1.69	0.24	0.91	0.99	0.6	0.42	1.32	0.76	1.48	2.02	12.54	7.1	0.59	2.14
k38-30-mz5-8	1.83	0.24	0.98	1.02	0.59	0.42	1.32	0.76	1.48	2.02	9.73	7.76	0.62	2.15
k38-30-mz5-9	2.64	0.24	1.08	0.75	0.59	0.42	1.33	0.77	1.41	1.91	7.72	8.89	0.76	1.46
k38-30-mz5-10	2.48	0.24	1.15	1.18	0.59	0.42	1.33	0.76	1.38	2.1	12.91	9.86	0.81	1.84
k38-30-mz5-11	1.97	0.24	0.92	0.81	0.6	0.42	1.36	0.77	1.43	1.89	8.01	6.62	0.61	1.73
k38-30-mz5-12	1.89	0.24	0.93	4.57	0.59	0.42	1.33	0.76	1.43	2.59	27.64	8.13	0.62	1.99
k38-30-mz5-13	2.72	0.24	1.08	0.78	0.59	0.42	1.32	0.76	1.38	1.92	7.81	8.12	0.73	1.56
k38-30-mz6-1	1.44	0.24	0.87	0.48	0.61	0.43	1.34	0.76	1.39	1.79	5.76	5.42	0.56	2.54
k38-30-mz6-2	1.63	0.24	1.00	0.51	0.60	0.42	1.31	0.75	1.44	2.25	7.45	6.38	0.61	2.88
k38-30-mz6-3	1.58	0.24	0.94	0.51	0.60	0.42	1.30	0.76	1.46	2.25	6.13	6.44	0.59	2.81
k38-30-mz6-6	1.20	0.24	0.96	0.53	0.60	0.42	1.33	0.76	1.40	2.36	6.90	6.42	0.59	2.99

k38-30-mz6-7	0.67	0.24	1.57	0.67	0.59	0.42	1.31	0.75	1.39	2.01	7.41	7.82	0.58	6.61
k38-30-mz6-8	1.41	0.24	0.86	0.48	0.61	0.42	1.32	0.76	1.47	2.19	6.54	5.20	0.55	2.32
k38-30-mz6-9	1.57	0.24	0.89	0.51	0.60	0.42	1.35	0.76	1.44	2.23	7.72	5.32	0.57	2.31
k38-30-mz6-10	1.42	0.24	0.82	0.48	0.60	0.42	1.34	0.76	1.48	2.28	7.06	4.67	0.53	2.28
k38-30-mz6-11	1.39	0.24	0.80	0.47	0.61	0.42	1.36	0.76	1.47	2.20	6.50	4.63	0.51	2.13
k38-30-mz6-12	1.35	0.24	0.83	0.49	0.61	0.43	1.34	0.76	1.34	1.73	5.90	5.02	0.54	2.43
k38-30-mz6-13	1.50	0.24	0.87	0.48	0.60	0.42	1.32	0.76	1.45	2.11	6.09	4.93	0.55	2.44
k38-30-mz6-14	1.39	0.24	0.84	0.47	0.61	0.42	1.34	0.76	1.45	2.19	6.48	4.74	0.53	2.22
k38-30-mz6-15	1.31	0.24	0.76	0.46	0.61	0.43	1.37	0.76	1.44	2.20	6.21	4.22	0.50	2.00
k38-30-mz8-1	3.69	0.24	1.34	0.51	0.59	0.42	1.30	0.76	1.45	1.88	5.81	9.40	0.92	1.69
k38-30-mz8-2	3.14	0.24	1.24	0.49	0.59	0.42	1.31	0.76	1.42	1.83	5.19	8.50	0.81	2.16
k38-30-mz8-3	4.79	0.24	1.58	0.54	0.59	0.42	1.30	0.76	1.37	1.85	6.12	11.31	1.16	1.98
k38-30-mz8-4	2.96	0.24	1.19	1.27	0.59	0.41	1.29	0.76	1.40	2.03	14.31	8.18	0.76	2.20
k38-30-mz8-5	1.88	0.24	0.94	6.95	0.59	0.42	1.34	0.76	1.47	2.90	20.82	8.50	0.60	2.30
k38-30-mz8-6	4.63	0.24	1.47	0.58	0.59	0.42	1.28	0.76	1.38	1.90	5.59	9.94	1.05	1.98
k38-30-mz8-7	2.77	0.24	1.10	0.46	0.61	0.42	1.33	0.76	1.40	1.82	4.85	8.05	0.76	1.88
k38-30-mz8-8	2.47	0.24	1.01	0.44	0.60	0.42	1.34	0.76	1.44	1.78	5.25	6.09	0.68	1.87
k38-30-mz8-9	2.13	0.24	0.91	0.44	0.61	0.42	1.34	0.76	1.41	1.80	5.13	6.19	0.61	1.69
k38-30-mz8-10	1.98	0.24	0.91	5.87	0.59	0.42	1.31	0.76	1.46	2.70	72.77	7.49	0.59	2.33
k38-30-mz8-11	1.72	0.24	0.94	100.00	0.57	0.41	1.29	0.76	1.65	5.32	183.19	9.04	0.60	2.92
k38-30-mz8-12	2.02	0.24	0.92	2.49	0.58	0.42	1.31	0.76	1.48	2.58	25.59	8.18	0.61	2.38
k38-30-mz8-13	2.95	0.24	1.08	0.71	0.60	0.42	1.31	0.76	1.38	1.86	7.03	7.70	0.75	2.06
k38-30-mz8-14	2.60	0.24	1.11	0.48	0.60	0.42	1.34	0.76	1.40	1.82	4.93	7.81	0.72	2.34
k38-30-mz8-15	2.84	0.24	1.22	0.55	0.59	0.42	1.29	0.76	1.44	1.92	5.33	9.18	0.83	2.16
k38-30-mz8-16	2.29	0.24	0.90	0.73	0.59	0.42	1.35	0.76	1.51	2.52	9.69	6.96	0.60	1.87
k38-30-mz10-1	9.35	0.24	0.68	0.97	0.60	0.42	1.37	0.77	1.52	2.61	11.61	4.32	0.55	0.79
k38-30-mz10-2	6.71	0.24	0.69	0.79	0.61	0.42	1.35	0.76	1.48	2.25	11.76	4.73	0.55	0.80
k38-30-mz10-3	8.37	0.24	0.66	1.20	0.60	0.42	1.38	0.79	1.60	2.80	15.91	4.07	0.54	0.75
k38-30-mz10-4	7.92	0.24	0.68	2.69	0.59	0.42	1.35	0.78	1.68	3.55	21.47	4.28	0.56	0.73
k38-30-mz10-5	3.55	0.24	0.73	7.70	0.58	0.42	1.33	0.77	1.64	4.18	40.34	5.32	0.56	0.91
k38-30-mz10-6	2.08	0.24	0.85	56.95	0.58	0.41	1.33	0.76	1.65	6.23	61.73	6.33	0.58	1.78
k38-30-mz10-7	2.41	0.24	0.98	0.95	0.60	0.42	1.35	0.76	1.40	1.96	11.18	7.35	0.67	1.54
k38-30-mz10-8	1.92	0.24	0.89	27.02	0.57	0.41	1.32	0.76	1.60	4.11	294.63	8.12	0.59	2.17

k38-30-mz10-9	7.64	0.24	0.69	0.82	0.60	0.42	1.36	0.78	1.51	2.26	10.50	4.31	0.55	0.84
k38-30-mz10-10	3.03	0.24	0.87	2.31	0.59	0.42	1.37	0.76	1.51	2.89	33.71	5.73	0.63	1.12
K45.10-mz1-1	2.74	0.24	0.86	0.42	0.62	0.43	1.27	0.74	1.27	1.69	4.90	5.17	0.55	1.66
K45.10-mz1-2	3.17	0.24	0.98	0.45	0.61	0.43	1.26	0.73	1.28	1.69	4.91	6.47	0.63	1.98
K45.10-mz1-3	2.94	0.24	0.92	0.43	0.62	0.43	1.25	0.74	1.29	1.68	4.82	5.82	0.59	1.81
K45.10-mz1-4	2.79	0.24	0.89	0.43	0.62	0.43	1.26	0.74	1.29	1.65	4.98	5.85	0.57	1.79
K45.10-mz1-5	2.81	0.24	0.88	0.43	0.62	0.43	1.27	0.74	1.27	1.67	5.16	5.60	0.57	1.63
K45.10-mz1-6	2.87	0.24	0.93	0.49	0.61	0.43	1.24	0.74	1.28	1.59	5.26	5.60	0.61	1.55
K45.10-mz1-7	2.97	0.24	0.98	0.52	0.61	0.43	1.22	0.74	1.26	1.58	6.23	6.42	0.64	1.81
K45.10-mz1-8	2.79	0.24	0.94	0.52	0.61	0.43	1.23	0.74	1.27	1.61	6.09	6.19	0.61	1.68
K45.10-mz2-1	9.64	0.24	0.73	1.64	0.61	0.43	1.23	0.74	1.30	2.13	16.50	4.97	0.56	0.86
K45.10-mz2-2	1.71	0.24	0.71	8.43	0.61	0.43	1.28	0.74	1.35	2.35	48.83	4.45	0.46	1.31
K45.10-mz2-3	2.47	0.24	0.77	0.42	0.62	0.43	1.27	0.75	1.29	1.57	4.46	4.87	0.51	1.41
K45.10-mz2-4	10.72	0.24	0.71	2.13	0.61	0.43	1.25	0.74	1.32	2.19	25.36	4.65	0.55	0.83
K45.10-mz2-5	5.39	0.24	0.72	3.63	0.61	0.43	1.23	0.74	1.30	2.33	24.79	4.77	0.54	0.83
K45.10-mz2-6	5.37	0.24	0.72	3.30	0.61	0.43	1.24	0.74	1.31	2.25	29.12	4.53	0.53	0.88
K45.10-mz2-7	7.56	0.24	0.71	2.69	0.61	0.43	1.23	0.74	1.34	2.34	38.45	4.59	0.54	0.83
K45.10-mz2-8	2.09	0.24	0.76	8.55	0.61	0.43	1.25	0.75	1.37	2.45	100.00	4.96	0.49	1.43
K52.40-mz1-1	5.11	0.24	1.18	0.41	0.61	0.43	1.22	0.74	1.50	2.57	8.97	9.10	0.78	3.10
K52.40-mz1-2	4.81	0.24	1.28	0.41	0.61	0.43	1.23	0.74	1.48	2.45	7.53	9.33	0.80	3.57
K52.40-mz1-3	3.26	0.24	1.05	0.37	0.61	0.43	1.24	0.74	1.34	1.82	4.77	6.96	0.64	2.56
K52.40-mz1-4	4.90	0.24	1.51	0.41	0.61	0.43	1.19	0.72	1.27	1.81	5.92	10.00	0.91	6.07
K52.40-mz1-5	4.72	0.24	1.53	0.39	0.61	0.43	1.21	0.73	1.25	1.81	5.94	12.75	0.98	4.69
K52.40-mz1-6	4.15	0.24	1.13	0.38	0.61	0.43	1.23	0.74	1.33	1.79	5.28	9.00	0.70	5.39
K52.40-mz1-7	4.89	0.24	1.43	0.41	0.61	0.43	1.21	0.74	1.34	1.96	5.43	10.93	0.88	4.68
K52.40-mz1-8	4.77	0.24	1.22	0.41	0.60	0.43	1.19	0.73	1.57	2.73	8.19	11.36	0.81	3.39
K52.40-mz2-1	3.61	0.24	1.78	0.48	0.60	0.43	1.20	0.72	1.28	1.72	5.27	14.13	0.99	3.47
K52.40-mz2-2	6.73	0.24	1.19	0.44	0.61	0.43	1.21	0.73	1.24	1.70	4.84	10.41	0.83	1.92
K52.40-mz2-3	3.32	0.24	1.85	0.53	0.60	0.43	1.22	0.72	1.29	1.86	5.87	13.55	0.97	4.36
K52.40-mz2-4	3.27	0.24	1.80	0.56	0.60	0.43	1.21	0.72	1.30	1.87	6.51	18.62	0.97	3.70
K52.40-mz2-5	3.05	0.24	1.97	0.62	0.60	0.43	1.22	0.72	1.27	1.83	5.99	14.23	0.99	5.66

K52.40-mz2-6	5.29	0.24	1.32	0.52	0.60	0.43	1.20	0.72	1.29	1.81	5.04	11.94	0.88	2.53
K52.40-mz2-7	2.95	0.24	1.35	0.50	0.61	0.43	1.22	0.73	1.29	1.80	5.69	10.47	0.80	2.84
K52.40-mz2-8	3.08	0.24	1.40	0.53	0.61	0.43	1.19	0.73	1.22	1.85	6.08	10.26	0.84	3.01
K52.40-mz2-9	5.33	0.24	1.02	0.47	0.61	0.43	1.23	0.73	1.30	1.76	5.35	7.12	0.74	1.65
K52.40-mz2-10	3.59	0.24	1.93	0.55	0.60	0.43	1.19	0.71	1.27	1.85	5.09	16.56	1.06	5.32
K52.40-mz3-1	0.88	0.24	0.54	6.30	0.64	0.45	1.40	0.81	1.84	3.85	77.90	2.67	0.35	1.61
K52.40-mz3-2	0.59	0.24	0.50	6.14	0.64	0.45	1.44	0.83	1.83	4.00	100.00	2.17	0.33	1.38
K52.40-mz3-3	0.63	0.24	0.49	9.62	0.64	0.46	1.44	0.84	1.99	5.02	116.57	2.16	0.33	1.44
K52.40-mz3-4	0.82	0.24	0.51	8.25	0.63	0.45	1.40	0.82	1.93	4.84	135.46	2.53	0.34	1.50
K52.40-mz3-5	0.77	0.24	0.49	6.34	0.66	0.46	1.39	0.82	1.89	4.47	265.36	2.32	0.33	1.41
K52.40-mz3-6	0.94	0.24	0.52	2.62	0.65	0.45	1.38	0.79	1.53	2.64	26.13	2.69	0.35	1.31
K52.40-mz3-7	1.54	0.24	0.62	1.38	0.63	0.44	1.30	0.75	1.31	2.06	12.88	3.57	0.42	1.23
K52.40-mz3-8	2.63	0.24	0.84	1.10	0.61	0.43	1.23	0.73	1.26	1.79	9.64	5.38	0.55	1.21
K52.40-mz3-9	0.72	0.24	0.48	3.63	0.67	0.46	1.44	0.83	1.69	3.04	29.93	2.13	0.33	1.23
K52.40-mz3-10	1.21	0.24	0.56	1.70	0.64	0.44	1.35	0.77	1.41	2.18	14.47	3.04	0.38	1.24
K52.40-mz4-1	3.87	0.24	1.30	0.91	0.62	0.43	1.23	0.74	1.31	1.90	7.45	7.56	0.77	1.39
K52.40-mz4-2	2.47	0.24	0.97	0.93	0.63	0.43	1.28	0.76	1.32	1.97	7.51	5.71	0.55	1.38
K52.40-mz4-3	1.61	0.24	0.73	1.54	0.63	0.44	1.31	0.76	1.48	2.48	13.04	4.16	0.43	1.67
K52.40-mz4-4	2.33	0.24	0.94	0.94	0.62	0.43	1.27	0.76	1.34	1.95	7.93	5.62	0.55	1.37
K52.40-mz4-5	1.15	0.24	0.64	1.25	0.65	0.45	1.38	0.78	1.39	2.22	10.83	3.17	0.38	1.30
K52.40-mz4-6	3.56	0.24	0.92	1.17	0.62	0.43	1.27	0.75	1.35	2.12	12.77	5.10	0.59	0.99
K52.40-mz4-7	2.72	0.24	0.93	0.98	0.62	0.43	1.29	0.76	1.38	1.96	10.40	5.82	0.54	1.42
K52.40-mz4-8	5.25	0.24	0.83	2.99	0.61	0.43	1.27	0.78	1.52	2.65	18.06	4.86	0.57	0.87
K52-40A-mz1-1	5.40	0.24	1.48	0.87	0.62	0.43	1.23	0.75	1.32	1.87	7.51	10.36	1.04	1.64
K52-40A-mz1-2	5.87	0.24	1.47	0.91	0.61	0.43	1.21	0.75	1.33	1.86	7.78	9.78	1.05	1.58
K52-40A-mz1-3	4.96	0.24	1.26	0.86	0.62	0.43	1.24	0.76	1.33	1.86	7.46	9.04	0.90	1.30
K52-40A-mz1-4	5.04	0.24	1.49	0.81	0.62	0.43	1.27	0.74	1.33	1.85	7.21	10.37	1.05	1.55
K52-40A-mz1-5	5.59	0.24	1.45	0.85	0.62	0.43	1.23	0.74	1.29	1.79	7.95	10.08	1.02	1.53
K52-40A-mz1-6	4.80	0.24	1.43	0.88	0.62	0.43	1.23	0.74	1.31	1.86	8.35	9.04	0.99	1.57
K52-40A-mz1-7	4.12	0.24	1.08	0.73	0.63	0.43	1.25	0.75	1.25	1.68	6.90	6.76	0.75	1.19
K52-40A-mz1-8	3.97	0.24	1.06	0.77	0.63	0.43	1.25	0.75	1.29	1.75	7.42	7.41	0.73	1.31
K52-40A-mz1-9	4.27	0.24	1.08	0.75	0.63	0.43	1.26	0.75	1.28	1.77	7.86	6.86	0.74	1.21
K52-40A-mz1-10	3.68	0.24	1.01	0.76	0.63	0.43	1.24	0.75	1.28	1.78	6.76	6.86	0.69	1.24

K52-40A-mz2-1	2.28	0.24	0.75	0.84	0.64	0.44	1.31	0.76	1.32	1.85	7.84	4.45	0.50	1.09
K52-40A-mz2-2	1.79	0.24	0.73	1.03	0.64	0.44	1.28	0.76	1.38	2.00	7.91	4.67	0.47	1.39
K52-40A-mz2-3	1.99	0.24	0.77	0.98	0.64	0.44	1.30	0.76	1.36	1.90	8.85	5.41	0.49	1.34
K52-40A-mz2-4	1.82	0.24	0.77	1.02	0.64	0.44	1.30	0.76	1.34	1.97	9.69	5.14	0.48	1.42
K52-40A-mz2-5	2.60	0.24	0.76	0.86	0.63	0.44	1.31	0.77	1.40	1.90	6.88	5.00	0.52	1.00
K52-40A-mz2-6	2.94	0.24	0.80	0.83	0.63	0.44	1.32	0.76	1.34	1.81	8.33	4.90	0.55	1.02
K52-40A-mz2-7	2.19	0.24	0.72	0.94	0.63	0.44	1.33	0.77	1.36	1.99	8.82	4.51	0.47	1.16
K52-40A-mz2-8	2.31	0.24	0.74	0.78	0.64	0.44	1.31	0.76	1.30	1.73	8.03	4.65	0.50	1.09
K52-40A-mz2-9	2.25	0.24	0.81	0.99	0.63	0.44	1.30	0.76	1.32	1.91	8.89	5.51	0.52	1.40
K52-40A-mz2-10	2.80	0.24	0.88	1.00	0.63	0.43	1.29	0.76	1.35	1.86	8.19	5.73	0.58	1.44
K53-30-mz1-1	N/A	N/A	N/A	0.36	N/A	N/A	N/A	N/A	N/A	N/A	N/A	5.42	0.45	2.93
K53-30-mz1-2	N/A	N/A	N/A	0.35	N/A	N/A	N/A	N/A	N/A	N/A	N/A	4.49	0.39	2.66
K53-30-mz1-3	N/A	N/A	N/A	0.35	N/A	N/A	N/A	N/A	N/A	N/A	N/A	3.48	0.34	2.34
K53-30-mz1-4	N/A	N/A	N/A	0.35	N/A	N/A	N/A	N/A	N/A	N/A	N/A	4.01	0.36	2.44
K53-30-mz1-5	N/A	N/A	N/A	0.36	N/A	N/A	N/A	N/A	N/A	N/A	N/A	3.59	0.34	2.36
K53-30-mz1-6	N/A	N/A	N/A	0.34	N/A	N/A	N/A	N/A	N/A	N/A	N/A	2.87	0.32	2.11
K53-30-mz1-7	N/A	N/A	N/A	0.34	N/A	N/A	N/A	N/A	N/A	N/A	N/A	2.34	0.30	2.12
K53-30-mz1-8	N/A	N/A	N/A	0.34	N/A	N/A	N/A	N/A	N/A	N/A	N/A	5.09	0.40	2.65
K53-30-mz1-9	N/A	N/A	N/A	0.36	N/A	N/A	N/A	N/A	N/A	N/A	N/A	5.41	0.43	2.79
K53-30-mz1-10	N/A	N/A	N/A	0.37	N/A	N/A	N/A	N/A	N/A	N/A	N/A	7.16	0.52	2.95
K53-30-mz1-11	N/A	N/A	N/A	0.34	N/A	N/A	N/A	N/A	N/A	N/A	N/A	4.34	0.39	2.60
K53-30-mz1-12	N/A	N/A	N/A	0.36	N/A	N/A	N/A	N/A	N/A	N/A	N/A	5.78	0.49	2.76
K53-30-mz2-1	N/A	N/A	N/A	0.38	N/A	N/A	N/A	N/A	N/A	N/A	N/A	5.36	0.46	2.27
K53-30-mz2-2	N/A	N/A	N/A	0.39	N/A	N/A	N/A	N/A	N/A	N/A	N/A	6.64	0.49	2.33
K53-30-mz2-3	N/A	N/A	N/A	0.39	N/A	N/A	N/A	N/A	N/A	N/A	N/A	6.90	0.54	2.63
K53-30-mz2-4	N/A	N/A	N/A	0.40	N/A	N/A	N/A	N/A	N/A	N/A	N/A	6.36	0.53	2.54
K53-30-mz2-5	N/A	N/A	N/A	0.39	N/A	N/A	N/A	N/A	N/A	N/A	N/A	7.21	0.55	2.56
K53-30-mz2-6	N/A	N/A	N/A	0.39	N/A	N/A	N/A	N/A	N/A	N/A	N/A	7.68	0.59	2.93
K53-30-mz2-7	N/A	N/A	N/A	0.35	N/A	N/A	N/A	N/A	N/A	N/A	N/A	5.17	0.42	2.09
K53-30-mz2-8	N/A	N/A	N/A	0.37	N/A	N/A	N/A	N/A	N/A	N/A	N/A	4.68	0.42	2.28
K53-30-mz2-9	N/A	N/A	N/A	0.38	N/A	N/A	N/A	N/A	N/A	N/A	N/A	6.79	0.55	2.76
K53-30-mz2-10	N/A	N/A	N/A	0.38	N/A	N/A	N/A	N/A	N/A	N/A	N/A	6.84	0.39	1.93

K53-30-mz2-11	N/A	N/A	N/A	0.39	N/A	N/A	N/A	N/A	N/A	N/A	N/A	6.06	0.53	2.43
K53-30-mz2-12	N/A	N/A	N/A	0.47	N/A	N/A	N/A	N/A	N/A	N/A	N/A	4.93	0.42	2.97
K53-30-mz2-13	N/A	N/A	N/A	0.37	N/A	N/A	N/A	N/A	N/A	N/A	N/A	9.15	0.59	2.56
K53-30-mz2-14	N/A	N/A	N/A	0.37	N/A	N/A	N/A	N/A	N/A	N/A	N/A	6.69	0.56	2.52
K53-30-mz2-15	N/A	N/A	N/A	0.40	N/A	N/A	N/A	N/A	N/A	N/A	N/A	8.32	0.54	2.79
K53-30-mz4-1	N/A	N/A	N/A	0.41	N/A	N/A	N/A	N/A	N/A	N/A	N/A	5.35	0.44	1.19
K53-30-mz4-2	N/A	N/A	N/A	0.38	N/A	N/A	N/A	N/A	N/A	N/A	N/A	4.30	0.44	0.85
K53-30-mz4-3	N/A	N/A	N/A	0.33	N/A	N/A	N/A	N/A	N/A	N/A	N/A	4.56	0.48	0.81
K53-30-mz4-4	N/A	N/A	N/A	0.28	N/A	N/A	N/A	N/A	N/A	N/A	N/A	4.91	0.60	0.79
K53-30-mz4-5	N/A	N/A	N/A	0.23	N/A	N/A	N/A	N/A	N/A	N/A	N/A	4.34	0.65	0.62
K53-30-mz4-6	N/A	N/A	N/A	0.39	N/A	N/A	N/A	N/A	N/A	N/A	N/A	4.49	0.43	0.92
K53-30-mz4-7	N/A	N/A	N/A	0.39	N/A	N/A	N/A	N/A	N/A	N/A	N/A	4.51	0.43	0.85
K53-30-mz4-8	N/A	N/A	N/A	0.31	N/A	N/A	N/A	N/A	N/A	N/A	N/A	4.34	0.48	0.78
K53-30-mz4-9	N/A	N/A	N/A	0.23	N/A	N/A	N/A	N/A	N/A	N/A	N/A	4.21	0.62	0.63
K53-30-mz4-10	N/A	N/A	N/A	0.37	N/A	N/A	N/A	N/A	N/A	N/A	N/A	4.85	0.48	0.94
K53-30-mz4-11	N/A	N/A	N/A	0.34	N/A	N/A	N/A	N/A	N/A	N/A	N/A	4.70	0.46	0.84
K53-30-mz5-1	N/A	N/A	N/A	0.34	N/A	N/A	N/A	N/A	N/A	N/A	N/A	6.60	0.51	1.49
K53-30-mz5-2	N/A	N/A	N/A	0.34	N/A	N/A	N/A	N/A	N/A	N/A	N/A	7.10	0.50	1.44
K53-30-mz5-3	N/A	N/A	N/A	0.33	N/A	N/A	N/A	N/A	N/A	N/A	N/A	6.23	0.51	1.38
K53-30-mz5-4	N/A	N/A	N/A	0.28	N/A	N/A	N/A	N/A	N/A	N/A	N/A	8.47	0.63	1.60
K53-30-mz5-5	N/A	N/A	N/A	0.25	N/A	N/A	N/A	N/A	N/A	N/A	N/A	6.80	0.58	1.35
K53-30-mz5-6	N/A	N/A	N/A	0.34	N/A	N/A	N/A	N/A	N/A	N/A	N/A	6.40	0.55	1.60
K53-30-mz5-7	N/A	N/A	N/A	0.34	N/A	N/A	N/A	N/A	N/A	N/A	N/A	6.07	0.50	1.47
K53-30-mz5-8	N/A	N/A	N/A	0.35	N/A	N/A	N/A	N/A	N/A	N/A	N/A	5.93	0.48	1.38
K53-30-mz5-9	N/A	N/A	N/A	0.26	N/A	N/A	N/A	N/A	N/A	N/A	N/A	6.37	0.58	1.46
K53-30-mz6-1	N/A	N/A	N/A	1.12	N/A	N/A	N/A	N/A	N/A	N/A	N/A	5.45	0.41	1.79
K53-30-mz6-2	N/A	N/A	N/A	2.72	N/A	N/A	N/A	N/A	N/A	N/A	N/A	4.15	0.35	1.38
K53-30-mz6-3	N/A	N/A	N/A	1.15	N/A	N/A	N/A	N/A	N/A	N/A	N/A	4.41	0.36	1.21
K53-30-mz6-4	N/A	N/A	N/A	0.39	N/A	N/A	N/A	N/A	N/A	N/A	N/A	4.33	0.39	1.29
K53-30-mz6-5	N/A	N/A	N/A	0.44	N/A	N/A	N/A	N/A	N/A	N/A	N/A	4.69	0.40	1.43
K53-30-mz6-6	N/A	N/A	N/A	0.37	N/A	N/A	N/A	N/A	N/A	N/A	N/A	4.77	0.40	1.29
K53-30-mz6-7	N/A	N/A	N/A	0.45	N/A	N/A	N/A	N/A	N/A	N/A	N/A	4.12	0.38	1.17
K53-30-mz6-8	N/A	N/A	N/A	0.40	N/A	N/A	N/A	N/A	N/A	N/A	N/A	4.32	0.39	1.23

K53-30-mz6-9	N/A	N/A	N/A	0.41	N/A	N/A	N/A	N/A	N/A	N/A	N/A	4.58	0.39	1.21
K53-30-mz6-10	N/A	N/A	N/A	0.56	N/A	N/A	N/A	N/A	N/A	N/A	N/A	4.78	0.39	1.30
K53-30-mz6-11	N/A	N/A	N/A	0.79	N/A	N/A	N/A	N/A	N/A	N/A	N/A	4.62	0.38	1.26
K53-30-mz7-1	N/A	N/A	N/A	0.67	N/A	N/A	N/A	N/A	N/A	N/A	N/A	5.21	0.44	1.08
K53-30-mz7-2	N/A	N/A	N/A	0.74	N/A	N/A	N/A	N/A	N/A	N/A	N/A	5.25	0.44	1.09
K53-30-mz7-3	N/A	N/A	N/A	0.73	N/A	N/A	N/A	N/A	N/A	N/A	N/A	5.48	0.44	1.07
K53-30-mz7-4	N/A	N/A	N/A	0.55	N/A	N/A	N/A	N/A	N/A	N/A	N/A	5.40	0.45	1.11
K53-30-mz7-5	N/A	N/A	N/A	0.31	N/A	N/A	N/A	N/A	N/A	N/A	N/A	5.26	0.47	1.66
K53-30-mz7-6	N/A	N/A	N/A	0.51	N/A	N/A	N/A	N/A	N/A	N/A	N/A	4.64	0.38	1.48
K53-30-mz7-7	N/A	N/A	N/A	0.64	N/A	N/A	N/A	N/A	N/A	N/A	N/A	5.15	0.45	1.11
K53-30-mz7-8	N/A	N/A	N/A	0.67	N/A	N/A	N/A	N/A	N/A	N/A	N/A	4.89	0.44	1.06
K53-30-mz7-9	N/A	N/A	N/A	0.61	N/A	N/A	N/A	N/A	N/A	N/A	N/A	5.53	0.42	1.40
K53-30-mz7-10	N/A	N/A	N/A	0.87	N/A	N/A	N/A	N/A	N/A	N/A	N/A	4.18	0.35	1.70
K53-30-mz7-11	N/A	N/A	N/A	0.49	N/A	N/A	N/A	N/A	N/A	N/A	N/A	4.67	0.41	1.57
K53-30-mz7-12	N/A	N/A	N/A	0.40	N/A	N/A	N/A	N/A	N/A	N/A	N/A	6.67	0.45	1.96
K53-30-mz8-1	N/A	N/A	N/A	0.89	N/A	N/A	N/A	N/A	N/A	N/A	N/A	8.33	0.59	1.74
K53-30-mz8-2	N/A	N/A	N/A	0.84	N/A	N/A	N/A	N/A	N/A	N/A	N/A	6.12	0.51	1.61
K53-30-mz8-3	N/A	N/A	N/A	0.44	N/A	N/A	N/A	N/A	N/A	N/A	N/A	5.13	0.51	1.39
K53-30-mz8-4	N/A	N/A	N/A	0.32	N/A	N/A	N/A	N/A	N/A	N/A	N/A	5.59	0.54	1.42
K53-30-mz8-5	N/A	N/A	N/A	0.28	N/A	N/A	N/A	N/A	N/A	N/A	N/A	6.02	0.55	1.45
K53-30-mz8-6	N/A	N/A	N/A	0.92	N/A	N/A	N/A	N/A	N/A	N/A	N/A	6.80	0.59	1.63
K53-30-mz8-7	N/A	N/A	N/A	0.94	N/A	N/A	N/A	N/A	N/A	N/A	N/A	5.94	0.49	1.46
K53-30-mz8-8	N/A	N/A	N/A	0.51	N/A	N/A	N/A	N/A	N/A	N/A	N/A	6.21	0.49	1.27
K53-30-mz8-9	N/A	N/A	N/A	0.45	N/A	N/A	N/A	N/A	N/A	N/A	N/A	6.49	0.52	1.41
K53-30-mz8-10	N/A	N/A	N/A	0.33	N/A	N/A	N/A	N/A	N/A	N/A	N/A	4.88	0.50	1.28
K59.90-mz1-1	2.60	0.24	0.84	1.67	0.61	0.43	1.25	0.73	1.27	1.90	11.73	4.87	0.55	1.36
K59.90-mz1-2	2.39	0.24	0.80	1.75	0.61	0.43	1.25	0.74	1.25	1.87	13.87	4.88	0.52	1.27
K59.90-mz1-3	3.61	0.24	1.08	2.01	0.60	0.43	1.23	0.73	1.31	2.08	16.88	9.19	0.70	1.66
K59.90-mz1-4	3.98	0.24	1.23	2.33	0.59	0.42	1.21	0.72	1.31	2.09	15.30	9.85	0.82	2.04
K59.90-mz1-5	3.90	0.24	1.14	2.14	0.60	0.43	1.22	0.73	1.33	2.11	15.77	9.29	0.78	1.66
K59.90-mz1-6	2.05	0.24	0.77	1.71	0.61	0.43	1.25	0.74	1.30	1.90	12.50	4.80	0.51	1.19
K59.90-mz1-7	3.76	0.24	1.14	1.93	0.60	0.43	1.20	0.73	1.35	2.10	15.58	9.94	0.74	1.85

K59.90-mz1-8	3.15	0.24	0.94	1.79	0.60	0.43	1.23	0.73	1.29	1.94	13.14	6.37	0.62	1.56
K59.90-mz1-9	3.04	0.24	1.00	1.90	0.45	0.60	1.27	0.75	1.38	2.04	17.08	6.84	0.59	1.62
K59.90-mz2-1	1.77	0.24	0.81	2.96	0.45	0.62	1.28	0.75	1.35	2.13	30.79	5.12	0.47	1.55
K59.90-mz2-2	2.23	0.24	0.90	2.94	0.45	0.61	1.27	0.76	1.37	2.13	23.23	6.44	0.53	1.61
K59.90-mz2-3	1.57	0.24	0.76	3.02	0.46	0.62	1.29	0.76	1.38	2.22	24.52	4.91	0.45	1.43
K59.90-mz2-4	4.26	0.24	0.79	0.29	0.47	0.63	1.38	0.79	1.42	1.36	2.79	4.78	0.51	1.49
K59.90-mz2-5	3.43	0.24	0.81	0.34	0.46	0.63	1.33	0.78	1.37	1.52	3.66	5.00	0.50	1.59
K59.90-mz2-6	1.35	0.24	0.71	2.78	0.46	0.63	1.31	0.76	1.38	2.10	45.29	4.43	0.42	1.42
K59.90-mz2-7	1.41	0.24	0.72	3.05	0.46	0.63	1.33	0.77	1.36	2.14	29.08	4.11	0.43	1.48
K59.90-mz2-8	2.12	0.24	0.86	2.99	0.45	0.61	1.28	0.76	1.35	2.07	31.62	5.54	0.51	1.52
K59.90-mz2-9	1.45	0.24	0.72	1.47	0.46	0.62	1.31	0.76	1.38	2.07	18.03	3.95	0.42	1.39
K63.120-mz1-1	5.29	0.24	1.25	2.78	0.60	0.43	1.21	0.72	1.28	2.12	15.35	9.44	0.89	1.21
K63.120-mz1-2	7.61	0.24	1.57	3.25	0.60	0.42	1.20	0.71	1.26	2.17	30.86	15.21	1.15	1.44
K63.120-mz1-3	5.74	0.24	1.25	2.76	0.61	0.43	1.20	0.73	1.26	2.13	24.62	8.59	0.89	1.13
K63.120-mz1-4	6.35	0.24	1.34	2.94	0.60	0.43	1.21	0.74	1.29	2.17	22.06	9.47	0.95	1.15
K63.120-mz1-5	7.03	0.24	1.40	3.87	0.60	0.43	1.19	0.72	1.28	2.34	155.46	11.42	1.00	1.33
K63.120-mz1-6	7.61	0.24	1.65	5.75	0.59	0.42	1.22	0.73	1.36	2.53	79.42	14.25	1.26	1.78
K63.120-mz1-7	5.50	0.24	1.19	2.27	0.60	0.43	1.24	0.74	1.34	2.22	16.71	7.66	0.80	1.27
K63.120-mz1-8	5.81	0.24	1.45	3.07	0.60	0.42	1.21	0.72	1.25	2.21	30.69	8.73	1.00	1.32
K63.120-mz1-9	5.94	0.24	1.33	3.24	0.60	0.43	1.22	0.72	1.26	2.14	83.58	10.24	0.95	1.23
K63.120-mz1-10	6.20	0.24	1.55	3.74	0.61	0.43	1.25	0.75	1.32	2.38	96.36	11.31	1.00	1.38
K63.120-mz2-1	0.59	0.24	0.48	0.43	0.66	0.47	1.75	0.94	1.92	1.54	5.64	1.80	0.32	1.36
K63.120-mz2-2	0.58	0.24	0.49	0.44	0.66	0.47	1.67	0.94	1.81	1.57	5.36	1.84	0.32	1.39
K63.120-mz2-3	0.69	0.24	0.49	0.43	0.65	0.46	1.66	0.93	1.85	1.53	4.80	2.04	0.33	1.44
K63.120-mz2a-1	0.59	0.24	0.47	0.42	0.67	0.48	1.67	0.95	1.85	1.55	5.53	1.75	0.31	1.29
K63.120-mz2a-2	0.63	0.24	0.47	0.41	0.67	0.47	1.66	0.94	1.78	1.48	4.70	1.90	0.32	1.33
K63.120-mz2a-3	0.73	0.24	0.52	0.43	0.64	0.46	1.57	0.89	1.69	1.44	4.88	2.29	0.34	1.65
K63.120-mz3-1	0.60	0.24	0.47	0.40	0.68	0.48	1.74	0.97	1.92	1.53	4.97	1.78	0.32	1.27
K63.120-mz3-2	0.64	0.24	0.50	0.42	0.65	0.47	1.64	0.95	1.89	1.57	5.10	1.94	0.33	1.50
K63.120-mz3-3	0.72	0.24	0.52	0.42	0.64	0.46	1.63	0.91	1.79	1.46	4.85	2.15	0.33	1.52
K63.120-mz3-4	0.57	0.24	0.49	0.36	0.68	0.48	1.72	0.94	1.83	1.45	4.01	1.86	0.32	1.32
K63.120-mz3-5	0.70	0.24	0.51	0.40	0.65	0.46	1.66	0.90	1.69	1.46	4.28	2.06	0.33	1.47

K63.120-mz3-6	0.83	0.24	0.54	0.42	0.63	0.46	1.59	0.90	1.71	1.45	4.52	2.44	0.35	1.60
K63.120-mz4-1	6.24	0.24	1.68	2.81	0.61	0.43	1.23	0.74	1.31	2.24	17.08	13.27	0.95	1.68
K63.120-mz4-2	5.99	0.24	1.51	2.52	0.61	0.43	1.23	0.73	1.32	2.19	20.31	11.89	0.96	1.66
K63.120-mz4-3	5.52	0.24	1.56	2.85	0.61	0.43	1.22	0.73	1.28	2.19	18.42	11.53	1.00	1.46
K63.120-mz4-4	4.55	0.24	1.28	2.37	0.61	0.43	1.23	0.74	1.35	2.17	16.25	10.98	0.77	1.57
K63.120-mz4-5	5.98	0.24	1.56	3.45	0.61	0.43	1.21	0.73	1.31	2.43	23.41	11.15	0.96	1.57
K63.120-mz4-6	2.94	0.24	0.96	2.23	0.62	0.43	1.28	0.76	1.39	2.25	19.84	6.17	0.55	1.56
K63.120-mz4-7	5.31	0.24	1.30	2.09	0.62	0.43	1.24	0.75	1.31	2.17	20.41	9.28	0.82	1.48
K63.120-mz4-8	7.00	0.24	1.48	2.28	0.61	0.43	1.24	0.74	1.32	2.26	16.34	10.18	0.90	1.62
K63.120-mz4-9	4.44	0.24	1.17	2.27	0.62	0.43	1.25	0.75	1.34	2.28	18.82	6.57	0.70	1.53
K63.120-mz4-10	6.27	0.24	1.56	2.42	0.62	0.43	1.25	0.74	1.32	2.24	19.91	12.09	0.95	1.61
K63.120-mz4-11	6.60	0.24	1.65	3.77	0.61	0.43	1.27	0.75	1.34	2.33	21.37	10.41	1.05	1.48
K63.120-mz4-12	6.28	0.24	1.50	2.21	0.62	0.43	1.27	0.75	1.34	2.27	18.97	10.15	0.93	1.56
K63-120-mz6-1	8.95	0.24	0.75	2.51	0.63	0.43	1.26	0.76	1.43	2.52	68.56	4.89	0.64	0.77
K63-120-mz6-2	10.43	0.24	0.76	2.16	0.63	0.43	1.28	0.76	1.43	2.45	26.43	5.05	0.62	0.81
K63-120-mz6-3	11.62	0.24	0.79	2.67	0.63	0.43	1.29	0.75	1.42	2.59	39.89	6.16	0.66	0.79
K63-120-mz6-4	10.12	0.24	0.75	2.39	0.63	0.43	1.31	0.76	1.43	2.52	30.59	5.09	0.62	0.81
K63-120-mz6-5	12.65	0.24	0.79	2.55	0.62	0.43	1.31	0.75	1.43	2.54	18.29	5.78	0.66	0.81
K63-120-mz6-6	11.49	0.24	0.80	2.40	0.62	0.43	1.27	0.76	1.39	2.38	33.90	5.61	0.67	0.80
K63-120-mz6-7	13.27	0.24	0.78	2.66	0.62	0.43	1.27	0.76	1.39	2.56	46.98	5.49	0.66	0.81
K63-120-mz6-8	12.91	0.24	0.78	2.44	0.62	0.43	1.29	0.75	1.39	2.49	48.39	5.20	0.66	0.81
K63-120-mz6-9	13.81	0.24	0.79	2.45	0.62	0.43	1.28	0.76	1.40	2.38	33.10	4.34	0.66	0.80
K63-120-mz6-10	12.88	0.24	0.78	2.05	0.62	0.43	1.29	0.76	1.40	2.42	23.61	5.18	0.64	0.85
K63-120-mz6-11	10.21	0.24	0.76	2.36	0.63	0.43	1.26	0.75	1.39	2.42	26.88	5.24	0.64	0.77
K103.20-mz1-1	1.15	0.24	0.57	0.80	0.64	0.44	1.35	0.78	1.39	1.81	8.28	3.25	0.38	1.37
K103.20-mz1-2	1.27	0.24	0.64	0.83	0.63	0.44	1.30	0.76	1.38	1.76	10.12	3.66	0.42	1.68
K103.20-mz1-3	1.22	0.24	0.60	0.81	0.64	0.44	1.31	0.77	1.37	1.78	8.21	3.28	0.40	1.51
K103.20-mz1-4	1.31	0.24	0.63	0.82	0.63	0.44	1.30	0.76	1.39	1.81	10.55	3.53	0.42	1.65
K103.20-mz2-1	5.93	0.24	0.78	2.09	0.61	0.43	1.23	0.74	1.37	2.55	18.39	4.49	0.59	0.77
K103.20-mz2-2	4.78	0.24	0.69	7.59	0.61	0.43	1.29	0.76	1.51	3.04	46.21	3.92	0.53	0.68
K103.20-mz2-3	5.48	0.24	0.75	6.87	0.60	0.43	1.25	0.76	1.48	3.29	61.23	4.65	0.56	0.77
K103.20-mz2-4	3.19	0.24	0.92	1.77	0.61	0.43	1.24	0.74	1.38	2.40	16.68	6.27	0.61	1.42

K103.20-mz2-5	3.58	0.24	0.85	3.06	0.60	0.43	1.24	0.75	1.47	2.91	35.45	5.29	0.59	1.08
K103.20-mz2-6	3.16	0.24	1.11	0.90	0.61	0.43	1.24	0.74	1.33	2.11	12.60	8.26	0.70	2.05
K103.20-mz2-7	3.39	0.24	1.09	1.07	0.60	0.43	1.22	0.74	1.32	2.19	13.25	8.26	0.70	1.98
K103.20-mz2-8	2.77	0.24	1.12	0.86	0.61	0.43	1.22	0.73	1.33	2.08	9.66	8.28	0.70	1.89
K103-20A-mz2-1	3.19	0.24	0.87	100.00	0.61	0.43	1.25	0.76	1.48	3.83	60.33	6.80	0.60	1.63
K103-20A-mz2-2	2.61	0.24	0.80	17.71	0.61	0.43	1.28	0.77	1.52	3.54	154.54	5.03	0.56	1.59
K103-20A-mz2-3	3.69	0.24	0.84	2.64	0.62	0.43	1.25	0.76	1.50	3.12	59.43	5.93	0.59	1.74
K103-20A-mz2-4	3.49	0.24	1.00	1.72	0.61	0.43	1.25	0.73	1.38	2.31	17.93	7.68	0.65	2.11
K103-20A-mz2-5	2.45	0.24	0.77	2.57	0.61	0.43	1.27	0.76	1.52	3.70	47.52	5.35	0.55	1.87
K103-20A-mz2-6	2.65	0.24	0.84	0.50	0.64	0.43	1.31	0.75	1.33	1.61	5.68	5.66	0.56	1.98
K103-20A-mz2-7	4.28	0.24	1.08	0.96	0.62	0.43	1.23	0.74	1.36	2.04	11.46	8.65	0.73	2.18
K103-20A-mz2-8	3.21	0.24	0.89	1.60	0.61	0.43	1.26	0.75	1.47	2.86	15.53	6.77	0.60	2.06
K103-20A-mz3-1	3.52	0.24	0.79	4.48	0.62	0.43	1.26	0.75	1.39	2.92	32.50	5.72	0.58	1.20
K103-20A-mz3-2	3.24	0.24	0.79	2.95	0.62	0.43	1.29	0.75	1.46	2.87	25.93	5.06	0.57	1.14
K103-20A-mz3-3	3.02	0.24	0.93	0.56	0.63	0.43	1.28	0.75	1.33	1.80	6.56	6.29	0.63	1.69
K103-20A-mz3-4	3.64	0.24	0.80	7.07	0.61	0.43	1.24	0.76	1.49	3.38	40.94	5.40	0.59	1.19
K103-20A-mz3-5	2.30	0.24	0.80	0.51	0.64	0.43	1.30	0.77	1.37	1.71	4.58	5.41	0.54	1.75
K103-20A-mz3-6	3.83	0.24	0.67	1.08	0.63	0.43	1.31	0.78	1.56	2.60	15.66	4.64	0.52	1.01
K103-20A-mz3-7	8.60	0.24	0.69	3.52	0.62	0.43	1.26	0.77	1.60	3.32	52.93	4.53	0.55	0.92
K103-20A-mz3-8	2.37	0.24	0.77	0.57	0.63	0.43	1.29	0.77	1.38	1.76	6.87	4.38	0.53	1.70
K103-20A-mz3-9	4.15	0.24	0.77	7.30	0.61	0.43	1.25	0.76	1.52	3.41	87.71	5.29	0.57	1.06
K103-20A-mz3-10	4.00	0.24	0.75	0.76	0.63	0.43	1.29	0.76	1.44	2.23	9.22	5.16	0.55	1.12
m54-83-mz2-1	0.73	0.24	0.62	0.56	0.65	0.44	1.47	0.82	1.52	1.79	5.85	3.06	0.40	1.20
m54-83-mz2-2	0.75	0.24	0.62	0.54	0.63	0.44	1.45	0.82	1.53	1.71	5.91	3.21	0.39	1.18
m54-83-mz2-3	0.85	0.24	0.66	0.66	0.63	0.43	1.40	0.79	1.48	1.87	7.22	3.49	0.43	1.37
m54-83-mz2-4	5.22	0.24	0.77	0.41	0.61	0.43	1.38	0.78	1.45	2.33	7.45	5.07	0.54	1.80
m54-83-mz2-5	5.61	0.24	0.75	0.41	0.61	0.43	1.37	0.77	1.46	2.26	8.90	5.35	0.53	1.76
m54-83-mz2-6	1.51	0.24	0.87	1.29	0.61	0.43	1.34	0.77	1.42	2.31	17.25	5.76	0.55	1.71
m54-83-mz2-7	0.93	0.24	0.70	0.74	0.62	0.43	1.38	0.78	1.50	1.98	9.31	3.66	0.43	1.38
m54-83-mz2-8	1.58	0.24	0.83	1.16	0.61	0.43	1.35	0.76	1.40	2.23	12.86	5.06	0.53	1.35
m54-83-mz2-9	1.37	0.24	0.76	0.65	0.62	0.43	1.35	0.77	1.42	1.86	7.08	4.18	0.49	1.31
m54-83-mz2-10	1.33	0.24	0.73	0.61	0.62	0.43	1.40	0.79	1.46	1.82	6.42	4.05	0.48	1.28

m54-83-mz2-11	1.53	0.24	0.79	0.84	0.61	0.43	1.37	0.78	1.38	2.13	11.45	4.94	0.52	1.40
m54-83-mz2-12	1.54	0.24	0.83	0.60	0.61	0.43	1.36	0.77	1.43	1.75	7.36	4.62	0.51	1.46
m54-83-mz2-13	1.64	0.24	0.83	0.87	0.61	0.43	1.35	0.76	1.43	2.28	10.30	5.06	0.54	1.41
m54-83-mz2-14	1.78	0.24	0.90	0.73	0.61	0.43	1.34	0.76	1.40	1.89	8.13	6.22	0.58	1.56
m54-83-mz3-1	1.24	0.24	0.71	0.52	0.62	0.43	1.42	0.79	1.48	1.75	5.73	4.00	0.47	1.25
m54-83-mz3-2	0.92	0.24	0.59	0.42	0.65	0.44	1.51	0.83	1.51	1.57	5.38	2.75	0.39	0.90
m54-83-mz3-3	0.88	0.24	0.60	0.42	0.65	0.44	1.50	0.83	1.50	1.54	5.71	2.80	0.39	0.97
m54-83-mz3-4	1.33	0.24	0.79	0.89	0.62	0.43	1.37	0.78	1.47	2.19	10.43	4.68	0.50	1.45
m54-83-mz3-5	8.89	0.24	0.80	0.33	0.62	0.43	1.42	0.80	1.45	1.74	4.21	5.46	0.57	1.58
m54-83-mz3-6	0.81	0.24	0.56	0.41	0.66	0.45	1.51	0.83	1.52	1.53	5.03	2.53	0.38	0.86
m54-83-mz3-7	1.42	0.24	0.77	0.57	0.61	0.43	1.37	0.78	1.48	1.76	6.91	4.43	0.50	1.50
m54-83-mz3-8	7.04	0.24	0.82	0.34	0.61	0.43	1.41	0.79	1.46	1.82	5.26	5.28	0.58	1.64
m54-83-mz3-9	7.18	0.24	0.79	0.34	0.62	0.43	1.44	0.79	1.45	1.75	4.69	5.09	0.56	1.53
m54-83-mz3-10	1.00	0.24	0.64	0.44	0.64	0.44	1.46	0.81	1.48	1.57	5.30	3.33	0.42	1.02
m54-83-mz1-1	18.00	0.24	0.76	0.68	0.60	0.43	1.36	0.77	1.51	2.29	11.93	4.53	0.56	1.02
m54-83-mz1-2	14.44	0.24	0.75	0.68	0.60	0.43	1.36	0.78	1.50	2.21	11.48	4.59	0.56	1.02
m54-83-mz1-3	9.71	0.24	0.76	0.68	0.61	0.43	1.36	0.77	1.47	2.22	11.77	4.41	0.56	1.02
m54-83-mz1-4	10.32	0.24	0.76	0.67	0.61	0.43	1.36	0.78	1.48	2.31	12.11	4.82	0.56	1.03
m54-83-mz1-5	10.29	0.24	0.76	0.66	0.60	0.43	1.37	0.77	1.47	2.24	10.53	4.78	0.57	1.07
m54-83-mz1-6	10.80	0.24	0.76	0.65	0.61	0.43	1.36	0.77	1.50	2.23	9.98	4.58	0.57	1.05
m54-83-mz1-7	13.00	0.24	0.76	0.65	0.60	0.43	1.33	0.77	1.48	2.28	12.44	4.82	0.57	1.04
m54-83-mz1-8	13.08	0.24	0.77	0.66	0.60	0.43	1.36	0.78	1.48	2.22	11.33	4.51	0.57	1.06
m54-83-mz1-9	10.34	0.24	0.76	0.61	0.61	0.43	1.36	0.78	1.50	2.19	10.48	4.22	0.56	1.01
m54-83-mz1-10	13.87	0.24	0.76	0.65	0.61	0.43	1.33	0.77	1.50	2.31	11.26	5.21	0.57	1.04
m54-83-mz1-11	10.41	0.24	0.75	0.60	0.61	0.43	1.38	0.78	1.48	2.18	11.82	4.81	0.56	1.05
m54-83-mz1-12	12.97	0.24	0.77	0.65	0.61	0.43	1.34	0.77	1.46	2.24	13.59	5.10	0.57	1.06
m54-83-mz1-13	12.65	0.24	0.77	0.66	0.60	0.43	1.36	0.77	1.47	2.28	9.32	5.20	0.58	1.06
m54-83-mz12-1	5.53	0.24	0.77	0.74	0.61	0.43	1.38	0.79	1.49	2.02	8.55	4.79	0.56	0.94
m54-83-mz12-2	7.75	0.24	0.77	0.73	0.61	0.43	1.38	0.79	1.50	1.99	8.87	4.48	0.56	0.95
m54-83-mz12-3	8.24	0.24	0.75	0.77	0.61	0.43	1.37	0.79	1.46	1.92	9.96	4.34	0.56	0.87
m54-83-mz12-4	6.57	0.24	0.76	0.85	0.61	0.43	1.40	0.79	1.53	2.01	9.76	5.02	0.55	1.04
m54-83-mz12-5	7.88	0.24	0.75	0.81	0.61	0.43	1.40	0.79	1.50	1.94	11.13	4.35	0.55	0.96
m54-83-mz12-6	7.55	0.24	0.78	0.79	0.61	0.43	1.38	0.80	1.47	2.03	8.49	4.81	0.56	0.96

m54-83-mz12-7	6.00	0.24	0.76	0.84	0.61	0.43	1.38	0.79	1.56	2.17	9.27	4.54	0.55	1.00
m54-83-mz12-8	5.62	0.24	0.77	0.68	0.61	0.43	1.42	0.80	1.49	2.18	8.50	4.26	0.57	0.87
m54-83-mz12-9	2.79	0.24	1.03	0.45	0.61	0.43	1.38	0.78	1.57	1.87	5.73	6.38	0.65	1.81
m54-83-mz12-10	7.55	0.24	0.77	0.78	0.61	0.43	1.39	0.80	1.50	2.01	7.30	4.91	0.57	0.93
m54-83-mz12-11	5.86	0.24	0.75	0.57	0.61	0.43	1.38	0.78	1.49	1.98	9.37	4.42	0.57	0.77

Appendix F. Sample Catalogue

JCU #	Sample #	Lithology	Polished thin sections*	Location
72007	CH22	Grassy Branch Fm.	0, 30	see Fig. 2. (Chapter 2)
72011	CH27	Copper Hill Fm.	20, 50	see Fig. 2. (Chapter 2)
72014	CH35	Ammons Fm.	0	see Fig. 2. (Chapter 2)
72030	CH62	Ammons Fm.	150	see Fig. 2. (Chapter 2)
59421	CA1	Canton Schist/Fm.	100	see Fig. 2. (Chapter 3)
72678	CA2	Canton Schist/Fm.	120, 130, 150	see Fig. 2. (Chapter 3)
72679	CA3	Canton Schist/Fm.	0, 0A	see Fig. 2. (Chapter 3)
72680	CA4	Canton Schist/Fm.	30	see Fig. 2. (Chapter 3)
72681	CA5	Canton Schist/Fm.	0A-0F, 170A-170E	see Fig. 2. (Chapter 3)
72682	CA6	Canton Schist/Fm.	30	see Fig. 2. (Chapter 3)
72683	CA7	Canton Schist/Fm.	10, 170	see Fig. 2. (Chapter 3)
72684	CA10	Canton Schist/Fm.	30, 180	see Fig. 2. (Chapter 3)
72685	CA14	Canton Schist/Fm.	0A-0G	see Fig. 2. (Chapter 3)
72686	CA17a	Canton Schist/Fm.	90, 90A, 120, 150, 150A	see Fig. 2. (Chapter 3)
72687	CA19	Canton Schist/Fm.	90	see Fig. 2. (Chapter 3)
72688	CA20	Canton Schist/Fm.	120	see Fig. 2. (Chapter 3)
72689	CA23	Canton Schist/Fm.	140	see Fig. 2. (Chapter 3)
72690	CA29	Canton Schist/Fm.	170	see Fig. 2. (Chapter 3)
72691	CA30	Canton Schist/Fm.	0A-0G	see Fig. 2. (Chapter 3)
72692	CA31	Canton Schist/Fm.	0, 0A	see Fig. 2. (Chapter 3)
72693	CA37	Canton Schist/Fm.	30	see Fig. 2. (Chapter 3)
72694	GA13	Canton Schist/Fm.	160	see Fig. 2. (Chapter 3)
72695	W1	Canton Schist/Fm.	170	see Fig. 2. (Chapter 3)
72696	W2C	Canton Schist/Fm.	150, 170	see Fig. 2. (Chapter 3)
72697	K1	Littleton Fm.	30	see Appendix G
72698	K20	Littleton Fm.	20	see Appendix G
72699	K22	Erving Fm.	90	see Appendix G
72700	K31	Littleton Fm.	0	see Appendix G
72701	K34	Littleton Fm.	150	see Appendix G
72702	K36	Littleton Fm.	30	see Appendix G
72703	K37	Littleton Fm.	90	see Appendix G
60463	K38	Littleton Fm.	30	see Appendix G
72704	K42	Littleton Fm.	30, 170	see Appendix G
72705	K43	Littleton Fm.	10	see Appendix G
72706	K44	Littleton Fm.	150	see Appendix G
72707	K45	Littleton Fm.	10	see Appendix G
72708	K52	Littleton Fm.	40, 40A, 60	see Appendix G
60470	K53	Littleton Fm.	30	see Appendix G
72709	K53	Littleton Fm.	90A, 90B	see Appendix G
72710	K55	Littleton Fm.	90(A), 90(B)	see Appendix G
72711	K59	Littleton Fm.	0, 90, 90A	see Appendix G
72712	K60	Littleton Fm.	90	see Appendix G
72713	K63	Littleton Fm.	120	see Appendix G
72714	K66	Littleton Fm.	10	see Appendix G
72715	K74	Erving Fm.	90	see Appendix G
72716	K81	Littleton Fm.	30	see Appendix G
72717	K87	Littleton Fm.	130	see Appendix G
72718	K103	Littleton Fm.	20, 20A	see Appendix G

72719	K111	Littleton Fm.	30	see Appendix G
60501	M54	Mt. Mineral Fm.	83	see Appendix G

* value represents strike of vertical thin section

Appendix G. Massachusetts sample locations